

Oral Abstracts

Friday, January 20, 2006

10:30 AM–12:00 PM

Best Oral Abstracts: Clinical

101. CARDIOVASCULAR MAGNETIC RESONANCE, FIBROSIS AND PROGNOSIS IN DILATED CARDIOMYOPATHY

Ravi G. Assomull, MBBChir MRCP, Sanjay K. Prasad, MD, MRCP, Elisabeth Burman, Mohammed Khan, Mary Sheppard, MD, FRCPath, Philip A. Poole-Wilson, MD, FRCP, Dudley J. Pennell, MD, FRCP. *Royal Brompton Hospital, London, United Kingdom.*

Background: Non-ischemic dilated cardiomyopathy (DCM) is associated with significant morbidity and premature mortality. Accurate risk stratification of patients with DCM in the era of device implantation is problematic. Previous studies have shown that approximately 30% of patients with DCM have mid-wall fibrosis as detected by late gadolinium-enhancement (LGE) cardiovascular magnetic resonance (CMR). Myocardial fibrosis may be associated with increased susceptibility to arrhythmia and progression of heart-failure.

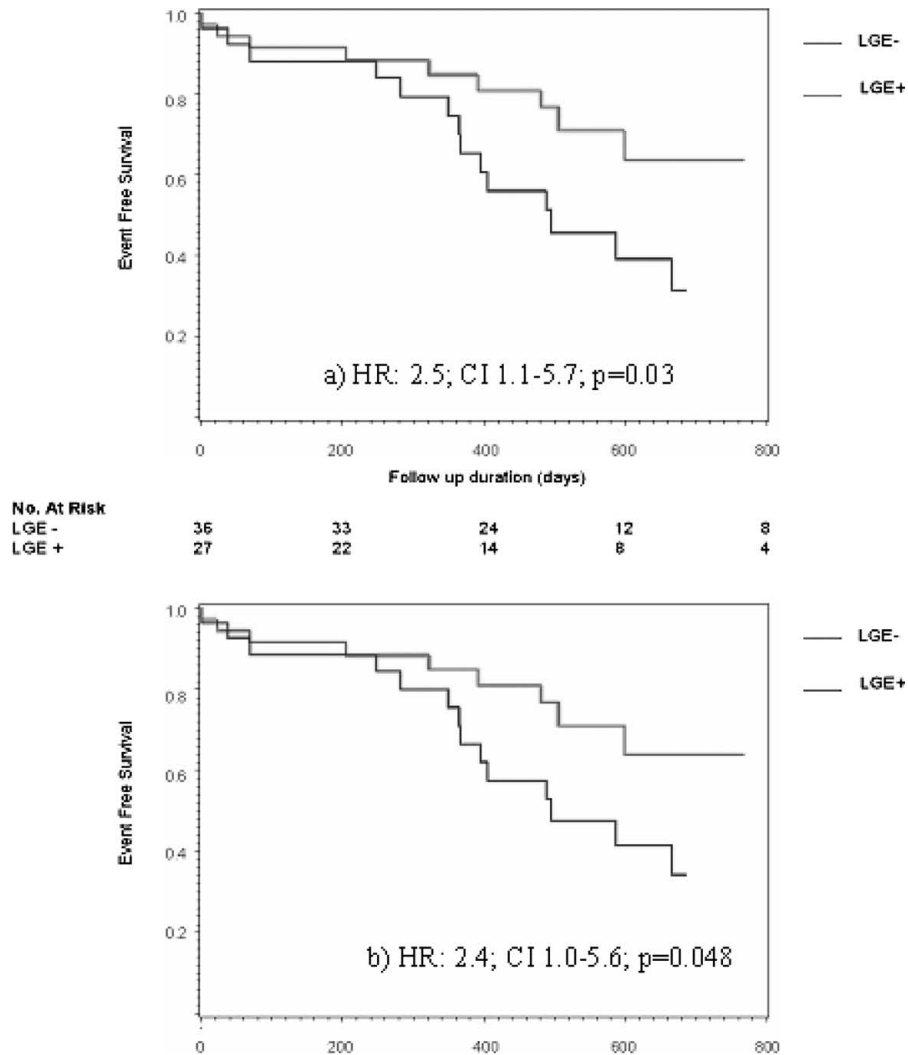


FIG. 1.

Purpose: We speculated that fibrosis in DCM might predict outcome. We tested this hypothesis in a prospective longitudinal study comparing the clinical outcomes in DCM patients according to the presence (LGE+) or absence (LGE-) of mid-wall fibrosis with a composite primary endpoint of all cause mortality or hospitalization for cardiovascular causes.

Methods: Consecutive patients diagnosed with DCM ($N = 63$, Male = 45, Mean age = 52 ± 13 years) and an EF of $\leq 40\%$ were recruited. All patients had a normal coronary angiogram and no CMR evidence of prior myocardial infarction. The patients were divided into 2 groups according to the presence or absence of mid-wall fibrosis and followed prospectively for 534 ± 318 days. Event data was collected and recorded by communication with patients, their cardiologists and general practitioners at regular intervals. Medical records were reviewed for recruited patients following attendance at outpatient clinics or hospitalization. Follow-up was complete.

Statistical Analysis: Continuous data are expressed as mean \pm SD. The baseline characteristics of the two groups were compared with the use of independent sample t-tests for continuous variables and chi-square or Fisher's tests for categorical variables where appropriate. Survival estimates and cumulative event rates were compared by the Kaplan-Meier method. The time to first event for each end-point was recorded for each patient. The log-rank test was used to compare the Kaplan-Meier survival curves in the two groups. The hazard ratio was calculated using a Cox regression model with computed 95% confidence intervals (CI). Multivariate analysis was also performed using 3 covariates known to affect the end-points, namely age, left ventricular (LV) ejection fraction (EF), and right ventricular (RV) EF. The duration of follow up was computed using the date of entry into the study (day of the CMR scan) to the date of the first end-point reached. For patients who did not reach an end-point, follow up data was collected to the time of their last clinical follow up. A p value of < 0.05 was deemed significant

Results: Mid-wall fibrosis was present in 27 patients (43%). There were no baseline differences in age, underlying etiology, left ventricular and right ventricular size and function between the two groups. In addition, the proportion of patients on treatment with beta blockers, ACE inhibitors and spironolactone in each group were comparable. The presence of mid-wall fibrosis was associated with a higher rate of all cause mortality and hospitalization (hazard ratio [HR] 2.5, $p = 0.03$; Fig. 1a). Multivariate analysis demonstrated mid-wall fibrosis as the sole significant predictor of death/hospitalization (HR 2.4, $p = 0.048$, Fig. 1b).

Conclusions: This is the first study to evaluate the prognostic significance of detecting myocardial fibrosis in DCM. Patients with myocardial fibrosis had a higher incidence of the pre-defined endpoint of all-cause mortality and hospitalization, and this finding persisted after correction for baseline patient differences in LV/RV volumes/function and age. These findings have potentially important implications for the risk stratification of DCM patients and further studies are required to establish whether LGE-CMR can be used for refinement of patients groups selected for device therapy.

102. DETECTION OF PULMONARY VEIN ABLATION WITH HIGH RESOLUTION MRI

Dana C. Peters, PhD,¹ John V. Wylie, MD,¹ Kraig V. Kissinger, RT,¹ Thomas Hauser, MD,¹ Rene M. Botnar, PhD,² Vidal Essebag, MD,¹ Mark E. Josephson, MD,¹ Warren J. Manning, MD.¹ ¹Beth Israel Deaconess Medical Center, Boston, MA, USA, ²Technical University Munich, Munich, Germany.

Introduction: The ability to directly visualize atrial scar tissue resulting from radiofrequency (RF) ablation would allow correlation of RF ablation locations with clinical outcomes in pulmonary vein and atrial ablation therapy. Cardiovascular

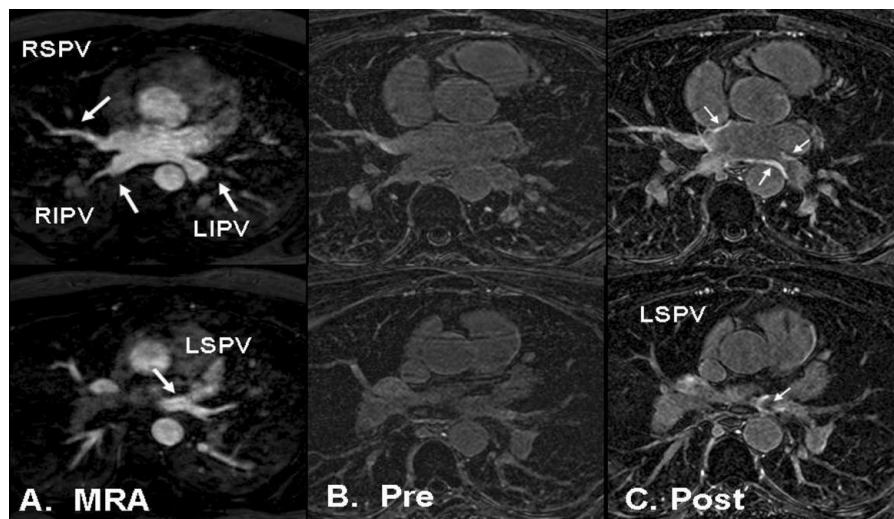


FIG. 1. A) Axial slices from the 3D pulmonary vein MRA showing the four pulmonary veins. B) Pre-ablation delayed enhancement image with the absence of hyperenhancement. C) Post-ablation delayed enhancement image demonstrating multiple areas of hyperenhancement (solid arrows). All slices were obtained from the same patient and are anatomically matched.

magnetic resonance (CMR) imaging identifies scar due to myocardial infarction (1) by imaging the accumulation of gadolinium contrast agent in the scarred regions, which appears bright (hyperenhanced) on a T1-weighted delayed enhancement (DE) image (2). We hypothesized that high resolution DE-CMR would similarly visualize the locations of RF ablations in patients after RF ablation.

Methods: Twenty-two patients (age = 58 ± 17 yrs) underwent CMR evaluation of pulmonary vein morphology before and/or after (43 ± 12 days post) an RF ablation procedure. Bi-directional pulmonary vein isolation was performed with an 8 mm non-irrigated tip ablation catheter and a circumferential catheter placed at each pulmonary vein ostium to confirm pulmonary vein entrance and exit block. The patients were studied using a T1-weighted DE-CMR 15–30 minutes after injection of 0.2 mmol/kg gadolinium. Imaging was performed on a Philips 1.5 T CMR scanner using a 3D ECG-triggered and respiratory motion compensated sequence (navigator-gating, 6 mm window) with an in-plane spatial resolution of 1.3×1.3 mm (scan time 6 min). Other scan parameters were: Cartesian acquisition, TR/TE/ $\theta = 5.4$ ms/2.5 ms/15°, $30 \times 30 \times 12.5$ cm field of view, full echo, 110 Hz/pixel receiver bandwidth, matrix $224 \times 224 \times 23$ –32 Nz, inversion time = 290 to 350 ms, zero-filling to $0.6 \times 0.6 \times 2.5$ mm resolution, vector ECG-gating with 32 views per segment (~150 ms in end-diastole), centric acquisition, navigator-gating with 5–7 mm window. Saturation bands were placed in the phase-encoding direction. Images were inspected for the presence of hyperenhancement in the left superior PV (LSPV), the left inferior PV (LIPV), the right superior PV (RSPV), and right inferior PV (RIPV). Signal to noise ratio (SNR) of the left atrial blood and left atrial/pulmonary vein walls were measured on both pre and post ablation images. Average contrast to noise ratio (CNR) was calculated for each PV with and without scar. The amount of scar in the left atrium was measured as the volume of left atrial/pulmonary vein wall with signal 5 standard deviations above the blood pool signal.

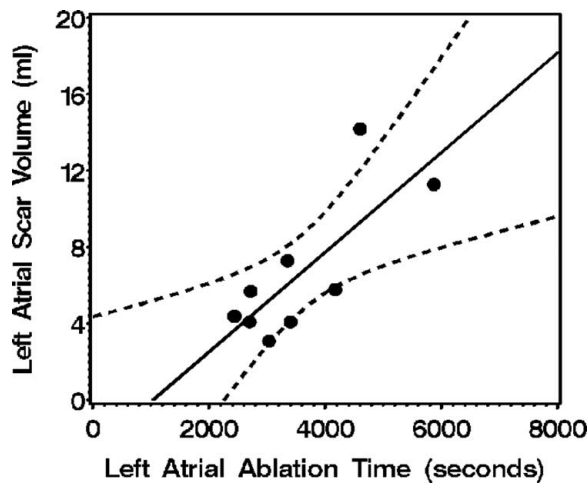


FIG. 2.

Results: Nineteen (86%) of scans were completed and interpretable. Four patients were imaged both pre and post-ablation (matched pairs). No pre-ablation patient images demonstrated positive left atrial wall scar while all post-ablation patients demonstrated evidence of left atrial wall hyperenhancement/scar in at least two veins (Fig. 1). Average CNR between left atrial blood and PV wall was 12 and 3.4 for scarred and unscarred regions, respectively ($P < 0.05$). A regression analysis of LA ablation time vs. volume of scar in the left atrium showed significant correlation with $R = 0.81$ (Fig. 2).

Conclusion: This study demonstrates that RF ablation scar can be visualized with this non-invasive CMR approach. Visualization of the left atrial scar may confirm procedural success of pulmonary vein isolation and scar anatomy may correlate with clinical outcomes.

REFERENCES

1. Kim RJ. N Engl J Med 2000;343:1445–1453.
2. Simonetti, OP. Radiology 2001; 218:215.

103. AUTOLOGOUS BONE MARROW-DERIVED STEM CELL TRANSFER IN PATIENTS WITH ST-SEGMENT ELEVATION MYOCARDIAL INFARCTION

Jan Bogaert, Maria Kalantzi, Lertlak Chaothawee, Frank E. Rademakers, Steven Dymarkowski, Frans Van de Werf, Stefaan Janssens. Gasthuisberg University Hospital, Leuven, Belgium.

Introduction and Purpose: The benefit of reperfusion therapies for ST-elevation acute myocardial infarction (STEMI) is limited by postinfarction left ventricular (LV) dysfunction. We investigated the effect of autologous bone marrow-derived stem cell (BMSC) transfer in the infarct-related artery on left ventricular (LV) function and structure in a randomized, double-blind, and placebo-controlled study.

Methods: One day after successful percutaneous coronary intervention for STEMI, 66 patients underwent bone marrow aspiration and were randomized to optimum medical treatment and injection of placebo (n = 34) or BMSC (n = 32). Primary endpoint was the increase in LV ejection fraction and secondary endpoints change in infarct size and regional LV function, all evaluated by magnetic resonance imaging (MRI).

Results: No differences were found in the area at risk or infarct size between groups. All 66 patients survived the 4 months follow-up and no complications could be attributed to BMSC transfer. BMSC transfer was associated with a greater reduction in myocardial infarct size, measured as reduction in late enhancement volume from baseline to follow-up (BMSC treatment effect 28%, $p = 0.036$). Global LV ejection fraction as measured by MRI 4 days after PCI, was 46.9 ± 8 in controls and 48.5 ± 7 in BMSC patients and increased after 4 months by 2.2 and by 3.4%, to $49.1 \pm 11\%$ and to $51.8 \pm 9\%$, respectively ($p = 0.38$ for treatment effect). Regional functional recovery

(i.e. systolic wall thickening) was not different between the control group, $21.8 \pm 19.2\%$ to $23.7 \pm 18.9\%$, and BMSC group, $23.6 \pm 17.9\%$ to $29.3 \pm 21.7\%$, in the infarct area ($p = 0.35$) or border zone ($32.7 \pm 15.3\%$ to $38.4 \pm 21.1\%$, and $36.6 \pm 18.9\%$ to $40.8 \pm 17.2\%$, respectively, $p = 0.87$).

Conclusions: Intracoronary transfer of autologous bone marrow cells does not augment global or regional left ventricular function recovery in timely reperfused myocardial infarcts but may enhance infarct remodeling.

104. RISK STRATIFICATION AFTER REPERFUSED ACUTE MYOCARDIAL INFARCTION USING DELAYED CONTRAST-ENHANCED CARDIOVASCULAR MAGNETIC RESONANCE: WHICH CMR PARAMETER PREDICTS MAJOR ADVERSE CARDIAC EVENTS MOST ACCURATELY

Matthias Regenfus,¹ Carolin Stingl,¹ Christian Schlundt,¹ Johannes von Erffa,¹ Michaela Schmidt,² Werner Adler,¹ Werner Daniel.¹ ¹FAU Erlangen-Nürnberg, Erlangen, Germany, ²Siemens Medical Solutions, Erlangen, Germany.

Objective: The established parameter for risk stratification after reperfused acute myocardial infarction (MI) is left ventricular (LV) ejection fraction (EF). With the use of delayed contrast-enhanced cardiovascular magnetic resonance (DE-CMR) further parameters for estimation of the extent of MI can be determined. We investigated which of these parameters would show the best performance in determining major adverse cardiac events (MACE) in patients with reperfused acute MI.

Methods and Materials: One hundred twenty-two patients (pts) with left ventricular (LV) dysfunction ($EF 40 \pm 7\%$) were examined on a 1.5T scanner within 5 ± 2 (3–9) days of an reperfused (percutaneous coronary intervention, TIMI III flow in post-interventional angiography) acute MI. Cine and DE-CMR (10 min after injection of $0.15 \text{ mmol/kg Gd-DTPA}$) was acquired and scored for regional wall thickening and contrast enhancement (HE) using a 17-segment model. Segments were considered to be viable if showing $<25\%$ HE. The dysfunctional area by CMR (No. of dysfunctional segments/No. of segments analyzed) and the dysfunctional but viable area by CMR (No. of dysfunctional segments considered viable by DE-CMR/No. of segments analyzed) were calculated. Additionally, infarct size, the extent of microvascular obstruction (MO), and LV ejection fraction (EF) were quantitatively determined by planimetry. Serial clinical follow-up was obtained in all patients (mean follow-up 3.5 ± 1.3 years) regarding occurrence of MACE, as there are cardiac death, reinfarction, further myocardial revascularization, and unstable angina or congestive heart failure requiring hospitalization. Patient-related and CMR data were analyzed by univariate hazard ratio analysis and in a multivariable Cox proportional hazard regression model.

Results: Among the 122 patients, there were 11 cardiac deaths and reinfarctions in the follow-up period. Additionally, there

TABLE 1
Prediction of MACE: univariate analysis

	Hazard ratio	Low limit 95% CI	Up limit 95% CI	p
EF	3.4	1.5	5.1	<0.0001
extent of MO	3.7	1.4	5.0	<0.0001
infarct size	1.7	0.8	3.6	0.007
dysfunctional/viable area	2.4	1.7	3.5	0.002

were 35 patients with further myocardial revascularization or hospitalization due to unstable angina or congestive heart failure. Patients with events at follow-up showed significantly lower EF ($35 \pm 12\%$ vs. $46 \pm 11\%$, $p = 0.002$), and more often presence of MO (63% vs. 20% , $p < 0.001$) than patients without events. In patients with cardiac deaths or reinfarction, the dysfunctional area by CMR (66% vs. 43% , $p = 0.02$) and the dysfunctional but viable area by CMR (28% vs. 13% , $p = 0.008$) were significantly higher than in patients without such events. By univariate analysis, EF, extent of MO, infarct size, and, the dysfunctional but viable area by CMR were related to occurrence of future events (Table 1). By the multivariable Cox regression model, extent of MO remained the strongest predictor after adjustment for LV EF (adjusted hazard ratio 3.1, CI 1.9–4.3, $p < 0.004$).

Conclusion: In patients after reperfused acute MI, DE-CMR can be used to predict major adverse cardiac events. Next to the established parameter for risk stratification-ejection fraction -, the extent of microvascular obstruction represents a highly predictive parameter.

105. DIAGNOSTIC VALUE OF CONTRAST ENHANCED MAGNETIC RESONANCE IMAGING AND SINGLE PHOTON EMISSION COMPUTED TOMOGRAPHY FOR THE DETECTION OF MYOCARDIAL NECROSIS EARLY AFTER ACUTE MYOCARDIAL INFARCTION

Tareq Ibrahim, MD,¹ Hubertus P. Bülow, MD,² Thomas Hackl,² Mira Hörnke,² Stephan G. Nekolla, PhD,² Josef Dirschinger, MD,¹ Albert Schömig, MD,¹ Markus Schwaiger, MD² ¹Deutsches Herzzentrum & Klinikum rechts der Isar der Technischen Universität München, Munich, Germany, ²Nuklearmedizinische Klinik und Poliklinik der Technischen Universität München, Munich, Germany.

Background: Reperfusion therapy has significantly reduced mortality in patients with acute myocardial infarction (AMI). However, the use of mortality as an end point in clinical trials evaluating the efficacy of reperfusion therapy after AMI requires increasingly large patient numbers. Measurement of infarct size is an attractive surrogate end point instead of early mortality because the number of study patients can be significantly reduced without the need for megatrials. Currently, single photon

emission computed tomography (SPECT) is widely accepted in the clinical setting for the detection and quantification of myocardial infarction. However, technical limitations of SPECT such as a low spatial resolution or attenuation artifacts predominantly within the inferior wall may impair the delineation of infarcted tissue. Contrast enhanced magnetic resonance imaging (CMR) offers several advantages compared to SPECT, particularly a higher spatial resolution, which may allow the detection of even very small infarcts. Because efficient reperfusion therapies aim for the restriction of infarct extent, CMR may be superior to SPECT for the accurate assessment of infarct size after AMI.

Purpose: In this study, we sought to investigate the diagnostic value of CMR and SPECT for the detection of myocardial necrosis early after reperfusion therapy in patients with AMI.

Methods: Seventy-eight patients (62 ± 12 years; 60 men) with AMI were examined by CMR and SPECT 7 ± 2 d after percutaneous coronary stenting. All subjects were imaged in supine position using a 1.5T Siemens Sonata scanner equipped with a cardiac coil. CMR short and long axis were acquired 20 minutes after bolus injection of Gd-DTPA (0.2 mmol/kg) using a segmented inversion recovery sequence. CMR and corresponding SPECT images of the left ventricle were analyzed using a 17-segment model. For CMR, each segment was scored for presence and location of hyperenhancement by two blinded observers by consensus using the following score: 0 = no enhancement, 1 = 1–25%, 2 = 26–50%, 3 = 51–75%, 4 = 76–100% enhancement extent of the transmural wall. For SPECT analysis, a similar scoring system was used: 0 = normal perfusion, 1 = mildly reduced, 2 = moderately reduced, 3 = severely reduced, 4 = absent tracer activity. Both modalities were evaluated in 1326 segments and results were compared to ECG-changes as well as angiographic findings.

Results: All patients had elevated troponin t-levels, and 83% of the patients had a Q-wave myocardial infarction by ECG. AMI was significantly more often detected by CMR than SPECT ($p < 0.008$). Overall sensitivity for CMR and SPECT was 97% and 87%, respectively. Both modalities identified Q-wave myocardial infarction with high sensitivity (CMR: 100% vs. SPECT: 95%). However, SPECT was less sensitive for the detection of non-Q-wave myocardial infarction (CMR: 85% vs. SPECT: 46%). While CMR offered high sensitivity and specificity for regional detection of infarcted tissue irrespective of the infarct related artery, SPECT was less sensitive particularly within the left circumflex artery territory and specificity was lowest within the right coronary artery region (Table 1).

Conclusion: CMR is more sensitive than SPECT in detecting myocardial necrosis early after AMI and reperfusion because CMR detects non-Q-wave infarctions that were missed by SPECT independent of the infarct location. Thus, CMR may help overcome limitations of SPECT imaging and therefore is an attractive alternative for the assessment of myocardial infarct size in patients with AMI.

106. HIGH RESOLUTION MYOCARDIAL PERFUSION IMAGING AT 3.0T: COMPARISON TO STANDARD 1.5T PERFUSION STUDIES AND DIAGNOSTIC ACCURACY IN PATIENTS WITH SUSPECTED CAD

Katharina A. Strach, MD, Carsten Meyer, MD, Claas P. Naehle, MD, Alexandra Schmiedel, MD, Matthias Hackenbroch, MD, Jürgen Gieseke, Hans Schild, MD, Torsten Sommer, MD. University of Bonn, Radiology, Germany.

Background: Recently, myocardial rest perfusion in healthy volunteers at 3.0T has been shown to significantly increase signal-to-noise-ratio (SNR) in comparison to 1.5T. However, the benefits of 3.0T with respect to image quality in comparison to 1.5T as well as diagnostic accuracy for the detection of coronary artery disease (CAD) have not been evaluated, yet.

Purpose: To evaluate: 1) high resolution myocardial rest perfusion in healthy volunteers (group 1) at 3.0T in comparison to a standard approach at 1.5T, as well as 2) the technical feasibility and diagnostic accuracy of 3.0T high resolution myocardial stress perfusion in patients with suspected CAD (group 2).

Methods: All perfusion studies were performed using a T1-weighted saturation-recovery k-space segmented gradient-echo sequence combined with parallel imaging (Gad-DTPA 0.05 mmol/kg BW).

Study group 1 consisted of 17 healthy volunteers (9 males, 8 females; mean age: 25.6 ± 4.1 years) with low likelihood of CAD (<5% Diamond & Forrester) receiving 1) a high resolution rest perfusion scan at 3.0T (in-plane resolution 1.8×2.1 mm², pixel size 3.78 mm², slice thickness 8 mm, TE/TR/ α 3.7/1.8 ms/15°, SENSE factor 3; Achieva 3.0T, Philips Medical Systems) and 2) a standard perfusion approach at 1.5T (in-plane resolution 2.9×3.4 mm², pixel size 9.86 mm², slice thickness 8 mm, TE/TR/ α 3.7/1.8 ms/ 20°, SENSE factor 2; Intera 1.5T, Philips Medical Systems). Both rest studies were performed in random order on two separate days (interval: 24 to 72 hours). Myocardial signal intensity increase [(peak signal intensity/baseline signal intensity) \times 100] was

TABLE 1
Regional detection of myocardial infarction according to the infarct related artery

	LAD Sensitivity	LAD Specificity	LCX Sensitivity	LCX Specificity	RCA Sensitivity	RCA Specificity
CMR	97%	100%	100%	97%	97%	100%
SPECT	89%	98%	79%	92%	87%	85%

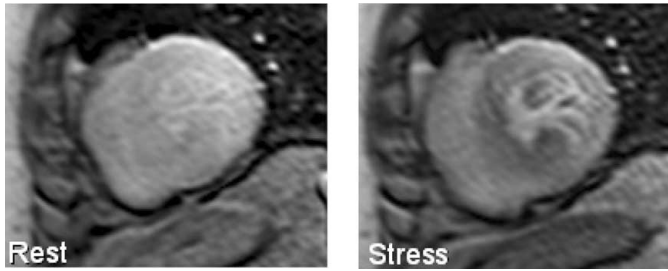


FIG. 1. Stress-induced perfusion deficit in the septal and inferior myocardium. X-ray coronary angiography revealed a proximal occlusion of a dominant RCA.

assessed for high resolution and standard scans. Image quality was evaluated by two observers on a four point grading scale (4: excellent, 1: non-diagnostic) with respect to homogeneity of myocardial enhancement, blurring and presence of artifacts.

Study group 2 consisted of 19 patients (12 males, 7 females; mean age: 59.3 ± 7.2 years) with suspected CAD scheduled for X-ray coronary angiography. Patients underwent a high resolution stress (adenosine $140 \mu\text{g}/\text{kg}$ BW over 6 min) and rest perfusion study at 3.0T (interval: 30 min) with equivalent Gd-DTPA concentration and scan parameters as for healthy volunteers at 3.0T. Perfusion studies were qualitatively assessed for stress-induced hypoperfusion by two experienced observers. Hemodynamically significant coronary artery disease was defined as luminal diameter stenosis $\geq 70\%$ in conventional coronary angiography.

Results: Study group 1: Myocardial signal intensity increase in high resolution rest perfusion studies at 3.0T was not significantly different to the standard approach at 1.5T ($207\% \pm 43$ vs. $199\% \pm 52$, $p > 0.05$). Image quality was significantly improved in high resolution perfusion imaging at 3.0T in comparison to the standard approach at 1.5T (3.1 ± 0.7 vs. 2.2 ± 0.4 , $p < 0.01$).

Study group 2: Mean score of image quality was 2.7 ± 0.7 . The mean myocardial signal intensity increase was $170\% \pm 30$. Sensitivity and specificity of high resolution perfusion studies at 3.0T for the detection of significant coronary artery disease was 90% ($n = 9/10$) and 78% ($n = 7/9$), respectively.

Conclusion: 1) MR myocardial perfusion imaging at 3.0T permits significantly improved spatial resolution allowing for a 60% reduction of pixel size. 2) High resolution perfusion at 3.0T provides significantly improved image quality in comparison to a standard approach at 1.5T. 3) 3.0T perfusion studies are also feasible in patients with suspected CAD in a clinical setting and yield promising results for the detection of significant coronary artery stenosis.

107. MYOCARDIAL PERFUSION RESERVE TO DETECT PHYSIOLOGICALLY SIGNIFICANT CORONARY DISEASE: QUANTITATIVE MAGNETIC RESONANCE VS.

INVASIVE PHYSIOLOGIC ASSESSMENTS AND QUANTITATIVE CORONARY ANGIOGRAPHY

Hideki Futamatsu, MD, Steven Shoemaker, MD, Bayar Batmunnh, MS, Christopher Klassen, MD, PHD, Alan Siuciak, MS, Minh Nguyen, MD, Marco Costa, MD, Norbert Wilke, MD. *University of Florida, Jacksonville, FL, USA.*

Introduction: The quantitative myocardial magnetic resonance perfusion reserve (MPR) provides an accurate noninvasive assessment of the physiologic significance of coronary artery disease (CAD) as compared to the fractional flow reserve (FFR). MPR also correlates with quantitative coronary angiography (QCA) in determining the anatomical severity of CAD.

Purpose: Determine the correlation of FFR and QCA with magnetic resonance MPR in patients with CAD.

Methods: Patients ($n = 30$) with indication for elective coronary angiography underwent non-invasive, stress and rest first-pass perfusion MR studies (0.04 mmol/kg gadolinium-DTPA bolus, 1.5T Sonata, Siemens). For both FFR and MPR, stress was induced with 140 mcg/kg/min Adenosine IV. Invasive FFR was obtained during stress using a .014 inch Jomed pressure wire. Automated QCA (CASS II 4.1, Pie Medical) was done in 2 orthogonal views. MPR was calculated from the ratio, between stress and rest, of the myocardial flows calculated from signal intensity time curves (Leonardo, Siemens). Quantitative MPR analysis was performed by propriety deconvolution analysis methods as previously validated in this lab. Visual perfusion assessment was also performed for rest and stress perfusion studies.

Results: Patients (19 vessels) had MPR, FFR measurements, and QCA performed. The MPR cutoff value of 2.3 yielded a sensitivity of 88.9% (95% CI, 51.8–99.7%), specificity of 85.7% (95% CI, 42.1%–99.6%), PPV of 88.8%, and NPV of 85.8% in predicting a significant FFR ($\leq .75$). The MPR to FFR correlation coefficient = .7181 with $p = .0017$. Qualitative analysis for ischemia yielded a sensitivity of 90.9% (95% CI, 58.7–99.8%), but a specificity of 60% (95% CI 14.7–94.7%) in predicting a significant FFR. % Diameter Stenosis and MPR were inversely correlated with a correlation coefficient of -0.66 with $p = .0025$.

Conclusions: This is the first study to suggest a strong correlation between noninvasive, quantitative MPR and invasive FFR measurements. Visual MR analysis showed also a good sensitivity but much lower specificity to detect physiologically significant CAD. Quantitative MPR had a better correlation with QCA than qualitative, visual MR perfusion assessment alone.

108. ASSESSMENT OF IRREVERSIBLE MYOCARDIAL INJURY USING THE DELAYED ENHANCEMENT TECHNIQUE AT 1.5 AND 3 TESLA

Adrian S. H. Cheng, MBBS, MRCP, Matthew D. Robson, PhD, Stefan Neubauer, MD, FRCP, Joseph B.

Selvanayagam, DPhil, FRACP. University of Oxford, Oxford, United Kingdom.

Introduction: In recent years, a number of studies have demonstrated the effectiveness of a segmented inversion-recovery fast gradient echo sequence for differentiating irreversibly injured from normal myocardium. This technique of delayed enhancement imaging (DE-MRI) has been shown in animal and human studies to identify the presence, location and extent of acute and chronic myocardial irreversible injury. DE-MRI is superior to single photon emission computed tomography for the identification of subendocardial myocardial infarction and has become a first-line indication for myocardial viability assessment. Recently, 3 Tesla (T) MRI systems have come into use for cardiac imaging, but it is uncertain how these systems perform in the assessment of myocardial viability using the delayed enhancement technique.

Purpose: To compare the visualisation of myocardial infarction using the same segmented inversion-recovery turbo fast low-angle shot (turbo-FLASH) pulse sequence at 1.5T and 3T.

Methods: Sixteen patients (mean age 66 ± 13 years) with evidence of myocardial infarction (clinical history and/or confirmation with previous imaging and/or troponin elevation) were recruited. Each participant was scanned by the same operator at both 1.5T (Sonata, Siemens Medical Solutions, Erlangen, Germany) and 3T (Trio, Siemens Medical Solutions) with the scans 30 minutes apart and done in random order. Following cine imaging covering the entire left ventricle (LV), a bolus of 0.1 mmol/kg of contrast agent (gadodiamide, Omniscan™, GE Healthcare) followed by a 10 mL saline flush was administered. Six minutes later, based on an inversion time (TI) pilot, the operator selected the TI value that best nulled the normal myocardium and acquired short axis images (typically 8–12) covering the entire LV using a breath-hold T1-weighted segmented inversion-recovery turbo-FLASH sequence (average voxel size: $2.4 \times 1.4 \times 8$ mm³). The operator adjusted TI to maintain optimum nulling of normal myocardium. Images were acquired every second cycle, unless the breath-hold time was prohibitive, in which case images were acquired every cycle. Identical sequence parameters were used on each system wherever possible.

Results: All images acquired were of sufficient quality for analysis despite the presence of sternal wires in 2 of 16 (13%) patients and coronary stents in 8 of 16 (50%) patients. No problems with electrocardiographic gating were encountered. Mean LV values were: ejection fraction 38 ± 15 %, end-diastolic volume 244 ± 62 mL, end-systolic volume 156 ± 67 mL, mass 138 ± 42 g. The average initial TI selected by the operator to null normal myocardium at 3 T was 51 ± 27 ms longer than at 1.5 T (351 ± 23 ms vs. 300 ± 18 ms; $p < 0.01$). There were no significant differences in the presence, location or quantification of hyper-enhancing myocardium at 1.5 T or 3 T (28.1 ± 15.7 g vs. 27.8 ± 15.7 g; $p = 0.599$). There was no significant difference (41 ± 288 %) in percent signal intensity elevation at 1.5 T and 3 T (555 ± 417 % vs. 514 ± 276 %; $p = 0.575$) and no significant

difference (1.7 ± 28) in contrast-to-noise ratio at 1.5 T and 3 T (34 ± 12 vs. 36 ± 24 ; $p = 0.813$).

Conclusions: We demonstrate that DE-MRI is feasible at 3 T in patients with evidence of myocardial infarction. When using the same turbo-FLASH pulse sequence, there was no significant difference in the quantification of hyper-enhancing myocardium at 1.5 T or 3 T. The values for percent signal intensity elevation and contrast-to-noise ratio were similar at both field strengths, comparable with previous studies using a similar sequence at 1.5 T.¹ Inversion time needs to be longer when imaging at 3 T when compared to 1.5 T at the same time after contrast injection.

REFERENCE

1. Simonetti OP, Kim RJ, Fieno DS, et al. An Improved MR Imaging Technique for the Visualization of Myocardial Infarction. *Radiology* 2001;218:215–23.

109. FUNCTIONAL AND STRUCTURAL VASCULAR REMODELING IN ELITE ATHLETES ASSESSED BY CARDIOVASCULAR MAGNETIC RESONANCE

Steffen E. Petersen, Frank Wiesmann, MD, Lucy E. Hudsmith, Matthew D. Robson, PhD, Jane M. Francis, Joseph B. Selvanayagam, DPhil, FRACP, Stefan Neubauer, MD, FRCP, Keith M. Channon, MD, FRCP. University of Oxford, Oxford, United Kingdom.

Introduction: Endothelial dysfunction is a cardinal feature of vascular disease states, such as atherosclerosis, and is associated with an increased risk for cardiovascular events. Physical activity protects against the development of coronary artery disease and a sedentary lifestyle is believed to contribute to approximately one-third of deaths caused by coronary artery disease. Physical activity has well-known beneficial effects on vascular function in subjects with endothelial dysfunction. Exercise also leads to beneficial effects on endothelial function in elderly athletes, possibly contributing towards the reduced risk associated with coronary artery disease in this age group. However, the training effects in the younger population remain controversial.

Purpose: We hypothesized that in young adult elite rowers (whole body exercise, high intensity training over years) vascular function would be normal, but that vascular remodeling would be present in peripheral and central conduit arteries. We aimed to non-invasively quantify the effects of chronic exercise training in a cross-sectional study design on both peripheral and central conduit artery function and structure using high-resolution magnetic resonance imaging in a single examination.

Methods: A total of 48 young (20–35 years of age) non-smoking participants comprising 15 male and 13 female elite rowers and 21 (15 male/6 female) age-sex matched sedentary controls underwent cardiovascular magnetic resonance (CMR) imaging (1.5 Tesla) using steady state free precession. None of the subjects had received any vasoactive medication or had any factor known to cause endothelial dysfunction. As described in

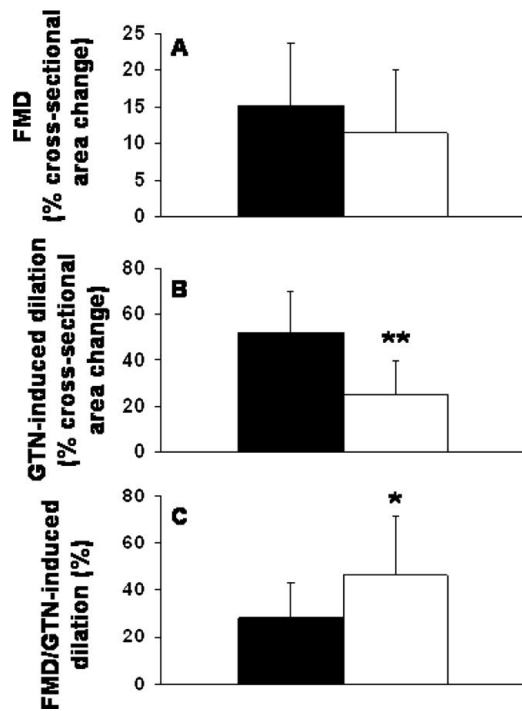


FIG. 1.

detail elsewhere, the ascending (AA), the proximal descending (PDA), the distal descending aorta (DDA), the right common carotid artery (CCA) and the brachial artery (BA) were assessed for diastolic and systolic area, absolute and relative area change, aortic and carotid artery distensibility. Flow-mediated, or endothelial-dependent dilatation (FMD) was assessed in the right brachial artery comparing cross-sectional baseline diastolic brachial artery areas with those acquired 1 min after reactive hyperemia was induced by release of a forearm cuff inflated to suprasystolic pressure for 4.5 min. Endothelial-independent brachial artery dilation was determined as the brachial artery area change compared to baseline 3 min after sublingual application of 400 g glyceroltrinitrate (GTN).

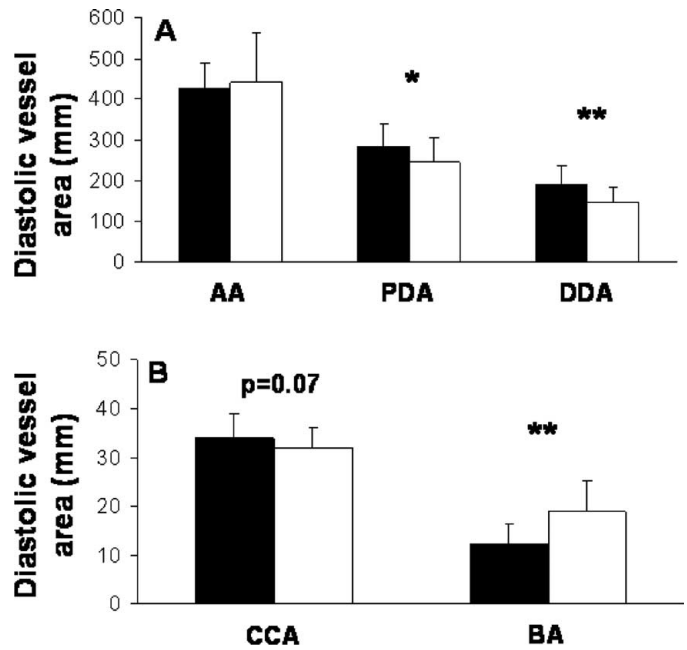


FIG. 2.

Results: Vessel distensibilities (mmHg^{-1}) were similar for elite rowers when compared to sedentary controls at the level of the ascending, proximal and descending aorta, the carotid artery and the brachial artery ($p > 0.05$ for all). Endothelial-dependent dilation (%) was similar for rowers and controls ($p > 0.05$), but rowers showed reduced (by 106%) endothelial-independent dilation ($p = 0.015$, Fig. 1). Rowers showed vascular remodeling with enlarged brachial (by 51%, $p < 0.001$) and reduced central conduit artery areas (Fig. 2).

Conclusions: Young elite rowers demonstrate normal endothelial-dependent, but reduced endothelial-independent dilation, possibly reflecting smooth muscle cell desensitization to NO. Chronic, whole body, combined endurance- and strength-training does not lead to changes in arterial stiffness, but to vascular remodeling.

Friday, January 20, 2006
 10:30 AM–12:00 PM
 Best Oral Abstracts: Basic

³Imaging Science Laboratories, New York, NY, USA, ⁴Johns Hopkins University School of Medicine New York, NY, USA, ⁵Guerbet, Paris, France.

110. ASSESSING ATHEROSCLEROSIS WITH IN VIVO IMAGING OF MATRIX METALLOPROTEINASES (MMPS) USING P947, A NOVEL SPECIFICALLY-TARGETED MRI CONTRAST AGENT

Smbat Amirbekian,^{1,2,3} Juan Gilberto S. Aguinaldo,^{2,3} Vardan Amirbekian,^{2,3,4} Fabien Hyafil,^{2,3} Esad Vucic,^{2,3} Eric Lancelot,⁵ Claire Corot,⁵ Zahi A. Fayad.^{2,3,4} ¹Emory University School of Medicine, New York, NY, USA, ²The Mount Sinai School of Medicine, New York, NY, USA,

Introduction and Purpose: Matrix Metalloproteinaes (MMPs) play an important role in the pathogenesis of atherosclerosis and vascular remodeling. Most notably, over-expression of MMPs is associated with plaque rupture and instability. MMPs are often highly expressed at the shoulder regions of plaques that rupture. P947 (Guerbet) is a short peptide (7 residues) ligand for MMPs. P947 has a DOTA-Gadolinium chelate attached to it, making it into an MRI contrast agent. Here we investigated the in-vivo efficacy of P947 in detecting atherosclerotic plaque using ApoE KO mice.

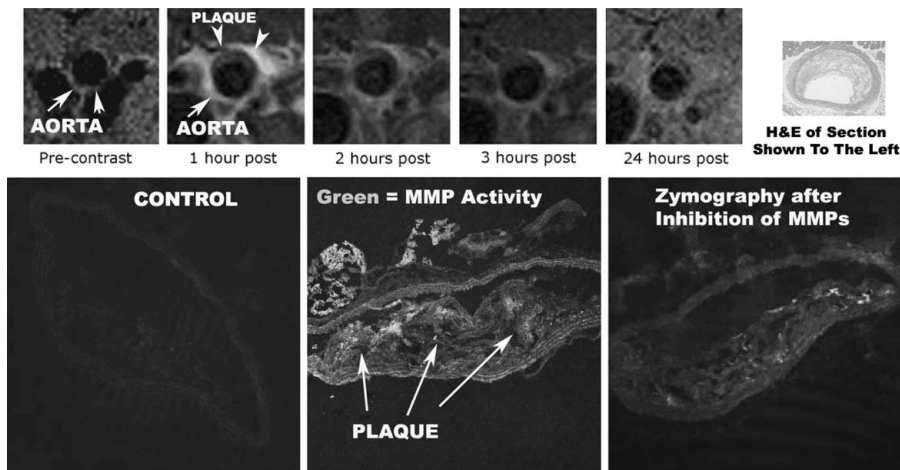


FIG. 1. Top Row: IN-VIVO Matched axial MR images (using P947) corresponding to the H&E section shown of the abdominal aorta of an ApoE KO mouse. Bottom Row: MMP Zymography—Left Panel is a control MMP Blank Section; Middle Panel is MMP targeted Zymography; Right Panel is MMP targeted Zymography following inhibition of MMPs with EDTA.

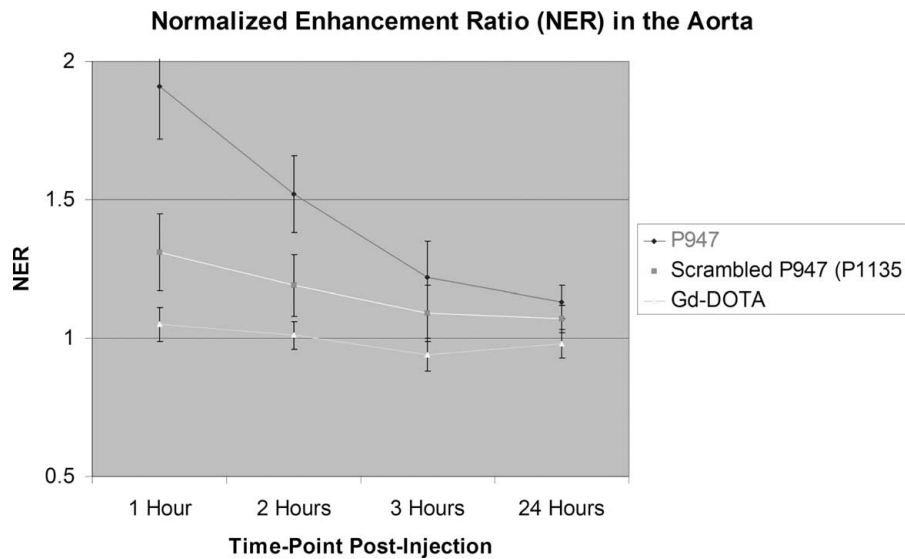


FIG. 2.

TABLE 1
Summary of MRI Results

NER = Normalized Enhancement Ratio	P947	Scrambled P947 (P1135)	Gd-DOTA (Dotarem)
NER at 1 Hour Post-Injection	1.91 ± 0.19 (91% Enhancement)	1.31 ± 0.14 (31% Enhancement)	1.05 ± 0.06 (5%)
NER at 2 hrs Post-Injection	1.52 ± 0.14 (52%)	1.19 ± 0.11 (19%)	NS
NER at 3 hrs Post-Injection	1.22 ± 0.13 (22%)	1.09 ± 0.1 (9%)	NS
NER at 24 hrs Post-Injection	1.14 ± 0.06 (14%)	1.07 ± 0.05 (7%)	NS
Injection	(14%)		

Methods: Fifteen-month-old ApoE KO mice (n = 12) underwent in vivo MRI of the abdominal aorta using a 9.4T MRI system. Pre-contrast enhanced (CE) and post-CE MRI was performed at 1, 2, 3, and 24 hours post injection using a T1W black blood sequence. P947 (100 umol/kg) was injected via the tail vein. As a powerful control, we used the peptide contrast agent P1135, which is P947 with the peptide sequence completely scrambled. By scrambling the peptide sequence specificity for MMPs is lost. As a second control, another group of ApoE KO mice (n = 5) was injected with non-targeted Gd-chelate (Gd-DOTA, Dotarem, Guerbet). After MRI, the aortas were isolated, fixed and immunohistochemistry was performed for MMPs. MMP Zymography was performed to show expression of MMPs in imaged sections.

Results: In ApoE mice that were injected with P947 there was heterogeneous enhancement seen on MRI, with a significant increase in the contrast-to-noise ratio (CNR) post-contrast-enhanced images (1, 2 and 3 hrs post-injection; Fig. 1). In the Gd-DOTA control group, there was no significant enhancement of the wall. The ratio of the post to the pre contrast signal intensity of the wall, normalized to an externally placed standard, with P947 was 2.21 ± 0.19 (121% enhancement) in ApoE-KO mice at 1 hr, 1.74 ± 0.14 (74%) at 2 hrs, 1.31 ± 0.13 (31%) at 3 hrs, and 1.18 ± 0.06 (18%) at 24 hrs. The ratio of the post to the pre contrast signal intensity of the wall, normalized to muscle, with P947 was 1.91 ± 0.19 (91% enhancement) in the ApoE-KO mice at 1 hr, 1.52 ± 0.14 (52%) at 2 hrs, 1.22 ± 0.13 (22%) at 3 hrs, and 1.14 ± 0.06 (14%) at 24 hrs. Using P1135 (P947 scrambled) we saw enhancements of only 1.31 ± 0.14 (31% enhancement) in the ApoE-KO mice at 1 hr, 1.19 ± 0.11 (19%) at 2 hrs, 1.09 ± 0.1 (9%) at 3 hrs, and 1.07 ± 0.05 (7%) at 24 hrs (Table 1). MMP Zymography demonstrated significant MMP activity in imaged sections (controls were negative; Fig. 1).

Conclusions: Targeting MMPs with P947 showed highly significant MRI enhancement of aortic atherosclerotic plaque in Apo E KO mice. P947 may be useful in in-vivo noninvasive detection of atherosclerosis and assessment of plaque stability using MRI.

111. EFFICIENT QUANTITATION OF ²³Na CONCENTRATIONS INCLUDING FAST AND SLOW T₂

COMPONENTS IN THE HUMAN HEART USING UTE-CSI AND THE BLOOD POOL AS A REFERENCE

Matthew D. Robson, MA, PhD, Damian J. Tyler, PhD, Joseph B. Selvanayagam, FRACP DPhil, Jane M. Francis, DCRR, DNM, Stefan Neubauer, MD, FRCP. OCMR, Oxford University, Oxford, United Kingdom.

Introduction: Sodium concentrations in the human heart increase during ischemia due to failure of the Na-K pump, which results in increases in intra-cellular sodium (²³Na). This has been demonstrated extensively in animal models (1), and has also been demonstrated in humans (2). Here we describe technical developments that further advance this field. ²³Na exists as a 3/2-spin nucleus its quadrupolar moment results in it having bi-exponential relaxation under typical biological conditions. The relative concentration of these two relaxation components, and T₂'s of each of these components may indicate the environment of the nucleus. The sum of these two components yields the total sodium concentration.

Purpose: Develop an approach to:

1. Measure the rates of fast and slow relaxation
2. Quantify the amount of sodium in terms of the mM concentrations for each relaxation component.

Theory: Use of the ultra-short TE Chemical Shift Imaging acquisition method allows us to acquire images with a TE as short as 70us, and to acquire the free-induction decay so as to capture both the short and long T₂ components efficiently (3). After reconstruction we can fit the two relaxation components to evaluate the relative amounts and relaxation rates of the two signal components. To provide quantitation we use the blood pool as a reference. The left ventricular blood pool is a good choice for a reference as it has a known Na concentration 135 mM/l–145 mM/l, which can be tested, has a similar T₂ to the myocardial tissue, contains a high level of Na, and finally is located close to the tissue of interest and hence will be similarly affected by the transmit RF fields.

Methods: All work was performed on a Siemens Sonata 1.5T system with multinuclear capabilities and a ²³Na coil (Rapid-Biomedical). UTE-CSI was used in a cardiac gated fashion using the Ernst angle and a repetition time of 20 ms.

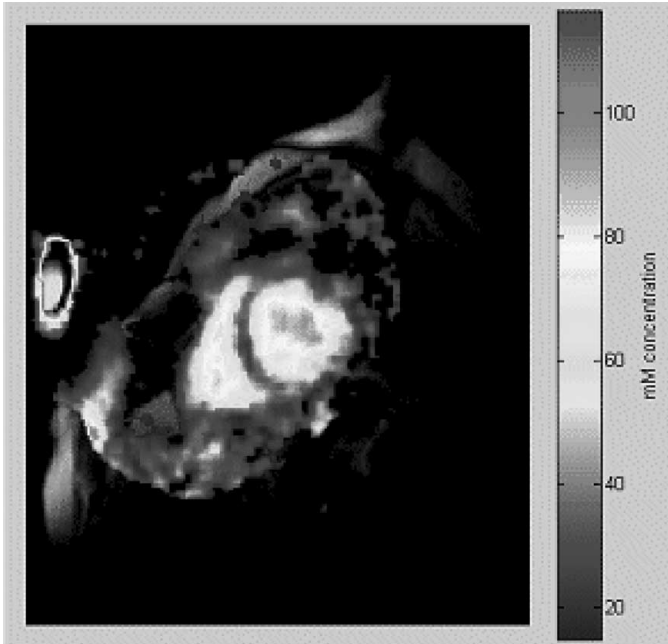


FIG. 1.

Five male volunteers were imaged supine. The ²³Na acquisition required around 25 minutes (dependent on heart rate), total exam time was around 40 minutes. Fiducial markers and proton images were used to determine the exact coordinates of the RF coil for each run enabling correction of the receive field profile.

Results: An example image of the long T₂ component is shown in Fig. 1.

The blood pool contains tiny amounts of short T₂ components. Relaxation and concentration parameters for the heart as a whole are shown in the Table. Each of the 16 segments of the conventional cardiac model were analyzed. Regionally consistent long T₂ relaxation rates were found, but the T₂ of the short relaxation rate could not be quantified regionally owing to the noise level. Concentrations of the long T₂ component were regionally consistent with coefficients of variation of ~15%. The short T₂ concentrations (using a T₂ value of 1.21 ms) exhibited high coefficients of variation ~60%. The high variability in these regional measurements is due to the intrinsically low SNR of the ²³Na acquisition.

Conclusions: A method has been described and validated that allows quantitative measurements of the Na concentration

Group	Total left ventricular myocardial wall Na concentration			Relaxation time	
	Long T ₂ (mM/l)	Short T ₂ (mM/l)	Total Na (mM/l)	Short T ₂ T ₂ [*] (ms)	Long T ₂ T ₂ [*] (ms)
Volunteers	43.6 ± 1.9	10.5 ± 2.4	54.1 ± 2.9	1.21 ± 0.45	18.4 ± 1.6

in the myocardium using a time efficient acquisition. Short T₂ components can be separately evaluated using this approach, but have low SNR. The basis of the method is the knowledge that the blood pool has the same T₁ and observes the same transmit field as the ²³Na in the myocardium. This simplification removes complex corrections and their associated error sources from the calculation.

REFERENCES

1. Ouwerkerk R, et al. JMRI 2005;21:546.
2. Constantinides, CD, et al. MRM 2001;46:1144.
3. Robson MD, et al. MRM 2005;53:267.

112. SIGNAL-ENHANCED VISUALIZATION OF MAGNETIC NANOPARTICLE-LABELED STEM CELLS USING INVERSION RECOVERY ON-RESONANT WATER SUPPRESSION (IRON)

Matthias Stuber, PhD,¹ Wesley D. Gilson, PhD,² Dorota Kedziorek, MD,² Jeff W. Bulte, PhD,³ Dara L. Kraitchman, VMD, PhD,² ¹Russell H. Morgan Department of Radiology and Radiological Science, Department of Medicine, and Department of Electrical Engineering, Johns Hopkins University School of Medicine, Baltimore, MD, USA, ²Russell H. Morgan Department of Radiology and Radiological Science, Johns Hopkins University School of Medicine, Baltimore, MD, USA, ³Russell H. Morgan Department of Radiology and Institute for Cell Engineering, Johns Hopkins University School of Medicine, Baltimore, MD, USA.

Introduction: The use of superparamagnetic nanoparticles has shown promise for contrast generation in stem cell research and atherosclerosis imaging. However, the resultant negative contrast created by susceptibility artifacts can be difficult to discriminate from other potential sources of signal voids. Therefore, we have developed Inversion-Recovery ON-Resonant water suppression (*IRON*), an imaging methodology that enables the hyperintense visualization of superparamagnetic particles.

Purpose: The development of an MRI method that enables the hyperintense visualization of superparamagnetic particles and investigation of its use for *in vivo* imaging of magnetic nanoparticle-labeled mesenchymal stem cells (MSCs).

Theory and Methods: The local external field-shift of a non-diamagnetic particle exposed to the static magnetic field (B₀), can be described as:

$$\Delta B_{\text{External}}(\mathbf{r}, \Theta) \sim (\Delta K^* a^3 / 3^* r^3) * (3^* \cos^2(\Theta) - 1) * B_0 \quad [1]$$

where ΔK is the difference in magnetic susceptibility, and *r* and *a* refer to the distance from the particle and to its radius,

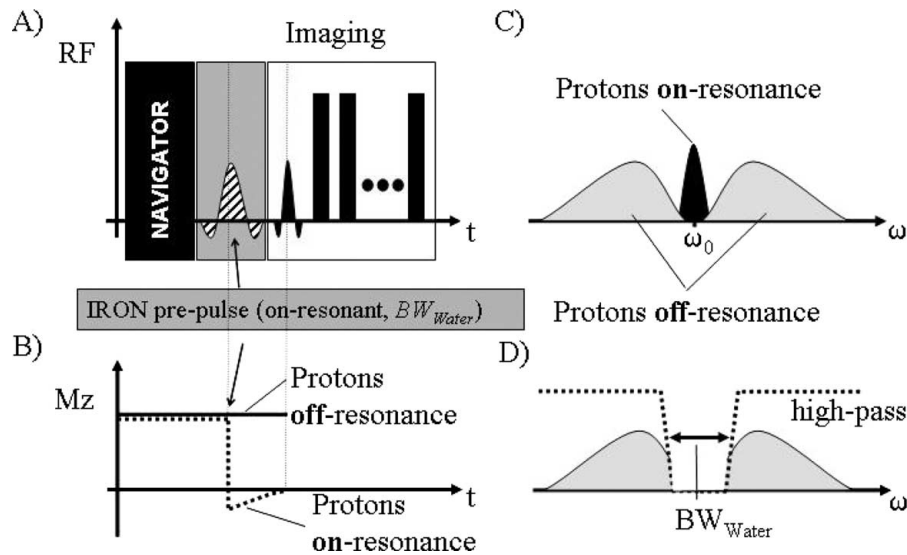


FIG. 1. IRON concept for signal-enhanced visualization of superparamagnetic particles (A) and the corresponding M_z of off-resonant and on-resonant protons (B). The frequency spectrum of a 'regular' MR image mainly consists of on-resonant protons (C). However, in the presence of superparamagnetic particles, off-resonant protons are now part of the spectrum (C). By suppressing on-resonant protons (with the IRON pre-pulse) in a certain bandwidth (BW_{Water}) as shown in D, only signal from off-resonant protons remain visible in the image.

respectively. The angle between r and B_0 is Θ . External to the particle, the frequency shift is $\Delta\omega_{External} = \gamma \Delta B_{External}$. *Concept IRON*: Using a spectrally selective saturation pre-pulse with the frequency ω_0 and the bandwidth BW_{Water} , the signal from on-resonant protons can be suppressed (Fig. 1).

However, this saturation pulse does not affect off-resonant protons in close proximity to the iron particles (Fig. 1B & D). Therefore, signal enhancement adjacent to these particles is expected while the on-resonant background should appear signal-attenuated (Fig. 1B). *Implementation*: IRON was implemented on a 1.5T Philips Intera system and was combined with ECG triggering and real-time navigator technology. *In vitro*, fast spin-echo (FSE) imaging of a 5 mm thick slice (FOV/matrix = 180 mm/256, TE/TR = 4.6 ms/2RR, inter echo spacing = 4.6 ms, echo train length (ETL) = 24) was performed *with* (= IRON imaging ($BW_{Water} = 100$ Hz, $FA_{Iron} = 95^\circ$)) and *without* on-resonant water suppression in an agarose phantom ($T_1 = 850$ ms) in which a strand of 1.5×10^7 /mL iron-loaded (PLL Feridex) MSCs were injected (Fig. 2).

For the *in vivo* study, a mongrel dog was subjected to a 90-min closed-chest myocardial infarction (MI). At 48 hrs post-reperfusion, four injections of $\sim 7 \times 10^6$ allogeneic Feridex-PLL-labeled MSCs were placed under MR fluoroscopy into the MI based on delayed contrast enhanced images (DCE, Fig. 3A). At 24 hrs post-injection, the dog was imaged using navigator-gated and corrected 3D IRON FSE imaging (Fig. 1A, 1 mm gating window, tracking factor = 1.0, FOV/matrix = 280 mm/512, slice thickness = 2 mm, TE/TR = 8.4/1200 ms, inter echo spacing = 8.4 ms, ETL = 18, $BW_{Water} = 100$ Hz, $FA_{IRON} = 95^\circ$). Additional navigator-gated and corrected 3D segmented k-space gradient-echo (TE/TR = 2.85/10 ms,

thickness = 3 mm, FOV/matrix = 270 mm/489, FA = 25°) and DCE images were also acquired. The dog was then sacrificed, the heart excised, and IRON/gradient-echo imaging was repeated.

Results: In Fig. 2A, a signal void is apparent in the phantom at the injection site of the magnetic nanoparticle-labeled MSCs on the conventional FSE image.

In contrast, IRON imaging leads to a substantial visual signal enhancement in the same region (Fig. 2B).

In vivo mid-ventricular DCE, FSE, IRON, and gradient-echo images are shown in Fig. 3A–D. On the IRON image (Fig. 3C), an excellent suppression of the myocardium with selective enhancement of the MSC injection (arrow) is visible. The

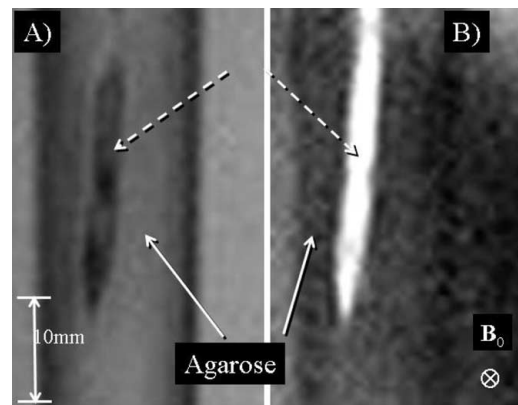


FIG. 2. *In vitro* fast spin-echo imaging of iron-loaded stem cells (dashed arrows) was performed *without* (A) and *with* (B) on-resonant water suppression (= IRON pre-pulse).

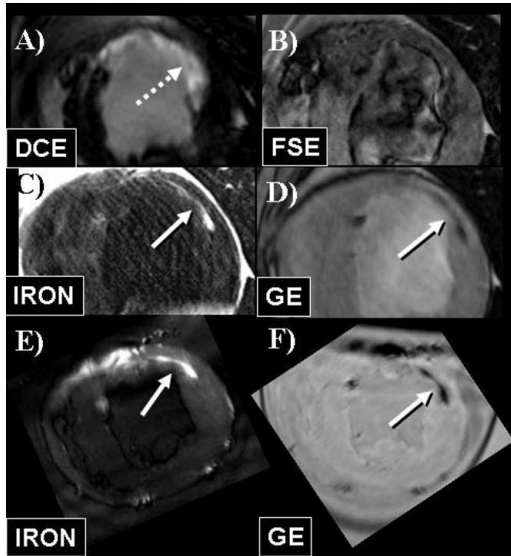


FIG. 3. Short axis view of infarct dog model before (A) and after (C–F) stem cell injection. In-vivo imaging is shown in A–D and ex-vivo imaging in E & F. A) Delayed hyper enhancement (DCE) imaging. B) Fast spin-echo imaging (FSE) C) IRON imaging D) Gradient-echo (GE) imaging. E) IRON imaging F) Gradient-echo imaging.

injection site corresponds well with areas of signal void in the gradient-echo image (Fig. 3D, arrow) and mapped directly to the infarcted myocardium (Fig. 3A, arrow). Signal enhancement and engraftment of the MSCs was further confirmed on the *ex vivo* IRON and gradient-echo images shown in Fig. 3E & F (arrows).

Conclusions: IRON is an MR imaging methodology that enables the hyperintense visualization of superparamagnetic nanoparticles. Extended with ECG triggering, real-time navigator technology, and 3D imaging, *in vivo* high-resolution IRON imaging was successful in selectively enhancing magnetic nanoparticle-labeled MSCs that were injected into the infarcted myocardium. The method remains to be compared with alternative approaches (1–3).

REFERENCES

1. Seppenwolde. MRM 2003.
2. Coristine. ISMRM 2004.
3. Cunningham. MRM 2005.

113. DERANGEMENT OF CARDIAC HIGH-ENERGY PHOSPHATE METABOLISM IN PATIENTS WITH LEFT VENTRICULAR NON-COMPACTION AND PRESERVED EJECTION FRACTION

Steffen E. Petersen,¹ Michaela Scheuermann-Fresstone, MD,¹ Lucy E. Hudsmith, MA, MRCP,¹ Jane M. Francis, DCRR, DNM,¹ Damian T. Tyler, PhD,¹ Matthew D. Robson, PhD,¹ Robert H. Anderson, FRCPATH,² Hugh Watkins, MD, PhD, FRCP,¹ Stefan Neubauer, MD, FRCP¹. ¹University of

Oxford, Oxford, United Kingdom, ²University College London, London, United Kingdom.

Introduction: Left ventricular non-compaction (LVNC) is characterised by the presence of an extensive non-compacted layer of myocardium, which can lead to chronic cardiac failure. The non-compacted myocardium likely represents an embryological arrest of normal myocardial compaction, albeit that the pathophysiological mechanisms leading to cardiac failure remain unknown. One attractive mechanism which may underlie the progression into cardiac dysfunction may be altered metabolism of cardiac high-energy phosphates, since similar changes have been described in patients with dilated or hypertrophic cardiomyopathy (1, 2). If this was the case, there would be two clinical implications: First, it would suggest treatment strategies aimed at improving myocardial energetics. Second, altered cardiac energetics may potentially serve to distinguish patients with non-compaction at low and high risk developing complications, analogous to the situation in dilated cardiomyopathy (3).

Purpose: We aimed to investigate cardiac energy metabolism in a group of patients with preserved cardiac function in the setting of ventricular non-compaction.

Methods: We studied 7 patients (5 male, mean age 39 ± 13 years) with clear evidence of non-compaction, comparing them with 7 age- and sex-matched controls (5 male, mean age 37 ± 16 years). Left ventricular end-diastolic, end-systolic, stroke volumes and, ejection fraction (EF) and mass were determined using magnetic resonance (MR) imaging, and cardiac high-energy phosphate metabolism (phosphocreatine to ATP ratios, PCr/ATP) was measured in the compacted basal anterior myocardium using ³¹Phosphorus-MR spectroscopy (3D acquisition weighted chemical shift imaging, interpolated spatial resolution 7.5 ml). The fitted amplitudes of the spectral peaks were individually corrected for blood contamination and saturation effects using T1 and contamination values from the literature.

Results: Patients with LVNC had preserved EF (68 ± 5 vs. $72 \pm 4\%$, $p = 0.16$) and no evidence of abnormalities of regional wall motion, but showed significantly increased end-diastolic (146 ± 33 vs. 116 ± 16 ml, $p = 0.049$) and end-systolic (46 ± 11 vs. 33 ± 8 ml, $p = 0.019$) volumes when compared to controls. The cardiac PCr/ATP ratio was significantly reduced by 19% in LVNC (1.81 ± 0.10 vs. 2.25 ± 0.36 , $p = 0.005$). Figure 1 shows typical ³¹P-magnetic resonance spectra of a healthy volunteer and a patient with non-compaction with a decrease of the ratio of PCr to ATP in the patient. There was no correlation between LV end-diastolic volumes and PCr/ATP ratio, suggesting that LV dilation was not responsible for the derangement of cardiac energetics.

Conclusions: The metabolism of cardiac high-energy phosphate is deranged in patients with non-compaction and preserved ejection fractions. This is the first study to show such abnormal findings, suggesting that derangements in cardiac energetics may precede the development of cardiac dysfunction in non-compaction. Future long-term follow-up studies are

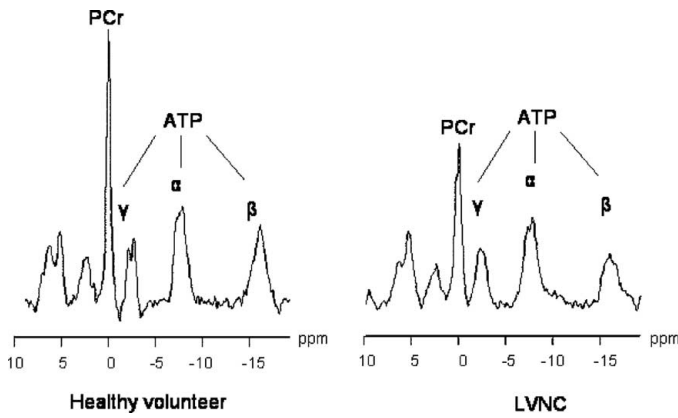


FIG. 1. Typical spectra of a healthy volunteer and a patient with left ventricular non-compaction (LVNC) and preserved systolic LV function. Please note the substantially reduced PCr/ATP ratio in LVNC.

needed to test whether the deranged metabolism has prognostic value.

REFERENCES

1. Crilly JG, Boehm EA, Blair E, Rajagopalan B, Blamire AM, Styles P, McKenna WJ, Ostman-Smith I, Clarke K, Watkins H. Hypertrophic cardiomyopathy due to sarcomeric gene mutations is characterized by impaired energy metabolism irrespective of the degree of hypertrophy. *J Am Coll Cardiol* 2003;41:1776–1782.
2. Beer M, Seyfarth T, Sandstede J, Landschutz W, Lipke C, Kostler H, von Kienlin M, Harre K, Hahn D, Neubauer S. Absolute concentrations of high-energy phosphate metabolites in normal, hypertrophied, and failing human myocardium measured noninvasively with $(31)\text{P}$ -SLOOP magnetic resonance spectroscopy. *J Am Coll Cardiol* 2002;40:1267–1274.
3. Neubauer S, Horn M, Cramer M, Harre K, Newell JB, Peters W, Pabst T, Ertl G, Hahn D, Ingwall JS, Kochsiek K. Myocardial phosphocreatine-to-ATP ratio is a predictor of mortality in patients with dilated cardiomyopathy. *Circulation* 1997;96:2190–2196.

114. RECONSTRUCTION OF MYOCARDIAL FIBER SHEETS USING DIFFUSION TENSOR IMAGING

Marcel Jackowski, PhD,¹ Zakir Sahul, PhD, MD,² Maolin Qiu, PhD,¹ Lawrence Staib, PhD,¹ Albert J. Sinusas, MD².
¹Dept. of Diagnostic Radiology, Yale University, New

Haven, CT, USA, ²Internal Medicine (Cardiology), Yale University, New Haven, CT, USA.

Introduction: Diffusion Tensor Magnetic Resonance Imaging (DT-MRI) has emerged as a noninvasive imaging modality capable of characterizing cardiac fiber orientation (1). DT-MRI has confirmed that myofiber orientation varies as a function of transmural location. Tseng et al. demonstrated that the tensor's primary eigenvector correlates with fiber direction, while the second eigenvector correlates with the more complex sheet architecture (2). While studies have demonstrated the existence of different fiber sheet distributions in animal hearts, their explicit 3D reconstruction has not yet been attempted. In this work, we present preliminary results on recovering the laminar cardiac structure by tracing myofibers and sheet architecture.

Purpose: Depiction of microstructure with DT-MR can provide insights into the myocardial molecular-structure-function relationship. Reconstruction of myofiber continuity and sheets allows for the 3D visualization of cardiac tissue architecture that has not been possible by histological means.

Methods: A canine heart was harvested after euthanasia, washed, and placed in a beaker with densely packed wet gauze. The beaker and cavities were filled with a buffered formalin solution. The beaker was placed in a 3T MR scanner (Siemens, Germany) oriented with the long axis of the heart along the y-axis of the scanner, and diffusion-weighted segmented echoplanar imaging was implemented. The standard CP head coil was employed for signal transmission and reception. Forty-four slices were acquired along the long axis of the excised heart. The in-plane matrix size (short axis) is 128×68 , resulting in a voxel size of $1.5 \times 1.5 \times 2$ cubic millimeters. The EPI factor was set to 3 (with each shot, 3 of the phase encoding lines were filled), TR = 4600 ms, TE = 76 ms and b-factor = 800 s/mm². An icosahedral 6-direction set was selected as the gradient directions. Segmented DTI was repeated 9 times to improve the SNR resulting in a total scan time of ~9 hours. After acquisition, the diffusion tensor was computed and diagonalized in order to extract the eigenvectors and corresponding eigenvalues. Fractional anisotropy (FA) maps were calculated using the tensor eigenvalues. Connectivity was established by a 4th-order

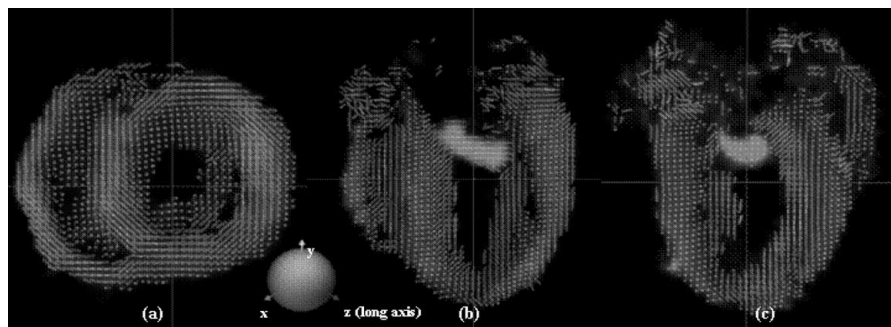


FIG. 1. Depiction of the primary eigenvector overlaid on the orientation color-coded FA map (red color = x axis, green color = y axis, blue color = z-axis) (a) Short-axis cross-section (b) Long axis (four-chamber) view (c) Long axis (two-chamber) view.

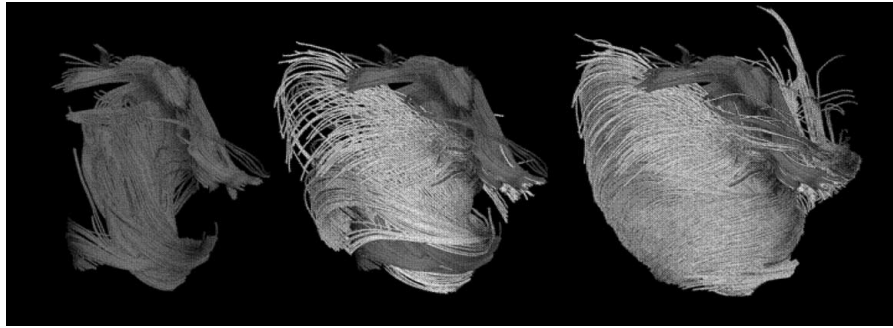


FIG. 2. Left: Cardiac fibers traced from the endocardium. Middle: Fibers traced from mid-wall. Right: Fibers traced from the epicardium.

Runge-Kutta integration scheme along the principal eigenvector. Fiber tracing was initiated from selected transmural regions (endocardium, mid-wall, epicardium). Sheet architecture analysis was performed by integration along the secondary eigenvector.

Results: Our findings are summarized in Figs. 1 to 3. Fig. 1 shows the direction of the diffusion tensor's primary eigenvectors which correspond to the fiber angle orientation. Endocardial and epicardial fibers are mainly oriented longitudinally while the midwall fibers are oriented more circumferentially. Fig. 2 shows the connectivity of the cardiac fibers initialized separately from endocardial, mid-wall and epicardial regions. The fibers originating from the endocardium form a left-handed helix while the fibers originating from the epicardium form a right-handed helix. Fibers originating from the mid-wall tend to be circumferential although seem to provide a transition between the two helix directions. Fig. 3 shows a comprehensive map of transmural sheet architecture. There is a transmural apex-to-base gradient in the sheet orientation which appears to reverse around the circumference of the heart.

Conclusions: Analysis of primary and secondary eigenvectors from DTI-MR provides a unique non-invasive approach for defining myofibril and sheet architectures. Selective regional seeding of fiber connectivity permits interrogation of subsets of

the myofiber architecture. This technique may permit the assessment of myocardial molecular-structure-function relationships in the setting of disease.

REFERENCES

1. Hsu EW, et al. Magnetic resonance myocardial fiber-orientation mapping with direct histological correlation. *Am J Physiol Heart Circ Physiol* 1998;274:H1627–1634
2. Helm P, et al. Measuring and Mapping Cardiac Fiber Architecture Using Diffusion Tensor MR Imaging. *Ann NY Acad Sci* 2005;1047:296–307.

115. DETECTING MYOCARDIAL OXYGEN DEFICITS WITH CINE 2D-BALANCED STEADY-STATE FREE PRECESSION IMAGING AT 1.5T

Rohan Dharmakumar, PhD,¹ Richard Tang, MD,¹ Kathleen Harris, BS,¹ Andrew C. Larson, PhD,¹ Yucho Chung, PhD,² Graham A. Wright, PhD,³ Debiao Li, PhD.¹ ¹Northwestern University, Chicago, IL, USA, ²Siemens Medical Solutions, Chicago, IL, USA, ³University of Toronto, Toronto, ON, Canada.

Introduction: Myocardial oxygen deficits (MODs) secondary to coronary occlusions may be detected with blood-oxygen-level-dependent (BOLD) MRI (1). Long scan times, poor image quality and/or poor oxygen sensitivity have limited the clinical utility of this technique (1–3). Steady-state acquisition strategies provide opportunities for obtaining temporally resolved high quality images. Recent findings also show that 2D-balanced steady-state free precession (2D-b-SSFP) imaging can detect BOLD signal changes (4).

Purpose: This work investigates (1) whether 2D-b-SSFP imaging can detect MODs secondary to coronary stenosis in a canine model and (2) whether such BOLD contrast may be obtained within the framework of cine imaging.

Methods: Four Mongrel dogs underwent thoracotomies and three catheters were routed for injections into the aorta and LA and RA. In all animals, a proximal portion of the LCX was also isolated, and an occluder was secured around the LCX. A Doppler flow probe was secured distal to the occluder to estimate blood velocity within the LCX. Each study consisted of four cardiac-gated and breath-held

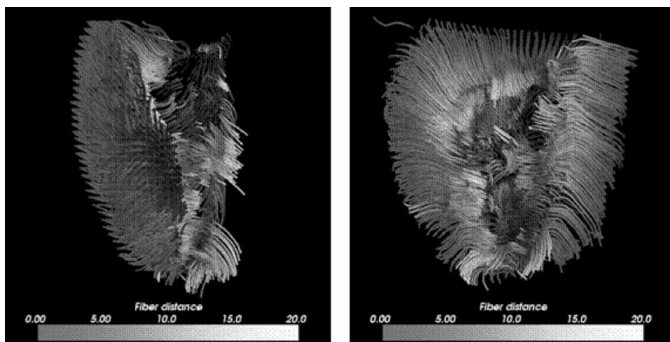


FIG. 3. Sheet architecture reconstructed by tracing the secondary eigenvector from the diffusion tensor. Sheet architecture is shown for one-half of the ventricle from two perpendicular projection colored according to their distance to the epicardium (mm).

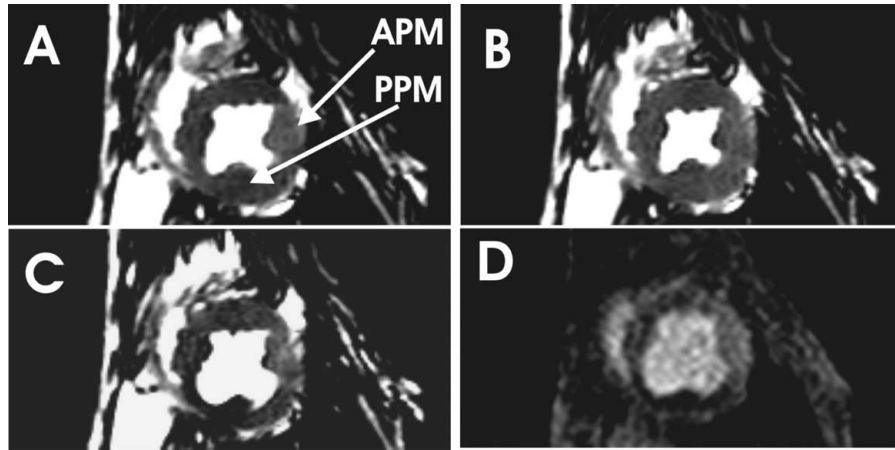


FIG. 1. Short axis images showing 2D-b-SSFP BOLD contrast at pre-adenosine baseline (A), adenosine baseline (B), and severe stenosis (C). Image D represents the associated first-pass perfusion image obtained at severe stenosis state at the same image position as images A–C. Note the severe signal loss in the posterior papillary muscle (PPM) region (supplied by the LCX) during stenosis of LCX and its close correspondence to the flow deficit region identified by the first-pass perfusion image. Also note that the signal in the anterior papillary muscle (APM) region (Supplied by the LAD) remains unaffected at the severe stenosis state.

scans (19–25 s) employing 2D-b-SSFP sequence on a Siemens Sonata 1.5T scanner: (A) baseline scan; (B) baseline adenosine scan with constant adenosine infusion (0.14 mg/min) into the RA catheter; (C) and (D) two scans at different LCX stenosis levels (mild/severe occlusion $\sim 50\%/88\%$) with adenosine. Stenosis levels were estimated from Doppler measurements. In all 7 studies, heart rates remained approximately constant with adenosine infusion. The scan parameters were: voxel size = $1.8 \times 1.4 \times 6.0 \text{ mm}^3$, segments/cardiac phase $\sim 5\text{--}7$, 10–12 phases/heart beat, $T_E/T_R = 3.1/6.3 \text{ ms}$, flip angle = 90° , bandwidth = 241 Hz/pixel, and averages = 3. Note that consistent with previous findings (4), a long T_R was used compared to those that are typically used in conventional cine SSFP imaging in order to detect BOLD contrast and the same cardiac slice was continuously excited to maintain steady state. Each

study was terminated with a first-pass perfusion exam at the severe stenosis state. From the signals measured at the anterior and posterior papillary muscles (PM) at the cardiac phase with the greatest systolic thickening, BOLD contrast was computed as:

$$\text{SSFP BOLD Contrast} = 100\% \times (S_{\text{adeno}} - S_{\text{var}})/S_{\text{adeno}}, \quad [1]$$

where S_{adeno} and S_{var} are myocardial signal magnitudes at adenosine baseline and at other experimental conditions (pre-adenosine, mild and severe occlusions), respectively.

Results: Fig. 1 shows a set of typical short axis cardiac BOLD 2D-b-SSFP MR images (A–C) obtained under various experimental conditions and a first pass perfusion image (D) obtained during severe stenosis. Regional BOLD contrast was observed at the posterior PM region. This contrast increased with the severity of LCX occlusion and was reversible when the occlusion was released. There is also good agreement between first pass and BOLD 2D-b-SSFP images (C and D). Fig. 2 shows the mean contrast values obtained from Eq. 1. There was a significant signal loss in the region supplied by the LCX (posterior PM) and no signal loss in the myocardium supplied by the LAD (anterior PM). This absence of BOLD contrast was also observed in other regions not supplied by the LCX. Cine SSFP images also showed that wall motion abnormalities can be observed within a single scan when MODs are severe.

Conclusions: This work demonstrated that 2D-b-SSFP cine imaging can provide high quality temporally resolved images that show MODs due to acute coronary stenosis. Since 2D-b-SSFP combines the capabilities of volumetric measurements and detection of wall motion abnormalities of cine MRI with BOLD MRI, it is anticipated that this technique will be very important in the diagnosis of ischemic heart disease.

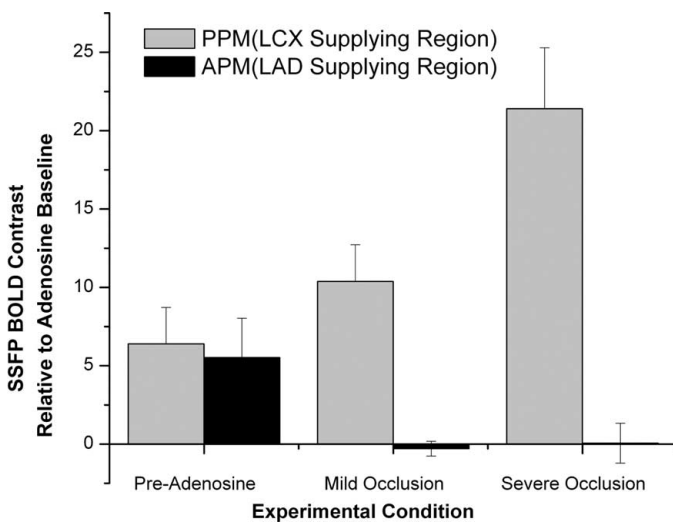


FIG. 2.

REFERENCES

1. Li D. MRM 1996;36:16–20.
2. Wacker CM. JACC 2003;41:834–840.
3. Foltz WD. Circulation 2002;106:2714–2719.
4. Dharmakumar R. Circulation 2004;110:685–685;3171 Suppl. S.

116. SELF-GATED, REDUCED FIELD-OF-VIEW DIFFUSION TENSOR IMAGING OF THE HUMAN HEART AT 3.0T

Urs Gamper, Sebastian Kozerke, Peter Boesiger. *Institute for Biomedical Engineering, Zurich, Switzerland.*

Introduction: Myocardial fiber structure correlates with anisotropy in the water self-diffusion of the myocardium (1), which can be assessed using diffusion tensor MRI. In vivo measurement of myocardial diffusion (2) proves to be difficult due to cardiac bulk motion, respiratory motion, chemical shift and susceptibility gradients around the heart.

Purpose: In this work, several techniques previously described were combined, addressing the aforementioned problems and allowing in vivo myocardial diffusion tensor imaging.

Methods: The gradient lobes in the standard Stejskal-Tanner experiment were replaced with bipolar gradients to zero out the first gradient moment of the diffusion gradients. This reduces the motion sensitivity of the diffusion sequence by a factor of about 10 and prevents loss of signal due to cardiac motion. To reduce the echo-train length of the single-shot EPI acquisition, the slice-select gradient of the excitation pulse was set perpendicular to the echo pulse slice-select gradient (3). Thus the actual field-of-view was reduced to the region covering the myocardium allowing for a short acquisition time and thereby making the EPI acquisition less sensitive to off-resonances. Furthermore, localized second order shimming was used (4). The measurements of the reference image and the 6 diffusion weighted images were performed during free breathing, but only the images acquired at expiration were used for averaging and diffusion cal-

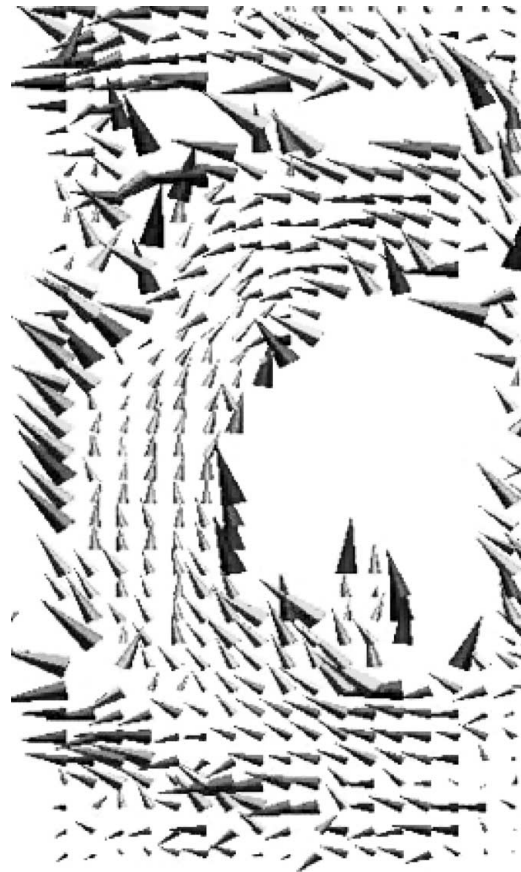


FIG. 2. The direction of largest eigenvector of the diffusion tensor shows a circumferential structure due to the myocardial fiber structure.

ulation (5). The measurements were performed on a 3T Philips Intera whole body MR system (Philips Medical Systems, Best, NL) using a 6-element coil array. Imaging parameters were: FOV = $320 \times 44 \text{ mm}^2$, resolution = $2.2 \times 2.2 \times 6 \text{ mm}^3$, TE = 61 ms, $\alpha = 90^\circ$, $b = 350 \text{ s/mm}^2$. Cardiac trigger delay was set to $\sim 80\%$ of end systole. The eigenvectors of the resulting diffusion

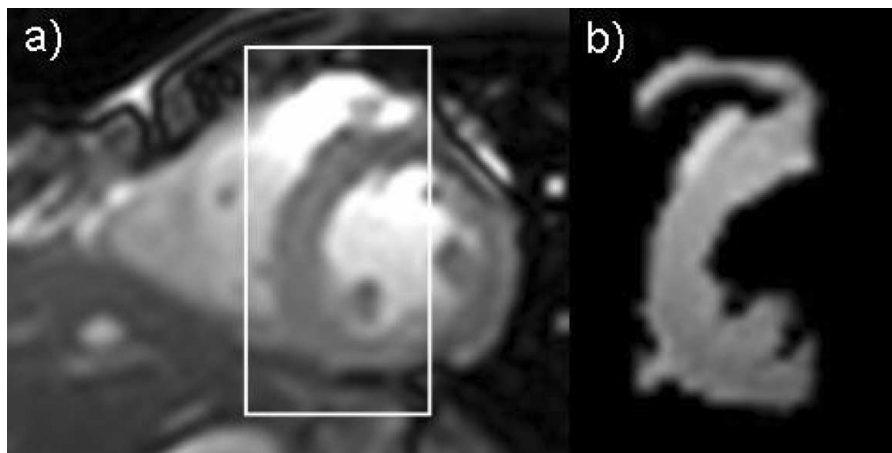


FIG. 1. Short axis view of the left ventricle at end systole. A SSFP image is shown in a) and a reduced field-of-view diffusion weighted image in b).

tensor were calculated using MATLAB (The MathWorks, Natick, MA, USA).

Results: Fig. 1a shows a balanced SSFP image of a short axis view of the left ventricle. A representative diffusion weighted image with reduced FOV is shown in Fig. 1b.

On the myocardium no signal loss due to cardiac motion is observed despite the relative large cardiac bulk motion (~ 1.0 mm) during diffusion encoding. The direction of the largest eigenvector is shown in Fig. 2, revealing the circumferential orientation of the heart muscle fibers (2, 6, 7).

Conclusions: The proposed combination of self gating and reduced field-of-view imaging with bipolar diffusion encoding gradients at 3.0T allows in vivo diffusion weighted imaging of the human heart at high resolution.

REFERENCES

1. Hsu EW, et al. Am J Physiol 1998;274:1627-1634.
2. Dou J, et al. Magn Reson Med 2002;48(1):105-114.
3. Feinberg DA, et al. Radiology 1985;156(3):743-747.
4. Schar M, et al. Magn Reson Med 2004;51(4):799-806.
5. Hardy CJ, et al. J Magn Reson Imaging 2003;17(2):170-176.
6. Reese TG, et al. Magn Reson Med 1995;34(6):786-791.
7. Tseng WY, et al. Magn Reson Med 1999;42(2):393-403.

117. REAL-TIME ACQUISITION OF BLACK-BLOOD CINE CARDIAC IMAGES AT 3.0T

Ahmed S. Fahmy, MS, Li Pan, MS, Nael F. Osman, PhD.
Johns Hopkins University, Baltimore, MD, USA.

Introduction: Cine black-blood images of the heart were successfully produced using stimulated echo mode (STEAM) after correction of deformation-induced artifacts (1). Because of the splitting of the image acquisition over several cardiac cycles,

the method required at least one breath-hold in order to acquire the entire cine sequence. Similar to other techniques that require cardiac gating and breath-holding, the method is vulnerable to artifacts generated by irregular R-R intervals (arrhythmia) and improper breath-holding. Also, using the method to examine patients undergoing administration of dobutamine, i.e. stress test, was not appropriate.

Purpose: Implementing real-time STEAM sequence on 3.0T systems that produces black-blood cine sequences of the heart acquired in a period of a single cardiac cycle.

Methods: The presented real-time STEAM sequence uses optimal techniques for fat suppression and k-space excitation and acquisition in order to acquire one image in 44ms (capture 20 frames in a single cardiac cycle with heart rate = 75 bpm). First, an optimal fat suppression scheme is used which consists of only one fat-saturation pulse applied prior to the STEAM modulation (Fig. 1). Consequently, no fat suppression pulses are needed during the acquisition of images; therefore, the imaging time is significantly reduced than the current fat suppression techniques (1). In order to reduce the acquisition time further, spatially-selective modulating RF pulses are used to modulate a small region of interest (ROI) around the heart, which allows imaging of a reduced FOV, i.e. traversing the k-space using sparse trajectories, without aliasing artifacts (2). In the current technique, interleaved multi-shot spiral acquisitions are used to provide fast acquisition with reasonable image quality. To maintain constant myocardial signal intensity throughout the cardiac cycle, a ramped flip angle is used to compensate for the T1-related signal decay.

Four-chamber images of a healthy volunteer's heart were obtained using the proposed real-time STEAM sequence. An Intera 3.0T scanner (Phillips Medical Systems, Best) was used. The imaging parameters are slice thickness 8 mm, 22 cardiac

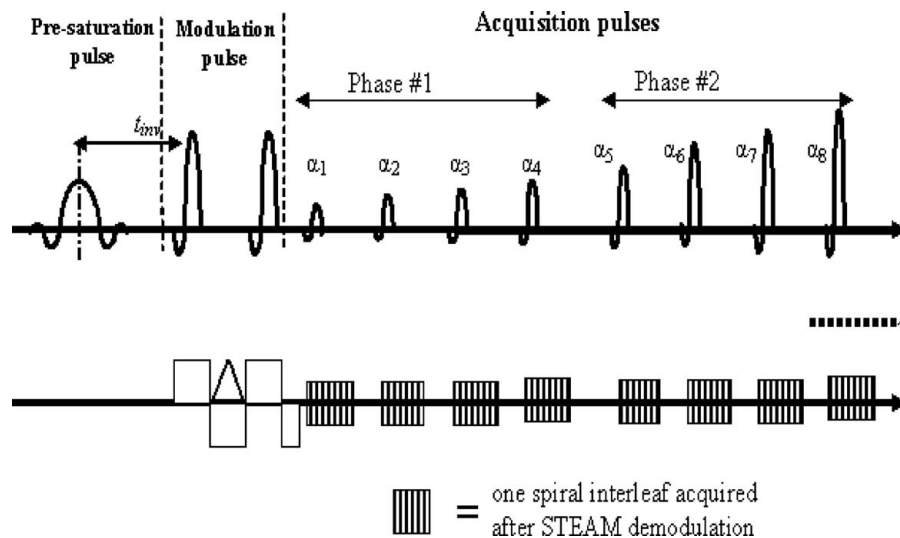


FIG. 1. The pulse diagram of the proposed cine black-blood sequence. A fat-selective pre-saturation pulse is applied prior to the modulation pulse resulting in suppression of the fat in the stimulated echo. Acquiring one image consists of 4 shots of spiral interleaves. The flip angle is incremented to compensate the expected signal decay caused by T1 relaxation.

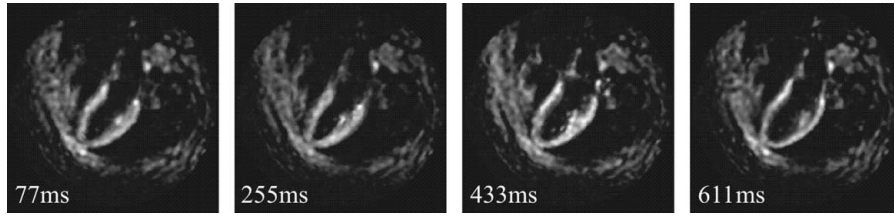


FIG. 2. Four time frames selected from a cine sequence of the heart of a normal volunteer.

phases, reduced FOV 160 mm, ramped flip angle with maximum 40°, and STEAM modulation frequency 0.3 mm⁻¹. A correction of the deformation-related artifact was used as described previously (1).

Results and Discussion: Fig. 2 shows the acquired images at four time frames (at 77, 255, 433, and 611 ms after ECG trigger) where each image is acquired in 44 ms. High contrast between the myocardium and the blood can be shown throughout the entire cardiac cycle. In addition, real-time images of high quality were acquired despite the expected field inhomogeneity in a 3.0T magnet.

Conclusion: The proposed method successfully produces real-time cine images of the heart on 3.0T magnet. The sequence is acquired in a single cardiac cycle and provides quality images with black-blood contrast.

Acknowledgments: The authors would like to thank and Dr. Matthias Stuber for his help in developing the pulse sequence. This research was supported by a grant from the National Heart, Lung, and Blood Institute (RO1 HL072704).

REFERENCES

1. Fahmy AS, et al. Proc. of SCMR, San Francisco, 2005.
2. Pan L. et al. Proc. of SCMR, San Francisco, 2005.

118. TRUE MYOCARDIAL PLANAR STRAIN: RESOLVING THROUGH-PLANE ROTATION AMBIGUITY IN TAGGED MRI USING ZHARP

Khaled Z. Abd-Elmoniem, Msc, Matthias Stuber, PhD, Jerry L. Prince, PhD. Johns Hopkins University, Baltimore, MD, USA.

Introduction: Quantitative strain maps can be used to identify and characterize healthy and diseased myocardial tissues. Strain maps are calculated for a cardiac imaging plane after a image slice is acquired using functional cardiac MRI methods, eg, tagging (1), displacement encoding (2), or velocity encoding (3). Because of through-plane motion, the imaged slice is not necessarily the same slice that was motion-encoded, which may cause the computed strain to be inaccurate. With slice-following tagging (SF-CSPAMM) (4), the same tissue of the myocardium is always examined; however, through-plane rotation can still be misinterpreted as a false strain. As a result, only the in-plane motion and apparent strain can be computed when only a single slice is imaged.

Purpose: The purpose of this research was to develop and test a method that provides a true planar strain map for a given imaged slice. The method takes the through-plane motion into consideration and corrects for the false strain component caused by through-plane rotation. First results demonstrating the ability to remove the through-plane rotation effect from the strain maps are presented.

Methods: Concept: A method for true planar strain mapping has been developed using zHARP tagging MRI. ZHARP is a recently developed tagging MRI methodology, which images and automatically tracks the 3-D myocardial displacement of all

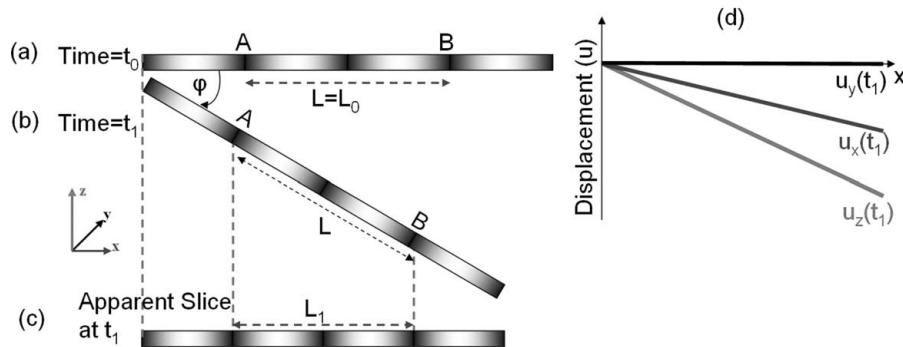


FIG. 1. An example of false apparent strain due to through-plane rotation ϕ . (a) Original slice plane location at t_0 . The length of the segment AB (L) is the same as the imaged length (L_0); (b) True slice location at t_1 . The segment AB has the same length; (c) The imaged projection or the apparent slice. The imaged segment AB has a false length L_1 . Apparent false strain = $(L_1 - L_0)/L_0 = \cos(\phi) - 1$; (d) The components of the displacement vector (u) at t_1 . At t_0 $u = 0$. In SF-CSPAMM, only u_x and u_y can be computed.

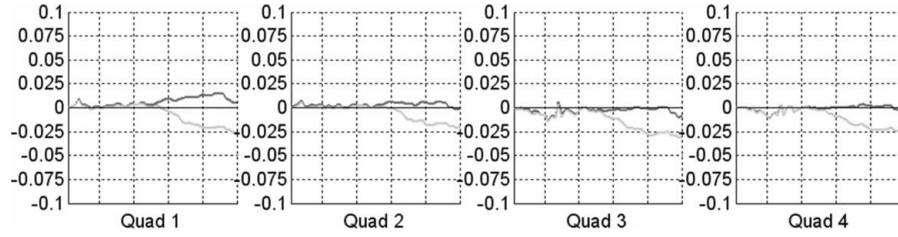


FIG. 4. Regional Eulerian Strain before and after correction. The LA slice is divided into four quadrants and the Eulerian strain is computed (Green). Ignoring u_z through-plane rotation not corrected. False strain of $\sim 2\%$ is apparent (Red). Using u_z to remove the effect of the through-plane rotation. Due to the vibration of the gel-phantom especially in the upper quadrants near the free surface, correction was not perfect.

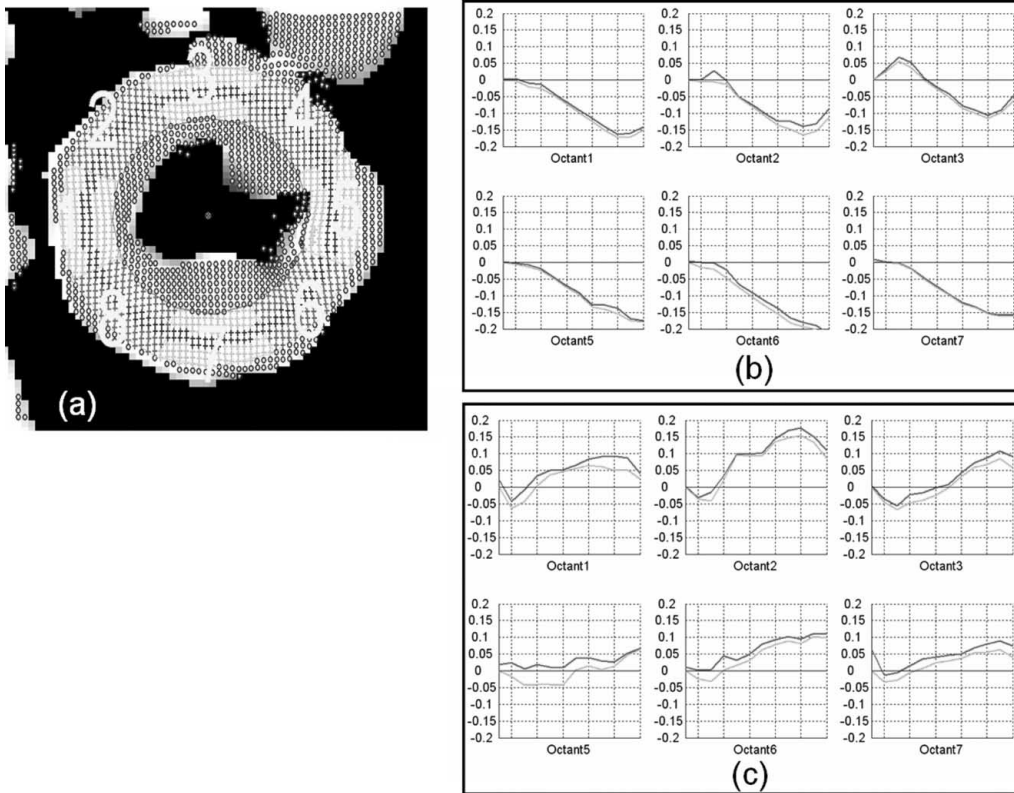


FIG. 5. Human volunteer equatorial SA slice. Segment Strain Comparison. Through-plane rotation adds false negative strain. True Ecc (compression) is less than the apparent Ecc. While True Err (thickening) is higher than the apparent Err. (a) 8-Segments position. 1,2: Septal, 3,4: Interior, 5,6: Lateral, 7,8: Inferior; (b) Ecc before correction (green) and after correction (red); (c) Err before correction (green) and after correction (red); Acquisition Window: 15 ms.; Res. 256×256 . FOV 350 mm; Slice Thickness 6 mm; Spiral Interleavs: 12; TE 4.0 ms. TR 30 ms; Tag-spacing 8 mm.

Friday, January 20, 2006

10:30 AM–12:00 PM

Best Oral Abstracts: Congenital

119. RIGHT VENTRICULAR (RV) DIASTOLIC FUNCTION AFTER REPAIR IN TETRALOGY OF FALLOT AT REST AND DURING STRESS: RESTRICTIVE PHYSIOLOGY IS ASSOCIATED WITH WORSE OUTCOME

Jochem van den Berg, MD,¹ Piotr A. Wielopolski, PhD,² Folkert J. Meijboom, MD, PhD,² Maarten Witsenburg, MD, PhD,¹ Ad J. J. C. Bogers, MD, PhD,² Peter M. T. Pattynama, MD, PhD,² Willem A. Helbing, MD, PhD.¹ ¹Erasmus MC - Sophia Children's Hospital, Rotterdam, The Netherlands, ²Erasmus MC, Rotterdam, The Netherlands.

Introduction: Right ventricular (RV) dysfunction is common after repair of tetralogy of Fallot (TOF). Diastolic dysfunction may precede systolic dysfunction and contribute to early detection of RV dysfunction. Reports on how restrictive RV diastolic dysfunction affects clinical outcome in patients with repaired TOF are equivocal.

Purpose: Study-aims were to: 1) assess RV diastolic function after repair of TOF, 2) study the relationship between end-diastolic forward flow in the pulmonary artery (EDFF, indicative of restriction to RV filling), and pulmonary regurgitation % and exercise performance, 3) test the usefulness of stress imaging in assessing RV diastolic function.

Methods: Thirty-six patients with corrected TOF (15.5 ± 4.5 years after repair at <2 years of age) underwent rest and stress (dobutamine $7.5 \mu\text{g}/\text{kg}/\text{min}$) MRI, and exercise testing. MRI flow curves of the tricuspid and pulmonary valve were combined into RV time-volume change curves, from which indices of RV filling were derived. Patients were subdivided in two subgroups according to the presence of EDFF in the main pulmonary artery.

Patient characteristics. Restrictive and non-restrictive patients

Parameter	Total group (n = 36)	EDFF positive (n = 24)	DFF negative (n = 12)
Age at repair (y)	0.9 ± 0.5	1.0 ± 0.5	0.9 ± 0.5
Interval since repair (y)	15.4 ± 4.5	16.4 ± 3.8	13.4 ± 5.2
BSA (m ²)	1.62 ± 0.35	1.65 ± 0.28	1.55 ± 0.46
RVEDV (ml/m ²)	138 ± 40	145 ± 41	104 ± 59
RVESV (ml/m ²)	72 ± 29	75 ± 29	65 ± 28
RVEF (%)	49 ± 7	49 ± 6	49 ± 9
PR (%)	30 ± 17	35 ± 16*	21 ± 18
Watts (%)	92 ± 13 [†]	98 ± 16	89 ± 11 [†]

*Significant difference according to the presence of EDFF (p value ≤ 0.05).

[†] Significant lower compared to the predicted 100%.

RV indices of diastolic function: Restrictive and non-restrictive patients

Parameter	EDFF positive (rest)	EDFF positive (stress)	EDFF negative (rest)	EDFF negative (stress)
Stroke volume (ml)	69 ± 14	60 ± 14	84 ± 18*	61 ± 26*
AFV (%)	18 ± 8 [†]	35 ± 11	25 ± 13* [†]	34 ± 10
FF (%)	52 ± 11 [†]	39 ± 7	47 ± 10*	42 ± 10
E/A ratio	2.6 ± 1.2 [†]	1.2 ± 0.3	1.9 ± 1.1* [†]	1.3 ± 0.5
Deceleration time (ms)	216 ± 61	219 ± 64	249 ± 72*	224 ± 66

*p < 0.05 by paired analysis (rest versus stress).

[†]p < 0.05 according to the presence of EDFF (ANCOVA corrected for BSA and HR).

Results: RV filling was abnormal in all patients, including impaired relaxation (prolonged deceleration time, smaller early filling fraction) for the entire group compared to controls, and impaired compliance (smaller atrial filling fraction, higher E/A ratio) in patients with EDFF (n = 24) compared to those without EDFF (n = 12). Stress response was abnormal in patients with EDFF, who developed impaired RV relaxation, not appreciated at rest. Patients with EDFF had more severe pulmonary regurgitation compared to patients without EDFF and had poorer exercise performance compared to controls.

Conclusions: All patients with repaired TOF, operated at relatively young age, showed RV diastolic dysfunction, with both signs of impaired relaxation and restriction to filling. EDFF in the pulmonary artery is a marker of highly abnormal RV dysfunction and relates to worse exercise performance and more severe PR. RV diastolic abnormalities may be 'unmasked' by dobutamine stress imaging.

120. IS GENERAL ANESTHESIA NECESSARY FOR CARDIAC MAGNETIC RESONANCE IMAGING IN ALL INFANTS AND SMALL CHILDREN?

Laura K. Diaz, MD, Michael D. Taylor, MD, Taylor Chung, MD, Rajesh Krishnamurthy, MD, G. Wesley Vick, MD, John P. Kovalchin, MD. *Texas Children's Hospital/Baylor College of Medicine, Houston, TX, USA.*

Introduction: General anesthesia with controlled breathing (GA) is often used for cardiac magnetic resonance imaging (CMRI) in infants and children. Deep sedation with free breathing (DS) may be a useful and safe alternative in some children undergoing CMRI, and the utility and safety of DS without GA for CMRI in these patients has received limited evaluation.

Purpose: The purpose of this study was therefore to evaluate the feasibility and safety of DS in infants and children undergoing CMRI.

Methods: The medical records of patients who received DS or GA for CMRI from January 2002 to March 2005 were reviewed.

Patient characteristics including age, weight, ASA physical status, inpatient/outpatient status, presence of cyanotic congenital heart disease and/or single ventricle physiology were noted, as well as scan duration and any complications.

Results: A total of 129 pts were included with a median age of 5.2 years (range 2 days to 17.3 years), and median weight 19.5 kg (range 1.1–110.4). GA was used in 53% and DS in 47% of patients. Twenty-eight percent of the patients were infants, and a higher percentage of infants (72%) required GA, compared to older patients (44%) ($p < 0.004$). The ASA classes of the patients were I (0), II (7%), III (39%), IV (54%), and V (0). Patients in higher ASA classes required GA more often than patients in lower ASA classes. Thirty percent of class II patients, 48% of class III, and 59% of class IV patients required GA. Seventy-eight percent were outpatients, and 22% were inpatients at the time of the scan. Fourteen percent of patients were in an intensive care unit (ICU). One outpatient with tetralogy of Fallot and cyanosis who received GA remained hospitalized overnight for observation. Five percent of patients were intubated ICU patients prior to the scan. Thirteen percent of patients had cyanotic congenital heart disease, and 9% had single ventricle physiology. The average scan length was 70 ± 24 minutes, with an average of 73 minutes for GA and 70 minutes for DS. Two patients required conversion from DS to GA because of upper airway obstruction with DS. Both of these patients remained outpatients and were discharged home. There were no complications in any of the patients who received GA or DS.

Conclusions: DS is a feasible and safe alternative to GA in many infants and children undergoing CMRI. A higher percentage of infants and patients with higher ASA classes require GA. DS is a useful alternative technique to GA in CMRI and may eliminate the need for GA in select groups of patients.

121. EVALUATION OF MYOCARDIAL PERFUSION BY MAGNETIC RESONANCE IMAGING IN CHILDREN WITH CONGENITAL OR ACQUIRED CORONARY ARTERY DISEASE

Emanuela R. Valsangiacomo Buechel, MD,¹ Urs Bauersfeld, MD,¹ Christian J. Kellenberger, MD,¹ Juerg Schwitzer, MD.² ¹Children's University Hospital Zurich, Zurich, Switzerland, ²University Hospital Zurich, Zurich, Switzerland.

Introduction: Abnormal myocardial perfusion may occur in children after inflammatory disease or cardiac surgery for congenital heart disease (CHD) and congenital coronary artery anomalies. Detection of myocardial ischemia by perfusion cardiac magnetic resonance (perfusion CMR) in adults has been demonstrated to be accurate and reliable.

Purpose: We sought to assess the feasibility of perfusion CMR in children and to compare the results with coronary angiography (CA).

Methods: A hybrid echo-planar pulse sequence with saturation recovery preparation was used (GE Healthcare, 1.5T) for assessing contrast medium first-pass (Gd-DTPA-BMA, 0.1 mmol/kg, 5ml/sec) in the myocardium under pharmacological stress (adenosin 0.14 mg/kg/min IV). Mean duration of examinations, including data acquisition for myocardial perfusion and ventricular function, was 66 ± 11 min; the maximal heart rate under vasodilatation was 95 ± 18 bpm. Three examinations were performed in general anesthesia, one under conscious sedation. Coronary artery disease (CAD) was defined by the presence of a $\geq 50\%$ diameter reduction in ≥ 1 coronary vessel.

Results: Nineteen consecutive patients, median age 13 y (range 3.5–18.2y) underwent perfusion CMR between January 2003 and December 2004. Underlying diagnosis was CHD in 8, inflammatory disease in 5, cardiomyopathy in 2, congenital coronary artery anomalies in 1 and others in 3 children. Six patients had undergone coronary surgery during repair of CHD, 2 had an aorto-coronary bypass. Perfusion CMR was diagnostic in all cases, and no complications were observed. Perfusion CMR depicted normal and abnormal myocardial perfusion in 14 and 5 patients, respectively. Regarding abnormal first pass perfusion findings, a stenosis of a coronary artery was suggested in 3 patients, a global subendocardial hypoperfusion was related to severe left ventricular hypertrophy in one patient, and in another patient abnormal perfusion was present in an epicardial scar territory of a hypokinetic region suggestive for a residue after myocarditis. In this last case CA showed absence of CAD. Twelve patients underwent CA with a median time interval of 19 months (range 1 day–6 years) between perfusion-CMR and CA. The findings of both examinations were concordant in all 12 cases.

Conclusions: Perfusion CMR is feasible in children, shows high agreement with CA results and may add hemodynamic information to the anatomic findings provided by CA. Perfusion CMR may be useful in selecting patients requiring invasive investigation.

122. MYOCARDIAL VELOCITIES MEASURED WITH MRI: COMPARISON BETWEEN PATIENTS WITH CORRECTED TETRALOGY OF FALLOT (TOF) AND PATIENTS AFTER ATRIAL SWITCH OF D-TRANSPOSITION OF THE GREAT ARTERIES (D-TGA)

Claudia Seibt,¹ Julia Wiethoff,¹ Mirko Fröhlich,² Birgit Spors,¹ Matthias Grothoff,¹ Hashim Abdul-Khaliq,³ Felix Berger,³ Roland Felix,¹ Matthias Gutberlet.¹ ¹Klinik für Strahlenheilkunde, Charité - Universitätsmedizin Berlin, Campus Virchow Klinikum, Berlin, Germany, ²Franz-Volhard-Klinik, Charité Campus Buch, Universitätsmedizin Berlin, Helios-Kliniken, Berlin, Germany, ³DHZZ, Abteilung f. angeborene Herzfehler/Kinderkardiologie, Berlin, Germany.

Background: MRI allows for quantification of myocardial velocities and gives a refined statement about cardiac function. Aim of this investigation was to find out differences between myocardial velocities in different congenital heart diseases and how those differ from normal velocities found in healthy subjects.

Methods: We examined 48 patients (23 female, 25 male) between 6 and 61 years old 3 to 24 years after corrective surgery of tetralogy of Fallot and 27 patients (10 female, 17 male) with d-TGA between 9 and 26 years old 18 ± 4 years after atrial switch procedure. Furthermore, we examined 13 normal control subjects (4 female, 9 male). Examination was performed on a 1.5 T MRI scanner. Results were compared between the two patient groups and with those of the control subjects. Myocardial velocities were measured in a four chamber view for each of the subjects using 3D-phase contrast imaging in three directions (longitudinal, radial, circumferential). Three intramyocardial ROIs (interventricular septum, free wall of the left and right ventricle) in the myocardium close to the AV-valves were defined for each data set and myocardial velocity-time curves were generated.

Results: In longitudinal and radial direction we found velocity-time curves, which showed a systolic (s-wave), an early (e-wave) and late diastolic (a-wave) motion for each intramyocardial ROI. In longitudinal direction mean myocardial systolic peak velocities in the left ventricle (LV) in d-TGA patients were significantly higher compared to TOF patients (7.6 vs. 6.6 cm/s, $p = 0.02$). In the right ventricle (RV) lower mean velocities were measured in systole (5.6 vs. 6.7 cm/s, $p = 0.02$), in early (5.5 vs. 6.6 cm/s, $p = 0.01$) and late diastole (3.3 vs. 5.4 cm/s, $p < 0.01$). Septal early diastolic mean velocities were significantly lower in patients with d-TGA than in patients with TOF (5.4 vs. 7.2 cm/s, $p < 0.01$).

There was an unphysiologic motion of the interventricular septum (IVS) in radial direction in half of the patients after atrial switch and in one third of the patients after corrective surgery of TOF. This paradoxical septal motion leads to a significantly lower LV ejection fraction (LV-EF) of those TOF patients as compared to TOF patients with normal septal motion (mean LV-EF = 51% vs. 57%, $p = 0.03$). In radial direction mean myocardial peak velocities of the left ventricle were significantly higher in patients with d-TGA than in patients with TOF (6.8 vs. 5.4 cm/s, $p < 0.01$). There were no significant differences in the right ventricle. In circumferential direction lower septal and right ventricular velocities were measured in patients with d-TGA than in patients with TOF ($p \leq 0.03$).

Conclusions: Like in echocardiographic tissue Doppler, MRI can describe regional systolic and diastolic myocardial function in more detail as compared to the simple calculation of global ejection fraction. In contrast to tissue Doppler, velocities in all three directions can be measured. This approach might provide a better diagnostic parameter than EF alone in patients with congenital heart disease and showed significant differences in the different diseases.

123. TIME-RESOLVED "CINE" 3D CONTRAST-ENHANCED MR ANGIOGRAPHY USING CENTRA-KEYHOLE AND SENSE IN CONGENITAL HEART DISEASE WITH PULMONARY ARTERY PATHOLOGY

Philipp Beerbaum, MD,¹ Hermann Koerperich, PhD,¹ Samir Sarikouch, MD,¹ Juergen Gieseke, MSc,² Romhild Hoogeveen, PhD,² Peter Barth, MSc,¹ Matthias Peuster, MD,¹ Hans Meyer, MD.¹ ¹Heart Center NRW, Bad Oeynhausen, Germany, ²Philips Medical Systems, Best, The Netherlands.

Introduction: Conventional 3D contrast-enhanced MRA (3D-CE-MRA) allows to delineate complex pulmonary artery pathology at acquisition durations between 20–40 seconds. However, more rapid scanning in children may optimize bolus timing and simplify postprocessing by reducing pulmonary venous overlay.

Purpose: To validate time-resolved 3D-CE-MRA in children with congenital heart disease.

Methods: A novel CE-MRA sequence using SENSE and CENTRA-keyhole to achieve multiple acquisitions at temporal resolution of ~0.6–1.5 seconds (spatial resolution ~1.3*1.3*72.0 mm, 50–70 coronal slices) was tested in 21 pediatric patients with congenital heart defects referred for evaluation of pulmonary artery pathology. Results were compared with conventional 3D-CE-MRA using identical spatial resolution/SENSE-factor.

Results: Mean scan time was comparable between both techniques. CENTRA-keyhole CE-MRA allowed to generate 9–22 sequential 3D data sets during 1 bolus transit (conventional CE-MRA, 2–3). Minor artifacts were observed, but SNR/CNR considered sufficient. Grading of image quality (1 = poor, 2 = borderline-diagnostic, 3 = diagnostic/blurred, 4 = good, 5 = excellent) of a blinded observer revealed a mean grade of 4.1 (± 0.8 SD) for keyhole-CE-MRA and 4.5 (± 0.6 SD) for conventional CE-MRA, respectively. Vessel contours appeared slightly less sharp with keyhole-CE-MRA, but no grading <3 occurred. Vessel contrast between pulmonary arteries and pulmonary veins was improved with CENTRA-keyhole 3D-CE-MRA, and post-processing including generation of segmented models was much easier especially in children with multifocal pulmonary blood supply ($n = 8$).

Conclusions: Time-resolved 3D-CE-MRA using CENTRA-Keyhole and SENSE may replace conventional CE-MRA in terms of image quality. Advantages include optimal bolus timing with sequential imaging of all thoracic vascular compartments with minimal overlay, improved contrast between vessel compartments, and thus easier model generation in complex pulmonary artery pathology.

124. CARDIOVASCULAR MAGNETIC RESONANCE IMAGING IN PATIENTS OPERATED ON FOR

TETRALOGY OF FALLOT: USEFULNESS OF MYOCARDIAL TISSUE CHARACTERIZATION IN THE ARRHYTHMIC RISK STRATIFICATION

Giulia Russo, Francesco Corbetti, Elisa Mazzotti, Barbara Bauce, Luisa Cacciavillani, Francesca D'Ambrosio, Luciano Daliento. University of Padua, Padova, Italy.

Introduction: Tetralogy of Fallot is the most common cyanotic congenital heart disease. Although surgical repair has low mortality and good quality of life, late sudden death, related to sustained ventricular tachycardia and ventricular fibrillation, remains a problem, with an incidence up to 5–6% at 30 yrs after surgical correction. Fibro-fatty substitution around infundibular resection, intraventricular septal scar and patchy myocardial fibrosis may provide the anatomical substrates for re-entrant ventricular arrhythmias. Several non invasive tests based on 12-lead ECG and echocardiographic parameters have been proposed to identify patients at high risk of sudden death.

Purpose: To assess the usefulness of cardiac magnetic resonance (CMR) particularly with gadolinium injection in the arrhythmic risk stratification of patients operated on for tetralogy of Fallot.

Methods: Twenty seven consecutive patients (13 males, 14 females, mean age 33 ± 10 yrs) were enrolled in the study. In 8 of them a history of at least one episode of sustained ventricular tachycardia was reported. CMR was performed with 1.0 Tesla system (Siemens, Medical Solutions), and images were obtained on transverse, coronal and sagittal planes using a standard multislice spin echo sequence. In order to evaluate areas of late-enhancement a segmented gradient echo inversion recovery turbo FLASH sequence was used, after injection of Gadolinium chelate (Gd-DTPA) at a dose of 0.1 mmol/Kg.

Results: MRI with Gd-DTPA revealed in 9 subjects (33%) the presence of late-enhancement; this was localized both on the infundibular region and anterior wall of the right ventricle in 4, in the infundibular region in 3 and in the right ventricular anterior wall in 2. The late-enhancement was present in 7 out of 8 patients with previous life-threatening arrhythmic events, compared with 2 patients without history of sustained ventricular tachycardia ($p < 0.001$).

Conclusions: There is a correlation between detection of late-enhancement at CMR and presence of life-threatening ventricular arrhythmias in patients with tetralogy of Fallot; thus, this parameter could be a useful tool in identifying subjects at risk of sudden death.

125. THE EFFECT OF REGIONAL DYSFUNCTION ON GLOBAL RIGHT VENTRICULAR SYSTOLIC FUNCTION IN PATIENTS WITH REPAIRED TETRALOGY OF FALLOT

Rachel M. Wald, MD,¹ Idith Haber, PhD,¹ Ron Wald, MD,² Anne Marie Valente,³ Andrew J. Powell, MD,¹ Tal

Geva, MD.¹ ¹Children's Hospital Boston, Boston, MA, USA, ²University of Toronto, Toronto, ON, Canada.

Introduction: In patients with repaired tetralogy of Fallot (TOF), depressed global right ventricular (RV) systolic function is associated with impaired clinical status. The underlying mechanisms contributing to global RV dysfunction in these patients are incompletely understood.

Purpose: We sought to quantitatively evaluate the relationship between RV regional wall motion abnormalities (RWMA) and global RV systolic function.

Methods: Subjects with TOF repair who underwent cardiac magnetic resonance imaging (CMRI) (1.5T GE scanner) from 2002–2005 were reviewed. Patients with a prosthetic pulmonary valve were excluded. Steady state free-precession cine images of the ventricles in short axis were analyzed. RV endocardial borders were contoured at end-diastole and end-systole to determine ventricular volumes, ejection fraction (EF) and pulmonary regurgitation (PR) fraction. A 3-dimensional surface was reconstructed using a triangulation algorithm. The septal portion was removed and remaining analysis of RWMA was restricted to the RV free wall (RVFW). The surface normals were calculated and oriented away from the left ventricle. Magnitude and direction of RVFW systolic surface displacement was calculated by establishing the correspondence between the surface at end-diastole and end-systole. For each triangle on the end-diastolic surface, a vector was defined along the local normal and its intersection with the end-systolic surface was found. The vector between the original triangle center and the intersection point determined the displacement of that triangle. Each triangle comprising the reconstructed endocardial surface area was analyzed for systolic inward (negative) or systolic outward (positive) displacement. Positive triangular displacement was labeled dyskinetic (see figure of RV outflow tract dyskinesis, shown in orange). Two quantitative measures were derived: (1) the spatial extent of dyskinesis defined as the ratio of the dyskinetic area to total RVFW area (expressed as %), and (2) the magnitude of dyskinesis defined as the total displacement of all dyskinetic segments indexed to the total RVFW area (in mm) (i.e. $A_1D_1 + A_2D_2 + \dots + A_nD_n$ /total RVFW area; where A is the triangle area, D the dyskinetic displacement and n is the number of triangles in the RVFW). Phase velocity cine MR flow measurements in the main pulmonary artery were used to calculate PR fraction.

Results: CMRI data of 40 patients were analyzed (median age 19.7 years, range 4.2–67.2 years, 20 males). Median RVEF was 51% (range 24–70%), median RV end-diastolic volume indexed to body surface area (RVEDVi) was 151 cc/m² (range 78–372 cc/m²) and median PR fraction was 37% (range 3–67%). Locations of RWMA included the RV outflow tract (RVOT) (n = 36) and/or RV sinus (n = 6). Median spatial extent of dyskinesis (as defined above) was 3.6% of the RVFW (range 0–21%). Median magnitude of dyskinesis (as defined above) was 0.03 mm (range 0–0.45 mm). RVEF correlated negatively with RVEDVi ($r = -0.52$, $p < 0.0001$). Negative

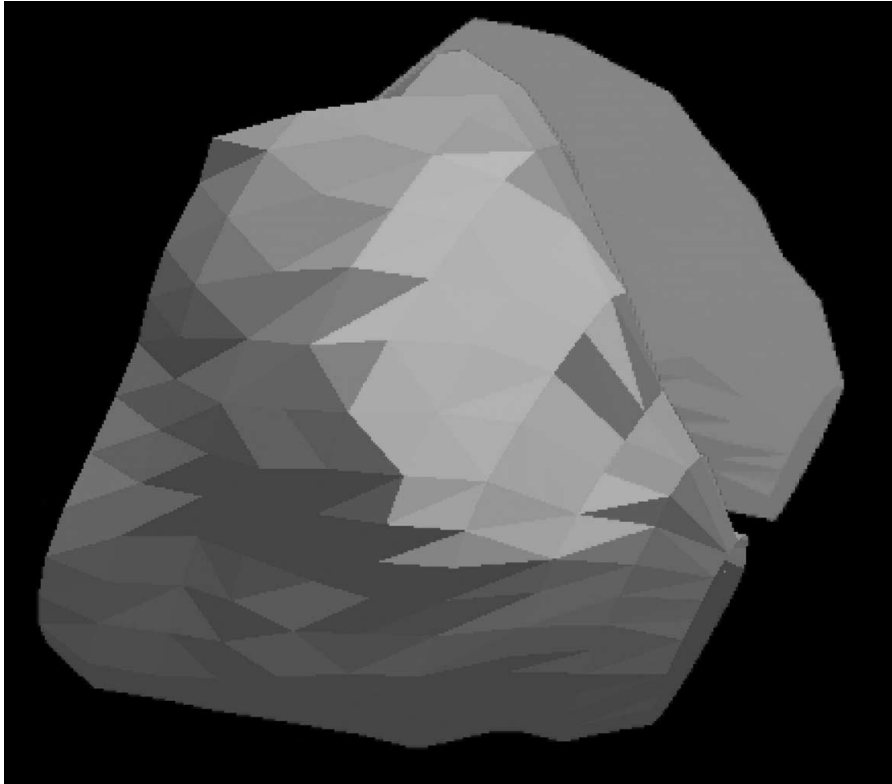


FIG. 1

correlations were found between spatial extent of dyskinesia and RVEF ($r = -0.665$, $p < 0.0001$) and magnitude of dyskinesia and RVEF ($r = -0.58$, $p = <0.0001$). There were no significant correlations between RV dyskinetic area or RV dyskinetic displacement and either PR or RVEDVi, respectively.

Conclusion: This study demonstrates that RWMA of the RV, principally in the RVOT, negatively impact global RV systolic function in patients with repaired TOF. These findings may have important implications for surgical management, including RVOT reconstruction to exclude the dyskinetic wall segments at the time of pulmonary valve replacement.

126. FEASIBILITY OF NON-SEDATED, FREE BREATHING CARDIAC MAGNETIC RESONANCE IMAGING IN CHILDREN AGES 5–10 YEARS

William Gottliebson, MS, MD, Robert Fleck, MD, Eric Crotty, MBBCh, Janaka Wansapura, PhD. Cincinnati Childrens Hospital and Medical Center, Cincinnati, OH, USA.

Introduction: Cardiac magnetic resonance imaging (CMRI) is an important non-invasive tool for evaluation of cardiac anatomy, function, and flow characteristics in pediatric patients with congenital and acquired heart disease. At many institutions, general anesthesia is considered a necessity to perform CMRI cases on

children less than 8–10 years of age, as a means to overcome scan times of 60 minutes or more, claustrophobia, and concern regarding image artifact from respiratory motion. Alternative sedation techniques, including deep sedation with free breathing, have also been suggested and validated. We sought to determine the feasibility of non-sedated, free-breathing CMRI in patients ages 5–10 years, using a modified video display system as a substitute for all sedation and anesthesia.

Methods: From 9/1/2004 through 8/31/2005, 16 patients between the ages of 5–10 years of age underwent CMRI based on clinical indications; 2 control patients in the same age range also underwent scans. Scans were performed on a Siemens 3T *Trio* Magnet with a phased-array multichannel cardiac coil. Imaging sequences performed were based on the patient's diagnosis and specific clinical questions that were requested by the referring clinicians; for the control patients, cine SSFP 2 chamber, 4 chamber, and short axis stacks, phase contrast of each valve and the great vessels, and axial and sagittal SSFP stacks were performed. At the onset of the scan, onto each patient/subject was placed a pair of custom-made spectral inverting goggles that allowed visualization of a DVD or VCR movie being broadcast behind them via a commercially-available MRI-compatible LCD Projection Visual System (Avotec, Stuart, FL). To compensate for lack of breath-holding, non-breathhold cine images were acquired using a segmented TrueFISP (SSFP) sequence with GRAPPA parallel acquisition (acceleration factor = 2).

Unsedated cardiac MRIs, 2004–2005

Patient Number	Age (yrs)	Diagnosis	Sedation used	IV
1	5.17	TOF	movie	y
2	5.67	Normal Control	movie	n
3	5.58	CoA	movie	y
4	6.92	DMD	movie	n
5	7.08	Normal Control	movie	n
6	7.42	TOF	refused/GA	y
7	8.08	r/o ARVD	movie	n
8	8.17	TOF	movie	y
9	8.25	TOF	movie	y
10	8.50	L-TGA, s/p Fontan	movie	y
11	8.83	DMD	movie	n
12	9.25	DMD	movie	n
13	9.50	DMD	Valium	n
14	9.67	TOF	movie	y
15	9.75	DMD	movie	n
16	9.75	DMD	movie	n
17	9.92	TOF/PA	movie	y
18	9.92	s/p ALCAPA, Supra PS, PI	movie	y

TOF = Tetralogy of Fallot; ARVD = Arrhythmogenic RV Dysplasia; DMD = Duchenne Muscular Dystrophy; PA = Pulmonary Atresia.

Image blurring due to chest motion was suppressed by long term signal averaging (Nex = 4). Scans were assessed for diagnostic quality by 2 independent expert readers.

Results: 14 patients and both control subjects successfully completed their scans with no pharmacologic sedation. 2 patients did require sedation. One (patient number 6 in Table 1) refused to get in the scanner, so underwent general anesthesia-assisted CMRI the following week. The other required an oral anxiolytic a few minutes into the scan, but did thereafter complete the study. Mean scanning time was 47.3 mins (± 13.2) for the 7 “functional” scans (patients with DMD or r/o ARVD). Mean scanning time was 93.5 mins (± 22 mins) for the other 8 patients and both control patients. One patient fell asleep during the scan. All studies were considered diagnostic, and functional data (biventricular volumetry and phase contrast flow measures) were measurable without significant post-analysis discrepancy between the two readers (for example, mean LVEF discrepancy 5.6%, RVEF 12.2%). Gadolinium MRA images were obtained from the 8 patients who had intravenous lines placed, and 3D reconstructions were rated as good or excellent in all.

Conclusion: Movie-assisted CMRI without pharmacological sedation, anesthesia, or breatholding is a feasible alternative in patients aged 5–10 years. Data obtained are reliable and diagnostic. Use of this technique can enhance pediatric CMRI referral patterns, by decreasing the additional logistical considerations, risk and expense of general anesthesia.

127. CARDIAC MAGNETIC RESONANCE IMAGING EVALUATION OF SINUS VENOSUS DEFECTS: COMPARISON TO SURGICAL FINDINGS

Anne Marie Valente, MD, Lauren Sena, MD, Andrew J. Powell, MD, Pedro Del Nido, MD, Tal Geva, MD. Children’s Hospital Boston, Boston, MA, USA.

Background: Sinus venosus defect (SVD) is an uncommon type of interatrial communication which may pose a diagnostic challenge. Because cardiac magnetic resonance (CMR) is used as an alternative imaging modality in this condition, we sought to determine its accuracy in patients with SVD by comparing CMR and surgical findings.

Methods: The CMR studies and operative reports of all patients who had CMR followed by surgical repair of SVD (n = 14) from 1996–2005 were reviewed and discrepancies were recorded. CMR studies included assessment of anatomy (evaluated by a combination of gradient echo cine, spin echo, and Gd-enhanced 3D MR angiography), ventricular volumes and function, and flow measurements.

Results: The median age at CMR was 14 yrs (range 0.4–42 yrs). Compared with operative findings, there were no major discrepancies with CMR. The SVD was clearly imaged in all patients and 38 anomalously draining pulmonary veins were identified (Fig. 1). The median pulmonary-to-systemic flow ratio was 2.4 (range 1.3–4.6). Patients had an average of 1.7 previous diagnostic tests (range 1–3; 16 transthoracic echo, 5 catheterizations, 2 transesophageal echo). Before CMR, SVD was diagnosed in 1 patient, suspected in 7, and not suspected in 6. Additional unsuspected findings identified by CMR included malposition of septum primum (n = 2), left superior vena cava (LSVC) to coronary sinus (n = 2), and aortic arch anomalies (n = 2).

Conclusion: CMR accurately depicts SVD anatomy, may reveal additional abnormalities, and provides the information necessary for surgical planning.

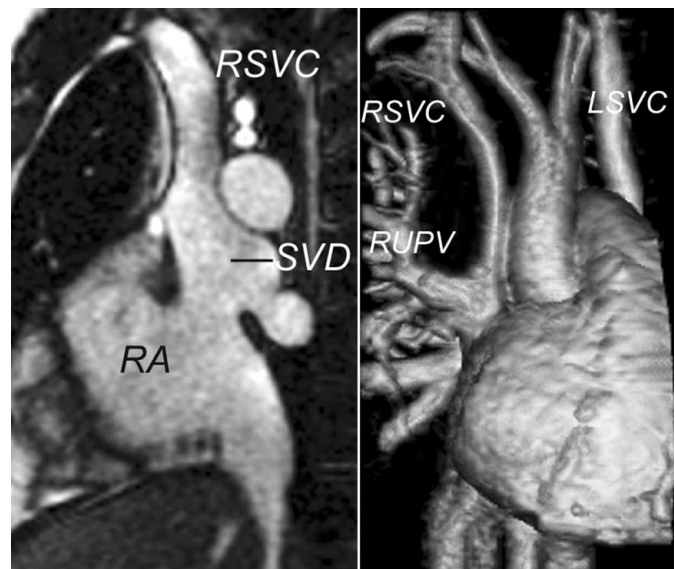


FIG. 1.

Friday, January 20, 2006

1:30 PM–3:00 PM

**Clinical Abstracts: Non-Ischemic Heart Disease:
Tissue Characterization in Myocardial
Inflammation and Beyond**

**128. COMPARISON OF DIFFERENT CARDIAC
MAGNETIC RESONANCE IMAGING (MRI) SEQUENCES
IN PATIENTS WITH PERSISTENT VIRUS MYOCARDITIS**

Birgit Spors, MD, Tobias Thoma, MD, Henriette Bertram, MD, Claudia Seibt, MD, Roland Felix, MD, Hans Peter Schultheiss, MD, Uwe Köhl, MD, PhD, Matthias Gutberlet, MD. Charité, Campus Virchow Klinikum, Berlin, Germany.

Purpose: To evaluate different cardiac MRI sequences and analyse global relative myocardial enhancement, late enhancement and function analysis in patients with chronic myocarditis.

Methods: Cardiac MRI was performed in 62 patients (mean age 49 ± 13) with positive endomyocardial biopsies (EMB) acquired more than 3 months after the clinical onset of acute myocarditis. To assess different CMR approaches for myocarditis evaluation we acquired: STIR-, T2- and T1-weighted Fast Spin Echo (FSE) images before and after contrast agent administration to detect myocardial edema and inflammation as well as inversion recovery gradient-echo sequences (IR-GRE) and steady-state free-precession (SSFP) sequences to assess myocardial fibrosis and function.

Results: Forty five patients had a single virus infection, 17 double infections (parvovirus B19, $n = 59$; human herpes type 6 [HHV 6], $n = 16$; enterovirus, $n = 4$ Edema) was present in 4%, increased global relative enhancement in 40% as indicators for active inflammation, which was histopathologically (EBM) obvious in 61%, and late enhancement (LE) in 22 of the patients as an indicator for irreversibly injured myocardium. LE was slightly more common in patients with double infections (37% vs. 24%).

Conclusions: In patients with chronic myocarditis and cardiotropic viral persistence LE is a common finding but less common as in acute myocarditis. Furthermore, it is more frequent in patients with double infections. In patients with chronic myocarditis different types of MR sequences are necessary to distinguish between persistent inflammation, irreversibly injured or healed myocardium.

**129. ECG FINDINGS COMPARED TO CMR RESULTS
IN THE SETTING OF BIOPSY PROVEN MYOCARDITIS**

Christina Deluigi,¹ Heiko Mahrholdt,¹ Stefan Hager,¹ Martina Mangin,¹ Holger Vogelsberg,¹ Anja Wagner,² Reinhardt Kandolf,³ Udo Sechtem.¹ ¹Robert Bosch Med Ctr., Stuttgart, Germany, ²Duke Cardiovascular MR Center, Durham, NC, USA, ³Institute of Pathology, Tuebingen, Germany.

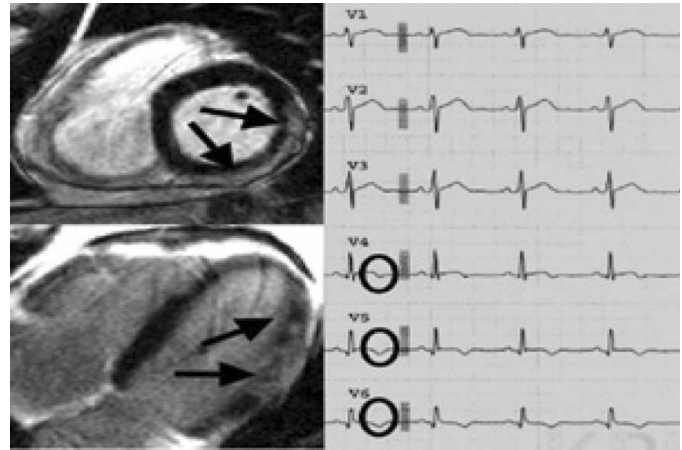


FIG. 1.

Introduction: CMR has recently emerged as a new non-invasive technique for the diagnosis of myocarditis and the identification of myocardial regions with maximum inflammatory involvement. We wondered whether ECG changes were related to CMR findings in patients with biopsy proven myocarditis.

Method: We evaluated the ECGs upon admission in 72 pts with biopsy proven myocarditis and contrast enhancement (CE) on CMR images. CAD was ruled out by coronary angiography. CMR images were read for CE and ECG's were evaluated for QRS and ST-T abnormalities.

Results: The reason to seek medical attention was severe chest pain ($n = 36$), heart failure ($n = 18$) or malaise ($n = 18$). Almost all pts had an abnormal ECG at initial presentation (92%, $p < 0.01$). Most pts presenting with severe chest pain (86%) had ST-abnormalities, compared to only 30% presenting with heart failure or malaise ($p < 0.01$). Interestingly, pts with LV lateral CE ($n = 41$) had ST abnormalities in V3–V6 more frequently than pts without involvement of the lateral wall ($p < 0.05$). Pts with CE confined to the septum were nearly twice as likely to show bundle branch block (40% vs. 13%, $p < 0.01$) than those without CE involving the septum. Q-waves were rare and only present in two cases with severest LV lateral CE. Patients with biopsy proven myocarditis do not have normal ECGs at initial presentation.

Conclusion: ECG findings are related to the area of maximal damage as seen by CMR.

**130. A RANDOMIZED, PLACEBO CONTROLLED,
DOUBLE BLIND TRIAL OF THE EFFECT OF COMBINED
THERAPY WITH DEFEROXAMINE AND DEFERIPRONE
ON MYOCARDIAL IRON IN THALASSAEMIA MAJOR
USING CARDIOVASCULAR MAGNETIC RESONANCE**

Mark A. Tanner, MBBS,¹ Renzo Galanello, MD,² Carlo Dessi, MD,² Mark A. Westwood, MD,¹ Gill C. Smith, MSc,¹ Mohammed Khan, MSc,¹ Sunil Nair, MBBS,³ Lisa J. Anderson, MD,¹ Malcolm J. Walker, MD,³ Dudley J. Pennell,

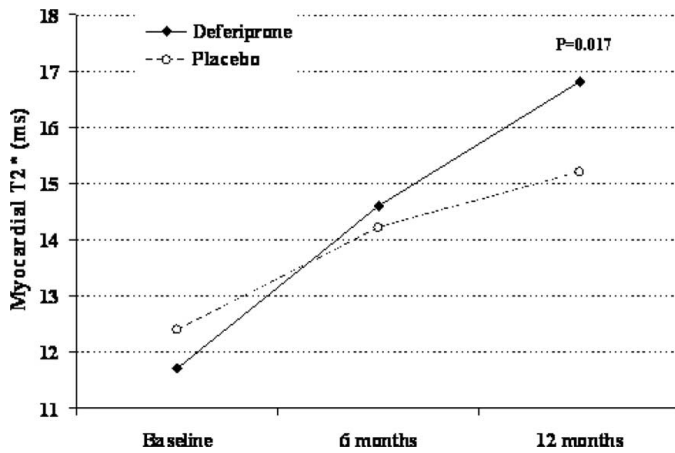


FIG. 1.

MD.¹ ¹Royal Brompton Hospital, London, United Kingdom, ²Ospedale microcitamico, Cagliari, Italy, ³University College London, London, United Kingdom.

Introduction: β -thalassaemia major (TM) is a hereditary anaemia affecting 60000 births worldwide each year. Survival is dependent upon lifelong blood transfusions with cardiac failure secondary to myocardial iron loading being the commonest cause of death. Approximately two-thirds of patients maintained on the parenteral iron chelator, deferoxamine, have myocardial iron loading. More recently, the oral iron chelator, deferiprone has been demonstrated to remove myocardial iron and it has been proposed that in combination with deferoxamine it may have an additive or synergistic effect. Myocardial iron can be rapidly and reproducibly quantified using the validated cardiac magnetic resonance (CMR) T2* technique. CMR is therefore well suited to assess the efficacy of new therapies for the removal of myocardial iron in TM.

Purpose: To report the changes in myocardial and hepatic iron loading (changes in T2*) from a randomized placebo controlled trial comparing the combined therapy of deferiprone

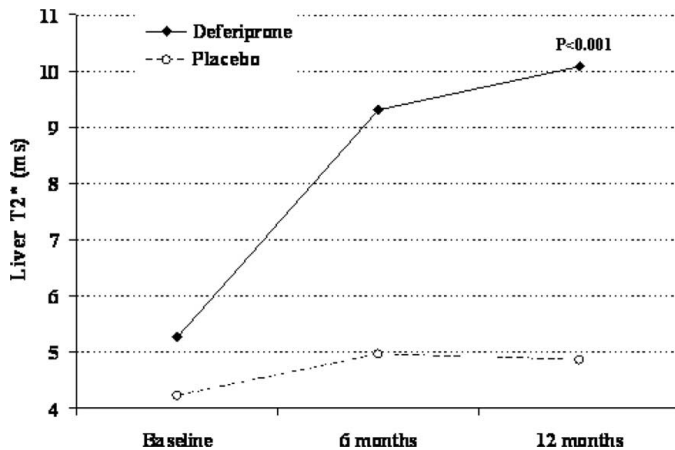


FIG. 2.

and deferoxamine with the standard therapy of deferoxamine alone.

Methods: A mobile CMR scanner (1.5T Siemens Sonata) was transported to Cagliari, Italy. The myocardial T2* was assessed in 167 patients with TM. 65 patients (male 27, female 38, age 30 ± 5.2 years) with mild-moderate myocardial iron loading (T2* 8–20ms) were randomized to receive either deferoxamine and placebo, or deferoxamine and deferiprone. Myocardial and hepatic T2* were assessed at baseline, 6 and 12 months.

Results: Analysis of covariance showed a significant difference between the two groups, with the combined group showing superior effects in improving both myocardial T2* ($p = 0.017$) and liver T2* ($p < 0.001$). (Figs. 1 and 2)

Conclusion: In patients with mild-moderate cardiac iron loading the combined therapy of deferiprone and deferoxamine is superior to deferoxamine alone in the removal of myocardial and hepatic iron.

131. DELAYED ENHANCEMENT REVEALS TYPICAL FIBROSIS PATTERNS IN VARIOUS NON-ISCHEMIC HEART DISEASES

Steffen Bohl, MD, Ralf Wassmuth, MD, Petra Bock, MD, Andr  Rudolph, MD, Daniel Messroghli, MD, Philipp Boy , MD, Rainer Dietz, MD, Jeanette Schulz-Menger, MD. Franz-Volhard Klinik, Helios Klinikum Berlin, Charite Campus Berlin Buch, Universit tsmedizin Berlin, Berlin, Germany.

Background: Delayed contrast enhancement (DE) Cardiac Magnetic Resonance Imaging (CMR) can visualize fibrosis after myocardial infarction. Furthermore fibrosis occurs in a variety of myocardial pathologies such as inflammation, vasculitis and pressure-volume overload. Aim of our study was to assess the distribution patterns of myocardial fibrosis in patients with non-ischemic heart diseases of 8 different causes.

Patients and Methods: We retrospectively analyzed the image data sets of 143 patients (mean 49 ± 16 years, 102 males) who had undergone a CMR with positive DE between 6/2001 and 6/2005. Coronary artery disease (CAD) had been ruled out by coronary angiography in 61 patients, 30 were younger than 40 years of age. The remainder had no history of CAD. CMR was conducted on a 1,5 T clinical scanner. LV-function was assessed by cine-SSFP. DE was assessed using a breathhold IR-GRE (TR 5.5, TE, 1.4, matrix 256×192) 10 minutes after intravenous administration of 0.2 mmol/kg Gadolinium-DTPA in a set of contiguous short axis slices with a slice-thickness of 10 mm. TI was adjusted to suppress remote myocardium. Artefacts were ruled out e.g. by change of the read-out direction. DE was defined by a signal increase of at least 2 fold of the standard deviation of

Table 1.

Clinical Diagnosis	n	Ejection fraction (%)	Enddiastolic volume (ml)
Myocarditis (itis)	41	55 ± 12	189 ± 99
Hypertrophic cardiomyopathy (HCM)	29	72 ± 9	130 ± 32
Aortic stenosis (AS)	21	66 ± 10	163 ± 52
Dilated cardiomyopathy (DCM)	11	24 ± 7	371 ± 78
Vasculitis (Vasc)	8	46 ± 41	174 ± 22
Sarcoidosis (Sarc)	4	57 ± 12	248 ± 99
Lupus erythematoses (SLE)	4	64 ± 4	158 ± 54
Miscellaneous (Msc)	16	49 ± 17	207 ± 112

remote myocardium. Image review was based on the 17 segment model and addressed the amount, regional distribution and the transmural extent of the lesions.

Patient characteristics are shown in Table 1.

Results: We found a considerable variability in lesion patterns depending on the underlying pathology. Overall 85% of all lesions were focal, diffuse lesions were only observed in HCM (27% of the lesions in this group). Out of a total of 441 affected segments subendocardial and transmural lesions (e.g. sarcoidosis, Fig. 1) were only observed in 18 and 15 segments, respectively. Yet, in vasculitis circumfer-



FIG. 1.

Table 2.

Diagnosis	No. of affected segments/patient (mean)	Predominantly affected LV-regions	Predominantly affected myocardial layer
itis	3	50% inferolateral	62% subepicardial
HCM	3	84% anteroseptal/ anterior	45% intramural
AS	1.8	41% RV-insertions	38% subepicardial
DCM	5.3	even distribution	no predominance
Vasc	7	43% septal/ RV-insertion	80% intramural
Sarc	4	even distribution	60% subendocardial
SLE	1	75% inferolateral	50% transmural
			100% intramural

ential subendocardial lesions were frequent but were confined to less than 25% of myocardial wall (Fig. 2). Remarkably, in myocarditis 50% of all lesions were inferolateral whereas lesions in HCM were mainly anterior and anteroseptal (84%).

Details are summarized in Table 2. By nature, in the miscellaneous subgroup no typical pattern of DE could be elucidated.

Conclusion: Non-ischemic heart disease features different patterns of myocardial fibrosis. There are substantial differences in the number of affected segments, regional distribution and transmural extent of the fibrosis. Subendocardial lesions are a



FIG. 2.

rare finding but do occur. The differentiation of distinct delayed enhancement patterns allows for discerning various forms of non-ischemic heart disease.

132. EVOLUTION OF ACUTE MYOCARDITIS BY CARDIAC MAGNETIC RESONANCE

David I. Paterson, MD,¹ Wiphada P. Bandettini, MD,² Anthon R. Fuisz, MD,³ Andrew E. Arai, MD.² ¹*University of Alberta, Edmonton, AB, Canada,* ²*National Institutes of Health, Bethesda, MD, USA,* ³*Washington Hospital Center, Washington, DC, USA.*

Background: Gadolinium delayed enhancement (DE) cardiac magnetic resonance (CMR) has been used to characterize and diagnose myocarditis. This technique has also been used in longitudinal studies of patient with coronary artery disease (CAD) to follow infarct size and to predict myocardial viability.

Objectives: The purpose of this study was to describe the evolution of the extent of CMR DE of acute myocarditis. A secondary aim was to assess whether the extent of DE predicts subsequent recovery of the left ventricular function.

Methods: Consecutive, troponin-positive patients with suspected myocarditis underwent conventional cine CMR followed by DE. All CMR measures were performed on standard image analysis software by 2 blinded readers. The cine images were used to calculate the left ventricular volumes, mass and ejection fraction (LVEF). Using a 17 segment model of the heart, segmental DE was scored on a scale ranging from 0–4 according to the transmural extent (0%, 1–25%, 26–50%, 51–75%, >75% respectively). Consequently, for each patient, the total DE score ranged from 0–68. Each patient was asked to return for a follow-up CMR study at least 30 days after diagnosis.

Results: Twenty three patients (19 male, mean age 40 ± 10) were identified over a 26 month period. Each patient had an abnormal elevation of troponin i, mean 133 ± 225, at presentation

but only 1 or no risk factors for CAD. Acute myocardial infarction was excluded by coronary angiography in 14 or by clinical history and non-invasive testing in the remaining 9. On the initial CMR scan, mean LVEF was 53% (range 29–69%) with 13 of the 23 patients having left ventricular dysfunction (LVEF <55%). All patients had evidence of midmyocardial or subepicardial DE characteristic for myocarditis. The mean DE score was 16 ± 10. 20 patients agreed to return for follow-up scan at a mean of 63 days (range 30–148). On follow-up CMR, 6 patients had residual left ventricular dysfunction. Overall, the extent of DE had diminished with a mean DE score of 10 (p < 0.001). The best predictor for impaired LV function at follow-up was the extent of DE at presentation (Table).

Conclusion: Our CMR follow-up of patients with acute myocarditis, revealed that the extent of DE: (1) significantly diminished over time and (2) was predictive of recovery of left ventricular dysfunction. These two findings agree with DE CMR studies of acute myocardial infarction.

133. COMBINED EARLY AND DELAYED MYOCARDIAL CONTRAST ENHANCEMENT IN CARDIAC AMYLOIDOSIS

Ralf Wassmuth, MD, Steffen Bohl, MD, Rainer Dietz, MD, Jeanette Schulz-Menger, MD. *Franz-Volhard-Clinic Charite University Berlin, Berlin, Germany.*

Background: Amyloidosis is a multi-organ infiltrative disease with cardiac involvement limiting the prognosis. Preliminary reports have focused on delayed enhancement patterns. We applied multi-contrast cardiac magnetic resonance (CMR) including cine, T2-weighted, early and delayed contrast enhancement imaging in a large group of amyloidosis patients.

Methods: We scanned 24 patients (median 61 years, 16 male) in a clinical MR scanner. Five had positive myocardial biopsy, all others had positive extracardiac biopsy plus accepted markers for cardiac amyloidosis including hypertrophy on echo and peripheral low voltage ECG. SSFP or turboFLASH cine gradient echo loops were acquired in 3 long axes. Left ventricular (LV) mass and function were measured. Short axis T2-weighted triple inversion fast spin echo images were acquired. Myocardial signal 2.5 times higher than skeletal muscle signal was considered myocardial edema. Axial T1-weighted fast spin echo images were obtained before and over the first 4 minutes after administration of 0.1 mmol/kg Gd-DTPA. Early enhancement was calculated as the ratio of myocardial and skeletal muscle uptake and compared to data derived in normal volunteers before. We obtained contiguous stacks of long and short axis delayed enhancement inversion recovery gradient echo images 10–30 minutes after a second contrast dose in 10 patients.

Results: LV mass was increased in all but one patient (mean 1.4 ± 0.4 g/cm, normal < 1g/cm in males). On average LVEF was normal (59 ± 10%). T2-weighting showed normal or low signal in all cases (1.4 ± 0.4 vs. 1.5 ± 0.2 in controls). Early

Accuracy for predicting LVEF < 55% at follow-up

	Sensitivity	Specificity	Positive Predictive Value	Negative Predictive Value
Age ≥42	100%	62%	55%	100%
Female sex	100%	62%	75%	80%
Troponin i ≥200	83%	92%	83%	92%
No ST elevation on ECG	83%	54%	45%	88%
LVEF < 55% on initial scan	83%	54%	45%	88%
DE of interventricular septum	100%	36%	43%	100%
DE score ≥25 on initial scan	100%	100%	100%	100%

myocardial contrast enhancement was markedly increased in 21/24 (88%, mean 6.7 ± 2.4) compared to normal values (3.1 ± 1.1), non-diagnostic in one and negative in two patients. Delayed enhancement was normal in 3 and showed focal lesions in 2 patients. In 5 out of 10 patients the myocardial signal could not be suppressed in the usual way, but appeared inhomogeneous across various inversion times. Small pericardial effusions were present in 19/24 patients (79%), pleural effusions in 16/24 patients (67%). Taken together CMR detected cardiac amyloidosis in 22/24 cases (92%). The two cases with positive myoacardial biopsy but negative CMR were slight senile cardiac amyloidosis and AL amyloidosis, respectively. The latter had normal echo and ECG, was not hypertrophic, had no abnormal contrast uptake but a small pericardial effusion only.

Conclusion: In our series, CMR detected cardiac amyloidosis in 22/24 cases. In addition to LV hypertrophy and pericardial effusion early myocardial contrast enhancement adds diagnostic benefit to inconsistent delayed enhancement patterns in cardiac amyloidosis.

134. SIGNIFICANCE OF GADOLINIUM MYOCARDIAL DELAYED ENHANCEMENT ON CARDIAC MAGNETIC RESONANCE IMAGING IN PATIENTS WITH PULMONARY HYPERTENSION

Susan M. Sallach, MD, Vivian Mo, MD, Sharon C. Reimold, MD, Fernando Torres, MD, Clyde Yancy, MD, Ron Peshock, MD. *University of Texas Southwestern, Dallas, TX, USA.*

Introduction: Pulmonary hypertension (PH) is a rapidly progressive disease with cardiac sequelae leading to poor survival. Although the mechanisms of cardiac involvement are not well understood, recent therapeutic advances show promise in improving survival, emphasizing the need for early detection. Cardiac magnetic resonance imaging (CMR) is an effective tool in right ventricular (RV) evaluation due to its ability to accurately measure volumes and function without geometric assumptions. Additionally, the use of delayed enhancement (DE) CMR imaging has been shown to successfully differentiate ischemic from non-ischemic cardiomyopathies involving the left ventricle. However, it is unknown if DE-CMR imaging may offer benefit in the evaluation of patients with cardiac manifestations of PH.

Purpose: Thus we pose the following questions: (1) what is the prevalence of DE in PH? and (2) what is the relationship between DE or other CMR measures of RV dysfunction and PH severity?

Methods: With Institutional Review Board approval, we performed a retrospective analysis of 119 patients with PH who underwent DE-CMR from 9/29/03-8/2/05. Medical records were abstracted for clinical and diagnostic data. CMR studies were performed on a 1.5 Tesla scanner (General Electric Signa

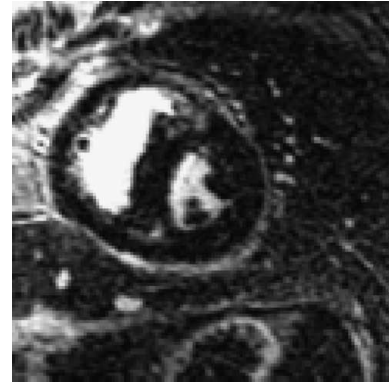


FIG. 1.

Twin Speed CV/I) to obtain standard 2-chamber, 3-chamber, 4-chamber, and short-axis cine images. DE images were acquired with an inversion recovery technique 7–10 minutes following the intravenous administration of 0.2 mmol/kg of gadolinium-DTPA, with adjustment of inversion times to null ventricular myocardium. Interpretation of volumes, size, and function, and assessment of DE were done using the MASS analysis program. Abnormal ventricular septal motion (AVSM) was defined as flattening or paradoxical motion. New York Heart Association (NYHA) Functional Classification results were grouped into 2 categories where Classes I and II were assigned a value of 1, while Classes III and IV were assigned a value of 2. Right heart catheterization (RHC) determined pulmonary pressures and pulmonary vascular resistance were unavailable in 30 and 43 patients, respectively.

Table 1.

	(+) RVIP-DE (abnormal) (n = 85)	(-) RVIP-DE (normal) (n = 34)	(+) AVSM (abnormal) (n = 64)	(-) AVSM (normal) (n = 50)
RHC				
PA systolic pressure (mmHg)	74 ± 22	76 ± 24	78 ± 21 [†]	68 ± 21
PA diastolic pressure (mmHg)	31 ± 10	33 ± 13	34 ± 11 [†]	27 ± 8
Mean PA pressure (mmHg)	46 ± 13	45 ± 14	48 ± 13 [†]	41 ± 12
PVR (dynes.s.cm-5)	543 ± 302	625 ± 344	685 ± 331 [†]	445 ± 252
CMR				
PA diameter (cm)	3.5 ± 0.6	3.4 ± 0.6	3.5 ± 0.5	3.4 ± 0.7
RVESV (cc)	44 ± 51	83 ± 47	93 ± 59 [†]	64 ± 27
RVEDV (cc)	147 ± 59	146 ± 52	155 ± 67	140 ± 41
RVEF (%)	51 ± 14	47 ± 15	44 ± 14 [†]	55 ± 12
Functional Status				
NYHA (I + II = 1, III + IV = 2)	1.6 ± 0.5	1.6 ± 0.5	1.5 ± 0.5	1.7 ± 0.5
6 minute walk (m)	358 ± 121	338 ± 129	369 ± 138	332 ± 103

All p = NS except [†]p < 0.05.

Results: In total, 119 patients underwent contrast CMR. Average age was 52 ± 16 years, and 95 (80%) were women. Mean pulmonary capillary wedge pressure by RHC was 20 ± 16 mmHg ($n = 84$). Although only 3 (2.5%) patients reported a history of myocardial infarction and no patients had received coronary angiography, cardiac risk factors were uncommon (hypertension 58 (50%), past/present tobacco abuse 42 [35%], diabetes 27 [23%], and dyslipidemia 26 [22%]). A mid-wall non-ischemic DE pattern of the left ventricular antero-septum and/or infero-septum (RV insertion points [RVIP] to the left ventricle) (Fig. 1) was present in 85/119 (71%) patients—no patient in this group displayed an ischemic pattern of DE. Table 1 represents RHC, CMR and functional status findings in the presence and absence of RVIP-DE and AVSM. Only the presence of AVSM was statistically significantly related to pulmonary artery pressures and resistance, and RV end-systolic volume and ejection fraction.

Conclusions: Non-ischemic DE at one or both RVIP's occurs in 71% of patients with PH undergoing DE-CMR imaging. DE findings by CMR were not significantly related to measures of disease severity by RHC, CMR, or functional measures. However, the presence of AVSM on CMR correlated with elevated pulmonary pressures and pulmonary vascular resistance by RHC, increased RV end-systolic volume by CMR, and decreased RV ejection fraction by CMR.

135. A DOUBLE-INVERSION GRADIENT AND SPIN-ECHO METHOD FOR THE DETECTION OF LIPID IN THE HEART

Zhiqiang Li,¹ Scott W. Squire,¹ Vincent L. Sorrell,¹ David A. Bluemke,² Maria I. Altbach.¹ ¹The University of Arizona, Tucson, AZ, USA, ²John Hopkins University, Baltimore, MD, USA.

Introduction: Arrhythmogenic right ventricular dysplasia (ARVD) is a condition characterized by progressive lipid infiltration in the right ventricle (RV) leading to ventricular malfunction and death. Current techniques to detect lipid infiltration in the RV rely on a water-plus-fat image obtained with a double-inversion fast spin-echo (DIR-FSE) method. Due to poor contrast-to-noise ratio, blurriness, and artifacts from unsuppressed flow, the visualization of the small lipid structures is a challenging task (1).

Recently, we developed a DIR-FSE method where the acquisition of water- and lipid-suppressed k-space lines is alter-

nated between TR periods (2) From these data, a lipid and a water image are obtained in one breath hold. The advantage of the method over the conventional DIR-FSE (where water and lipid are observed together) is that the lipid image has a high contrast-to-noise ratio and does not have artifacts caused by flow. Because the lipid and water images are co-registered, the anatomical location of lipids can be readily assessed. A recent technique based on steady-state free-precession (SSFP), has also been developed to separate the water and lipid components in the heart (3).

In this work we present a new approach to image lipids in the heart. The method uses a double-inversion gradient and spin-echo sequence (DIR-GRASE) to obtain co-registered in- and out-of-phase data in one breath hold. From these data a lipid and a water image are generated.

Methods: The DIR-GRASE method shown in Fig. 1 was implemented on a 1.5T GE Signa scanner. Ex vivo tissue data were acquired with: FOV = 14 cm², matrix size = 256 × 256, ETL = 2, BW = ±62.5 kHz, slice thickness = 5 mm, and NEX = 1. In vivo data were acquired in a breath hold, with ETL = 6, matrix size = 256 × 144, TR = 1RR, NEX = 1, and FOV = 26 cm². The delay between the gradient (GRE) and spin-echo (SE) was 2.27 ms, which is the out-of-phase condition for lipid and water. Lipid and water images were obtained from the GRE and SE images using a Dixon algorithm. Functional data were acquired with regular SSFP methods.

Results: Images of ex vivo tissue from a subject that died from ARVD are shown in Fig. 2. Note that lipid infiltration (arrows), penetrating from the epicardium into the myocardium, is clearly seen in the fat and water images as bright and dark pixels, respectively. Also, in regions of lipid infiltration, there is a clear difference between the in- and out-of-phase images. The dark regions in the latter are due to signal intensity cancellation in pixels with both lipid and water. Images of a patient diagnosed with ARVD are shown in Fig. 3. Lipid infiltration is seen in the lipid image (see insert). The area can be mapped in the water image to the outflow tract. As with the ex vivo tissue, there is signal loss in the out-of-phase image relative to the in-phase image where there is lipid infiltration. Lipid infiltration correlates with focal functional abnormalities as evidenced by the bulging in the systolic image (arrow).

Conclusions: A DIR-GRASE sequence was developed for detecting lipids in the heart. Compared to the interleaved DIR-FSE method, DIR-GRASE has the advantage that in addition to the lipid and water image, the in- and out-of-phase image can

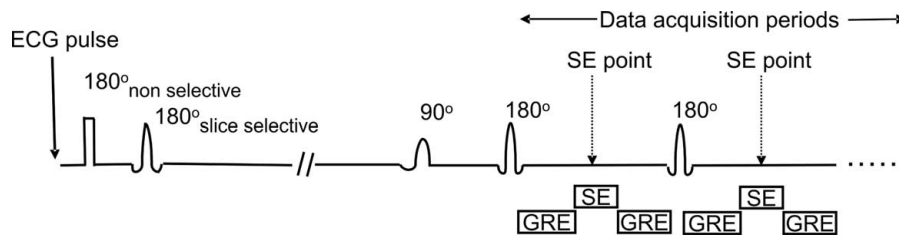


FIG. 1.

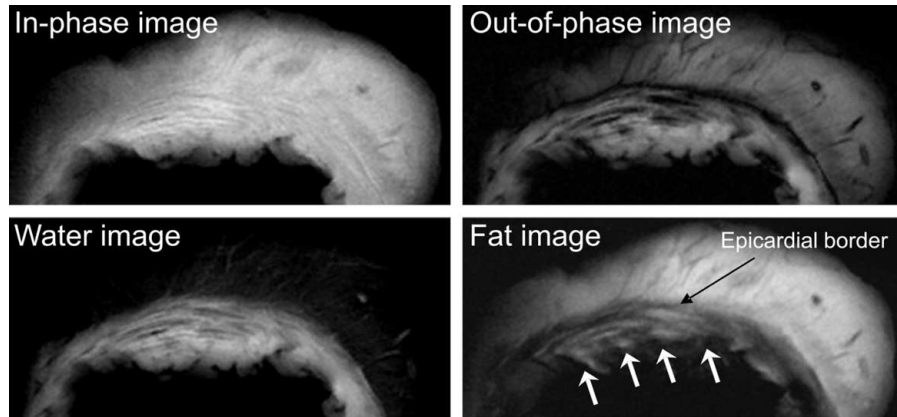


FIG. 2.

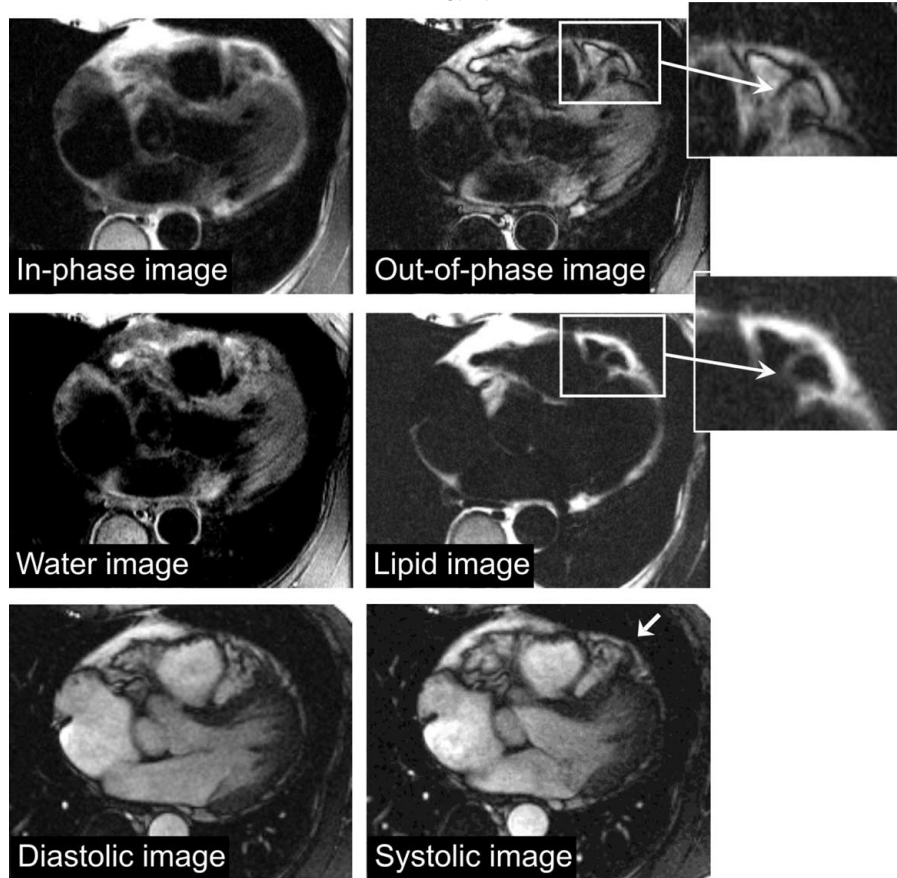


FIG. 3.

be used to evaluate regions of lipid infiltration. Also, with DIR-GRASE errors in separating lipid and water data due to field inhomogeneities can be corrected. The DIR-GRASE method also permits imaging with small FOV's which provides high spatial resolution. This is an advantage over the previously developed SSFP method.

Acknowledgements: Work supported by the AHA grant 0355490Z (MIA), NIH grants HL65549 (DAB), CA099074 (MIA), and the Arizona Hispanic Center of Excellence (MIA).

REFERENCES

1. Castillo. Radiology 2004;232:38.
2. Altbach. MRM in press.
3. Reeder SB. JMRI 2005;22:44.

136. ECHOCARDIOGRAPHIC TISSUE DOPPLER-DERIVED SEPTAL MITRAL EARLY VELOCITY PREDICTS MYOCARDIAL SIDEROSIS ASSESSED BY MR T2* IMAGING IN MAJOR THALASSAEMIA

Ru-San Tan, MBBS, MRCP,¹ Angeline H. M. Lai,² Ivy S. L. Ng,² Lisa J. Anderson,³ Tai-Gang He,³ Kevin K. W. Chen,⁴ Dudley J. Pennell.³ ¹*National Heart Centre, Singapore, Singapore,* ²*KK Women's and Children's Hospital, Singapore, Singapore,* ³*Imperial College, London, United Kingdom,* ⁴*Singapore General Hospital, Singapore, Singapore.*

Introduction: The magnetic resonance (MR) relaxation parameter $T2^*$ in liver and myocardial tissue has been shown to be inversely related to liver iron concentration and myocardial function, respectively, and is useful in diagnosis of transfusion-induced siderotic cardiomyopathy in thalassaemia major (TM) patients. Unlike MR $T2^*$ imaging, which is not widely available currently, echocardiography is ubiquitous. However, conventional echocardiographic assessment of cardiac dimensions and function have not been sensitive for detection of heart iron overload. The recent advent of echocardiographic tissue-Doppler imaging offers potential for echocardiographic diagnosis of myocardial siderosis.

Purpose: In this pilot study, we aim to compare the echocardiographic (including Tissue Doppler imaging) and MR findings in TM patients.

Methods: Ten beta-TM patients underwent heart MR $T2^*$ scans as part of an NIH-funded multicentre trial to validate the intersite reproducibility of MR $T2^*$ liver and myocardial imaging (No.1 RO1 DK066084-01). All ten subjects underwent further full echocardiographic studies (including tissue Doppler imaging) within 4 weeks. Echocardiographic systolic and diastolic functional measurements were correlated with myocardial MR $T2^*$ measurements.

Results: Demographics: M:F = 4:6; age 18–30 years (mean 21.5 years); transfusion frequency 3–6 weeks (mode 4). All received chelation therapy: 5 desferrioxamine; 1 deferiprone; 4 combined. Patients were classified into two groups: myocardial overload (Group 1, $T2^* \leq 20$ ms, $n = 6$) versus no myocardial iron overload (Group 2, $T2^* > 20$ ms, $n = 4$). Between groups 1 and 2, there are no statistically significant differences in left ventricular ejection fractions, atrial volumes and ejection fractions, echo-Doppler assessed mitral early velocities and deceleration times, and velocities of mitral colour flow propagation.

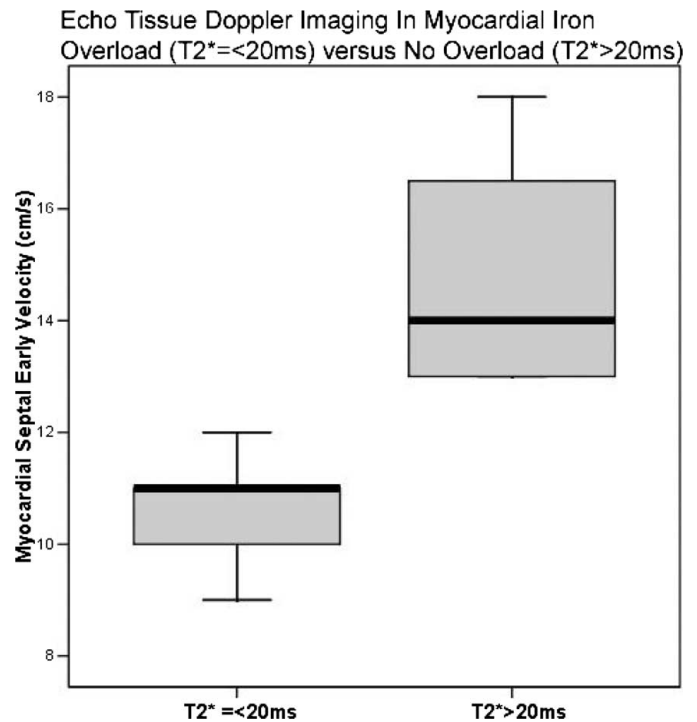


FIG. 1.

However there is significant difference in the septal myocardial early velocities (septal E') measured using tissue Doppler imaging: mean 10.7 cm/s (95% confidence interval 9.9 cm/s to 11.5 cm/s) versus 14.9 cm/s (95% confidence interval 12.6 cm/s to 17.2 cm/s) in groups 1 and 2 respectively, $p = 0.03$. Linear regression reveals good correlation between septal E' (y) and myocardial $T2^*$ (x):

Regression equation, $y = 9.90 + 0.12x$ ($R^2 = 0.71$, $p = 0.002$).

Conclusions: Echocardiographic tissue Doppler-derived mitral annular septal early velocities (E') correlate positively with myocardial $T2^*$ values, and may potentially be used in predicting myocardial iron overload in transfusion-dependent TM patients, especially in centres without access to MR $T2^*$ imaging facilities.

Friday, January 20, 2006

3:30 PM–5:00 PM

**Oral Abstracts: Ischemic Heart Disease:
The Impact of Stress Perfusion**

**137. FIRST PASS MYOCARDIAL PERFUSION
MAGNETIC RESONANCE IMAGING (MRI) FOR THE
DETECTION OF MYOCARDIAL ISCHAEMIA AS
DETERMINED BY INVASIVE CORONARY PRESSURE
MEASUREMENT—FRACTIONAL FLOW RESERVE (FFR)**

Stuart Watkins,¹ Tracey Steedman,¹ Jonathan Lyne,² Stephen Frohwein,³ John Foster,¹ Bjoern Groenning,¹ Ian Ford,¹ Henry J. Dargie,¹ Keith G. Oldroyd.¹ ¹Western Infirmary, Glasgow, United Kingdom, ²Royal Brompton Hospital, London, United Kingdom, ³American Cardiovascular Research Institute, Atlanta, GA, USA.

Introduction: Myocardial perfusion imaging with MRI during the first pass of a bolus of gadolinium has previously been compared to nuclear perfusion tests: single photon emission tomography (SPECT) and positron emission tomography (PET) as well as quantitative coronary angiography (QCA). In a recent comparison, Schwitter et al. (1) noted perfusion MRI to be more sensitive and specific than SPECT for the detection of coronary artery disease (Sensitivity 91% v 74% & Specificity 67% v 57%). However comparisons with SPECT, PET and QCA have their limitations as they may not represent the true gold standard for the diagnosis of significant coronary artery disease.

Purpose: We have compared first pass perfusion MRI with the invasive pressure measurement of fractional flow reserve (FFR) to determine the sensitivity and specificity of this technique.

Methods: Forty two patients with suspected anginal chest pain who were referred to our centre for coronary angiography/coronary intervention underwent first pass perfusion MRI imaging in the week prior to angiography. This was performed on a Siemens Sonata 1.5Tesla scanner (Erlangen, Germany) with perfusion imaging of 3 short axis slices obtained using a turboFLASH sequence (TI 90 ms, TE 0.99 ms, TR 173 ms, Flip Angle 8°, Matrix 80 × 128). Maximal hyperaemia was achieved using intravenous adenosine (140 μg/kg/min). The first pass bolus contained 0.1 mmol/kg of gadolinium (Omniscan, Amersham Health, Oslo, Norway) power injected at 5ml/sec (Medrad, Pittsburgh, PA) followed by a 20 mL saline bolus. During coronary angiography the FFR was recorded in all patent major epicardial coronary arteries using a coronary pressure wire (RADI,™ Uppsala, Sweden) with hyperaemia induced using intravenous adenosine as above. An FFR value of ≤0.75 was taken as the cut off for the diagnosis of significant coronary disease. Perfusion scans were analysed by a blinded independent experienced observer.

Results: Thirty two of 42 (76%) patients were male. The mean age was 59 years (SD = 9, Range 37–80). First pass

perfusion MRI revealed 57 perfusion defects in 124 coronary artery segments (46%). A FFR ≤0.75 was found in 47 coronary arteries (38%) with 22 (47%) in the territory of the left anterior descending coronary artery, 12 (25%) in the right coronary artery and 13 (28%) in the distribution of the left circumflex coronary artery. The sensitivity of first pass perfusion MRI for the detection of significant coronary artery disease as determined by FFR was 94% and the specificity was 83%. Twenty three patients (55%) underwent follow-on coronary intervention, 6 (14%) were referred for coronary artery bypass grafting, 4 (10%) had significant disease for medical therapy only and 9 (21%) had normal coronary arteries.

Conclusions: First pass perfusion MRI can detect significant coronary artery disease with good sensitivity and specificity when compared to invasive coronary pressure measurements (FFR). This adds support to the growing evidence for the use of this technique as a potential alternative to nuclear perfusion techniques and the diagnostic coronary angiogram.

REFERENCE

1. Schwitter J, et al. European Heart Journal 2005;26:329.

**138. EVENT FREE SURVIVAL IN PATIENTS WITH
SUSPECTED CORONARY ARTERY DISEASE AND A
NEGATIVE TEST RESULT IN ADENOSINE STRESS
PERFUSION MAGNETIC RESONANCE IMAGING**

David Hardung, MD, Giso von der Recke, MD, Karol Miszalski-Jamka, MD, Christoph Hammerstingl, MD, Harald Schmidt, MD, Bernhard Saxler, Jan Schnapauff, Heyder Omran, MD. St.-Marien-Hospital, Bonn, Germany.

Background: Adenosine stress perfusion cardiac magnetic resonance (CMR) of patients with suspected coronary artery disease (CAD) has been demonstrated to provide a high diagnostic accuracy for identifying patients in need of revascularisation. However, there is no data regarding the long term follow up of patients with a negative test results, ie, that are declared of having no significant coronary artery disease according to the stress perfusion CMR.

The aim of this study was to protocol the event free survival of patients undergoing adenosine stress CMR in whom significant disease could be excluded at the time of investigation.

Method: The study was planned as a prospective study in a primary investigational centre. All patients who completed adenosine stress perfusion CMR (1,5T Magnetom Avanto, Siemens, Germany) for suspected coronary artery disease were included. Patients with negative or insignificant, ie, only mild subendocardial, inducible perfusion deficits during a first pass perfusion were contacted after a follow up period of at least 6 months either by telephone or through our outpatient clinic. Data was evaluated on the occurrence of major adverse cardiac

events, re-hospitalisation for persistent angina or other cardiac symptoms, or the need for invasive coronary artery disease and reperfusion therapy.

Results: Of the 606 patients undergoing adenosine stress perfusion CMR 432 had a negative result or insignificant perfusion deficit that was not considered clinically relevant. Up to date 412 patients completed at least 6 months of the follow-up period. Of patients with successful completion of the follow up questionnaire, 0.5% had a major adverse cardiac event. 7.9% underwent invasive coronary artery imaging for ongoing symptoms or other positive indicators of relevant disease. Two patients had proof of coronary artery stenosis >50%. One patient, in whom CMR had demonstrated a negative test result that had been confirmed by invasive coronary angiography died shortly after the latter procedure for complications of dilated cardiomyopathy.

Conclusion: In patients with a negative adenosine stress perfusion CMR the event free survival was 99% in a large cohort of patients with initially suspected CAD. This finding has important implications for risk stratification of these patients and their management.

139. OPTIMAL QUALITATIVE CRITERIA OF ADENOSINE PERFUSION CARDIAC MAGNETIC RESONANCE TO PREDICT CORONARY ARTERY STENOSIS

Quint Whitby, RT (MR), Scott E. Bingham, MD, Nicole T. Smith, MS. Central Utah Clinic, Provo, UT, USA.

Introduction: The accuracy of adenosine stress perfusion cardiac magnetic resonance (CMR) has been demonstrated using quantitative analysis of first-pass contrast signal intensity curves to predict angiographic coronary stenosis (CAD). However, current quantitative techniques involve time consuming image post-processing and are therefore not easily applied.

Purpose: To determine optimal qualitative diagnostic criteria of visual analysis of adenosine perfusion CMR to predict significant CAD in our patient population.

Methods: Five hundred four patients were referred for assessment of heart disease by combination adenosine perfusion, viability, and function CMR from July 2002 through Nov 2004. Of

Table 1. 138 Coronary territories

Defect		1 Slice	2 Slices	1 Systolic	2 Systolic
Duration	Cutoff result				
5 sec	Sensitivity	90	89	83	67
	Specificity	46	74	69	87
8 sec	Sensitivity	86	83	81	64
	Specificity	67	89	85	97
10 sec	Sensitivity	83	75	75	58
	Specificity	77	94	93	98
15 sec	Sensitivity	64	46	54	39
	Specificity	89	98	96	98

Table 2. 46 Patients

Defect		1 Slice	2 Slices	1 Systolic	2 Systolic
Duration	Cutoff result				
8 sec	Sensitivity	96	89	92	69
	Specificity	45	65	65	90
10 sec	Sensitivity	92	85	89	65
	Specificity	55	85	80	95

110 patients referred for x-ray coronary angiography, 46 had no myocardial infarction by delayed gadolinium myocardial contrast enhancement. These 46 patients composed the study group. After written informed consent, CMR was performed with a 1.5 Tesla Twinspeed scanner (General Electric Healthcare, Milwaukee, Wisconsin). Adenosine was infused via a peripheral vein for 2 minutes before Gadoversetamide 0.05 mmol/kg was given at 3 cc/sec during a cardiac gated interleaved notched saturation fast gradient echo-echo train sequence. Five to nine short axis slices were acquired every 2 cardiac cycles. The CMR reader was blinded to patient data and results of angiography. Perfusion defects were considered potentially abnormal when the defect was at least subendocardial, and conformed to a major coronary artery territory. The duration of perfusion defect from first pass bolus myocardial arrival time was measured for each of the three major coronary territories. Optimal accuracy for prediction of angiographic coronary stenosis was tested for a perfusion defect observed in any single slice, any two adjacent slices, a single systolic slice, or 2 systolic slices. Each slice pattern was then tested for duration of perfusion defect (at least 5, 8, 10, or 15 seconds). CAD was defined as a non-protected diameter stenosis $\geq 70\%$ by quantitative coronary angiography. No intervening cardiac event occurred between CMR and x-ray angiography.

Results: Of the 46 study patients, 22 were women. CAD was found in 26 of 46 patients and 36 of 138 coronary territories. Sensitivity and specificity varied by perfusion defect duration and myocardial slice criteria as shown in Tables 1 and 2. The optimal cutoff for detection of CAD was a perfusion defect duration ≥ 10 seconds in any two adjacent myocardial slices. This cutoff resulted in the highest receiver operating characteristic area = 0.907 ± 0.044 .

Conclusion: Qualitative descriptors of a CMR perfusion defect may enhance the accuracy of image interpretation for detection of CAD. Increasing the cutoff for perfusion defect duration or the number of required abnormal slices results in higher specificity at the expense of sensitivity. In the present study population, a perfusion defect ≥ 10 second duration in any two consecutive slices produced an overall patient sensitivity and specificity of 85% for prediction of CAD.

140. DIAGNOSTIC ACCURACY OF STRESS CMR PERFUSION IMAGING EARLY AFTER ACUTE MYOCARDIAL INFARCTION COMPARED TO EXERCISE TOLERANCE TESTING

John P. Greenwood, MB ChB, PhD, Sven Plein, MD PhD, Ehtesham Mustafa, Aleksandra Radjenovic, PhD, John Ridgway, PhD, Mohan Sivananthan, MD, Stephen Ball, PhD. Leeds General Infirmary, Leeds, United Kingdom.

Introduction: Following acute myocardial infarction (MI) the presence of on-going ischaemia outside of the infarct zone has independent prognostic significance. Using the technique of late gadolinium hyper-enhancement, cardiac MRI can reliably detect and quantify infarcted myocardium and hence identify areas of viable tissue. Furthermore, first pass CMR perfusion imaging during rest and stress identifies fixed and inducible ischaemia in patients with both stable coronary disease and in acute coronary syndromes. At present exercise tolerance testing (ETT) has a Class I indication for the assessment of post-infarct ischaemia as recommended by the ACC/AHA, although ETT is recognised to have limitations in terms of its diagnostic accuracy. CMR has the potential to be superior to ETT but at present there are no data relating to the safety and clinical applicability of using stress CMR perfusion in the immediate post-MI period.

Purpose: To assess the safety and diagnostic accuracy of a first pass rest/stress CMR perfusion study to identify inducible ischaemia outside of the infarct zone compared to ETT.

Methods: Forty patients admitted with their first acute myocardial infarction and treated with thrombolysis were recruited. During their index admission all underwent CMR, ETT and x-ray angiography. CMR imaging was performed between days 3 and 6 using a 1.5T Gyroscan Intera CV system (Philips Medical Systems, The Netherlands). Rest perfusion images were acquired using a bolus of 0.05 mmol/kg Dimeglumine gadopentetate and a T1-weighted saturation recovery segmented k-space gradient echo pulse sequence combined with Sensitivity Encoding (echo time, 1.6 msec; repetition time, 3.3 msec; flip angle 15°, four parallel short axis slices, spatial resolution 2.5–3.0 × 3.0–4.0 × 8 mm). Twenty minutes later stress perfusion was assessed during a 6-minute intravenous administration of adenosine (140 mcg/kg/min) using identical pulse sequence parameters. A further contrast bolus of 0.1 mmol/kg was given immediately after the stress perfusion acquisition and viability images were obtained using a segmented inversion-recovery gradient-echo pulse sequence 15 minutes later. Visual analysis of the CMR perfusion and viability images was performed off-line by two experienced observers using commercial software (Mass 5.0, Medis, The Netherlands). The CMR study was reported positive if there was inducible ischaemia outside of the infarct zone in the infarct related artery territory or in an area of remote myocardium.

The ETT was performed between day 5 and 7 post-infarct using a standard modified-BRUCE protocol and was reported by a cardiologist. All x-ray angiograms were undertaken after the CMR and reported by a single, blinded cardiologist. The diagnostic accuracy in terms of sensitivity, specificity, positive and negative predictive values of CMR and ETT was determined to identify: 1) major adverse cardiovascular events, MACE (death,

Table 1.

Modality	Diagnostic accuracy	Sensitivity	Specificity	Positive Predictive	Negative Predictive
				Value	Value
ETT	All MACE	67%	71%	76%	60%
ETT	Occurrence of revascularization	56%*	56%	67%	45%
ETT	Stenosis (≥70%)	51%*	50%	90%	50%
CMR Visual Assessment	All MACE	86%	47%	76%	64%
CMR Visual Assessment	Occurrence of revascularization	92%*	50%	73%	82%
CMR Visual Assessment	Stenosis (≥ 70%)	87%*	83%	97%	50%

recurrent MI, revascularisation, CV readmission) over the next 12 months, 2) occurrence of revascularisation, 3) ability to detect a significant coronary stenosis (≥70%) on x-ray angiography. Comparison between ETT and CMR to predict all three outcomes was made using a McNemar's test.

Results: There were no complications during either the CMR rest/stress perfusion study or the ETT in this patient group. Table 1 highlights the main results for diagnostic accuracy of CMR and ETT. CMR was significantly more sensitive than ETT to predict revascularisation and significant coronary stenosis. The difference in predicting MACE did not reach statistical significance ($p=0.14$) and no other statistical differences were found.

Conclusions: In this study CMR rest and stress perfusion imaging was safe in patients during their index admission for acute myocardial infarction. Furthermore the sensitivity of CMR perfusion imaging using visual assessment was superior to ETT.

141. CLINICAL IMPLICATION OF ADENOSINE-STRESS MAGNETIC RESONANCE IMAGING IN THE DIAGNOSIS OF CORONARY HEART DISEASE

Günter Pilz, Peter Bernhardt, Markus Klos, Stefanie Martin, Berthold Höfling. Cardiac MRI at the Hospital Agatharied, Hausham, Munich, Germany.

Background: Cardiac magnetic resonance imaging (CMR) with pharmacological induced stress is establishing in clinical routine for assessing coronary artery disease (CAD). Aim of our study was to investigate clinical implication of a standard protocol in patients with suspected or known CAD undergoing adenosine stress CMR.

Methods: Three hundred forty-seven patients referred for coronary angiography were additionally studied in a 1.5-T whole body CMR-scanner for myocardial function, ischemia and viability. The routine protocol for detection of CAD consisted of functional imaging (long and short axes), adenosine stress- and rest-perfusion and "late enhancement" imaging. Images were analyzed by two independent and blinded investigators. Inter-observer differences were resolved by a third reader. Patients

without strict class I indication (ACC/AHA criteria) for coronary angiography (N = 171) were evaluated for diagnostic accuracy of CMR and its potential clinical impact in the decision making for indication of coronary angiography.

Results: One hundred seven (63%) of our patients had relevant perfusion deficits as seen by CMR and matching coronary artery stenosis >70%. Four (2%) patients had false negative CMR findings. In 60 patients (35%) no relevant coronary artery stenosis could be observed. In 50 (83%) of these patients CMR correctly showed no significant perfusion deficit. In 10 (17%) of these patients CMR provided false positive results (6% of all patients). Sensitivity of CMR to detect relevant CAD (>70% luminal narrowing) was 0.96, specificity 0.83, positive predictive value 0.92 and negative predictive value 0.93.

Conclusion: As demonstrated by our study, CMR prior to coronary angiography could substantially reduce redundant coronary angiographies (patients without significant stenosis) in patients without class I indication for angiography: 35% to 6% in our patient population. Further studies are warranted to identify the cause of rare false negative CMR results.

142. MYOCARDIAL BLOOD FLOW IS INCREMENTALLY REDUCED ACCORDING TO TRANSMURAL EXTENT OF SCAR: AN MR STUDY OF QUANTITATIVE PERFUSION ASSESSMENT IN SEVERE CORONARY ARTERY DISEASE

Joseph B. Selvanayagam,¹ Michael Jerosch-Herold,² Italo Porto,³ Nick Searle,³ Adrian S. H. Cheng,¹ David Sheriden,² Helen Doll,¹ Adrian P. Banning,³ Stefan Neubauer.¹ ¹University of Oxford, Oxford, United Kingdom, ²Oregon Health & Science University, Portland, OR, USA, ³John Radcliffe Hospital, Oxford, United Kingdom.

Background: Absolute myocardial blood flow (MBF) in areas of scarred myocardium has not been previously reported. Cardiovascular magnetic resonance permits both absolute quantification of myocardial blood flow (first pass perfusion imaging), and quantification of myocardial scar (delayed enhancement imaging-DE-MRI).

Purpose: We hypothesized that the level of MBF in scarred myocardium is significantly different between segments with >50% transmural extent of infarction (TEI) and those with ≤50% TEI.

Methods: Twenty-seven patients with one or two vessel coronary disease undergoing PCI were studied with pre-procedure DE-MRI and first pass perfusion MR imaging at rest. For perfusion imaging, 3 short axis images were acquired during every heart-beat using a T1-weighted turboFLASH sequence, with low-dosage Gd-DTPA bolus injection. DE-MRI was performed after a further administration of 0.085 mmol/Kg Gd-DTPA. In each slice, MBF was determined for 8 myocardial sectors in ml/min/g by deconvolution of signal intensity curves with an arterial input function measured in the LV blood pool. MBF re-

sults were subdivided according to transmural extent of delayed hyperenhancement.

Results: Mean MBF normalized by rate pressure product (corrected MBF) was 1.2 ± 0.3 mL/min/g in segments without significant coronary stenosis and 0.7 ± 0.2 mL/min/g in segments with coronary stenosis pre PCI ($p < 0.0001$). Overall, 11 (31%) patients had evidence of myocardial hyperenhancement (HE) in their pre-PCI scan. Mean mass of HE per patient was 9.1 ± 7.0 g. Out of a total of 641 myocardial segments (7 segments were excluded from analysis), 521 (81%) had no HE, 91 (14%) had 1-50% HE and 29 (5%) had >50% HE. Non-stenosed segments were significantly more likely to have no HE and less likely to have both 1-50% and >50% HE ($z = 3.7$, $p < 0.001$). Both the extent of HE ($z = -10.3$, $p < 0.001$) and the presence of significant stenosis ($z = -11.1$, $p < 0.001$) were significantly associated with MBF pre-PCI. In segments with no HE, the mean corrected MBF pre-PCI was 1.2 ± 0.2 mL/min/g in segments without significant coronary stenosis and 0.8 ± 0.2 mL/min/g in segments with coronary stenosis pre PCI ($z = -23.9$, $p < 0.001$). In the 91 segments with 1-50% HE, the mean corrected MBF was 1.0 ± 0.4 mL/min/g in segments without significant coronary stenosis and 0.6 ± 0.1 mL/min/g in segments with coronary stenosis pre PCI ($z = -7.2$, $p < 0.0001$). In the segments with >50% HE, the respective corrected MBF were 0.4 ± 0.1 mL/min/g and 0.3 ± 0.2 mL/min/g ($z = -1.09$, $p = 0.28$).

Conclusion: Mean MBF is lower in myocardial segments with scar and this reduction is incrementally related to the transmural extent of scar. The presence of large amounts of myocardial scar attenuates the differences in MBF between stenosed and non-stenosed coronary territories.

143. ACCELERATING MR PERFUSION IMAGING USING K-T BLAST-A FEASIBILITY STUDY

Rolf Gebker, MD,¹ Cosima Jahnke, MD,¹ Ingo Paetsch, MD,¹ Axel Bornstedt, PhD,¹ Bernhard Schnackenburg, PhD,² Eckart Fleck, MD,¹ Eike Nagel, MD.¹ ¹German Heart Institute, Berlin, Germany, ²Philips Medical Systems, Hamburg, Germany.

Purpose: The purpose of this study was to develop and test the feasibility of k-t BLAST for an accelerated data acquisition with MR myocardial perfusion imaging for the detection of myocardial ischemia.

Methods: Forty consecutive patients scheduled for coronary catheterization were examined with first-pass magnetic resonance imaging (MRI) during adenosine stress and at rest. A balanced SSFP pulse sequence with a k-t acceleration factor of 5 (TR/TE/α = 3.2 ms/1.7 ms/50°), saturation preparation (pp delay 100 ms) and a spatial resolution of $2.6 \times 2.6 \times 10$ mm was applied. The sequence allowed the acquisition of 3 short axis views every heart beat up to a heart rate of 120/min without reducing spatial resolution. Visual assessment of myocardial

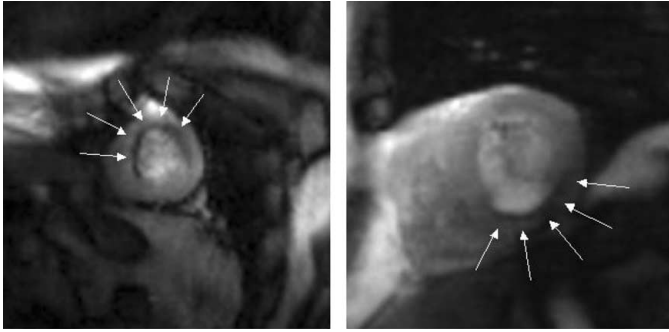


FIG. 1.

perfusion and grading of image quality (4 = excellent, 1 = non-diagnostic) was done patient based by two fully blinded experienced readers. Semiquantitative analysis was performed using commercial software.

Results: Prevalence of CAD was 53%. Sensitivity, specificity and diagnostic accuracy for the detection of coronary stenoses $\geq 50\%$ were 86%, 84% and 85%, respectively. Overall image quality was good (3.3 ± 0.7). Myocardial segments supplied by stenotic coronary arteries showed a significantly reduced peak signal enhancement compared to those supplied by normal coronary arteries (159 ± 46 vs. 192 ± 49 , respectively, $p < 0.05$).

Conclusion: Myocardial perfusion imaging using k-t BLAST accelerated imaging proved to be feasible and reliable for the detection of patients with significant CAD. The sequence allows the acquisition of images with a high spatial resolution even during high heart rates.

144. EVENT-FREE SURVIVAL OF PATIENTS WITH UNRECOGNIZED MYOCARDIAL INFARCTION BY CONTRAST ENHANCED MAGNETIC RESONANCE IMAGING

Raymond Kwong,¹ Anna Chan, MBBS,¹ Kenneth Brown, MD,² Carmen Chan, MBBS,¹ H Glenn Reynolds, MSc,³ Sui Tsang, BSc,¹ Roger B. Davis, ScD.⁴ ¹Brigham and Women's Hospital, Boston, MA, USA, ²Cardiology Unit, University of Vermont College of Medicine, Burlington, VT, USA, ³General Electric Healthcare, Boston, MA, USA, ⁴Beth Israel Deaconess Medical Center, Boston, MA, USA.

Background: Unrecognized myocardial infarction (UMI) is common and it is associated with higher rates of adverse cardiac events (MACE) than recognized MI.

Method: We examine whether myocardial delayed enhancement (MDE) by MRI can characterize UMI and can provide incremental prognostic value beyond clinical assessment. Patients with a suspicion of CAD underwent CMR for cardiac function and myocardial scar. Patients with MI by history, medical records, or cardiac enzymes were excluded. We quantified the normalized extent of myocardial delayed enhancement

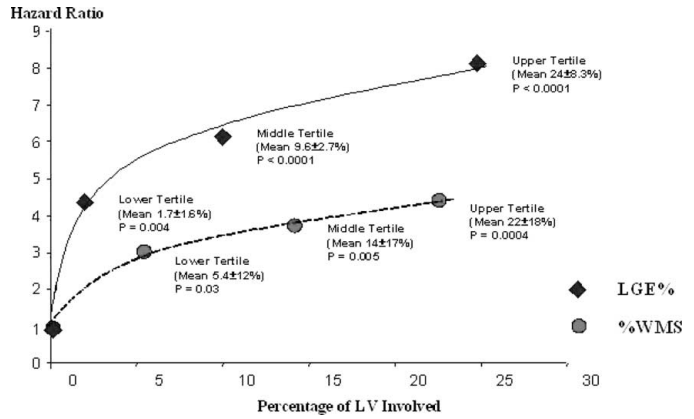


FIG. 1.

(MDE%), LV ejection fraction (LVEF), LV diastolic volume index, wall motion abnormality score, and assessed ECG evidence of UMI. Uni/Multivariable Cox proportional hazards regression models associated MDE% to MACE and assessed the incremental prognostic value by MDE% beyond a clinical model that considered all variables other than MDE.

Result: Of the initial 205 patients, 38 (19%) experienced MACE including 20 deaths and 18 non-fatal cardiac events at a median of 16 months. While LVEF, LVEDVI, LV hypertrophy by ECG (LVH), and any WMA associated with MACE, MDE% had the strongest association with MACE ($p < 0.0001$) and death ($p < 0.0001$). All %MDE tertiles indicated significant hazards, which progressed linearly from the lowest to the highest %MDE tertile (%MDE 1.7%, 9.7%, and 24%: hazard ratios of 4.5, 6.3, and 8.3, respectively). MDE% provided incremental prognostic value to the clinical model consisting of any WMA and LVH ($p = 0.02$).

Conclusion: MDE is a better method in characterizing UMI than ECG. While %MDE from all tertiles indicates strong increased hazards, MDE% provides incremental prognostic value to clinical variables and should be included in the workup of CAD.

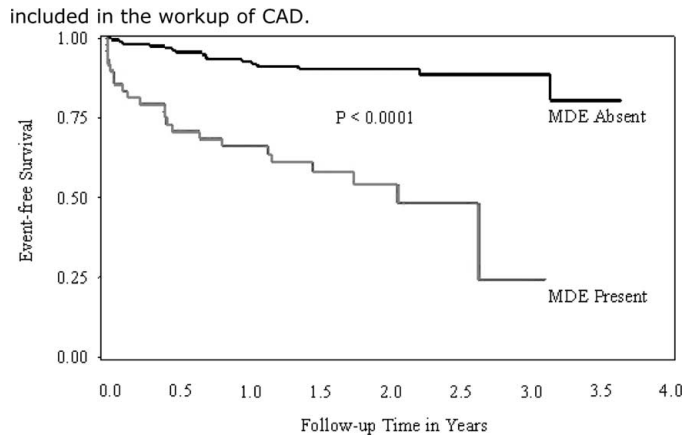


FIG. 2.

145. A PROSPECTIVE STUDY IN 645 CONSECUTIVE PATIENTS TO ASSESS SAFETY AND FEASIBILITY OF ADENOSINE STRESS MAGNETIC RESONANCE PERFUSION FOR DIAGNOSIS OF MYOCARDIAL ISCHAEMIA

Karol Miszalski-Jamka, MD, Giso von der Recke, MD, David Hardung, MD, Bernhard Saxler, Jan Schnapauff, Christoph Hammerstingl, MD, Harald Schmidt, MD, Heyder Omran, MD, PhD. St.-Marien-Hospital, Bonn, Germany.

Introduction: Adenosine stress cardiac magnetic resonance (CMR) is highly accurate and well established imaging modality for assessment of myocardial perfusion. However, there are no large studies which have evaluated safety and feasibility of adenosine CMR.

Purpose: To assess safety and feasibility of stress CMR with 140 microgram/kg/min adenosine intravenous infusion.

Methods: From September 2004 to August 2005, 645 consecutive in- and outpatients with known or suspected myocardial ischaemia underwent CMR with a 1.5 T scanner using a standard adenosine protocol. Adenosine infusion was discontinued to patient's wish or when major side effect occurred: myocardial infarction, severe angina, severe increase or decrease in blood pressure, persistent high-degree atrioventricular block, severe claustrophobia and bronchospasm. Facial flushing, chest

pain, palpitation, mild dyspnoe and headache were considered as physiological reactions and classified as minor side effects.

Results: Three hundred ninety-four patients were male (61,1%), 251 female (38,9%) with a mean age of 65.5 years. Because of mild claustrophobia, 66 patients (10,2%) needed intravenous short-acting benzodiazepine injection. The adenosine CMR was successfully performed in 642 patients (99,5%) and was prematurely terminated in 3 patients (0,5%). Two patients (0,3%) terminated early due to severe claustrophobia and 1 patient (0,2%) due to severe increase in blood pressure. Major side effects included also 23 cases (3,5%) of transient high-degree atrioventricular block which resolved spontaneously without cessation of adenosine infusion. At least one minor side effect (facial flushing, dyspnoe, headache, chest pain, palpitation) was reported by 523 patients (81,1%). All of those were transient and did not lead to premature termination. There were no deaths, no myocardial infarction, no sustained high-degree atrioventricular blocks, no episodes of bronchospasm and no severe hypotension. None of the patients needed to receive aminophylline or other drugs. The mean study time was approximately 29 min for whole CMR protocol. Interpretable images were obtained in all but above mentioned 3 patients.

Conclusions: Adenosine CMR is a very safe and feasible imaging modality. Premature termination occurs extremely rare (0,5%). Minor side effects occur often but are well tolerated and transient. Major side effects are rare and reverse after cessation of adenosine infusion.

Friday, January 20, 2006
3:30 PM–5:00 PM
Oral Abstracts: New Data
on Tissue Characterization

146. ACUTE MYOCARDIAL INFARCTION AND INCONSPICUOUS CORONARY ANGIOGRAPHY: DIFFERENTIAL DIAGNOSIS VIA CONTRAST ENHANCED CARDIAC MAGNETIC RESONANCE TOMOGRAPHY

Udo Sprengel,¹ Thomas Wetzel,¹ Katrin Hecking,¹ Thorsten Nitschke,¹ Martin Klocke,¹ Verona Lubienski,¹ Joachim Weber-Albers,¹ Thomas Scheffold,² Reinhard Kandolf,³ Hubertus Heuer¹ ¹*St. Johannes Hospital, Dortmund, Germany,* ²*Institut für molekulare und klinische Herz-Kreislaufforschung an der Universität Witten/Herdecke, Dortmund, Germany,* ³*Universitätsklinikum Thübingen, Abteilung für Molekulare Pathologie, Thübingen, Germany.*

Introduction: Often patients (p) with classical signs of acute myocardial infarction (typical clinic, specific ECG changes, positive CK; CKMB, troponin) show normal coronary arteries.

Methods: Forty-nine p. (45 ± 17 y) with clinical signs of acute myocardial infarction (positive CK, CKMB, troponin, infarct positive ECG) and exclusion of coronary heart disease via coronary angiography were investigated in a 1.5 T MR scanner (Sonata, Siemens) 1–4 days after the onset of the clinical symptoms. For functional analysis True FISP Cine sequences were used. Tissue characterization occurred by T1- and T2 weighted TSE and TIRM sequences and T1-weighted TFL images after injection of GD-DTPA in corresponding orientations. As control group we investigated 35 p (51 ± 12 y) with same changes in ECG, laboratory parameters and an established proof of significant coronary stenosis in the coronary angiography.

Results: Thirty-three p expressed an multifocal, subepicardial, intramural contrast enhancement in T1-weighted TLF images after 10 min. of Gd-DTPA injection. These changes were distributed over the whole left ventricular myocardium and could not assign to a perfusion area of a certain coronary artery. In 16 p. of these group a myocardial biopsy were taken and histological a acute myocarditis could be detected. Fourteen p showed unifocal, subendocardial to transmural contrast enhancement which could precisely assigned to an perfusion area of a certain coronary artery. All p in the control group showed an unifocal, subendocardial and/or transmural contrast enhancement which could be assign to a perfusion area of a coronary artery.

Conclusions: The contrast enhanced cardiac magnet resonance imaging is a sensitive, non invasive method to make differential diagnosis in patients with clinical sign of acute myocardial infarction and exclusion of coronary heart disease via coronary angiography and allows to devote the p to specific differential therapy.

147. CHARACTERIZATION OF PERI-INFARCT MYOCARDIAL TISSUE WITH CONTRAST-ENHANCED CARDIAC MRI PREDICTS POST-INFARCTION MORTALITY BEYOND LEFT VENTRICULAR EJECTION FRACTION

Andrew T. Yan, MD,¹ Adolphe Shayne, MD,¹ Carmen Chan, MBBS,¹ H. Glenn Reynolds, MSc,² Sui Tsang, BSc,¹ Marcelo F. Di Carli, MD,¹ Raymond Kwong, MD.¹
¹*Brigham and Women's Hospital, Boston, MA, USA,*
²*General Electric Healthcare, Boston, MA, USA.*

Introduction: Identifying post-MI patients at high-risk of cardiac death is crucial for treatment planning. Infarcted and peri-infarct viable myocardium quantified by contrast-enhanced cardiac MRI have been associated with electrophysiological substrates of malignant arrhythmias. We assessed the prognostic values of the morphologic or structural features of the left ventricle in post-infarct patients.

Methods: A consecutive series of 136 patients (105 males, mean age 63 ± 11 years) with prior MI (<1 month: 27%) underwent MRI for assessment of ventricular function and imaging of myocardial delayed enhancement (MDE). We quantified left ventricular ejection fraction (LVEF), left ventricular (LV) mass, and the total MDE mass. A threshold-detection algorithm quantified the total MDE mass (>2 SD above remote signal intensity) and divided it into core MDE (>3 SD) and peri-infarct MDE (2 to 3 SD). The total MDE mass was normalized to the LV mass (%MDE), and both core MDE and peri-infarct MDE to the total MDE mass (%MDE_{core} and %MDE_{peri_infarct}). Cox proportional hazards regression associated the MRI variables with adverse events.

Results: After a median follow-up of 10.6 months, 59 (44%) experienced events including 21 deaths and 38 nonfatal events (3 recurrent MI, 11 congestive heart failure, 15 unstable angina, and 9 appropriate ICD shocks). LVEF, %MDE, and %MDE_{peri_infarct} demonstrated significant Univariate associations with all adverse events ($p=0.02$, $p=0.03$, and $p=0.01$, respectively). Only LVEF and %MDE_{peri_infarct} demonstrated significant associations with death ($p=0.001$ and $p=0.03$) and with death or ICD shocks ($p=0.0002$ and $p=0.004$). By Multivariable analysis, %MDE_{peri_infarct} provided incremental values beyond LVEF for death (χ^2 increase = 4.17, $p=0.04$) and death or ICD shocks (χ^2 increase = 6.42, $p=0.01$), while LVEF maintained significant associations with death ($p=0.001$) and with death or ICD shocks ($p < 0.001$).

Conclusion: In patients with prior MI, %MDE_{peri_infarct} and LVEF provide strong and complementary prognostic values for all-cause mortality and for death or ICD shocks.

148. REAL-TIME COLOR OVERLAY CARDIAC PHASE CONTRAST SPIRAL IMAGING AT 3 TESLA

Chia-Ying Liu, Ph.D, Padimini Varadarajan, M.D., Gerald Pohost, M.D., Krishna Nayak, Ph.D. University of Southern California, Los Angeles, CA, USA.

Introduction: The ability of MRI to quantify blood flow with high spatial and temporal resolution has made it a method of choice for accurate blood flow mapping in-vivo. The challenges comprise the development of techniques to accurately assess blood flow through heart valves. Nayak et al. have performed the real-time color flow MRI (1) in 1.5T systems. In this work we develop a fast spiral phase contrast pulse sequence and real-time reconstruction to compute both velocity and density maps in 3T systems. The spiral was chosen because of its insensitivity to motion and flow, and time efficiency. No breath holding or gating is required. We design two spiral acquisitions including uniform (uds) and variable (vds) density trajectories with different spatial resolutions. Image quality and performance were compared qualitatively by independent observers.

Purpose: To demonstrate and evaluate the usefulness of real-time spiral phase contrast sequences at 3 Tesla for imaging cardiac flow.

Methods: We implemented the phase contrast sequence and image reconstruction algorithm based upon the MRI platform developed by Santos et al. (2). The system uses an external workstation for real-time control of sequence parameters and real-time reconstruction, and is capable of imaging dynamic processes. The pulse sequence consisted of a water selective spectral-spatial excitation (3), bipolar gradient, spiral readout, and gradient spoiler. The operator can interactively adjust the scan plane acquisition parameters. The scan plan prescription can be conveniently defined by deposition points and have the

ability to jump at any time to the standard axial, coronal, and sagittal planes. Flow encoding can be dynamically changed in three different directions. Symmetric encoding of two bipolar waveforms with equal and opposite first moments was used to reconstruct the phase and magnitude images. The following parameters were used for all studies: TR = 12.5 ms, TE = 6.12 ms, FOV = 24 cm, Flip Angle = 20 degree, velocity encoding of 100 cm/sec, and six interleaves. The temporal resolution of 150 ms and nominal spatial resolution of 2.3 mm and 1.5 mm can be achieved for uds and vds respectively. Experiments were performed on a GE Signa Excite HD 3T scanner equipped with gradients supporting 40 mT/m amplitude and 150 T/m/s slew rate, and fast receiver. An eight-channel cardiac phase array coil was used in human subject studies, with only three coil elements used for image reconstruction.

Results and Discussion: A feasibility study to evaluate the real-time performance and image quality was conducted with five healthy subjects. Each volunteer was scanned with the primary interest of visualization of cardiac flow into and out of the left ventricle. Axial, four chamber, three chamber, and two chamber views were scanned and saved. Representative real-time images of the left ventricle aortic outflow both with and without color overlay are shown in Fig. 1. Based on reviews from two independent observers trained in cardiac MR, the vds images were of higher image quality compared to uds. The temporal resolution can be improved by reducing the spatial resolution. For example, four interleaves can be used in the spiral design to achieve the temporal resolution of 100 ms with 3.0 mm of spatial resolution.

Conclusions: This study provides the first demonstration of real-time color flow MRI at 3 Tesla, based on spiral phase contrast imaging. This technique provides rapid visualization of cardiac flow. Further validation in patient cohorts with valvular stenosis and regurgitation are underway. The use of the interactive real-time system offers substantial reductions in scan time and complexity (free-breathing and no gating) for cardiovascular applications.

REFERENCES

1. Nayak KS, et. al. MRM 2000;43:21–258.
2. Santos JM, et.al. 26th Annual Int. Conference IEEE EMBS 2004;1048.
3. Nayak KS, Cunningham CH, et al. MRM 2004;51:655–660.

149. OPTIMIZATION OF A MULTIECHO T2* TECHNIQUE FOR THE MEASUREMENT OF MYOCARDIAL IRON OVERLOAD

Taigang He, Mark Tanner, Paul Kirk, Peter D. Gatehouse, Dudley J. Pennell, MD, David N. Firmin, Ph.D. Royal Brompton Hospital and Imperial College London, London, United Kingdom.

Introduction: Myocardial iron deposition is a common finding in the treatment of thalassaemia major. Cardiovascular magnetic

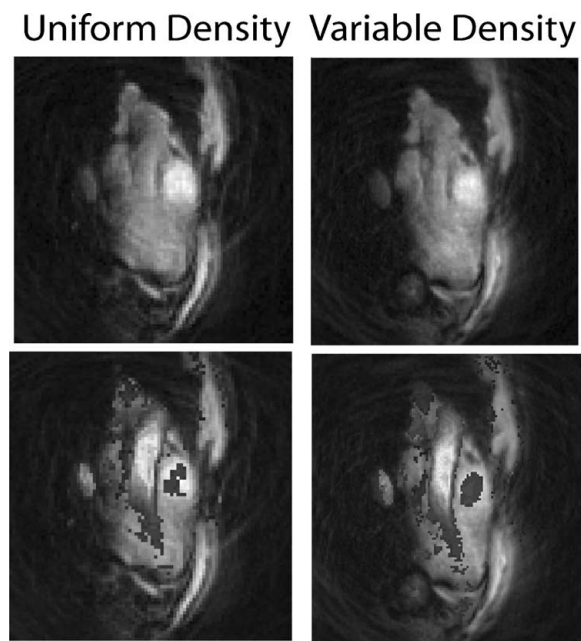


FIG. 1.

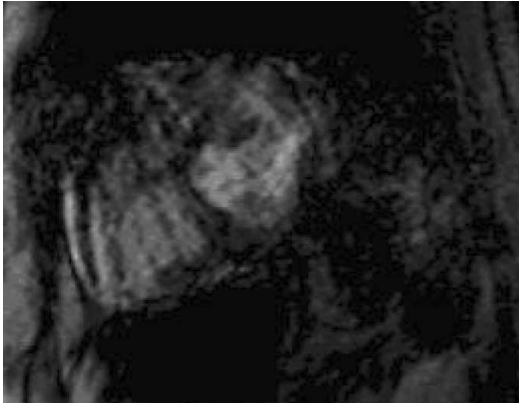


FIG. 1. TE = 32.9 ms.

resonance can provide a non-invasive procedure for assessing the iron content of the myocardium and a single breath-hold multi-echo $T2^*$ technique has been developed (1). $T2^*$ arises principally from local magnetic field irregularities that are increased by iron deposition. Nevertheless, $T2^*$ may also be more dependent on machine and sequence parameters such as shimming and pixel sizes, slice position, timing of data acquisition, flow and motion. The number of echoes and the range of echo times can affect the curve fitting algorithm. All this can introduce errors in $T2^*$ measurements. The aim of this study, therefore, was to optimize the $T2^*$ technique for a more accurate myocardial iron measurement for thalassemia patients.

Methods: A total of 20 thalassemia patients were scanned. A 1.5T scanner (Siemens Sonata) with 4-channel body array coil and gradient performance up to 40 mT/m and 200 T/m/s was used. A single short axis mid-ventricular slice was acquired at sixteen echo times (2.6–32.9 ms, increment 2.02 ms) in a single breath-hold. A spoiled gradient echo sequence was used (flip angle 20° , matrix 128×256 , field of view of 40 cm, TR 40 ms and bandwidth 810 Hz per pixel). A series of cine images were obtained to explain image quality through the cardiac cycle. Also, for non-cine acquisitions, a double inversion pulse was

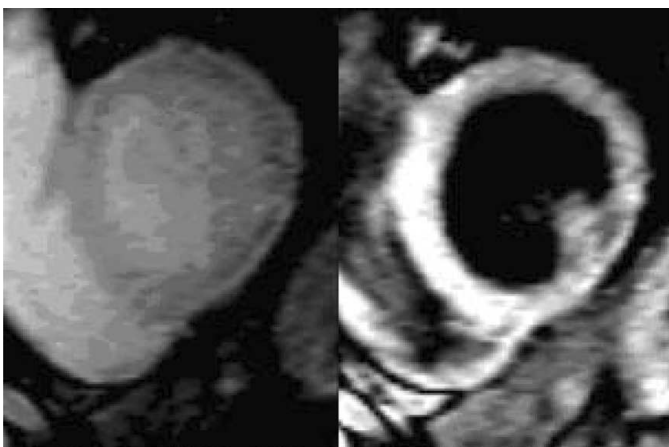


FIG. 2. Black-blood image (right), TE = 2.6 ms.

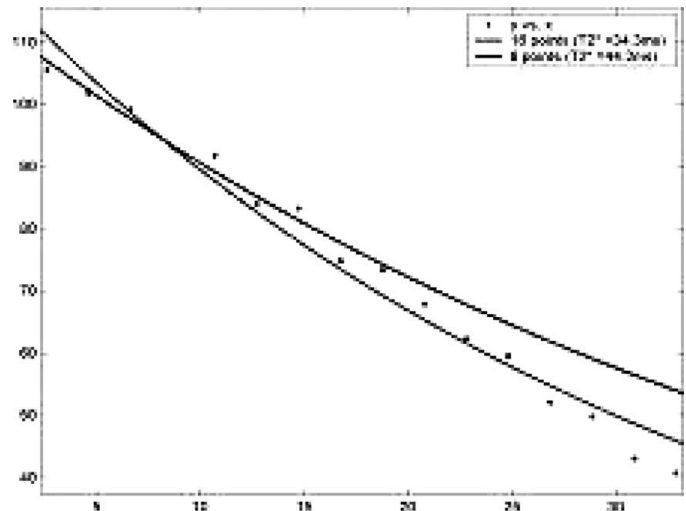


FIG. 3. $T2^*$ estimation with 8/16 echoes.

used to acquire black-blood images to suppress blood artifacts on the myocardium. A homogeneous full-thickness region of interest was chosen in the left ventricular septum. The signal intensity of this region was measured for each image, and a nonlinear curve fitting algorithm was used to derive $T2^*$ values.

Results:

- (1) Late echo images were found to be more sensitive to flow, motion and respiratory artifacts (Fig. 1).
- (2) The black-blood image (right) had very good contrast over the corresponding normal $T2^*$ image (Fig. 2).
- (3) Fig. 3 showed that significant difference of $T2^*$ estimation with different number of echo images.
- (4) Fig. 4 showed the images of different phases during one cardiac cycle (early, systole and late diastole from left to right) for a short (a, 2.6 ms) and a long (b, 32.9 ms) echo times. Images acquired late in the cardiac cycle were showed to be more robust with regard to motion artifacts.

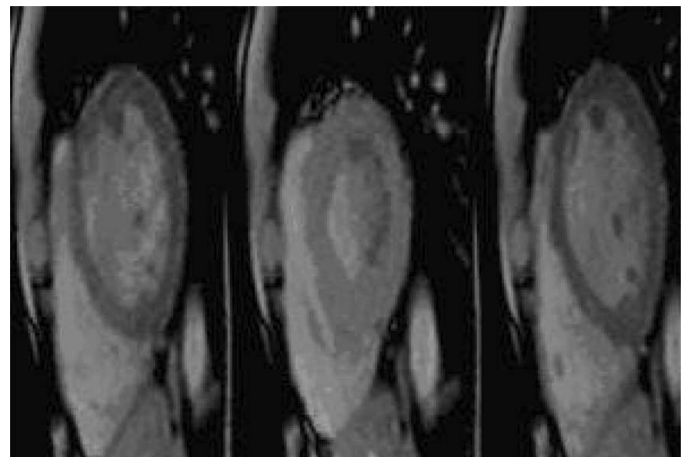


FIG. 4(a). First echo images, TE = 2.6 ms.

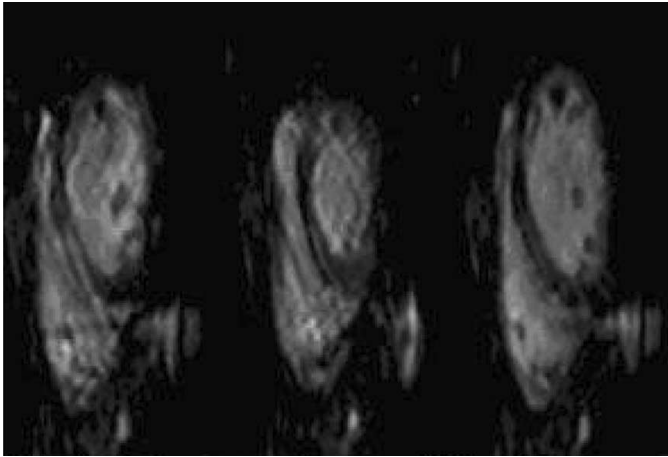


FIG. 4(b). Last echo images, TE = 32.9 ms.

Discussion: For longer $T2^*$ estimation, it is necessary to alter the echo times over a longer range. This can be achieved by extending the echo train while keeping the echo spacing to a minimum. Due to the cardiac motion, timing of the data acquisition and the length of acquisition window must be considered. In the early phase of cardiac cycle, blood flow and myocardial wall motion artifacts are minimized, but acquisition window should be relatively short because of the forthcoming cardiac motion. In systole, myocardium wall was shown to be thicker, but was still subject to motion artifacts (Fig. 4b), middle). Late diastole images proved to be more suitable for $T2^*$ measurements. From our preliminary results, the black-blood imaging compare favorably over the convention one for its contrast and for suppressing blood artifacts from myocardium, which corrupts the exponential fit.

The optimized $T2^*$ technique introduced here should allow relatively accurate and robust estimations of $T2^*$ for the thalassemia patients. It allows study of the factors influencing the $T2^*$ image qualities and makes optimal $T2^*$ estimation available. It may also find potential application in studying other iron overload induced diseases.

Acknowledgement: This work was supported by National Institutes of Health (R01 DK66084-01).

REFERENCE

1. Westwood M, et al. *J Magn Reson Imag* 2003;18:33–39.

150. EXTENT AND LOCALIZATION OF ULTRASMALL PARTICLES OF IRON OXIDE (USPIO) IN RABBIT ATHEROSCLEROTIC PLAQUES AND ITS RELATION TO MACROPHAGE DISTRIBUTION AND TISSUE FACTOR EXPRESSION

Raymond Migrino, MD,¹ Aaron Bubolz,¹ Yangping Liu, MD PhD,¹ Ming Zhao, PhD,¹ Paula Jacobs, PhD,² Eric Jensen,

DVM,¹ ¹Medical College of Wisconsin, Milwaukee, WI, USA, ²Advanced Magnetics, Inc., Cambridge, MA, USA.

Introduction: The vulnerable plaque plays a central role in the morbidity and mortality associated with atherosclerotic vascular disease. Ultrasmall particles of iron oxide (USPIO) have been shown to localize to plaques and have been used as negative contrast agents for plaque magnetic resonance imaging. The vulnerability of plaque to rupture and to subsequently produce a thrombotic event is related to macrophage content and tissue factor expression. However, the relationship in the distribution and localization of USPIO and these markers of plaque vulnerability is not well established.

Purpose: In this pilot study, the aim was to determine the distribution and localization of USPIO in rabbit atherosclerotic plaque and compare it to macrophage and tissue factor extent and distribution.

Methods: Two New Zealand white rabbits (weight 2.5 kg) were treated to 12 weeks of 2% cholesterol-6% peanut oil diet to produce atherosclerosis. A rabbit on regular chow served as control. At the end of 12 weeks, ferumoxtran USPIO (Advanced Magnetics, Cambridge MA) at 23 mg/kg IV was given and the rabbits sacrificed 5 days later. The thoracic aorta was harvested and 6 equidistant sections were obtained per rabbit. The aortic sections underwent Prussian blue staining for iron, RAM-11 staining for macrophages and staining with anti-tissue factor antibody. The distribution and extent of staining was determined and compared.

Results: In the normal control, iron, macrophage or tissue factor were not found in the intima/media. In atherosclerotic rabbits, 13 distinct plaques/neointima were seen. In 10 of these plaques (77%), iron was found. The extent of iron, macrophage and tissue factor expression in relation to total plaque areas were (mean \pm sem) 9 ± 3 , 48 ± 12 and $68 \pm 9\%$ respectively ($p = 0.02$ iron vs. macrophage, $p < 0.001$ iron vs. tissue factor,



FIG. 1.

p = 0.13 macrophage vs. tissue factor) (Fig. 1). Iron was found in the shoulder region in 7/10 plaques. Macrophages were distributed mostly in the shoulder region and in the base of the neointima. Tissue factor expression was diffuse but greatest in the luminal border. It was seen in both the neointima and adventitia.

Conclusions: The extent of distribution of ferumoxtran USPIO in rabbit atherosclerotic plaque is significantly less than the macrophage content and tissue factor expression in plaque. This may limit in-vivo magnetic resonance imaging of plaque. However, the distribution of USPIO in the shoulder region and in regions with high tissue factor expression may signify iron oxide localization in the plaque region most vulnerable to rupture, a finding potentially useful for vulnerable plaque imaging.

151. PRELIMINARY VALIDATION OF CIRCUMFERENTIAL STRAIN MEASUREMENTS USING DENSE AT 1.5T AND 3T

Alexander P. Lin, BS,¹ J. Michael Tyszka, PhD,¹ Eric Bennett, PhD,² Scott Fraser, PhD,¹ Han Wen, PhD.² ¹California Institute of Technology, Pasadena, CA, USA, ²National Heart Lung Blood Institute/National Institutes of Health, Bethesda, MD, USA.

Introduction: Carotid artery wall compliance has been implicated in a broad range of cardiovascular and neurological diseases and is directly correlated to increased cardiovascular morbidity and mortality. Regional compliance in the coronary artery wall is further correlated with the extent of rupture-prone vulnerable lesions. Current means of measuring regional wall compliance utilizes intravascular ultrasound; however, the procedure has inherent risks in the carotid artery. The development of a non-invasive means of mapping wall strain would allow the same assessment and potentially give non-invasive risk indicators of atherosclerotic cardiovascular disease. Displacement ENcoding with Stimulated Echoes (DENSE) is a MRI pulse sequence designed to encode motion over time intervals comparable to a cardiac cycle. DENSE has been primarily used to track motion of cardiac tissue, producing color-coded strain maps that can measure the elasticity or stiffness of the heart tissue. This technique has been applied at 1.5T and 3T where both displacement

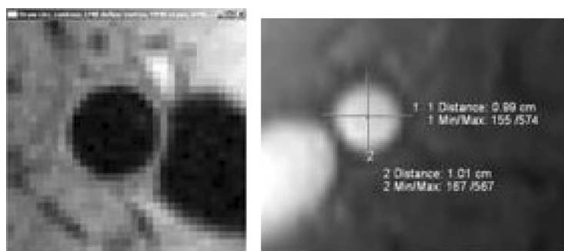


FIG. 1. a) left ROI of DENSE circumferential strain measurement b) right: Lumen diameter measurements from cine MRI.

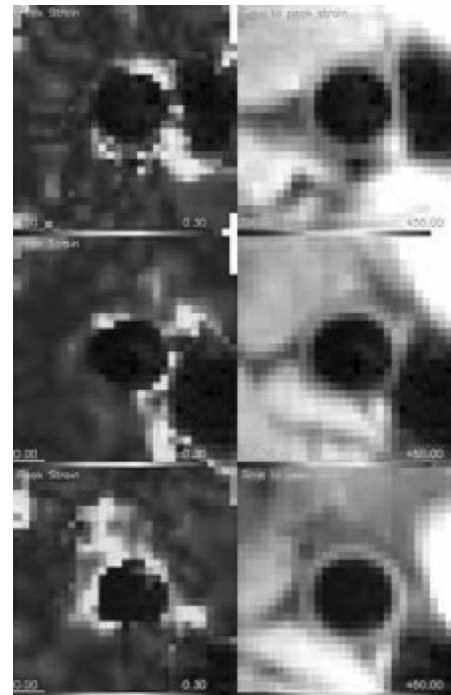


FIG. 2. Left: DENSE color-coded strain map. Right: DENSE image at 3T.

fields and circumferential strain can be measured around the common carotid artery. It is our aim to validate DENSE carotid strain measurements with manual measurements of lumen wall diameters at systole and diastole acquired by standard cine MRI at both field strengths.

Methods: Seven normal volunteers were scanned on a 3.0T whole-body clinical scanner (Trio, Siemens, Germany) using an 8 cm surface coil (Nova Medical, MA). Four normal volunteers were scanned on a 1.5T clinical scanner (Sonata,

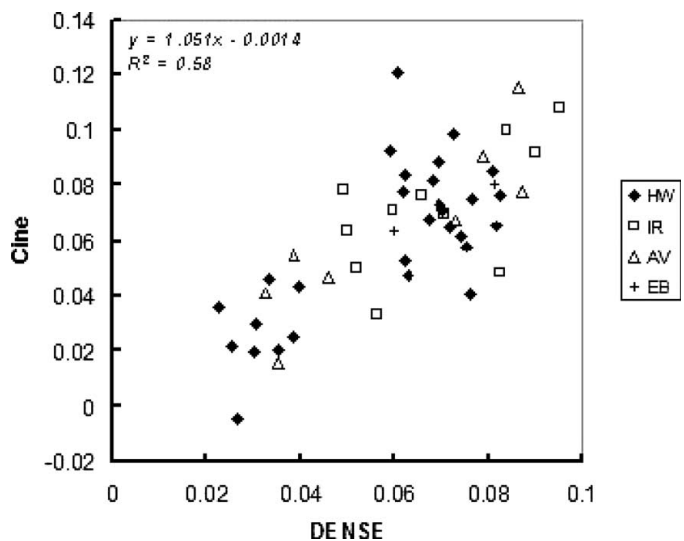


FIG. 3. DENSE and CINE comparison of average circumferential strain at 1.5T.

Siemens, Germany) using a 4-channel carotid coil array (Mach-Net, Netherland). Initial three plane scout images were acquired to localize of the left and/or right carotid artery and optimize coil location. 2D TOF images were acquired and MIPs used for slice positioning. Three or five slices were centered 1 cm below the bifurcation of the carotid arteries. DENSE images of the carotid artery wall were acquired at $0.6 \times 0.6 \times 4.0$ mm resolution, including displacement encoding in three oblique directions to produced a pixel-by-pixel 3D displacement map of the vessel wall and surrounding tissue. Image acquisition was consistently placed at the time of maximum lumen diameter, while in two separate scans the encoding portion was placed at 40 ms and 80 ms after the R-wave to capture the maximum wall strain and intermediate strain. Total scan time for the DENSE images was 30 minutes. An ECG-gated cine scan was acquired at the same location and resolution as DENSE images to determine maximum and minimum lumen diameter. DENSE raw data was processed to produce strain maps (DENSEView, Bethesda, MD) and compute average circumferential strain (Fig. 1a). For comparison, lumen vessel horizontal and vertical diameters were measured from the cine scans at the same time points as the DENSE images and the average circumferential strain was also calculated (Fig. 1b). The correlation between the two measurements provides a measure of accuracy.

Results: While the 1.5T scans were relatively routine, imaging at 3.0T introduced technical issues such as the lack of FDA approved dual surface coils, increased susceptibility artifacts, and greater effect on ECG gating. These obstructions were surmounted by optimizing coil placement, manual shimming, and centralized lead placement, respectively. The improvements resulted in well-resolved DENSE images of the carotid arteries (Fig. 2). The comparison between cine displacement and DENSE strain measurements demonstrated good correlation at both field strengths (Fig. 3). The main source of uncertainty came from the measurement of lumen diameter in the CINE images, which was limited by the spatial resolution.

Conclusion: DENSE measurement of carotid artery wall strain has been corroborated with direct lumen size measurements from CINE images at both 1.5T and 3T. Future effort will be focused on improving the RF coil at 3T and the spatial resolution of the CINE measurement for a more precise comparison.

152. POSITIVE MAGNETIC RESONANCE SIGNAL ENHANCEMENT FROM FERRITIN USING A GRASP (GRE ACQUISITION FOR SUPERPARAMAGNETIC PARTICLES) SEQUENCE: EX VIVO AND IN VIVO STUDY

Venkatesh Mani, PhD, Karen C. Briley-Saebo, PhD, Fabien Hyafil, MD, Vitalii V. Itskovich, PhD, Zahi A. Fayad, PhD. Mount Sinai School of Medicine, New York, NY, USA.

Introduction: White marker imaging sequences are currently being designed for identifying and tracking iron-laden cells. Recent *in vitro* studies using the GRASP sequence show that

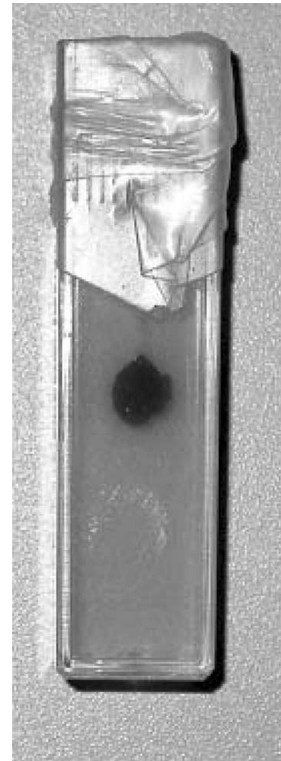


FIG. 1. Phantom of blood clot containing 100 mM ferritin in 2% agar gel.

modifications of traditional GRE sequences to include manually controlled dephasing gradients resulted in significant signal enhancement in gels containing iron particles. Enhancement was observed at low iron concentration levels, suggesting that this sequence may be useful for the identification of *in vivo* ferritin that is commonly found in intra-plaque haemorrhage.

Purpose: The purpose of our study was to verify the efficacy of white marker imaging technique (1) to produce positive signal in the presence of ferritin using both *ex vivo* clot models and *in vivo* rabbit models.

Methods: All imaging was performed at 1.5T using custom-built phased array carotid coils. T2* GRE and GRASP sequences were used with TR = 300 ms, TE = 5, 10, or 25 ms, and variable dephasing gradients. *Ex vivo* blood clots were prepared by drawing 25 mL of fresh human blood. The blood was immediately mixed with ferritin (0–100 mM Fe) and transferred to 0.5 mL plastic wells. The samples were incubated for 2 hours at 37°C and placed overnight at 4°C in order to allow for optimal clotting. Excess blood was removed and the clots were washed in PBS prior to placement in 2% agar gel (Fig. 1). *In vivo* ferritin imaging results were obtained by crushing the right carotid artery of New Zealand White rabbits. Imaging was performed every week after injury until significant T2* effects were observed on normal GRE sequences (38 days post injury). Immediately after imaging, the rabbits were sacrificed and the carotid arteries removed. The arteries were placed in formaldehyde overnight before being transferred to 2% agar gel. The *ex vivo* carotid

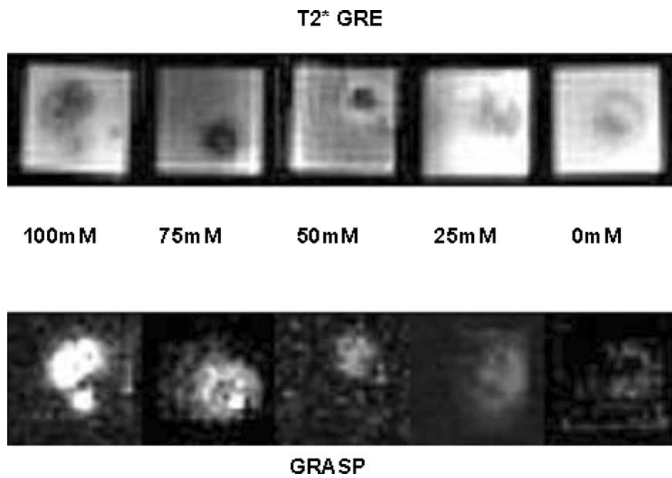


FIG. 2. Ex vivo MR images of blood clots containing different concentrations of ferritin, using T2* GRE and Grasp sequences. Imaging parameters: T2* GRE: TR/TE = 300/25 ms, GRASP: TR/TE = 300/10 ms, % gradient rephasing = 35%.

arteries (both injured and control) were also imaged using T2* GRE and GRASP sequences. Immediately after *ex vivo* imaging, the carotid arteries were removed from the 2% gel, fixed in paraffin, and stained for iron used Perls Prussian Blue. The histology results were compared to both the *in vivo* and *ex vivo* carotid images.

Results: The results from the *ex vivo* blood clots suggest that the GRASP sequence is able to detect ferritin in clotted blood (Fig. 2). Additionally, these results suggest that gain in signal enhancement is dependent upon the amount of ferritin present in the clot. Fig. 3 shows the *in vivo* results obtained 38 days post crush injury in the carotid artery of a rabbit. There was good correlation between the signal loss observed on T2* GRE sequences (TE = 25 ms) and the signal enhancement observed

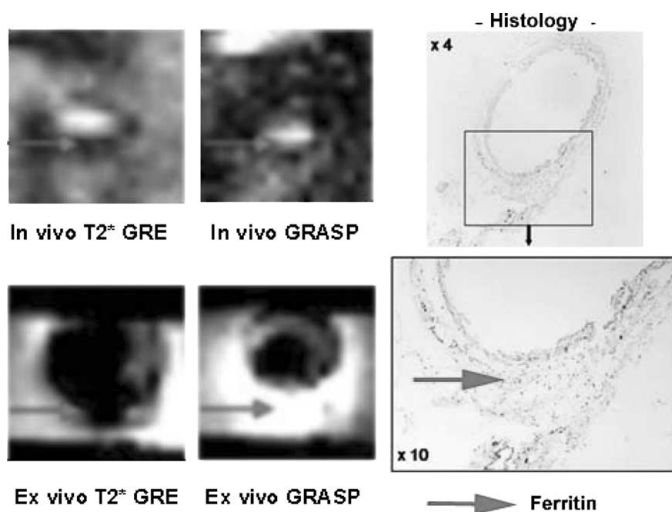


FIG. 3. In vivo and ex vivo images of carotid artery, 38 days after crush injury showing T2* signal loss and positive GRASP signal where ferritin is present as verified by histology.

with GRASP (35% rephasing, TE = 10 ms). Additionally, the *ex vivo* carotid results correlated well with the *in vivo* results, as shown in Fig. 3. The presence of ferritin in the injured areas was confirmed by histology. The location of ferritin observed by microscopy matched the location of the signal enhancement observed using the GRASP sequence.

Conclusions: This study shows that modified GRE sequences with variable dephasing gradients can be used *in vivo* to generate positive signal enhancement in the presence of ferritin.

REFERENCE

1. Seppenwoolde, et al. Magn Reson Med 2003;50:784-790.

153. POST-EXERCISE PHOSPHOCREATINE RECOVERY KINETICS IN PERIPHERAL ARTERIAL DISEASE: A NOVEL TOOL FOR PREDICTING CLINICAL DETERIORATION

David C. Isbell, MD, Craig H. Meyer, PhD, Stuart S. Berr, PhD, Arthur Weltman, PhD, Frederick H. Epstein, PhD, Walter J. Rogers, PhD, Klaus D. Hagspiel, MD, Nancy L. Harthun, MD, Christopher M. Kramer, MD. *University of Virginia, Charlottesville, VA, USA.*

Introduction: Modalities currently utilized to diagnose peripheral arterial disease (PAD) and assess its severity are inadequate. Although the presence of flow-limiting, macrovascular atherosclerosis can generally be established, these tests frequently fail to predict symptoms and clinical outcomes in PAD patients. Diagnostic techniques that focus on the skeletal muscle, the end-organ affected in PAD, may be better suited than conventional methods for characterizing disease severity, monitoring its progression, and predicting clinical events.

Purpose: We have previously demonstrated the utility of the post-exercise phosphocreatine (PCr) recovery time constant in identifying mild to moderate PAD. The purpose of this study was to examine the prognostic utility of the PCr recovery time constant acquired using ³¹P phosphorus magnetic resonance spectroscopy (MRS) in patients with mild to moderate PAD.

Methods: Twenty patients (mean age 67 ± 10 years) with mild to moderate PAD (mean ankle brachial index (ABI) 0.62 ± 0.13) were enrolled. Subjects were placed supine in the MR scanner with the calf at the isocenter of the magnet. After shimming to minimize non-uniformity of the magnetic field, 5 baseline spectra were acquired. An MRI compatible plantarflexion exercise device constructed for use in this protocol was then affixed to the MR table. The subject was instructed to exercise the calf muscle by pushing against the pedal at a steady rate until limiting symptoms developed. ³¹P spectra were acquired with a Siemens Sonata 1.5 T MR scanner using a single-pulse, surface coil-localized, 512-ms free induction decay (FID) acquisition with the coil centered on the mid-calf. A standard ³¹P surface coil embedded in the patient table was employed. Following 4 RF preparation pulses, twenty-five signal averages at

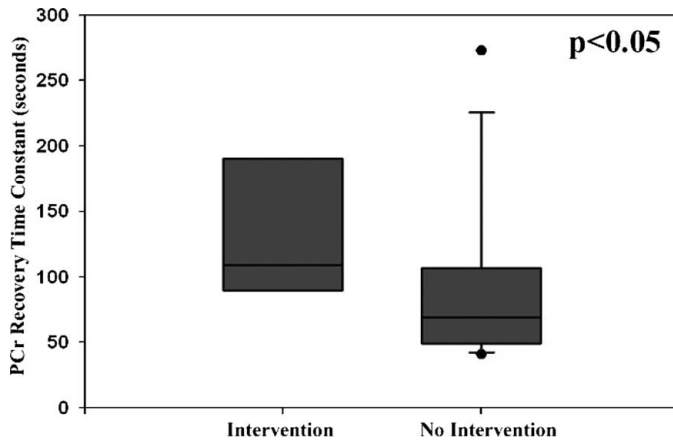


FIG. 1.

a repetition time of 550 ms were acquired for a total acquisition time of 16 s per spectrum. Siemens spectroscopy analysis software on a Leonardo workstation was used to estimate relative concentrations of ATP, PCr and Pi. FIDs were multiplied by an exponential with a time-constant of 110 ms and zero-filled from 1024 to 2048 points prior to Fourier transformation. Phase and baseline corrections, followed by Lorentzian fitting and integration of the spectral peaks corresponding to ATP, PCr, and Pi were carried out. The PCr recovery time constant was calculated by monoexponential fit of the PCr levels versus time. Clinical follow-up consisted of chart review and direct patient contact to determine clinical events and/or revascularization procedures following the one-time measurement of the PCr recovery time constant.

Results: Clinical follow-up was complete in 95% of PAD subjects. Six limbs required revascularization or amputation during a mean follow-up period of 14 ± 3 months. Median PCr recovery was 109.0 seconds (25th and 75th percentiles = 90.0 and 175.0 seconds) in limbs that required surgery, angioplasty, or amputation during the follow-up period compared to 69.0 seconds in limbs that did not (25th and 75th percentiles = 50.0 and 102.0 seconds; $p = 0.044$) (Fig. 1). Median ABI was similar in patients requiring revascularization or amputation (0.60; 25th and 75th percentiles = 0.52 and 0.66) and those that did not (0.60; 25th and 75th percentiles = 0.52 and 0.69; $p = \text{NS}$). During follow-up, there were 3 myocardial infarctions, 1 stroke, and 1 vascular death. The PCr recovery time constant was similar in patients who experienced one of these clinical events compared to those that did not ($p = \text{NS}$).

Conclusions: A one time measure of post-exercise PCr recovery kinetics identifies PAD subjects with mild to moderate disease at greater risk of clinical deterioration requiring intervention at one year while the resting ABI does not. This test

represents a potential advance in the risk stratification of patients with mild to moderate PAD.

154. GADOLINIUM-DTPA CONTRAST ENHANCEMENT IN ACUTE ENDOCARDITIS AS EXPRESSION OF MYOCARDIAL INVOLVEMENT

Jorge I. Parras, MD, Ricardo O. Obregón, MD, Edgar H. García, MD, Raúl Pelozo, MD, Raúl Cayré, MD, Walter J. García, MD, Mónica N. Cocco, MD. *Instituto de Cardiología, Corrientes, Argentina.*

Introduction: Contrast enhancement in myocarditis is a sign of myocardial involvement. It is unknown if in acute endocarditis occurred the same phenomenon.

Purpose: 1) To evaluate Gadolinium-DTPA contrast enhancement in acute endocarditis 2) To compare the results between three groups of subjects: normals, patients with diagnosis of acute myocarditis and patient with endocarditis.

Methods: All 24 of our patients had acute myocarditis on clinical grounds. Comparison was done with 10 patients with acute endocarditis and 10 healthy subjects as controls. Gadolinium-DTPA Magnetic Resonance Imaging (MRI) was done to all the patients within three days of diagnosis. Data were expressed as mean and standard deviation. Comparisons of continuous variables between groups were analyzed with student t test. Categorical variables were analyzed with Pearson Chi square test. A value lesser than 0.05 was considered significant. Intensity of signals of T1-weighted sequences was compared between myocardial and skeletal muscles before and after contrast administration.

Results: Table shows the different intensities of contrast enhancement according to the location.

Conclusions: Gadolinium-DTPA enhancement was detected in both groups of patients with diagnosis of endocarditis and myocarditis. The difference in grade of contrast enhancement between the two groups was not statistically significant. Our study shows that myocardial involvement is present during acute endocarditis.

Different intensities and their relationships with places of measurements

Variable	Normals	Myocarditis	Endocarditis
Difference	1.23 ± 0.21	$1.58 \pm 0.25^*$	$1.54 \pm 0.34^\#$
Myocardium/myocardium	1.19 ± 0.19	$1.57 \pm 0.24^*$	$1.55 \pm 0.34^\#$
Muscle/muscle	1.05 ± 0.17	1.08 ± 0.17	1.08 ± 0.20

* $p < 0.05$, myocarditis compared to normals.

^\# $p < 0.05$, endocarditis compared to normals.

Friday, January 20, 2006

3:30 PM–5:00 PM

Oral Abstracts: The Blood Vessel as a Diagnostic Target in Atherosclerosis

155. VASCULAR MRI DEMONSTRATES EARLY REDUCTION IN AORTIC ATHEROSCLEROSIS WITH INCREASED ARTERIAL DISTENSIBILITY AND IMPROVED ENDOTHELIAL FUNCTION AFTER INITIATION OF STATIN THERAPY

Justin Lee, Cheerag Shirodaria, Jane Francis, Clare Jackson, Matthew Robson, Stefan Neubauer, Keith Channon, Robin Choudhury, Frank Wiesmann *University of Oxford, Oxford, United Kingdom*

Introduction: In arteriosclerosis research, tools with greater sensitivity to evaluate response to treatment are urgently required. MRI shows promise in non-invasive assessment of both vascular structure and function. Cholesterol lowering with statins rapidly improves measures of endothelial and central arterial function and can reduce plaque size, assessed by MRI after 6–24 months. However, the relationship between structural and functional changes and their relative timings are not well established. This information is critical to both design and interpretation of treatment studies and an important component of comprehensive vascular phenotyping with MRI.

Purpose: We hypothesised that improvement in vascular function following statin initiation would precede and predict regression of atherosclerosis, providing an effective early measure of response to treatment in patients with coronary artery disease.

Methods: Thirty-four newly diagnosed coronary artery disease patients underwent MRI at 1.5 Tesla before as well as 3 and 12 months after commencing statin treatment. Aortic distensibility (relative change in cross-sectional area per mmHg of pulse pressure) was measured using trueFISP cine (TR/TE = 2.8 ms/1.4 ms, in plane resolution 2 mm, slice thickness 7 mm). To assess endothelial function, brachial artery flow

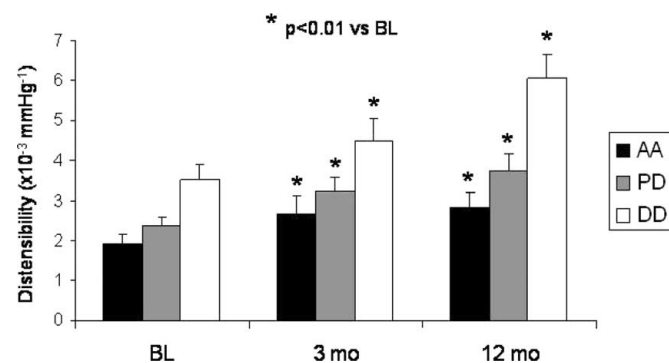


FIG. 1. Change in Aortic Distensibility.

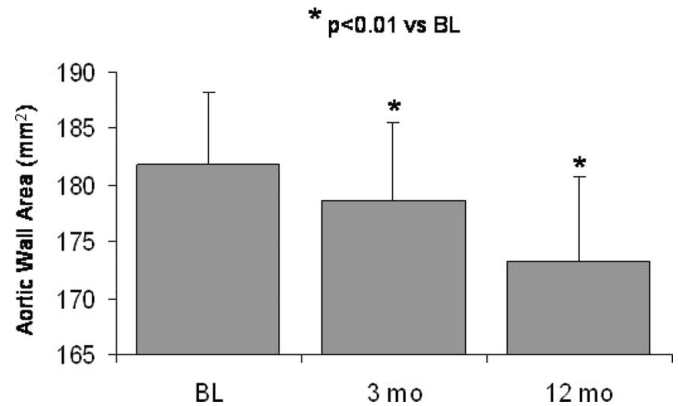


FIG. 2. Change in Aortic Atherosclerosis.

mediated dilatation or FMD (maximum relative change in area during postischemic hyperemia) and maximum response to sublingual 400 mcg glyceryl trinitrate (NTG) was measured using trueFISP cine. A stack of eleven transverse black blood turbo spin echo images of the descending thoracic aorta was acquired to determine vessel wall cross sectional area (TR/TE 750 ms/11 ms, in plane resolution 0.8 mm, slice thickness 5 mm).

Results: All patients received statin treatment (>80% simvastatin 40 mg daily). Mean total cholesterol was 202 ± 8 mg/dL at baseline, 151 ± 6 mg/dL at 3 months and 152 ± 6 mg/dL at 12 months. Significant ($p < 0.05$) increases in distensibility of the ascending (AA), proximal descending (PD) and distal descending (DD) aorta respectively occurred after 3 (and 12) months of 39% (46%), 37% (58%) and 28% (72%), of statin therapy (Fig. 1). Mean brachial artery FMD improved from 8.1% to 12.8% ($p < 0.003$) at 3 months and 13.7% at 12 months ($p < 0.001$). Response to NTG did not change significantly. Mean aortic wall cross sectional area decreased by 2.5% at 3 months and by 5.4% at 12 months (Fig. 2) while mean aortic lumen area remained stable throughout: 422 ± 14 mm², 422 ± 15 mm² and 427 ± 16 mm² at baseline, 3 and 12 months ($p = \text{NS}$ between timepoints). This implies that regression of atherosclerosis involves reversal of positive remodelling. Importantly changes between 0 and 3 months were strongly correlated with changes between 0 and 12 months, for aortic distensibility ($r = 0.55$, $p < 0.01$), FMD ($r = 0.49$, $p < 0.05$) and aortic wall area ($r = 0.77$ $p < 0.001$).

Conclusions: Using small numbers of patients MRI can detect significant changes in aortic distensibility, brachial artery FMD and aortic atherosclerosis within 3 months of commencing statin treatment. Changes at 3 months correlate well with changes at 12 months, suggesting that global vascular assessment with MRI may be valuable in allowing efficient, early quantification of response to treatment. Cholesterol levels appeared to plateau within 3 months, therefore further improvement in vascular parameters up to 12 months may represent non-cholesterol mediated statin effects.

156. CLINICAL FACTORS IMPACTING CORONARY ARTERY MRI QUALITY

April M. K. Chow, Susan B. Yeon, MD, Warren J. Manning, MD, Kraig V. Kissinger, Dana C. Peters. *Beth Israel Deaconess Medical Center, Boston, MA, USA.*

Introduction: Coronary artery imaging with MRI has been shown to be accurate compared with X-ray coronary angiography (1). However, a significant minority of scans are of suboptimal/poor quality. We sought to investigate the clinical predictors of these suboptimal/poor quality scans.

Methods: Data from 40 consecutive patients at our institution from February to August 2005, who underwent clinical targeted MR coronary angiography of their left and right coronary systems on a Philips 1.5 T scanner. The imaging method was similar to that described by Kim et al. Typical scan parameters were: 3D gradient echo imaging, TR/TE/ $\theta = 7.6$ ms/2 ms/30°, 270 mm FOV, 384 × 269 matrix, 13 3 mm slices, T2prep, fat-saturation, ECG-triggering, ~70 ms acquisition window, navigator-gating and tracking with a 5 mm window. For each scan (N = 77), subjective image quality was assessed by an experienced cardiologist (scale of 1–4, 1 = poor, 2 = fair, 3 = good, 4 = excellent). These ratings were then combined to compare high quality (rating 3 or 4) vs. low quality (1 or 2) scans. Patient clinical characteristics (e.g. age, body mass index (BMI)) were obtained. Heart-rate and diaphragmatic position were recorded continuously throughout the coronary scans. From these data, NAV efficiency, NAV quality (subjective rating of based on presence of drift or oscillation or improper NAV window) and the % of heart-beats which differed by 150 ms from the expected heart-beat length were measured. Whether the coronary scan was performed during a true (diastolic or systolic) rest period (RP) of the cardiac cycle was determined. Presence of motion artifact was assessed (yes/no). All continuous variables were tested with an unpaired two-tailed Student’s t-test. All yes/no parameters were studied using the Fisher’s exact test.

Results: Fig. 1 shows examples of excellent, good, fair and poor quality studies. Twenty (26%) of scans were low quality (fair, N = 16; poor, N = 4). All excellent scans (18%) were obtained within 40 minutes after the exam had started, while all poor quality (5%) scans were obtained more than 80 minutes after the onset of the exam. All scans with a NAV efficiency

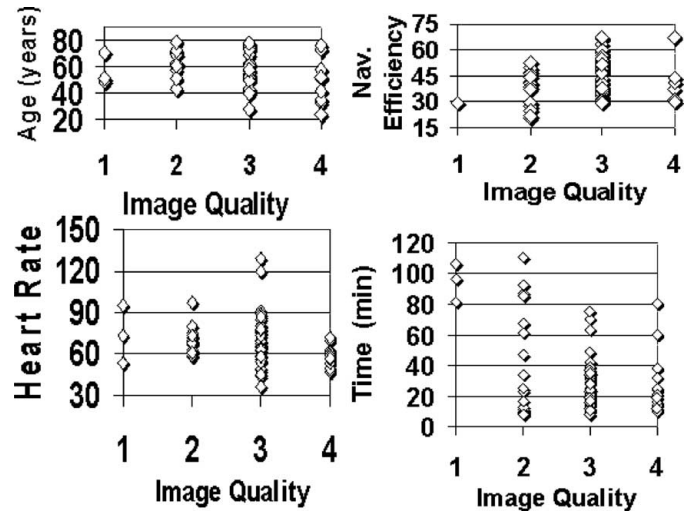


FIG. 2. Raw data from 77 coronary scans.

less than 29% (N = 6) were of poor/fair quality, while all scans with an efficiency >53% (N = 9) were of good/excellent quality. The Table summarizes results. High image quality was found to correlate with younger age, lower BMI, and high navigator efficiency, but not heart-rate or navigator quality. However, all scans of patients with HR < 53 bpm were high quality (N = 7). Figure 2 provides raw data on age, time of scan relative to beginning of exam, NAV efficiency and heart-rate.

Test	High quality	Low quality	p value
Age (years)	54	63	p < 0.05
Time* (min)	26	54	p < 0.05
Heart rate (bpm)	65	71	p = 0.2
Nav high quality?	87%	73%	p = 0.2
% of short beats†	5.7%	22%	p < 0.05
Motion artifacts?	5%	77%	p < 0.05
BMI (kg/m ²)	26	29	p < 0.05
RP match (yes, no)	91%	61%	p < 0.05
Nav Efficiency (%)	44%	37%	p < 0.05

*Time from beginning of exam to start of coronary scans.

†% of heart-beats shortened by at least 150 ms from expected length.

Discussion and Conclusion: The causes for low quality scans in our study are disparate, including imaging during systole

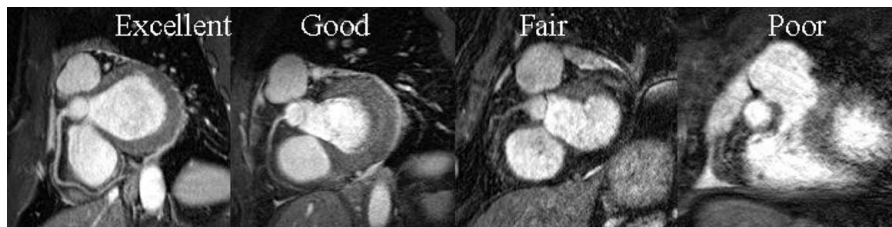


FIG. 1. Shows the RCA view for patients with (left to right) excellent, good, fair and poor quality scans.

(possibly indicative of ECG instability or lack of diastolic diastasis period), and scanning very late in the imaging session (which may result in increased patient motion due to restlessness). Motion plays a significant role in image quality, yet neither heart-rate nor NAV quality correlated with image quality, while time spent inside the scanner, NAV efficiency, age and BMI all did correlate. Low quality MRI does not appear to be related to failures of ECG-gating and NAV techniques to compensate for the wide range of cardiac and respiratory motion patterns found in patients. Instead, low quality is associated with sources of motion that are not currently compensated for at all (e.g. restlessness due to long scan times, late scans, and cardiac motion from a heart-beat with no period of diastasis). Efforts should be made to perform coronary MRI early in the examination period.

REFERENCE

1. Kim WY, et al. N Engl J Med. 2001;345:1863-9.

157. MRI ASSESSMENT OF SUBCLINICAL CORONARY ATHEROSCLEROSIS AND REMODELING IN OLDER PATIENTS WITH AND WITHOUT DIABETES

Masahiro Terashima, MD, PhD,¹ Patricia K. Nguyen, MD,¹ Geoffrey D. Rubin, MD,¹ Shoichi Ehara, MD, PhD,¹ Carlos Iribarren, MD, MPH,² Brian K. Courtney, MD,¹ Alan S. Go, MD,² Stephen P. Fortmann, MD,¹ Michael V. McConnell, MD, MSEE,¹ Donald W. Reynolds Cardiovascular Clinical Research Center, Stanford University School of Medicine, Stanford, CA, USA, ²Division of Reseach, Kaiser Permanente, Oakland, CA, USA.

Objectives: Noninvasive measures of subclinical coronary atherosclerosis may identify subjects at increased risk. Direct imaging of the coronary wall by MRI is challenging due to the small size of coronary arteries and rapid motion. We investigated high-resolution black-blood spiral coronary MRI in an asymptomatic older patient cohort who had coronary artery calcification (CAC) assessed by CT, including patients with diabetes.

Methods: A cohort of 1,007 older patients (age 60–72 years, 38% female) without a history of cardiovascular disease receiving care at Kaiser Permanente of Northern California underwent CT. A subset of 222 patients had coronary wall imaging using MRI. Cross-sectional images of the right coronary artery (RCA) were acquired using a gated, breathheld spiral black-blood coronary MRI sequence (0.7 mm resolution) on a 1.5T MR scanner. MR image quality was assessed first, blinded to patient information, with adequate images only subjected to quantitative analysis. Coronary vessel area (VA) and lumen area (LA) were traced, again blinded, with wall area (WA) calculated as $WA = VA - LA$. CAC quantification was performed on a multi-detector CT scanner with prospective ECG-gating using the Agatston scoring method.

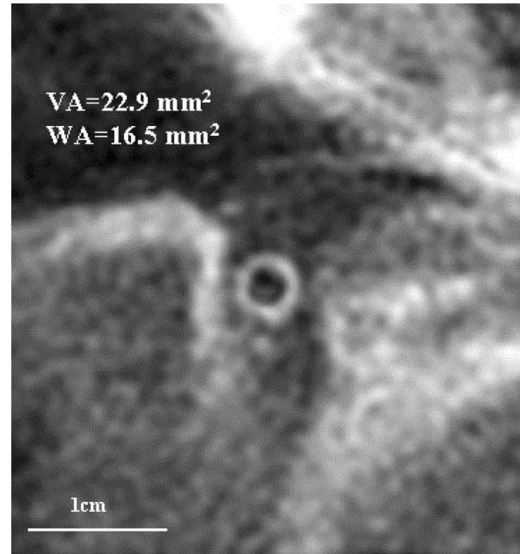


FIG. 1. Representative coronary wall imaging with MRI.

Results: In this older cohort, MR coronary wall image quality was adequate in 68% of subjects, leaving 150 (age 66 ± 3 , 37% female) for quantitative analysis (Fig. 1A). In patients with a high total CAC (≥ 100 , $n = 59$), both coronary WA and VA by MRI were significantly increased (WA: $24.6 \pm 6.1 \text{ mm}^2$ vs. $21.9 \pm 5.7 \text{ mm}^2$ for total CAC < 100 , $p = 0.008$, VA: 34.6 ± 8.3 vs. $30.7 \pm 7.9 \text{ mm}^2$, $p = 0.005$). The presence of any CAC in the RCA was more strongly associated with increased coronary WA and VA ($p < 0.001$ for both WA and VA). These findings remained significant in multiple stepwise regression analysis after adjustment for potential confounders (total CAC: $p < 0.01$ and RCA-CAC, $p < 0.001$). In patients with diabetes ($n = 22$), both CAC and WA were significantly increased compared with non-diabetic patients (CAC: 490 ± 866 vs. 166 ± 342 , $p = 0.03$, WA: 25.2 ± 6.5 vs. $22.4 \pm 5.8 \text{ mm}^2$, $p = 0.04$). There was a similar, but non-significant, increase in VA (DM vs. non-DM: 34.4 ± 8.2 vs. $31.7 \pm 8.2 \text{ mm}^2$, $p = 0.2$).

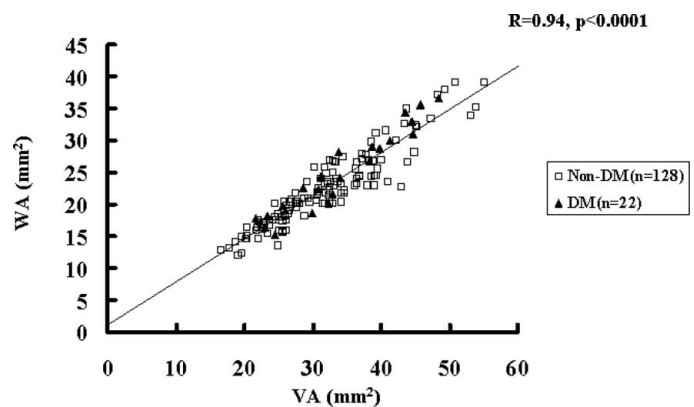


FIG. 2. Coronary artery remodeling: Correlation between coronary WA and VA. Patients with diabetes have a similar, but non-significant, increase in VA, but increased WA compared with non-diabetic patients.

Conclusions: Noninvasive coronary wall imaging by MRI can be performed in the majority of patients in an older cohort. In patients with evidence of subclinical atherosclerosis on CT, MRI demonstrated increased coronary wall area and positive remodeling. Diabetic patients had evidence of increased subclinical atherosclerosis on CT and MRI. While improvements in image quality are needed, black-blood coronary MRI has the potential to contribute to the noninvasive assessment of subclinical coronary atherosclerosis and remodeling in at-risk patient groups.

158. CONTRAST-ENHANCED WHOLE HEART CORONARY MRA WITH MS-325: EXPERIENCE IN 17 VOLUNTEERS

Sebastian Kelle, MD, Tarinee Tangcharoen, MD, Thomas Thouet, MD, Thaiz Schmal, MD, Ingo Paetsch, MD, Axel Bornstedt, PhD, Eckart Fleck, MD, Eike Nagel, MD. German Heart Institute Berlin, Berlin, Germany.

Introduction: Currently, magnetic resonance coronary angiography (MRCA) is rapidly attaining adequate quality for clinical use. It is, however, limited by low signal-to-noise ratios and restricted coverage of the whole coronary artery tree, which might be significantly improved by intravascular contrast agents.

Purpose: To evaluate the feasibility of contrast-enhanced MRCA using the intravascular contrast agent MS-325 (EPIX Pharmaceuticals, Cambridge, MA, USA) in the delineation of coronary arteries.

Methods: In 17 volunteers (6 men, 11 women; age range, 20–43 years; mean age, 30 ± 8 years) free-breathing navigator whole heart MR coronary angiography was performed before and after injection of MS-325 (0.05 mmol/kg body weight). Measurements were done in two groups; voxel size was between $1.02 \times 1.02 \times 1.4$ and $1.18 \times 1.18 \times 1.8$ mm. Signal intensity from the myocardium and left ventricular blood were assessed for non-enhanced and contrast-enhanced images and contrast calculated (signal intensity blood/signal intensity myocardium). Image quality (five-point scale) and MR angiograms (6 segment model: left main, proximal and middle left anterior descending, proximal left circumflex and proximal and middle right coronary artery segment) were evaluated. Visible vessel length was measured and visible side branches assessed.

Results: MR coronary artery imaging using MS-325 was successfully performed in all volunteers. Contrast improved significantly after administration of MS-325 (7.0 ± 4.6 vs. 2.1 ± 0.2 ; $p = 0.001$). Image quality increased significantly with MS-325 from 2.8 ± 0.5 to 3.1 ± 0.4 ($p = 0.009$). Overall vessel length of contrast enhanced MRCA vs. native images significantly increased ($p = 0.017$). The number of visible side branches improved significantly (2.9 ± 1.5 vs. 2.1 ± 1.5 , $p = 0.049$).

Conclusions: The intravascular contrast agent MS-325 significantly improves the blood-myocardial contrast, image qual-

ity and visible vessel length of whole-heart coronary MR angiography compared with non-contrast images.

159. LOWER EXTREMITY MRA WITH EXTENDED FIELD OF VIEW: USING A 32 CHANNEL MR SCANNER

Kambiz Nael, MD, Sergio Godinez, RT, Roya Saleh, MD, Stefan Ruehm, MD, Margaret Lee, MD, Gerhard Laub, PhD, J. Paul Finn, MD. UCLA, Los Angeles, CA, USA.

Purpose: To investigate a multi-station, whole body MR angiography protocol using multi coil technology and a 32 channel MR system in population with peripheral vascular disease.

Material and Methods: Forty-eight patients with suspected peripheral vascular disease (PVD) (30 M, age: 46–91) underwent a multi-station extended field-of-view (EFOV) contrast enhanced MR angiography (CEMRA) on a 32-channel 1.5 T MR system, equipped with multi coil technology, which enabled us to activate up to 28 coil elements per station. By integration of

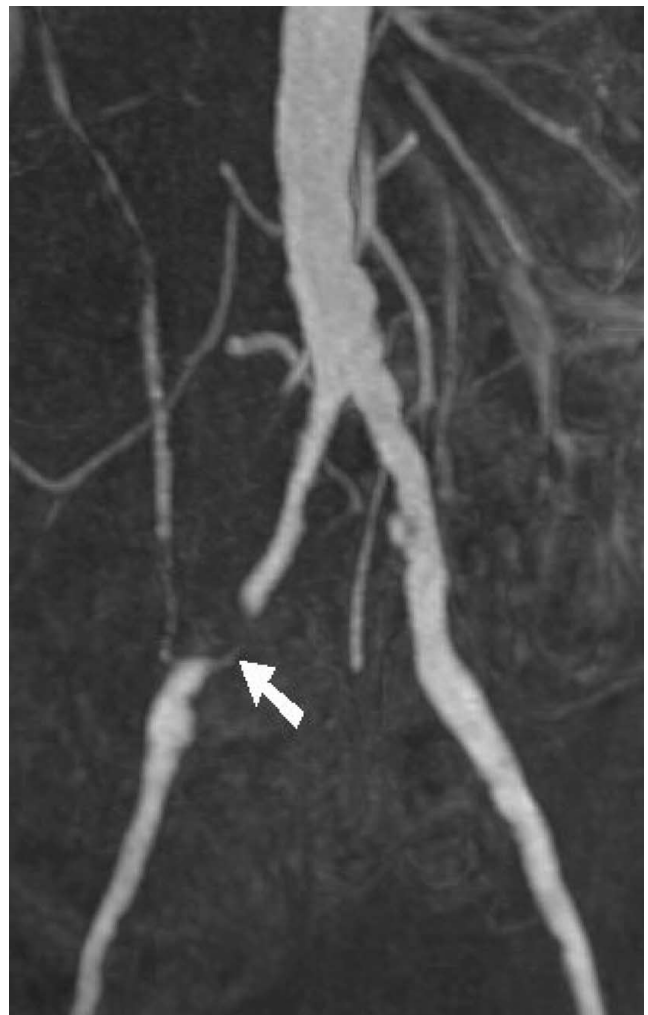


FIG. 1.



FIG. 2.

parallel acquisition technique based on generalized autocalibrating partially parallel acquisitions algorithm with acceleration factor of 2 (GRAPPA \times 2), a 3D data set with spatial-resolution of $1 \times 1 \times 1.5 \text{ mm}^3$ was acquired for each station. Two step-separate contrast injection protocol was used, where following the 1st injection, the most proximal station (1: head-neck) was acquired, followed by the most distal station (4:calves). The intermediate two stations (2: thoraco-abdominal & 3: thighs) were acquired following the 2nd injection. Twenty four patients followed by conventional catheter angiography. The image quality of the arterial segments and the presence and degree of the arterial stenosis were evaluated by two radiologists. The interobserver variability was tested by the kappa statistics and comparative analysis between the CEMRA and catheter angiography was performed by mean of the Spearman rank correlation coefficient.

Results: The majority of vascular segments were visualized by EFOV CEMRA with definition in the diagnostic range (96.6%). Arterial disease was detected with CEMRA in 694 (reader-1) & 672 (reader-2) segments and excellent interobserver agreement ($k = 0.84$). There was a significant correlation

between the CEMRA and DSA ($R_s = 0.92$ and 0.89 for reader 1 & 2 respectively) for the degree of stenosis. The sensitivity and specificity of the CEMRA for the detection of arterial stenoses greater than 50% were 92 & 96% for reader-1 and 93 & 97% for reader-2 respectively, compared with those of DSA.

Conclusion: Using a multi-channel RF system with multi-coil technology, EFOV MRA is able to provide high spatial-resolution data set sufficient for diagnosis in most vascular territories. Integrating of parallel imaging and innovative contrast injection protocol is efficient in minimizing the venous contamination. More clinical studies are required to explore the boundaries of this approach.

160. MAGNETIC RESONANCE ASSESSMENT OF AORTIC PULSE WAVE VELOCITY, AORTIC DISTENSIBILITY, AND CARDIAC FUNCTION IN UNCOMPLICATED TYPE 2 DIABETES MELLITUS

Rutger W. vd Meer, MD,¹ Michaela Diamant, MD, PhD,² Jos J. M. Westenberg, PhD,¹ Joost Doornbos, PhD,¹ Jeroen J. Bax, MD, PhD,¹ Albert de Roos, MD, PhD,¹ Hildo J. Lamb, MD, PhD¹ ¹Leiden University Medical Center, Leiden, The Netherlands, ²Free University Medical Center, Amsterdam, The Netherlands

Introduction: Type 2 diabetes mellitus (DM2) is associated with high morbidity and mortality due to cardiovascular complications. It has been shown that DM2 may augment arterial stiffening and thereby modulates left ventricular (LV) function. Magnetic resonance imaging (MRI) is well suited to assess aortic pulse wave velocity (PWV) and aortic distensibility, both markers of arterial stiffness. MRI has the advantage of being a non-invasive technique that allows direct imaging of the thoracic and abdominal aorta without the use of geometric assumptions. Furthermore, MRI has proven to be a reliable and accurate method for assessing left ventricular (LV) function.

Purpose: To assess aortic stiffness by measuring PWV and aortic distensibility in patients with DM2 using MRI. Furthermore, a correlation is sought between aortic stiffness and LV function.

Materials and Methods: The institutional review board approved the study and informed consent was obtained. Fourteen patients with uncomplicated DM2, and 16 age- and gender matched healthy subjects were included. PWV was calculated based on MR velocity mapping at two predefined aortic locations. Local aortic distensibility was measured just above the aortic valve level. LV volumes were measured by fast gradient-echo imaging to assess systolic function. Furthermore, mitral inflow was measured by MR velocity mapping to assess diastolic LV function. Moreover, fasting plasma glucose and insulin levels were measured. Groups were compared using a two-tailed sample T-test and correlations were assessed by Pearson r values.

Results: Mean PWV was higher in patients as compared to healthy subjects ($6.83 \pm 1.60 \text{ m/s}$ vs. $5.65 \pm 0.75 \text{ m/s}$, $P <$

0.05). PWV correlated significantly ($P < 0.05$) with fasting plasma glucose and insulin levels, the duration of diabetes, and blood pressure. Aortic distensibility was lower in patients as compared to healthy subjects ($4.50 \times 10^{-3} \pm 2.24 \times 10^{-3} \text{ mmHg}^{-1}$ vs. $7.42 \times 10^{-3} \pm 3.34 \times 10^{-3} \text{ mmHg}^{-1}$, $P < 0.05$). Distensibility correlated negatively with PWV and positively with LV diastolic function ($P < 0.05$).

Conclusion: Integrated assessment of aortic stiffness and heart function using MRI is feasible. MRI reveals abnormal aortic PWV and distensibility in patients with DM2. In addition, decreased aortic distensibility negatively affects left ventricular function.

161. CONTRAST-ENHANCED MRA AT 3.0T FOR EVALUATION OF THE PULMONARY ARTERIAL HYPERTENSION

Kambiz Nael, MD,¹ Rajan Saggar, MD,¹ Henrik Michaely,² Jonathan Goldin, MD,¹ Margaret Lee, MD,¹ Gerhard Laub, PhD,¹ J.Paul Finn, MD.¹ ¹UCLA, Los Angeles, CA, USA, ²University of Munich, Munich, Germany.

Background: MRI is being increasingly applied to the study of pulmonary hypertension. Results at 1.5T have, in general, been positive, and the promise is that performance and image quality can be further enhanced at 3.0T.

Purpose: To evaluate the morphological and functional assessment of patients with pulmonary arterial hypertension (PAH), using 3D contrast-enhanced MR angiography (CEMRA) at 3.0T, which to our knowledge, is the first at 3.0T.



FIG. 1.



FIG. 2.

Materials and Methods: Eight patients with PAH (3 M, 5F, 29–87 years old) were scanned on a 3.0T MR system, using an 8-channel body array coil. Following injection of 6 ml gadodiamide at 4 ml/s, time-resolved MRA was implemented using a fast 3D-GRE sequence, with integrated parallel acquisition technique (iPAT) based on generalized autocalibrating partially parallel acquisitions algorithm with acceleration factor of two (GRAPPA $\times 2$). With integration of a 3-segmented echo-shared k-space, the applied sequence acquired repetitive measurements of a 3D data set with in-plane resolution of $1 \times 1.2 \text{ mm}$ and temporal resolution of 1.5 s. Subsequently, high spatial-resolution MRA was acquired using a fast spoiled 3D-GRE sequence following injection of 0.2 mmol/Kg of gadodiamide. Integration of GRAPPA $\times 3$ resulted in a 3D data set with isotropic high spatial-resolution voxels: $0.7 \times 0.8 \times 1 \text{ mm}$ during a 19s breath-hold. Image analysis was performed by two thoracic radiologists independently. Pulmonary arteries (PA) were evaluated up to the highest branch order visualized, for the presence of PAH signs such as central dilatation, pruned tree sign, and corkscrew phenomenon. For quantitative assessment of the lung perfusion, signal intensity versus time-curves were obtained using a dedicated perfusion software. From the signal intensity time curves, perfusion indices including :mean transit time (MTT), time to peak

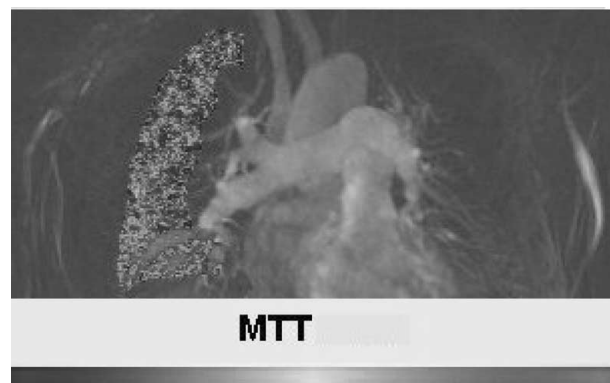


FIG. 3.

(TTP), maximal signal intensity (MSI), & maximal upslope of the curve (MUS), were obtained using a gamma-variate fit on a pixel by pixel basis. In addition, the time interval between peak enhancement of the PA and peak parenchymal enhancement (PE) was calculated. 5/8 patients had cardiac catheterization and pulmonary angiogram, and 3/8 patients had Tc-perfusion scintigraphy for correlation. Statistical analysis was performed by using a kappa test and Spearman rank correlation coefficient (Rs).

Results: Morphological abnormalities including the central dilatation, early cut off appearance and abnormal proximal to distal tapering, and corkscrew appearance of distal pulmonary branches were detected by both observers with excellent interobserver agreement ($k = 0.86$; 95% CI: 0.79, 0.93). Comparative analysis with angiogram showed excellent correlation ($R_s = 0.91$, $p < 0.0001$ & $R_s = 0.89$, $p < 0.0001$ for reader-1 & 2 respectively). Quantitative analysis of perfusion data showed significantly prolonged TTP: 8.19 s & MTT = 11.2 s, and lower MSI = 138.2 A.U. The time lag between the PA and PE was significantly prolonged ($p < 0.001$), and Eisenmenger physiology was detected in 3 patients. There was excellent correlation for detection of regional perfusion defects with those of Tc-perfusion scintigraphy ($R_s = 0.84$).

Conclusion: The combination of fast MR perfusion imaging and high spatial-resolution MRA with parallel acquisition techniques at 3.0T depict the pulmonary vasculatures in extreme details, enables the detection of abnormal morphological and dynamic abnormalities in patient with PAH. Further studies are indicated to establish the clinical application and the accuracy of this technique in a broader clinical setting.

162. RELATIONSHIP BETWEEN PLAQUE VOLUME AND THE OCCURRENCE AND LOCATION OF PERI-PROCEDURAL MYOCARDIAL NECROSIS FOLLOWING PCI: INSIGHTS FROM DELAYED ENHANCEMENT MRI AND INTRAVASCULAR ULTRASOUND

Joseph B. Selvanayagam,¹ Italo Porto,² Adrian S. H. Cheng,¹ William Van Gaal,² Stefan Neubauer,¹ Adrian Banning,² ¹University of Oxford, Oxford, United Kingdom, ²John Radcliffe Hospital, Oxford, United Kingdom.

Introduction: The exact mechanisms underlying myonecrosis after percutaneous coronary intervention (PCI) remain unclear, although both incidental minor side-branch impairment and microvascular obstruction from distal embolization of plaque contents have been implicated in recent CMR studies using delayed enhancement MRI (DE-MRI) (1, 2). It is unknown, however, if the occurrence of new myonecrosis after PCI is correlated to large changes in atheromatous plaque volume of the treated lesion.

Purpose: In patients undergoing complex PCI, we wanted to correlate changes in plaque volume measured by intravascular ultrasound (IVUS) with the magnitude and location of new myocardial necrosis measured by DE-MRI.

Methods: Fifty-two patients (64 vessels) undergoing complex PCI were studied with DE-MRI and two- and three-dimensional intravascular ultrasound (IVUS), both before and after PCI. "Adjacent" myonecrosis was defined as the presence of an area of new hyperenhancement (HE) adjacent to the stent, while "distal" myonecrosis was defined as new HE situated more than 10 mm downstream from the coronary stent.

Results: Fifteen (23%) vessels had evidence of new HE post-PCI. Of these, 8 (12%) had the "distal" type, while 7 (11%) had the "adjacent" type. IVUS showed a significantly greater reduction in plaque area ($2.6 \pm 0.8 \text{ mm}^2$ vs $0.3 \pm 0.6 \text{ mm}^2$ vs $0.4 \pm 0.2 \text{ mm}^2$, $p < 0.001$) and plaque volume ($91.6 \pm 51.5 \text{ mm}^3$ vs $8 \pm 14 \text{ mm}^3$ vs $20 \pm 35 \text{ mm}^3$, $p < 0.001$) in the group with distal new HE, as compared to patients without new HE or adjacent new HE, respectively. In the entire population, a significant correlation was seen between changes in plaque area ($r = 0.45$, $p < 0.001$) and volume ($r = 0.58$, $p < 0.001$) after PCI and the mass of new necrosis, which was mainly driven by the people with distal HE.

	DM (mean \pm se)	NON-DM (mean \pm se)	
AA distensibility	$1.6 \pm 0.2 \times 10^{-3} \text{ mmHg}^{-1}$	$2.6 \pm 0.4 \times 10^{-3} \text{ mmHg}^{-1}$	$p < 0.05$
PD distensibility	$2.0 \pm 0.2 \times 10^{-3} \text{ mmHg}^{-1}$	$3.5 \pm 0.4 \times 10^{-3} \text{ mmHg}^{-1}$	$p < 0.01$
DD distensibility	$3.1 \pm 0.5 \times 10^{-3} \text{ mmHg}^{-1}$	$5.8 \pm 0.7 \times 10^{-3} \text{ mmHg}^{-1}$	$p < 0.01$
Brachial FMD	$8.5 \pm 1.7\%$	$13.8 \pm 1.1\%$	$p < 0.05$
Brachial NTG	$31.8 \pm 3.0\%$	$38.6 \pm 2.7\%$	$p = 0.1$
Aortic wall area	$191 \pm 10 \text{ mm}^2$	$183 \pm 13 \text{ mm}^2$	$p = 0.6$
Aortic lumen area	$463 \pm 23 \text{ mm}^2$	$435 \pm 22 \text{ mm}^2$	$p = 0.4$
Body mass index	$31.0 \pm 1.2 \text{ kg/m}$	$27.9 \pm 1.1 \text{ kg/m}$	$p = 0.07$
Systolic BP	$136 \pm 3 \text{ mmHg}$	$128 \pm 4 \text{ mmHg}$	$p = 0.09$
Diastolic BP	$76 \pm 2 \text{ mmHg}$	$79 \pm 1 \text{ mmHg}$	$p = 0.2$
Total cholesterol	$146 \pm 5 \text{ mg/dL}$	$160 \pm 7 \text{ mg/dL}$	$p = 0.2$
LDL cholesterol	$94 \pm 4 \text{ mg/dL}$	$103 \pm 6 \text{ mg/dL}$	$p = 0.3$
HDL cholesterol	$35 \pm 1 \text{ mg/dL}$	$46 \pm 2 \text{ mg/dL}$	$p < 0.01$
Triglycerides	$191 \pm 17 \text{ mg/dL}$	$127 \pm 22 \text{ mg/dL}$	$p < 0.05$

Conclusions: The volume of embolized plaque material measured using IVUS is significantly related to the magnitude of peri-procedural myocardial necrosis occurring distal to inserted stent during PCI.

REFERENCES

1. Ricciardi MJ, Wu E, Davidson CJ, et al. Visualization of discrete microinfarction after percutaneous coronary intervention associated with mild creatine kinase-MB elevation. *Circulation*. 2001;103:2780–2783.
2. Selvanayagam JB, Porto I, Channon K, et al. Troponin elevation after percutaneous coronary intervention directly represents the extent of irreversible myocardial injury: insights from cardiovascular magnetic resonance imaging. *Circulation* 2005;111:1027–1032.

163. CMR PHENOTYPING OF VASCULAR DISEASE IN TYPE 2 DIABETICS AND CONTROLS

Justin Lee, Cheerag Shirodaria, Jane Francis, Clare Jackson, Jonathan Levy, Matthew Robson, Frank Wiesmann, Stefan Neubauer, Keith Channon, Robin Choudhury. University of Oxford, Oxford, United Kingdom.

Introduction: Type 2 diabetes (DM) and the associated metabolic syndrome are highly prevalent conditions that carry a substantially increased risk of arteriosclerosis and its complications. However, early diagnosis of arterial disease and determination of risk in individual patients remains challenging. MR has the potential to characterize multiple parameters of vascular function (aortic distensibility, endothelial function) and structure (quantification of atherosclerosis) at a single sitting. This would be of great value in further characterisation of vascular disease and in evaluation of anti-atherosclerotic agents or treatments for diabetes.

Purpose: To comprehensively phenotype vascular disease using MRI in patients with coronary artery disease, with and without type II diabetes.

Method: Twenty diabetic patients and 20 controls (matched for age, sex and height) with coronary artery disease underwent MRI at 1.5 Tesla (typical imaging time 45 min). Distensibility (relative change in cross-sectional area per mmHg of pulse pressure) of the ascending (AA), proximal descending (PD) and distal descending (DD) aorta was measured using trueFISP cine (TR/TE = 2.8/1.4; resolution $2 \times 2 \times 7$ mm). To assess endothelial function, brachial artery flow-mediated dilatation (FMD, maximum relative change in area during postischemic hyperemia) and the maximum response to 400 mcg sublingual nitroglycerin (NTG) were measured using trueFISP cine. A stack of eleven transverse black blood turbo spin echo images (TR/TE = 750/11; resolution $1.0 \times 0.8 \times 5$ mm) of the descending thoracic aorta was acquired to determine vessel wall cross sectional area (as a measure of atherosclerotic burden).

Results: For the population as a whole, distensibility in the AA, PD and DD aorta showed significant negative correlation with age ($r = -0.72, -0.63, -0.67$, all $p < 0.001$). Aortic distensibility was, as expected, negatively correlated with systolic ($r = -0.67, -0.74, -0.73$, all $p < 0.001$) but not diastolic blood pressure and also with mean aortic wall area ($r = -0.54, -0.48, -0.54$, all $p < 0.01$) but not with brachial FMD.

Conclusions: CMR demonstrates impaired endothelial function and aortic distensibility in diabetic coronary artery disease patients compared to matched controls. Age, aortic wall area and diabetes are strongly correlated with reduced aortic distensibility. CMR will be important in elucidating the complex relationship between endothelial function, blood pressure, arterial distensibility and development of atherosclerosis.

Saturday, January 21, 2006

11:15 AM–12:15 PM

Oral Abstracts: New Data on Ventricular Function in Ischemic Heart Disease

164. SERIAL CARDIAC MAGNETIC RESONANCE IMAGING AT 3 AND 12 MONTHS AFTER APPLICATION OF BLOOD-DERIVED PROGENITOR CELLS IN RECANALIZED CHRONIC CORONARY TOTAL OCCLUSIONS

Holger Thiele, MD, Andreas Schuster, Sandra Erbs, Volker Adams, Stephan Gielen, Karsten Lenk, Axel Linke, Gerhard Schuler, Rainer Hambrecht. University of Leipzig-Heart Center, Leipzig, Germany.

Introduction: MRI is an excellent diagnostic tool for serial assessment of changes in left ventricular function, infarct size and myocardial perfusion. Circulating progenitor cells (CPC) injected intracoronary improve myocardial perfusion and function after acute myocardial infarction as shown by MRI. In chronic total occlusions (CTO), similar effects could be observed at 3 months follow-up in our randomized, placebo-controlled, double-blind study, which evaluates the impact of CPC's on myocardial perfusion, infarct size and left ventricular function after successful recanalization of a CTO.

Purpose: If these effects are persistent at longer follow-up has not been evaluated.

Methods and Results: Twenty-six patients with reperfused CTO were randomized to either CPC's or inactive serum (control), which were infused into the target vessel. Serial contrast enhanced MRI performed initially, after 3 and 12 months revealed a significant increase in left ventricular ejection fraction in the CPC group (from 51 ± 14 to $58 \pm 13\%$ and $60 \pm 10\%$; $p < 0.01$ versus baseline), a decrease in endsystolic volume (from 68 ± 33 to 60 ± 33 ml and 60 ± 31 ml; $p < 0.05$ versus baseline) and unchanged enddiastolic volumes (136 ± 37 vs. 133 ± 33 and 147 ± 45 , $p = \text{n.s.}$ vs. baseline). Infarct size in percent of left ventricular mass, measured as delayed enhancement MRI, decreased significantly from 10.3 ± 7.7 to 9.0 ± 7.2 and $9.5 \pm 8.5\%$, $p < 0.05$ vs. baseline. First-pass myocardial perfusion MRI at rest and stress using adenosine at standard dose revealed a significant improvement of the myocardial perfusion reserve index in the affected segments by 1.1 ± 0.8 to 1.3 ± 0.9 and 1.3 ± 1.0 , $p < 0.05$. In the control group ejection fraction, left ventricular volumes, infarct size and myocardial perfusion reserve index remained unchanged.

Conclusions: Analysis of serial contrast-enhanced MRI suggests that intracoronary application of CPC post recanalization of CTO is associated with improved myocardial perfusion and subsequent improved recovery of left ventricular function as compared to a control group at mid-term and long-term follow-up. Further investigations of the pathophysiological

CPC effects on macro- and microvascular function are required.

165. ASSESSMENT OF DIASTOLIC DYSFUNCTION AFTER MYOCARDIAL INFARCTION USING PHASE-CONTRAST MAGNETIC RESONANCE IMAGING

Jose T. Ortiz, MD, Preeti Kansal, MD, Paula Tejedor, MD, Chiara Bucciarelli-Ducci, MD, Thomas A. Holly, MD, James C. Carr, MD, Francis J. Klocke, MD, Robert O. Bonow, MD, Edwin Wu, MD. Northwestern University, Chicago, IL, USA.

Background: Diastolic dysfunction may occur after acute ST-segment elevation myocardial infarction (STEMI) leading to an increase in adverse outcomes. Using phase-contrast flow cardiac magnetic resonance imaging (pc-CMR), we studied (LV) filling patterns in patients following reperfused acute STEMI and evaluated their relationship with infarct size.

Methods: Cine and contrast-enhanced CMR were performed in 50 patients (mean age 57 ± 11 years) 2.3 ± 1.5 days following a STEMI successfully treated with primary percutaneous intervention. CMR measurements included LV ejection fraction (EF), end-diastolic volume (EDV), LV mass and infarct size. LV filling patterns were obtained using a single pc-CMR image in a plane perpendicular to the mitral leaflet tips with the velocity encoding limit set to 100 cm/sec. Maximum velocities were measured at the peak of the E and A waves. The deceleration time (DT) was measured from the extrapolation of the deceleration interval between the peak E wave and baseline. The peak E to A wave velocity ratio (E/A) and the E wave DT were used to classify the LV filling pattern as normal ($E/A = 1-2$ and $DT > 200$ msec), impaired relaxation ($E/A < 1$), pseudonormal ($E/A = 1-2$ and

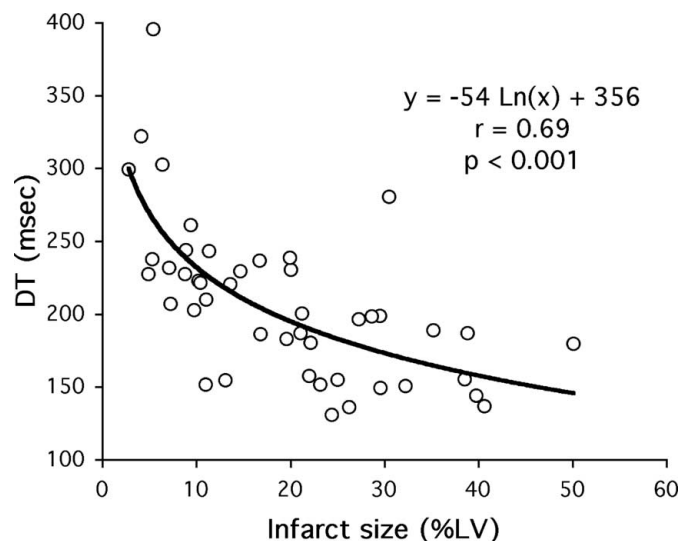


FIG. 1.

DT < 200 msec) or restrictive (E/A > 2 or E/A = 1–2 and DT < 160 msec).

Results: Mean infarct mass was 23 ± 13 g, ($20 \pm 13\%$ LV). Overall, 20 patients had a normal LV filling pattern (mean DT = 247 ± 47 msec) and 27 (54%) had diastolic dysfunction: 15 impaired relaxation (DT = 188 ± 39 msec), 7 pseudonormal (DT = 166 ± 23 msec), and 5 restrictive (DT = 152 ± 18 msec). Three patients with E/A fusion could not be evaluated. All patients were hemodynamically stable without overt symptoms of heart failure. Patients with diastolic dysfunction had significantly greater infarct sizes (30 ± 11 g vs 12 ± 6 g, $p < 0.001$) and lower EF ($39 \pm 9\%$ vs $49 \pm 7\%$, $p < 0.001$) than those with a normal mitral inflow pattern. However, there were no differences in EDV (160 ± 27 mL vs 153 ± 36 mL, $p = \text{NS}$) or LV mass (115 ± 20 g vs 122 ± 32 g, $p = \text{NS}$) between both groups. There was a significant inverse correlation between DT and infarct size ($r = -0.69$, $p < 0.001$, see graph), whereas there was no correlation between DT and EDV ($r = -0.25$, $p = \text{NS}$) or LV mass ($r = 0.13$, $p = \text{NS}$).

Conclusions: CMR evaluation of mitral inflow patterns to measure velocities in a manner analogous to Doppler echocardiography can detect diastolic dysfunction in patients acutely after STEMI. The severity of diastolic dysfunction is associated with the infarct size but is independent of LV volumes and mass. The use of a single pc-CMR acquisition can provide additional information without overly prolonging scan time.

166. THREE-DIMENSIONAL CARDIAC MAGNETIC RESONANCE: DETERMINATION OF LEFT VENTRICULAR FUNCTION AND MASS UTILIZING SINGLE BREATH-HOLD ACQUISITION

Carlos E. Rochitte, MD, PhD¹, Miguel A. RosÁirio, MD,¹ Maria H. R. Siqueira, MD,¹ ClÁrio F. Azevedo, MD,¹ Victor MonsÁo, MD,¹ JosÁ R. Parga, MD,¹ Luiz F. Ávila, MD,¹ Manoj Saranathan, PhD,² Thomas Foo, PhD,² JosÁ A. F. Ramires, MD.¹ ¹Heart Institute -InCor- University of São Paulo Medical School, São Paulo, Brazil, ²GE Healthcare, Baltimore, MD, USA.

Introduction : Measurements of left ventricular function are crucial for the cardiological assessment of any heart disease. Cardiac magnetic resonance (CMR) can evaluate left ventricle function precisely, using a conventional and two-dimensional cine magnetic resonance (2D), which requires multiple breath-holds to cover the whole left ventricle (LV). A new technique, a three-dimensional cine magnetic resonance (3D), was developed and requires only one single breath-hold to cover the entire LV. The cine 3D was made possible by the use of VAST (variable asymmetric sampling in time) technique, described elsewhere (1).

Purpose: Our objectives were to test the hypothesis that 3D could provide similar information to 2D, when used in clinical

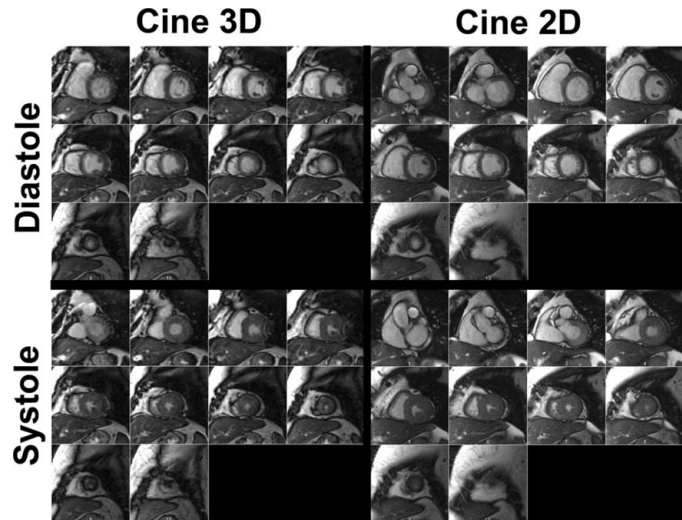


FIG. 1.

cardiological routine patients, and could lead to significant decrease of the exam duration.

Methods: We investigated 14 volunteers (to test the technique) and 43 outpatients from the clinical MRI service. All underwent cardiac magnetic resonance in a 1.5T GE Cv/i scanner, using both techniques. Parameters for 2D and 3D were respectively: FOV = 36/40 cm; Matrix = 256 × 160/256 × 128; Slice thickness = 8/8–10 mm; gap = 2/0 mm; voxel = 1.25 × 2 × 8/1.56 × 3.12 × 8–10 mm; TR = 3.9/4.9 ms; TE = 1.6/2.7 ms; NVP = 8–16/auto; cardiac phases = 20/20(view-sharing); rFOV = 0.75/0.8–0.9; NEX = 1/0,5; FA = 45/45 degrees, BW = 125/125 kHz. We measured, in 2 independent observations, left ventricular end diastolic and systolic volumes, ejective volume, ejection fraction and mass, in images generated by both techniques. Additional measurements were: imaging acquisition time, signal-to-noise and contrast to-noise ratios, temporal resolution and interobserver variability. We also

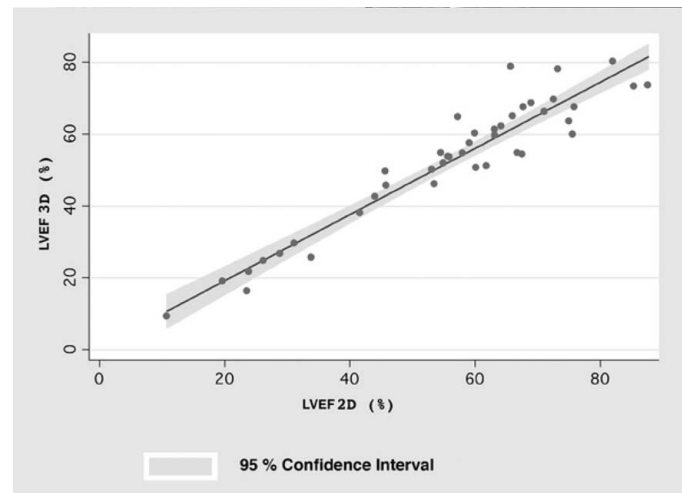


FIG. 2.

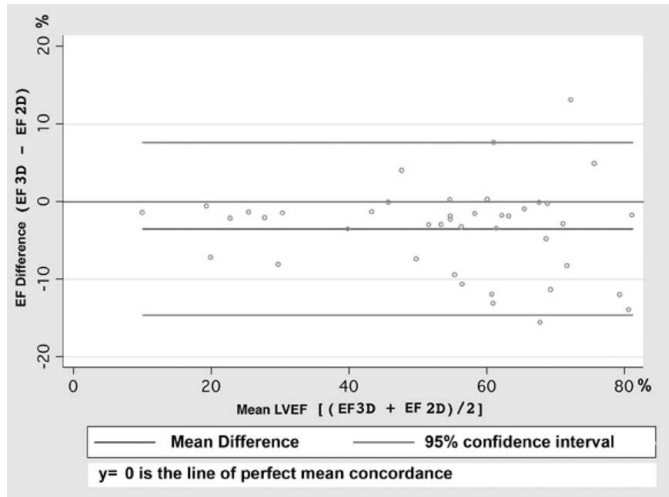


FIG. 3.

evaluated, qualitatively, the global and segmental LV functions and image quality.

Results: Patient group results showed that 3D is clinically applicable and provided similar results to the 2D (Fig. 1 shows an example of the entire data set in diastole and systole of 3D and 2D, short-axis view). An excellent correlation was noted between 2D and 3D LV ejection fraction (Fig. 2. $y = 0.92 \times + 0.92$, $r = 0.95$, $n = 43$, $p < 0.001$). Left ventricular mean differences (2D-3D) were small, not clinically significant and with narrow concordance interval: -16mL for the end diastolic volume, -2 mL for end systolic volume, -14mL for the ejective volume, -3.5% for the LV ejection fraction (Fig. 3 shows

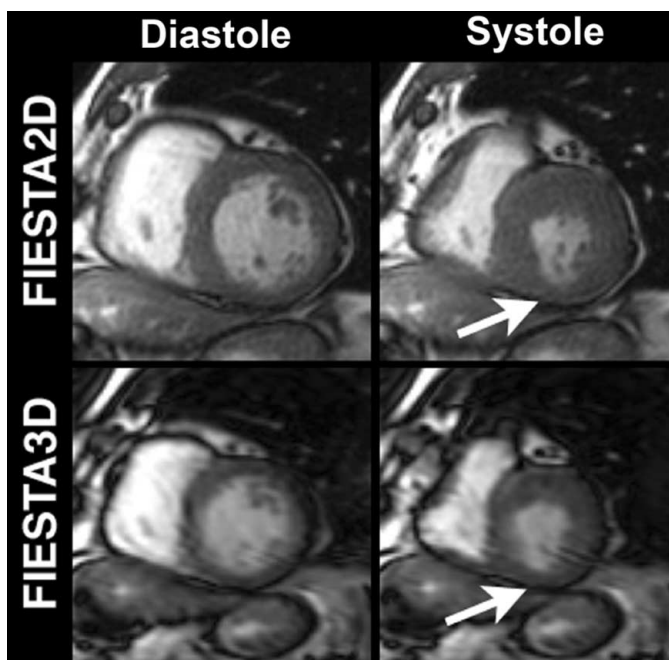


FIG. 4.

Bland-Altman graph for LV ejection fraction 2D vs. 3D: mean difference = $-3.5 \pm 5.7\%$; 95% CI = -14.9 to 7.9%) and 0.5 g for the mass. Similarly, qualitatively global and segmental functions were comparable between 2D and 3D (Fig. 4 depicts a regional wall motion abnormality detected clearly by 2D and 3D, an inferior hypokinesia). The image acquisition time was 24 s for 3D and almost 8 minutes for 2D ($p < 0.001$). Signal-to-noise and contrast-to-noise ratios were not different, while, the qualitative assessment indicated a worse image quality for 3D, due to image blurring, but without decreasing the diagnostic accuracy. Temporal resolution was better for 2D (42 ms vs. 58 ms for 3D). The interobserver variability was similar for both techniques.

Conclusions: 3D and 2D are similar, for the qualitative and quantitative assessment of left ventricular ejection fraction and mass, in routine cardiac patients, and 20 times faster. Our data support that 3D might be used in clinical practice, generating higher patient throughput, greater exam availability, easier exams for acute and more unstable patients, and still can be potentially useful for a faster and safer dobutamine stress magnetic resonance exam.

REFERENCE

1. Radiology 2004;230:845–851.

167. MITRAL ANNULAR DILATATION; IS IT ACTIVE OR PASSIVE? A CARDIAC MRI STUDY

Robert W. W. Biederman, MD, Ronald B. Williams, June Yamrozik, Ketheswaram Caruppannan, MD, Geetha Rayerao, Vikas K. Rathi, MD, Tarun Tewatia, MD, Diane A. Vido, Mark Doyle, PhD. Allegheny General Hospital, Pittsburgh, PA, USA.

Introduction: Multiple explanations exist for the etiology of LV annular dilatation. The current assumptions suggest an active process reflecting remodeling of adjacent myocardium. However, non-geometric, passive mechanisms have not been considered, yet are important. Cardiac MRI (CMR) delayed hyperenhancement (DHE) post-contrast techniques describe a myriad of LV histopathology such as infarct, infiltrative and inflammatory perturbations within the LV but may also be sensitive to non-myocardial pathology.

Hypothesis: We hypothesize that DHE may detect occult LV annular and/or mitral valvar enhancement in post MI patients.

Methods: Sixty patients; 48 S/P MI (20 F, 17 acute, 27 chronic) underwent CMR (1.5T GE) with 0.2 mmol/kg of Magnevist (Berlex, NJ). Notation of presence or absence of a DHE pattern involving the mitral annulus and/or valve was made. Patients were specifically excluded if MI pattern involved basal myocardium to avoid confounding signal etiology. Non MI patients (12) referred for contrast CMR served as controls.

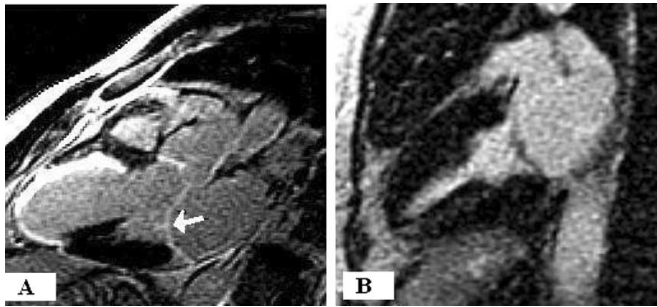


FIG. 1.

Results: All post-MI patients demonstrated an area of infarct by functional analysis, confirmed by DHE. Additional DHE was present involving the mitral annulus in 24/44 (55%) and in 42/44 (95%) the mitral valve (Fig. 1A). No controls demonstrated any degree of annular or valvar enhancement (Fig. 1B).

Conclusion: CMR DHE depicts focal annular and/or valvar enhancement in a large number of post MI patients, suggesting a specific, as yet unknown reactive process may contribute to annular dilatation and/or mitral leaflet pathology. This *passive* phenomena is currently not a suspected contributor to the post MI phenotype but may portend late LV dilatation and either primary or secondary mitral regurgitation.

168. RIGHT VENTRICULAR FUNCTION ASSESSMENT BY CARDIAC MAGNETIC RESONANCE IMAGING PREDICTS POOR PROGNOSIS AFTER MYOCARDIAL INFARCTION

Eric Larose, MD,¹ Carmen W. Chan, MBBS,¹ Andrew T. Yan, MD,¹ Adolphe J. Shayne, MD,¹ H. Glenn Reynolds, MSc,² Sharmila Dorbala, MD,¹ Marcelo F. Di Carli, MD,¹ Peter Ganz, MD,¹ Raymond Y. Kwong, MD.¹ ¹Brigham and Women's Hospital, Boston, MA, USA, ²General Electric Healthcare, Boston, MA, USA.

Background: Right ventricular (RV) failure predicts early in-hospital mortality after acute myocardial infarction (AMI). In patients surviving to discharge after AMI, impact of RV dysfunction on long-term mortality is poorly defined.

Purpose: Determine whether RV failure alters long-term prognosis in survivors of the early period following AMI.

Methods: We assessed RV ejection fraction (RVEF), left ventricular ejection fraction (LVEF), and LV infarct size by 1.5 Tesla Gadolinium-enhanced cardiac MRI (CMR) in 105 patients having survived the early period after AMI (>1 month). Right coronary artery (RCA) patency was assessed by x-ray angiography. Survival, major adverse cardiac events (death, new AMI, angina or heart failure requiring hospitalization, lethal arrhythmia) and risk factors for death were determined. We assessed hazard ra-

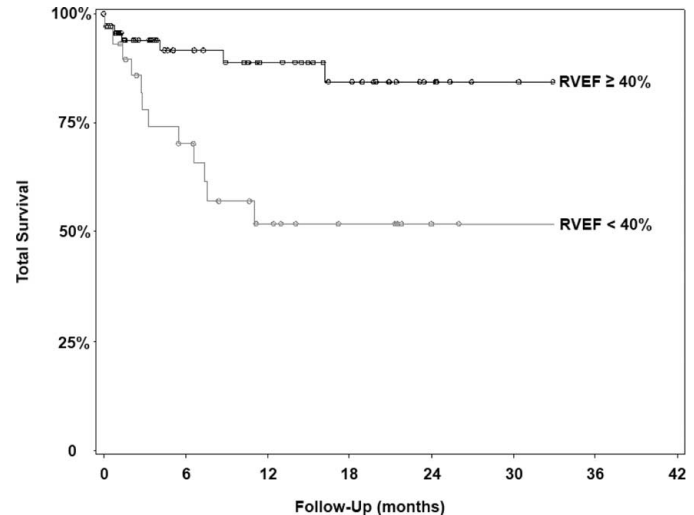


FIG. 1.

tios to death per RVEF. Association of RVEF with mortality was examined by Uni/Multivariable Cox proportional hazards regression models.

Results: Twenty deaths occurred during median follow-up of 11.5 months (range 6-45). RVEF showed a non-linear relationship to hazards ratio for mortality. Analysis per RVEF decile indicated a cutoff of 40% for excess death. By univariate analysis, RVEF < 40% was significantly associated with mortality ($p = 0.02$; Fig. 1; Kaplan-Meier estimate of total survival for population with decreased versus normal RVEF). By multivariate analysis RVEF < 40% remained a strong independent predictor of mortality late after AMI, an association that persisted after adjustment for decreased LVEF < 50%, LV infarct size, and severe RCA stenosis > 70%.

Conclusions: In survivors of the early period following AMI RVEF < 40% predicts death independently of decreased LVEF, LV infarct size and RCA patency. Evaluation of RVEF by CMR is valuable for risk-stratifying patients after AMI and assessing mortality risk beyond traditional assessment of LVEF and coronary artery patency.

169. FOLLOWING ACUTE MYOCARDIAL INFARCTION, MYOCARDIAL RESTRAINT WITH A NITINOL WRAP REDUCES LEFT VENTRICULAR DYSSYNCHRONY

Mark Doyle, PhD, Diane A. Vido, June Yamrozik, Ronald Williams, Geetha Rayarao, James A. Magovern, MD, Robert W. W. Biederman, MD. Allegheny General Hospital, Pittsburgh, PA, USA.

Introduction: A compliant Nitinol wrap (Paracor) placed around the heart following acute myocardial infarction (AMI) reduces left ventricular (LV) dilation and retards LV remodeling and has

been proposed as a human transplant sparing procedure. Yet, its effect on restoration of ventricular synchrony is not known.

Hypothesis: We hypothesize that the degree of dyssynchrony post AMI is reduced only in the myocardial region actively constrained by the Nitinol wrap.

Methods: Ten sheep (study group: 6, controls: 4) were imaged at baseline using 3D magnetic resonance imaging (MRI) to evaluate LV function. A proximal LAD myocardial infarction (MI) was created in all sheep. The study group received a prototype Nitinol wrap placed over the ventricle, extending from the apex to the mid level. At 6 weeks post MI, the 3D MRI evaluation was repeated. Contours outlining the epicardial and endocardial ventricular boundaries in the short-axis view were analyzed to assess time to maximal systolic contraction for 16 circumferential regions equally spaced around the LV for each slice (> 150 data points per heart). Excluded from analysis were scar and regions not contracting $\geq 20\%$. The t-test was used and the f statistic calculated to assess the degree of dyssynchrony, with $f < 0.05$ indicating significance.

Results: At baseline, there was no difference in time to end-systole between basal and mid ventricular regions within each group or between groups. When considering all sheep, the end-systolic time increased by an average of 35% from baseline to 6 weeks post MI (243 ± 86 ms vs. 326 ± 134 ms, $p < 0.001$). Comparing baseline to post MI, the degree of dyssynchrony present in the mid ventricular region was almost a factor 2 greater in controls vs. the wrap group (16% vs. 29%, $f < 0.05$). Conversely, the degree of dyssynchrony for the unrestrained basal region markedly increased and was equivalent for controls vs. the wrap group (99% vs. 107%, $f = \text{NS}$).

Conclusions: A Nitinol wrap placed immediately following AMI limits development of dyssynchrony only in the actively constrained LV region. Here, the unconstrained regions experienced up to a six-fold increase in dyssynchrony compared to the restrained myocardium. These results indicate that a ventricular restraining device, with potential for minimally invasive placement, reduces dyssynchrony, possibly negating need for future resynchronization or transplantation.

Saturday, January 21, 2006

11:15 AM–12:15 PM

Oral Abstracts: CMR on The Molecular Level

170. SERIAL IN VIVO MRI/³¹P MRS STUDY OF MURINE CARDIAC FUNCTION AND METABOLISM FOLLOWING CHRONIC PRESSURE-OVERLOAD STRESS

Mikhail Maslov, Ph.D, Vadappuram Chacko, Ph.D, Craig Smith, MD, Matthias Stuber, Ph.D, An Moens, MD, Hunter C. Champion, MD, Robert G. Weiss, MD. *Johns Hopkins University, Baltimore, MD, USA.*

Introduction: Pressure-overload of the heart causes LVH which can progress to chronic heart failure (CHF). Preserved energy metabolism is required for normal mechanical function but is depressed in human and large animal LVH. Because many promising genetic methods to modify cardiac function and metabolism can only be used in mice at this time, we implemented non-invasive MRI and MRS techniques to study mouse myocardial anatomy, function and metabolism to study the progression of LVH in a pressure-overload model.

Purpose: To study murine cardiac in vivo function and energy metabolism with high resolution MRI and image-guided ³¹P MRS following transverse aortic constriction (TAC).

Methods Cardiac function and metabolism were studied with ¹H MRI and image-guided, spatially localized ³¹P MRS at three and six weeks following TAC. In vivo experiments were carried out on a Bruker Biospec NMR/MRI spectrometer equipped with a 4.7T/40 cm Oxford magnet and a 12 cm (i.d.) actively shielded BGA-12 gradient set capable of developing gradient strength of up to 400 mT/m, using a custom-built dual coil system, as described elsewhere. LV function was quantified from the analyses of cardiac end diastolic and systolic images acquired with high temporal and spatial resolution multislice cine MRI covering the entire cardiac cycle with no gap between slices. Spatially localized ³¹P MRS was carried out using a 1D-chemical shift imaging sequence, with a field of view of 32 mm and 32 phase encode steps in direction perpendicular to the plane of the coil, 64 averages per phase encode steps and an adiabatic excitation pulse of 60° flip angle, and interpulse delay of 1s. Statistical analyses were carried out using two-tailed T-tests and data are expressed as mean ± SD.

Results: Three weeks after TAC there was a doubling of LV mass (Table 1) and evidence of dysfunction (increased ESV and reduced EF) and depressed cardiac PCr/ATP without an increase

in diastolic dimension. By six weeks mass increased further and EDV was now increased suggesting ventricular remodeling. This, however, was not associated with a further decline in EF and PCr/ATP.

Conclusions: TAC causes myocardial hypertrophy in mice within several weeks and results in morphologic, functional and metabolic alterations comparable to those of previously reported data in larger animals. Use of serial, non-invasive MRI/MRS allows long-term studies of dynamic changes associated with pressure-overload LVH in mice. This combination of a hypertrophy model and MRI/MRS methods may allow the serial study of the progression of LVH to CHF and the impact of genetic interventions on that process.

171. CMR DEMONSTRATES MARKEDLY ATTENUATED β-ADRENERGIC CONTRACTILE RESPONSE IN NNOS KNOCKOUT MICE

Moriel H. Vandsburger, B.S, Brent A. French, Ph.D, Patrick Helm, Ph.D, Rene J. Roy, Christopher M. Kramer, M.D, Frederick H. Epstein, Ph.D. *University of Virginia, Charlottesville, VA, USA.*

Introduction: While nitric oxide (NO) derived from neuronal nitric oxide synthase (nNOS) is thought to regulate calcium release from the sarcoplasmic reticulum in cardiomyocytes, recent studies using ex vivo and invasive in vivo methods have reported conflicting results on the role of nNOS in left ventricular (LV) function during β-adrenergic stimulation (1, 2, 3). Specifically, while some experiments show that myocytes or intact hearts from nNOS^{-/-} mice have a blunted response to β-adrenergic stimulation (2, 3), others show an enhanced response (1).

Purpose: The purpose of this study was to comprehensively assess the affect of nNOS ablation on LV size, function, and β-adrenergic responsiveness using cardiac MRI (CMR) at rest and during pharmacological stress.

Methods: Six nNOS^{-/-} and 6 wild type (WT) mice were studied on a 4.7T MRI system. Multislice black-blood cine CMR was used to measure end diastolic volume indexed to body weight (EDVI), end systolic volume indexed to body weight (ESVI), ejection fraction (EF) and myocardial mass index at rest. Black blood myocardial tagged cine CMR measured circumferential shortening (E_{cc}), rate of circumferential shortening (dE_{cc}/dt)_{sys}, and rate of relaxation (dE_{cc}/dt)_{dias} in 2 mid-ventricular slices at rest and during dobutamine infusion (20 and 40 μg/kg/min). Heart rate (HR) and temperature were

Table 1. Morphologic, Functional and Energetic Changes in Control and TAC Mice

	ESV, (mm ³)	EDV, (mm ³)	SV, (mm ³)	LV mass, (mg)	EF, (%)	Cardiac PCr/ATP
Control (n = 4)	20 ± 4	56 ± 7	36 ± 3	74 ± 4	63 ± 4	2.0 ± 0.5
3 wk TAC (n = 6)	36 ± 17	56 ± 17	19 ± 7*	146 ± 39*	36 ± 11*	0.9 ± 0.3*
6 wk TAC (n = 6)	47 ± 12*†	81 ± 9*†	33 ± 6†	195 ± 26*†	42 ± 12*	1.2 ± 0.2*

Table 1. LV Structure and Baseline Function

	WT	nNOS ^{-/-}
EDVI ($\mu\text{l/g}$)	2.26 \pm 0.26	1.36 \pm 0.23*
ESVI ($\mu\text{l/g}$)	0.99 \pm 0.15	0.47 \pm 0.18*
EF (%/g)	56.4 \pm 2.7	66.2 \pm 7.6*
Mass Index ($\mu\text{g/g}$)	3.9 \pm 0.7	3.4 \pm 0.4
Heart Rate	410 \pm 29	502 \pm 53*
Wall Thickness (mm)	11.1 \pm 1.3	11.1 \pm 1.6
Wall Thickening (%)	43.6 \pm 14.2	41.6 \pm 11.8
Blood Pressure (mmHg)	121.5 \pm 13.8	129.1 \pm 13.9

*P < 0.05 vs. WT, **P < 0.05 vs. Baseline.

monitored during imaging. In addition, systolic blood pressure was measured at baseline and at 20 $\mu\text{g/kg/min}$ dobutamine.

Results: At baseline, cine CMR demonstrated reduced EDVI and ESVI, similar wall thickness and wall thickening, and greater EF in nNOS^{-/-} mice compared to WT mice (Table 1). Also, baseline blood pressure was similar between groups while HR was higher in nNOS^{-/-} mice (Table 1). Peak E_{cc} and $(dE_{cc}/dt)_{sys}$ at baseline were also similar between groups, demonstrating similar baseline contractility (Table 2). However, at 20 and 40 $\mu\text{g/kg-min}$ dobutamine the change in peak E_{cc} vs. baseline was greater in WT vs. nNOS^{-/-} mice (Fig. 1, Table 2).

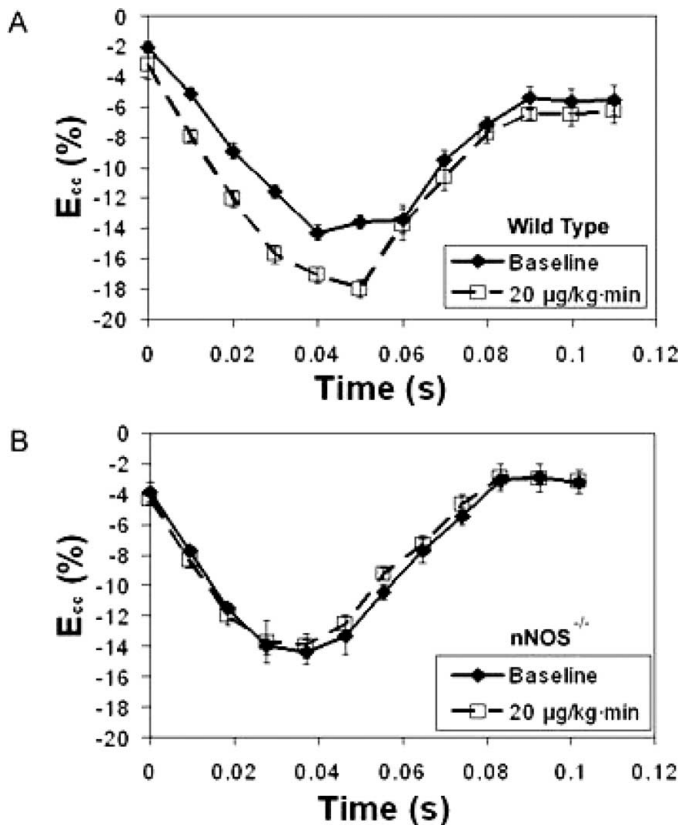


FIG. 1. Significant increases in strain (E_{cc}) and strain rate $(dE_{cc}/dt)_{sys}$ are observed in WT mice upon dobutamine infusion (A), however this increase is essentially absent in nNOS^{-/-} mice (B).

Table 2. Change in Function

	WT	nNOS ^{-/-}
E_{cc} (rest) (%)	14.7 \pm 1.3	14.2 \pm 2.5
ΔE_{cc} (20 $\mu\text{g/kg/min}$) (%)	2.1 \pm 1.2	0.2 \pm 1.1*
ΔE_{cc} (40 $\mu\text{g/kg/min}$) (%)	1.8 \pm 1.2	0.3 \pm 1.3*
$(dE_{cc}/dt)_{sys}$ (rest) (%/s)	-368.5 \pm 57.2	-409.4 \pm 34.3
$\Delta(dE_{cc}/dt)_{sys}$ (20 $\mu\text{g/kg/min}$) (%/s)	-88.0 \pm 65.1**	-15.1 \pm 39.3
$\Delta(dE_{cc}/dt)_{sys}$ (40 $\mu\text{g/kg/min}$) (%/s)	-90.0 \pm 63.8**	-28.6 \pm 18.6
$(dE_{cc}/dt)_{dias}$ (rest) (%/s)	228.4 \pm 37.2	253.37 \pm 32.5
$\Delta(dE_{cc}/dt)_{dias}$ (20 $\mu\text{g/kg/min}$) (%/s)	56.5 \pm 51.6	10.0 \pm 42.0
$\Delta(dE_{cc}/dt)_{dias}$ (40 $\mu\text{g/kg/min}$) (%/s)	71.8 \pm 62.8**	36.3 \pm 45.1

Also, $(dE_{cc}/dt)_{sys}$ increased in WT mice at 20 and 40 $\mu\text{g/kg} \cdot \text{min}$ dobutamine vs. baseline, however, no increase vs. baseline was seen at 20 or 40 $\mu\text{g/kg} \cdot \text{min}$ dobutamine in nNOS^{-/-} mice (Fig. 1, Table 2). In addition, WT mice showed an increase in $(dE_{cc}/dt)_{dias}$ over baseline at 20 and 40 $\mu\text{g/kg} \cdot \text{min}$ dobutamine, with statistical significance at 40 $\mu\text{g/kg} \cdot \text{min}$ dobutamine (Table 2), but no significant increase was measured in nNOS^{-/-} mice. HR increases were similar between groups at both 20 $\mu\text{g/kg} \cdot \text{min}$ dobutamine (43 \pm 46 WT vs 34 \pm 32 nNOS^{-/-}, P = NS) and 40 $\mu\text{g/kg} \cdot \text{min}$ dobutamine (61 \pm 72 WT vs. 64 \pm 53 nNOS^{-/-}, P = NS). The change in blood pressure at 20 $\mu\text{g/kg} \cdot \text{min}$ dobutamine was similar in both groups (2.9 \pm 6.9 WT vs -2.9 \pm 8.1 nNOS^{-/-}, P = NS).

Conclusions: CMR revealed reduced LV cavity size and increased baseline EF in nNOS^{-/-} mice. β -adrenergic contractile reserve was markedly reduced in nNOS^{-/-} mice despite a normal HR response to dobutamine. In addition, a measure of diastolic β -adrenergic responsiveness was attenuated in nNOS^{-/-} mice. These results support the hypothesis that nNOS derived NO stimulates, rather than attenuates, sarcoplasmic reticulum calcium release and reuptake, allowing a normal contractile response to catecholamines.

REFERENCES

- Ashely EA, et al. Cardiac Nitric Oxide Synthase 1 Regulates Basal and β -Adrenergic Contractility in Murine Ventricular Myocytes. *Circulation*. 2002;105:3011-3016.
- Barouch LA, et al. Nitric oxide regulates the heart by spatial confinement of nitric oxide synthase isoforms. *Nature*. 2002;416:337-340.
- Khan SA, et al. Nitric Oxide Regulation of Myocardial Contractility and Calcium Cycling: Independent Impact of Neuronal and Endothelial Nitric Oxide Synthases. *Circ Res*. 2003;92:1322-1329.

172. MAGNETIC RESONANCE MOLECULAR IMAGING FOR PREDICTION OF TARGETED DRUG DELIVERY EFFICACY IN ATHEROSCLEROSIS

Patrick M. Winter, PhD,¹ Shelton D. Caruthers, PhD,² Anne M. Neubauer,¹ John S. Allen,¹ Todd A. Williams,¹ Ralph W. Fuhrhop,¹ Thomas D. Harris, PhD,³ Samuel A. Wickline, MD,¹ Gregory M. Lanza, MD, PhD.¹ ¹Washington University, St. Louis, MO, USA, ²Philips Medical Systems,

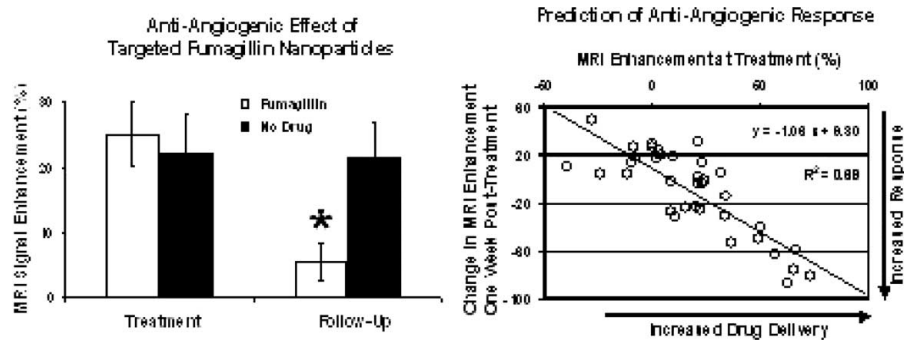


FIG. 1.

Cleveland, OH, USA, ³Bristol-Myers Squibb Medical Imaging, Billerica, MA, USA.

Introduction: Angiogenesis is integral to the progression of atherosclerosis. The $\alpha_v\beta_3$ -integrin is a cellular adhesion molecule that is selectively expressed on angiogenic endothelium but not mature vessels. Fumagillin is a potent anti-angiogenic agent, which directly inhibits endothelial cell proliferation by covalently binding to methionine aminopeptidase type II. $\alpha_v\beta_3$ -integrin-targeted paramagnetic nanoparticles maybe used to quantify early neovascular expansion of the vasa vasorum and to deliver an anti-angiogenic drug (fumagillin) directly to atherosclerotic plaques.

Purpose: This study evaluates the prognostic utility of MRI signal enhancement at the time of treatment to forecast anti-angiogenic response.

Methods: Male New Zealand white rabbits were fed a 0.5% cholesterol diet for 90 days. At the time of treatment, rabbits were imaged before and four hours post injection of $\alpha_v\beta_3$ -integrin-targeted paramagnetic nanoparticles with (n = 9) or without (n = 9) fumagillin (30 μ g/kg). Multi-slice, T1-weighted, black blood, fat suppressed images (250 μ m by 250 μ m resolution, 4 mm slices, TR/TE = 380/11 ms, NSA = 8) were collected of the thoracic aorta using a clinical 1.5T scanner and a quadrature birdcage coil. A semi-automated image segmentation program was used to define regions of interest within the aortic wall and MRI signal enhancement was averaged over all slices. Seven days after treatment, aortic angiogenesis was re-evaluated by imaging animals before and four hours post injection of $\alpha_v\beta_3$ -integrin-targeted paramagnetic nanoparticles without drug. The MRI data was split into proximal and distal aortic segments to assess the utility of signal enhancement at the time of treatment to predict the response to fumagillin at the seven day follow-up.

Results: MRI signal enhancement in the thoracic aorta at the time of treatment ($25.2 \pm 4.9\%$) was significantly lowered one week after fumagillin treatment ($5.5 \pm 2.7\%$). Animals receiving $\alpha_v\beta_3$ -integrin-targeted nanoparticles without fumagillin showed no reduction in MRI enhancement between the treatment and follow-up scanning ($22.2 \pm 6\%$ vs. $21.7 \pm 5\%$). Regional comparisons between the proximal and distal aortic

segments revealed that MRI enhancement concurrent with fumagillin treatment was highly predictive of the anti-angiogenic response as measured by the change in enhancement after treatment (Fig. 1).

Conclusions: $\alpha_v\beta_3$ -integrin-targeted paramagnetic nanoparticles allow early non-invasive quantification of atherosclerotic disease progression, which may be combined with effective delivery of fumagillin for anti-neovascular therapy. The magnitude of MRI signal enhancement from $\alpha_v\beta_3$ -integrin-targeted paramagnetic nanoparticles with fumagillin correlated well with the magnitude of the anti-angiogenic effect. These data illustrate the potential of molecular imaging and targeted drug delivery to improve atherosclerotic treatment and monitoring strategies, which may prevent subsequent myocardial infarction or stroke.

173. IN VIVO CARDIAC MR DETECTION OF PREVIOUSLY ISCHEMIC MYOCARDIUM IN A MURINE MODEL OF MYOCARDIAL INFARCTION USING SUPERPARAMAGNETIC IRON-OXIDE NANOPARTICLES TARGETING PE-CAM-1

Brent A. French, PhD, Zequan Yang, MD, PhD, Yi Zhang, PhD, Yunxiu He, BS, Bijoy K. Kundu, PhD, Mark B. Williams, PhD, Dongfeng Pan, PhD. *University of Virginia, Charlottesville, VA, USA.*

Introduction: Cell adhesion molecules are known to mediate many cellular interactions, and yet there are few methods currently available to non-invasively assess the function of cell adhesion molecules in the process of myocardial ischemia/reperfusion injury. Such information would be extremely useful in the design of therapeutic strategies to combat reperfusion injury.

Purpose: The purpose of this study was to test the hypothesis that intravascular expression of Platelet/Endothelial Cell Adhesion Molecule-1 (PE-CAM-1) might be elevated in previously ischemic regions of myocardium after myocardial infarction (MI) in mice.

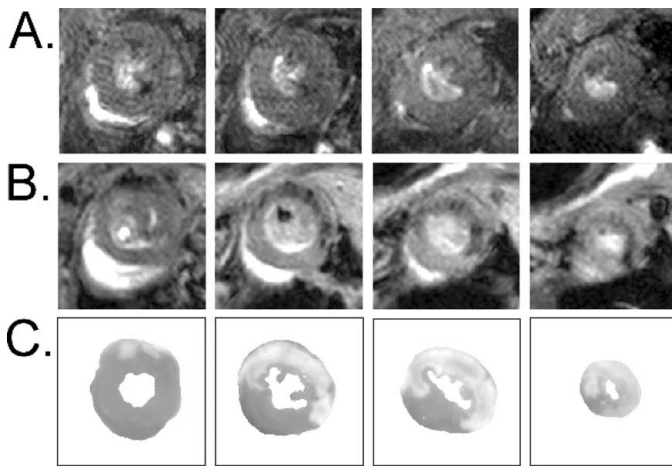


FIG. 1.

Methods: A clinically-approved MRI contrast agent (Feridex; Berlex Labs, Wayne, NJ) was targeted to PE-CAM-1 using a rat monoclonal antibody (mAb) against murine PE-CAM-1 (Ebioscience, San Diego, CA). This was accomplished by oxidizing the dextran coating of Feridex with sodium periodate, then conjugating the antibody to the activated Feridex. A negative control contrast agent was similarly prepared by substituting non-specific, rat IgG2a for the mAb. A total of 6 male, C57Bl/6 mice were used in these studies. All mice were subjected to a 45 min coronary occlusion followed by reperfusion as described previously (1). Three of the mice were injected with the targeted contrast agent (conjugated with the mAb), and 3 with the negative control contrast agent (conjugated with rat IgG2a). Cardiac MR was performed 60 min after contrast injection using an ECG-gated, 2D cine FLASH sequence on a 4.7T Varian scanner. After MR imaging, the mouse hearts were removed and assessed histologically for necrotic tissue via TTC staining (which stains viable tissue red and leaves dead tissue white).

Results: The administration of contrast agent was well tolerated in all animals. As shown in Fig. 1, no evidence of contrast agent was found in the 3 mice injected with the negative control contrast agent (Panel A). However, in the 3 mice injected with the mAb conjugated to Feridex, the accumulation of the iron oxide-based contrast agent could be identified as hypointense speckles in the anterolateral walls of the LV. As shown in Fig. 1, the distribution of the hypointense speckles in the MR image slices (Panel B) corresponded to the location of the infarct zone in TTC-stained tissue slices (Panel C, base to apex slices displayed left to right).

Conclusions: PE-CAM-1 is a cell adhesion molecule expressed on platelets and at the intercellular junction between endothelial cells. Thus the availability of vascular PE-CAM-1 to intravascular contrast agents may be increased in previously ischemic regions of myocardium due to increased platelet deposition and/or exposure of endothelial junctions to the bloodstream. The current study employed cardiac MR and superparamagnetic iron-oxide nanoparticles targeting PE-CAM-1 to demonstrate

that PE-CAM-1 immunoreactivity does indeed accumulate in regions of the mouse myocardium previously rendered ischemic by coronary occlusion. Similar methods may prove valuable in the assessment of jeopardized myocardium in patients with acute coronary syndromes.

REFERENCE

1. Yang Z, et al. *Circulation* 2004;109:1161-1167.

174. CHARACTERIZATION OF ANGIOGENESIS IN THE CHOLESTEROL-FED RABBIT AORTIC VALVE WITH MR FLUORINE SPECTROSCOPY OF INTEGRIN-TARGETED PERFLUOROCARBON NANOPARTICLES

Emily A. Waters, MS,¹ Junjie Chen, PhD,¹ Gregory M. Lanza, MD, PhD,² Samuel A. Wickline, MD,² ¹Washington University in St. Louis, St. Louis, MO, USA, ²Washington University Medical School, St. Louis, MO, USA.

Introduction: Understanding of the pathophysiology of valvular stenosis has evolved beyond the simplistic perception of a bland process of degeneration to one that comprises cellular infiltration, cytokine production, and active inflammatory components. Because angiogenesis is a feature of inflammation that is critical to many pathologies such as cancer and atherosclerotic plaque, we sought to develop a noninvasive approach to characterize angiogenesis in experimental valvular stenosis with the use of targeted molecular imaging contrast agents for magnetic resonance imaging. Because cholesterol-fed rabbits develop plaques in their aortic valves similar to those of human stenotic aortic valves, and they exhibit an inflammatory angiogenic component, we utilized $\alpha_v\beta_3$ -integrin targeted perfluorocarbon nanoparticles injected *in vivo* to bind to endothelium of valve plaque neovasculation, and identified the binding *ex vivo* with the use of fluorine spectroscopy of the aortic valve and root at 11.7 Tesla. We illustrate the concept of detecting a unique NMR signature (fluorine spectrum) of mechanisms critical for early valve degeneration, because the fluorine signal is definitive for nanoparticle binding, because the fluorine signal is definitive for nanoparticle binding, because the fluorine signal is definitive for nanoparticle binding, because the fluorine signal is definitive for nanoparticle binding.

Methods: Targeted perfluorocarbon (15-crown-5 crown ether) nanoparticles were prepared according to methods standard in our laboratory. The targeting ligand, an $\alpha_v\beta_3$ -integrin antagonist, is highly specific with a dissociation constant in the low nanomolar range versus other integrins. Three eight-month-old male New Zealand white rabbits (Harlan) were maintained on a 0.25% cholesterol diet for 6 months. The contrast agent, 2.2 mL/kg of nanoparticles containing 20M crown ether, was injected i.v. and allowed to circulate for 2 hours and bind to the angiogenic vessels. The heart and aorta were then excised and rinsed, and the leaflets carefully separated from the root. Imaging was performed on a Varian 11.7T MR scanner with a custom

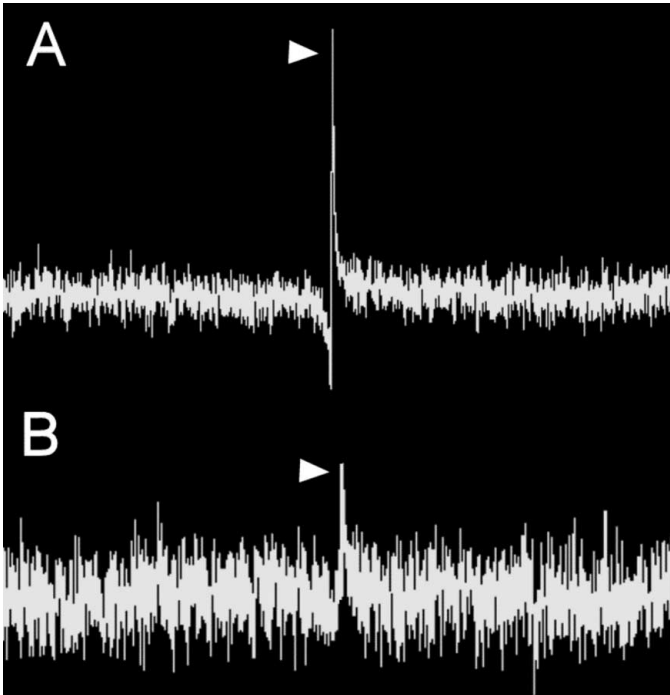


FIG. 1. Sample fluorine spectra obtained from (A) aortic root and (B) excised aortic valve leaflets (peaks shown by arrowheads).

designed 2-turn solenoid volume coil. Samples were immersed in fresh buffered saline solution, and scout proton images were acquired with a gradient echo sequence to guide subsequent ¹⁹F spectroscopy performed separately on the whole samples of root or valve leaflets. Scan time was approximately 30 seconds for each scout image and 20 minutes for spectroscopy (512 signal averages).

Results: The single fluorine peak in the crown ether nanoparticles bound to the aortic root was detected with excellent signal-to-noise in each of the three rabbits (Fig. 1A). A smaller peak was detected in the excised aortic valve leaflets of two of the three rabbits (Fig. 1B). No ¹⁹F signal was registered when the sam-

ples were removed from the coil. Histological analysis revealed macrophage infiltration (RAM-11 positive cells) and angiogenesis (CD-141 staining, Fig. 2) in both valve and root segments.

Discussion & Conclusions: In this pilot study, we have proposed and implemented a novel method for characterizing early valvular degeneration by targeting pathological angiogenesis. Because fluorine is not endogenous to living tissue, perfluorocarbon-based targeted nanoparticles provide a unique signature of the pathology. We have shown in other work that the fluorine signal is quantitative with respect to the number of nanoparticles bound (and thus, angiogenic $\alpha_v\beta_3$ -integrin epitopes present) (1), which could establish localized fluorine spectroscopy as a robust and specific method for noninvasive delineation of the extent of valvular angiogenesis.

REFERENCE

1. Morawski, et al. *Magnetic Resonance in Medicine* 2004;52:1255–62.

175. CHARACTERIZATION OF HDL AS A NEW CONTRAST AGENT FOR ATHEROSCLEROTIC LESIONS

Juan C. Frias, PhD,¹ Kevin Jon Williams, MD,² Edward A. Fisher, MD, PhD,³ Zahi A. Fayad, PhD¹ ¹*Mount Sinai School of Medicine, New York, NY, USA,* ²*Thomas Jefferson University, Philadelphia, PA, USA,* ³*New York University School of Medicine, New York, NY, USA.*

Introduction: HDL are well-know biocompatible lipoproteins that make them a good candidate for molecular imaging of atherosclerotic plaques. We have recently reconstituted HDL (rHDL) with a gadolinium complex and demonstrated in vivo MRI of plaques in atherosclerotic mice (Apo E-KO). Histopathology and fluorescent microscopy of the plaques showed a good agreement with the MRI findings and uptake of the fluorescently labeled rHDL-Gd complex by the macrophages in the plaques.

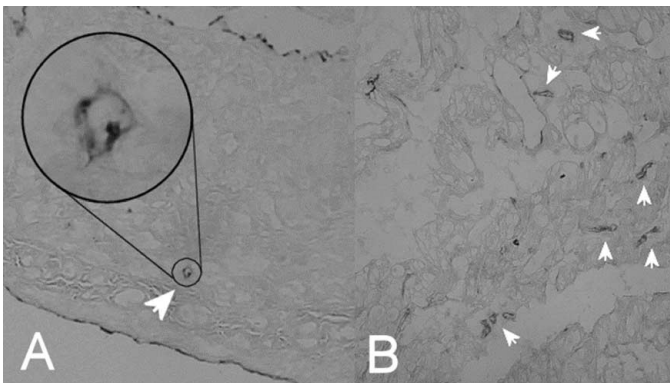


FIG. 2. CD-141 endothelial staining of aortic valve leaflet and root showing angiogenic vessels, indicated by arrowheads. (A) Valve leaflet: 100 × magnification; inset, 600 × magnification. (B) Root: 200×.

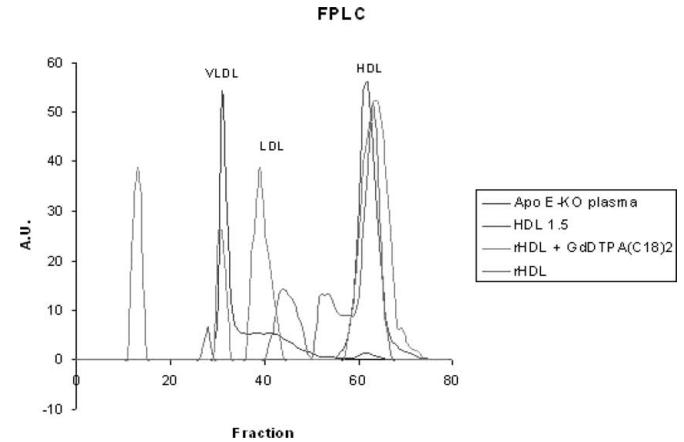


FIG. 1. FPLC profile of HDL contrast agent.

Methods: In this study, we present a new way to produce this new contrast agent avoiding the delipidation and the later sonication steps of the material. Incubation of HDL in the presence of the lipophilic gadolinium contrast agent (GdDTPA-(C₁₈)₂), afforded the desired MRI contrast agent. The resulting material was purified by FPLC (Fig. 1) and its size also characterized by light scattering measurements. ICP analysis provided the amount of gadolinium complex incorporated in the native HDL particle.

Results: Figure 1 shows how the delipidation of HDL and later reconstitution affords a mixture of particles with sizes similar to those of VLDL, LDL, HDL, and a population with a higher size that elutes at about fraction 14. The profile also shows

that HDL incubated in the presence of a lipophilic gadolinium complex has only one size that corresponds to the size of native HDL. MR images of in vivo ApoE-KO mice demonstrated a high uptake in atherosclerotic lesions and specific co-localization in macrophages as demonstrated by fluorescent microscopy.

Conclusion: Two different ways have been devised to produce a molecular MRI contrast agent based on HDL. The delipidation and sonication route affords a mixture of particles while incubation of HDL with a hydrophobic gadolinium complex produces only one type of nanoparticles. This study demonstrates the potential utility of this platform and new methodology for MRI molecular imaging of atherosclerotic plaque.

Saturday, January 21, 2006

11:15 AM–12:15 PM

Oral Abstracts: Increasing the Potential of Vascular MR

176. MEASUREMENT OF CORONARY ARTERIAL BLOOD FLOW BEFORE AND AFTER SUBMAXIMAL EXERCISE USING CARDIOVASCULAR MAGNETIC RESONANCE

Erica Dall'Armellina, MD, Timothy M. Morgan, PhD, Craig A. Hamilton, PhD, Ping Tan, PhD, David M. Herrington, MD, Kerry M. Link, MD, W. Gregory Hundley, MD. *Wake Forest University School of Medicine, Winston Salem, NC, USA.*

Introduction: The assessment of coronary arterial blood flow (CABF) during submaximal exercise is important for optimizing treatment designed to enhance one's ability to perform daily activities.

Purpose: We sought to assess the reproducibility of cardiovascular magnetic resonance (CMR) in assessing changes in submaximal exercise induced CABF.

Methods: On 2 occasions separated by 4 months, we measured CABF (mL/min) in 11 postmenopausal healthy women within the left anterior descending (LAD) coronary artery at rest and immediately after submaximal exercise. We selected women that had abstained from the use of hormone replacement and lipid lowering therapy for 2 months prior to enrollment and had no interval change in their medical condition throughout the study. For each exam, a point in the LAD 2.5 cm distal to its origin from the left main coronary artery was located and a breathheld, phase-contrast, gradient echo scan was acquired perpendicular to the vessel. Images were collected at rest and then participants were partially withdrawn from the bore and performed supine submaximal exercise using a nonferromagnetic electronically braked bicycle (Lode, the Netherlands) mounted at the end of the patient table. Within 30 seconds of exercise cessation, participants were returned to their original landmarked position, and CMR images were re-acquired in the same slice position used at rest. Imaging parameters included a TR/TE/flip angle of 13.8/6.7/45; a venc of 150 cm/sec; an 8 mm thick slice; a 256×256 matrix, 20 cm FOV and temporal resolution 98 msec.

Results: CABF in the LAD increased by $42 \pm 32\%$ on the first exam and $47 \pm 26\%$ ($p = 0.88$) on the second exam. Changes in CABF were highly correlated ($r = 0.86$). Interobserver variability for assessment of % increase in CABF after submaximal exercise was 14%. Based on the results of this study, one would need 24 subjects per treatment group to detect 20% difference in submaximal exercise induced CABF at 80% power.

Conclusions: CMR assessments of CABF within the left anterior descending coronary artery before and after submaximal exercise are feasible and reproducible. Twenty-four patients per

group would be needed to appreciate a 20% difference in exercise induced CABF measured by CMR. These results suggest CMR may be useful for testing noninvasively the efficacy of treatments designed to improve coronary artery blood flow with submaximal exercise.

177. COMPARISON OF LOWER VERSUS UPPER EXTREMITY ENDOTHELIAL DYSFUNCTION BY MRI MAY EXPLAIN DIFFERENCES IN SUSCEPTIBILITY TO ATHEROSCLEROSIS IN DIFFERENT ARTERIES

Harry A. Silber, MD, PhD,¹ Pamela Ouyang, MD,¹ David A. Bluemke, MD, PhD,¹ Sandeep N. Gupta, PhD,² Thomas K. Foo, PhD,² Joao A. C. Lima, MD¹ ¹*Johns Hopkins University School of Medicine, Baltimore, MD, USA,* ²*General Electric Healthcare Technologies, Milwaukee, WI, USA.*

Introduction: It is unclear why atherosclerosis usually involves the lower extremities more severely than the upper extremities within persons with cardiovascular risk factors. Endothelial dysfunction is an early occurrence in atherosclerosis development. We hypothesized that lower extremity endothelial function is more impaired than upper extremity endothelial function in an at-risk group assessed using MRI.

Purpose: This study compared a ratio of leg-to-arm endothelial function between older diabetics and older nondiabetics using phase contrast magnetic resonance imaging (PCMRI). We assessed endothelial function in by measuring post-ischemic hyperemic shear rate, which is dependent on nitric oxide release from the resistance arterioles.

Methods: We studied 32 subjects, ages 51–74: 18 nondiabetics with no cardiovascular risk factors (12M/6F), and 14 with type 2 diabetes (12M/2F). ECG-gated PCMRI was performed using a 1.5T scanner. To image the superficial femoral artery, a four-element phased array receiving coil was placed anterior and posterior to the upper thigh, and an inflatable cuff was placed on the lower thigh. For the brachial artery, a 3-inch receiving coil was placed medial to the upper arm and an inflatable cuff was placed on the forearm. PCMRI images were obtained at baseline. The cuff was inflated above the subject's measured systolic blood pressure for 5 minutes, then released. Images using the same fixed cross-sectional axial prescription as at baseline were obtained immediately after cuff release. A single imaging plane perpendicular to the artery of interest was prescribed. The imaging parameters were: Matrix size 256×128 , slice thickness 3 mm, flip angle 25 degrees, bandwidth 31.2 kHz, repetition time (TR) 11.43 msec, echo time (TE) 5.25 msec, 8 views per segment (VPS), first order flow compensation, no phase-wrap, and no magnitude weighting. Settings of 16 signal averages (NEX) were used at baseline, and 2 NEX after cuff release. Field-of-view was 10 by 10 cm for the femoral artery, and 8 by 8 cm for the brachial artery. During peak hyperemia, 10 VPS was used if necessary to keep the scanning time at 35 seconds or less.

Maximum encoded velocity (VENC) was 60–70 cm/sec during baseline, and 120–150 cm/sec during peak hyperemia. Resulting temporal resolution was 90–180 msec. A user-independent algorithm was employed to measure arterial radius and shear rate from the phase images. A radial plot of the velocity of each pixel versus its distance from the optimal center of the cross-section was created. The velocity pixels near the lumen wall were fit by least-squares method to a parabola. Shear rate was calculated as the slope of the velocity profile at the lumen-wall interface during systole. Radius was defined as where the best-fit parabola equals zero.

Results: There was no difference between diabetics and nondiabetics at baseline with regard to age (61 ± 7 vs. 58 ± 6 years, $p = .12$), femoral radius (3.77 ± 0.34 vs. 3.66 ± 0.50 mm, $p = .43$), femoral shear rate (397 ± 96 vs. 424 ± 86 sec⁻¹, $p = .29$), brachial radius (2.45 ± 0.34 vs. 2.39 ± 0.33 mm, $p = .33$), brachial shear rate (402 ± 145 vs. 358 ± 110 sec⁻¹, $p = .18$), or ratio of femoral radius to brachial radius ($1.56 \pm .20$ vs. $1.57 \pm .22$, $p = .37$). The ratio of baseline femoral-to-brachial shear rate tended to be lower in diabetics but did not reach statistical significance ($1.06 \pm .32$ vs. $1.23 \pm .27$, $p = .07$). During hyperemia, the ratio of femoral-to-brachial shear rate was significantly reduced in diabetics compared with nondiabetics (0.59 ± 0.16 vs. 0.78 ± 0.27 , $p = .01$).

Conclusions: Endothelial function is more impaired in the lower extremity than the upper extremity in type 2 diabetics. This suggests that there are regional differences in endothelial dysfunction that may explain why atherosclerosis development is usually more severe in the leg than arm vessels. Measuring hyperemic shear rate using MRI is useful in explaining mechanisms underlying atherogenesis.

178. NOVEL MAGNETIC RESONANCE IMAGING TECHNIQUE FOR PASSIVE TRACKING OF MR-COMPATIBLE ENDOVASCULAR DEVICES IN VIVO

Wesley D. Gilson, PhD, Matthias Stuber, PhD, Lawrence V. Hofmann, MD, Meiyappan Solaiyappan, MS, Parag Karmarkar, MS, Dara L. Kraitchman, VMD, PhD. *Johns Hopkins University, Baltimore, MD, USA.*

Introduction: Much effort has been put forth developing passive and active coil tracking systems and special MR-compatible devices for interventional MR imaging. Typically, passive tracking approaches have shown relatively poor results for device localization. Moreover, when endovascular devices are rendered MR-compatible, MR visualization is often further diminished. On the other hand, concerns about device heating and device dimensions have limited the adoption of active tracking systems. Recently, a magnetic susceptibility imaging method, Inversion Recovery with ON-resonant water suppression (IRON), was developed that yields positive signal enhancement for endovascular devices (1, 2) that overcomes some of these shortcomings.

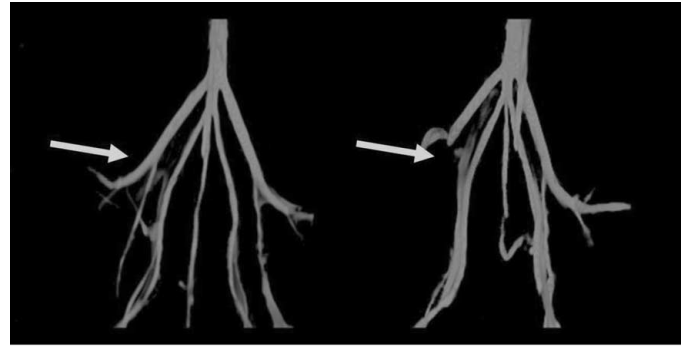


FIG. 1. Maximum intensity projections (MIPs) from a 3D MR angiography of the pelvic arteries before (left) and after (right) deployment of a stainless steel stent in the right external iliac artery. As is typical with conventional stents, blood flow interrogation by 3D MRA is not possible after placement of a metallic stent (arrow on right).

Purpose: The purpose of this study was to investigate using the IRON signal-enhancement method for passive tracking and visualization of conventional and MR-compatible endovascular devices *in vivo*.

Methods: The IRON technique was implemented on a 1.5T MR scanner (Intera, Philips Medical Systems). For this study, IRON was performed using 2D and 3D fast spin echo (FSE) and a real-time 2D gradient and spin echo (GRASE) (3) acquisition. However, in theory, IRON can be combined with any acquisition scheme. A mongrel dog was anesthetized, and carotid arterial access was obtained. Prior to IRON imaging, 3D MR angiography (SSFP time-of-flight; TR/TE = 6.4/3.2ms, flip angle (FA) = 75°, resolution = $0.58 \times 0.58 \times 3\text{mm}^3$) was performed to provide a roadmap for iliac artery catheterization. Under MR fluoroscopic imaging with IRON, a conventional stainless steel stent (7 mm × 15 mm, Genesis, Cordis Corp.) was advanced from the carotid artery into the right iliac artery using real-time GRASE with an IRON prepulse (TR/TE = 190/6 ms, FA = 90°, resolution = $2.7 \times 2.7 \times 5\text{mm}^3$, ETL = 16, IRON angle = 95°, IRON angle bandwidth = 170 Hz, and IRON inversion time = 300 ms). High resolution IRON FSE images were acquired after stent placement. Maximum intensity projections

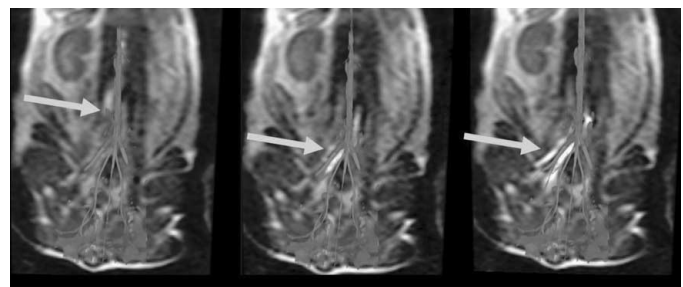


FIG. 2. Real-time IRON GRASE images overlaid on MR angiography MIPs. Arrows indicate the location of the stainless steel stent as catheter is passed through the aorta (left), into the right iliac artery (middle), and after deployment in the iliac artery (right).

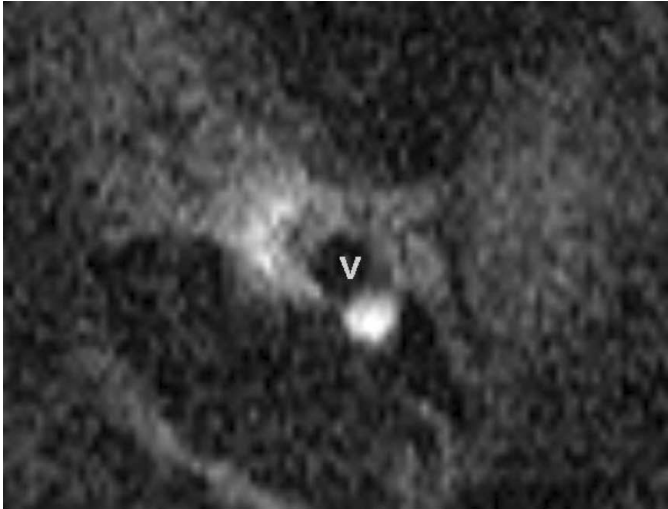


FIG. 3. High resolution cross-sectional IRON image of a stainless steel stent deployed in a canine external iliac artery. Signal enhancement is present around the vessel (v) due to the presence of the stent.

(MIP) were created from the 3D MRA and registered with the 2D IRON GRASE images using stereoscopic viewing software (Dextroscope, Volume Interactions).

Results: MIPs provided an excellent roadmap (Fig. 1) for successful MR-guided placement of a stainless steel stent in the left external iliac artery using IRON with a real-time GRASE acquisition. Guidance of the stent from a carotid approach into the descending aorta and deployment in the external iliac artery was clearly visualized (Fig. 2) on the real-time scans at a frame rate of 5 frames/second. Signal enhancement (arrows) along the vessel was used to guide the catheter and properly place the stent. Blood flow through the right external iliac artery was not visible by MRA following stent deployment as expected for the time-of-flight sequence (Fig. 1, right arrow). The high resolution cross-sectional 2D image in Fig. 3 shows positive signal enhancement of the conventional stainless steel stent.

Conclusions: IRON can be combined with real-time MR imaging to passively track catheter motion in endovascular procedures with conventional stents. Furthermore, high resolution IRON imaging can be used to visualize deployed endovascular devices *in vivo*. The IRON technique provides a means of performing interventional MR imaging without the need for passive markers or active coil systems.

REFERENCES

1. Stuber M. ISMRM. 2005;2608.
2. Kraitchman D. ISMRM. 2005;2165.
3. Feinberg D.A. Radiology. 1991;181:597–602.

179. HYPEREMIC SHEAR RATE MEASURED USING MRI IS BETTER THAN FLOW MEDIATED DILATION IN IDENTIFYING ENDOTHELIAL DYSFUNCTION, AN EARLY MARKER OF ATHEROSCLEROTIC RISK

Harry A. Silber, MD, PhD,¹ Joao A. C. Lima, MD¹, David A. Bluemke, MD, PhD,¹ Dhananjay Vaidya, MBBS, PhD,¹ Sandeep N. Gupta, PhD,² Thomas K. Foo, PhD,¹ Pamela Ouyang, MD.¹ ¹Johns Hopkins University School of Medicine, Baltimore, MD, USA, ²General Electric Healthcare Technologies, Milwaukee, WI, USA.

Introduction: Arterial endothelial dysfunction occurs early in atherosclerosis and predicts future cardiovascular events. Endothelial function is usually assessed noninvasively by measuring flow-mediated dilation stimulated by post-ischemic hyperemia. However, the induced hyperemia is also endothelial-dependent. Hyperemic shear rate, the stimulus for flow-mediated dilation, has not been directly measured in relation to cardiovascular risk factors such as increased age.

Purpose: Using phase contrast magnetic resonance imaging (PCMRI), we investigated whether hyperemic shear rate differs between older and younger men.

Methods: In 20 healthy men—10 ages 20 to 33 years and 10 ages 50 to 74 years—the superficial femoral artery was imaged before and after a 5 minute distal occlusion. PCMRI was performed using a 1.5T scanner A four-element phased array receiving coil was placed anterior and posterior to the upper thigh. An inflatable cuff was placed on the lower thigh. PCMRI images were obtained at baseline. The cuff was inflated above the subject's measured systolic blood pressure for 5 minutes, then released. Images using the same fixed cross-sectional axial prescription as at baseline were obtained immediately after cuff release, and at one minute after release. A single imaging plane perpendicular to the artery of interest was prescribed. The imaging parameters were: Matrix size 256 × 128, field-of-view 10 by 10 cm, slice thickness 3 mm, flip angle 25 degrees, bandwidth 31.2 kHz, repetition time (TR) 11.43 msec, echo time (TE) 5.25 msec, 8 views per segment, first order flow compensation, no phase-wrap, and no magnitude weighting. Settings of 16 signal averages (NEX) were used at baseline, and 2 NEX after cuff release. During peak hyperemia, 10 views per segment was used if necessary to keep the scanning time at 35 seconds or less. Maximum encoded velocity (VENC) was 60–70 cm/sec during baseline, 120–150 cm/sec during peak hyperemia, and 80–100 cm/sec at one minute after cuff release. Resulting temporal resolution was 90–180 msec. A user-independent algorithm was employed to measure arterial radius from the magnitude images, and to measure blood flow and shear rate from the phase images. The variables were measured in each phase of the cardiac cycle, and then averaged. The radius of the artery was defined during systole using the full-width, half-maximum approach. The velocity pixels near the lumen wall in a radial plot were fit by least-squares method to a parabola. Shear rate was calculated as the slope of the velocity profile at the lumen-wall interface. Average shear rate was calculated by averaging shear rates among the cardiac phases. Flow-mediated dilation was calculated as the percent change in systolic radius from baseline to one minute after cuff release.

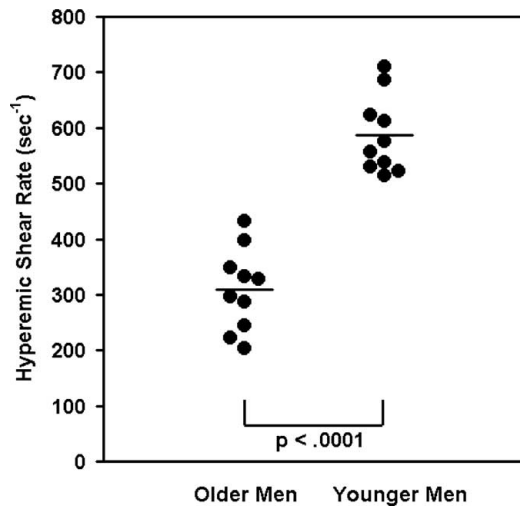


FIG. 1.

Results: Older and younger men had similar baseline femoral artery radius ($3.52 \pm .42$ vs. $3.46 \pm .37$ mm, $p = .36$) and baseline shear rate (134 ± 42 vs. 123 ± 46 sec⁻¹, $p = .28$). Flow-mediated dilation was decreased in older versus younger men (0.68 ± 1.65 vs. $1.79 \pm 2.02\%$, $p = .10$), but did not achieve statistical significance. Hyperemic shear rate was markedly decreased in older versus younger men and there was no overlap between groups (309 ± 74 vs. 587 ± 69 sec⁻¹, $p < .0001$, Fig. 1).

Conclusions: Endothelial-dependent hyperemic shear rate measured directly using PCMRI is markedly impaired in femoral arteries of older healthy men. Unlike flow-mediated dilation, which is the more commonly used noninvasive measure of endothelial function, hyperemic shear rate distinguished completely between older and younger men. Measuring femoral hyperemic shear rate directly using PCMRI may improve the identification of abnormal endothelial function, which is one of the earliest signs of atherosclerosis.

180. GADOLINIUM-ENHANCED INTRAVASCULAR MAGNETIC RESONANCE IMAGING IMPROVES DEFINITION OF LIPID VERSUS FIBROUS CONTENT OF ATHEROSCLEROTIC PLAQUES IN PATIENTS

Eric Larose, DVM, MD,¹ Scott Kinlay, MBBS, PhD,² Andrew Selwyn, MD,³ Daniel Kacher, MSc,³ Yerem Yeghiazarians, MD,⁴ Kent Yucel, MD,² Peter Ganz, MD³ ¹Quebec Heart Institute, Quebec, PQ, Canada, ²VA Boston Healthcare System, Boston, MA, USA, ³Brigham and Women's Hospital, Boston, MA, USA, ⁴University of California at San Francisco, San Francisco, CA, USA.

Background: Vulnerable atherosclerotic plaques are characterized by a high content of lipid relative to fibrous tissue. We have recently demonstrated that intravascular magnetic resonance imaging (IVMRI) provides high resolution imaging of ar-

teries deep within the body and identifies lipid, fibrous, and calcified tissues with superior sensitivity and specificity. Gadolinium-DTPA (Gd-DTPA), a T1-shortening agent, may selectively enhance the appearance of fibrous tissue on T1w MRI.

Purpose: Determine whether Gd-DTPA infusion during IVMRI enhances discrimination of fibrous versus lipid tissue of plaques in human arteries deep within the body.

Methods: A miniaturized 0.030" diameter IV receiver coil coupled to a 1.5T MR scanner was positioned in iliac arteries of 7 subjects with advanced atherosclerosis. Multi-parametric T1w and moderate T2w imaging identified lipid and fibrous tissues within 35 arterial segments. T1w imaging was repeated in all 35 segments after 0.1 mmol/kg IV Gd-DTPA infusion. Percent increase in T1w signal intensity with Gd-DTPA was determined for lipid and fibrous regions.

Results: Computerized mean grayscale measurements in T1w images for fibrous regions increased by 34.2% with Gd-DTPA (95% CI 24.3 to 43.5%, $p = 0.0001$) while lipid regions showed a non-significant increase of 4.3% (95% CI -0.6 to 9.2%, $p = 0.0825$). Percent increase in mean grayscale value with Gd-DTPA was significantly greater for fibrous tissue than for lipid ($p = 0.0001$). Selective enhancement of fibrous regions by Gd-DTPA was also readily discerned by visual inspection.

Conclusion: Gd-DTPA contrast selectively enhances signal intensity of fibrous tissue relative to lipid within human atherosclerotic plaques during T1w IVMRI. The addition of Gd-DTPA to IVMRI facilitates identification of tissue characteristics associated with plaque vulnerability. These findings have important implications for the development of novel plaque-stabilizing therapies and ultimately for reducing cardiovascular events.

181. AORTIC PULSE WAVE VELOCITY USING SINGLE BREATH-HOLD MRI: AGE EFFECTS IN NORMALS

Yi Wang, DSc, Kripa Jayaraman, MS, William Schapiro, RT, Nathaniel Reichel, MD. St. Francis Hospital, Roslyn, NY, USA.

Introduction: We evaluated aortic pulse wave velocity (PWV) with a single breath hold phase contrast (PC) imaging, and studied its relationship to age in normal volunteers.

Methods: Fifty volunteers with informed consent (age: 57.3 ± 14.9) were screened to exclude hypertension, elevated total cholesterol and cardiovascular disease. Using the 'candy cane' view of aorta, an axial plane through the ascending and descending aorta at the pulmonary artery level was prescribed (Fig. 1) and a breath hold cine PC was acquired using the through-plane velocity encoded PC imaging technique with VENC of 150 cm/s and voxel resolution $1.3 \times 2 \times 6$ mm³ on a 1.5T MRI scanner. Signal intensities of phase data within each aortic cross-section were averaged for each time point. A time delay of Δt between maximal flows in ascending and descending aortic regions of interest was determined from time

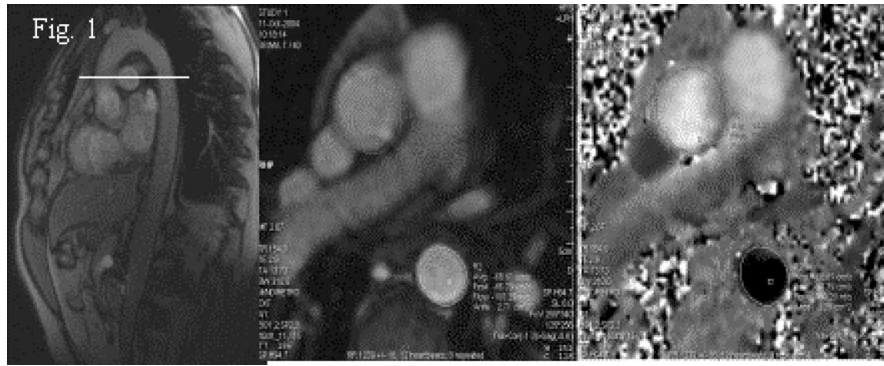


FIG. 1.

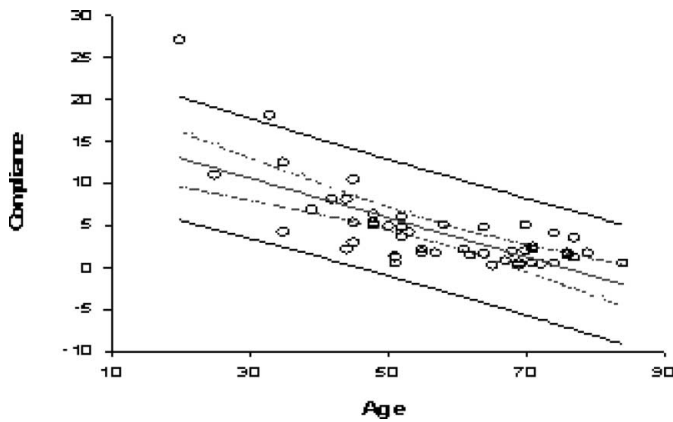


FIG. 2. Linear regression of compliance vs. age. $r^2 = 0.52$. $n = 50$.

intensity curves by a matlab program. The distance D between ascending and descending aortic cross-sections was measured in the ‘candy cane’ image. We calculated $PWV = \Delta D / \Delta t$ and aortic compliance as $C = 1 / (\rho * PWV^2)$, where $\rho = 1057 \text{ kg/m}$. Linear regression was used to determine the relationships between C and age.

Results: Illustrative PC magnitude and phase images are shown in Fig. 1 with the ascending aorta contour as upper and descending as lower vessel. The mean \pm sd of PWV and C were $7.3 \pm 4.4 \text{ m/s}$ and $(4.2 \pm 4.8) * 10^{-5} / \text{Pa}$, respectively. Linear regression of C vs. age had an R^2 of 0.52 and $p < 0.0001$ (Fig. 2).

Conclusions: Through-plane PC is an easy and robust approach to evaluate aortic pulse wave velocity and compliance in a single breath-hold. It has the potential to be an efficient clinical tool for assessment of vascular stiffness.

Saturday, January 21, 2006

1:30 PM–3:00 PM

Clinical Abstracts: LV Function: There is More to See

182. IMPROVED TRANSIENT BALANCED GRADIENT ECHO CORONARY MRA AT 3 TESLA EMPLOYING BINOMIAL PRE-SATURATION, VARIABLE-RATE SELECTIVE EXCITATION, AND ADIABATIC T2-PREPARATION

Michael Schär,¹ Reza Nezafat,² Matthias Stuber,³ Peter Boesiger,¹ Sebastian Kozerke.¹ ¹University and ETH Zurich, Zurich, Switzerland, ²National Institutes of Health, Bethesda, MD, USA, ³Johns Hopkins University, Baltimore, MD, USA.

Introduction: Balanced steady-state free precession (bSSFP) sequences have shown great potential for coronary angiography at 1.5T (1, 2). In its application to coronary imaging, this sequence type will be referred to as transient balanced gradient echo (tbGE) sequence to emphasize that the acquisition is performed during a transient rather than in steady-state. At 3.0T, increased inhomogeneities of the static magnetic field B_0 and of the radio frequency field B_1 together with power deposition limitations necessitate adaptations of the sequence. Simulations have shown that a flip angle sweep (3) in conjunction with a fifth-order binomial pulse to pre-saturate the darkband resonances (4) is the favored startup scheme as it provides most homogenous excitation across the off-resonance range encountered while suppressing artifacts originating from darkband resonances (5). This scheme will be called BIPS5 in the following.

Subjects and Methods: The BIPS5 scheme was implemented together with variable-rate selective excitation (VERSE) (6) pulses to shorten pulse duration and/or to reduce the specific absorption rate (SAR) to comply with power deposition limitations. Furthermore, the initial flip angle sweep (3) was modified according to a Kaiser-Bessel function (7) rather than a linear function. To further compensate for B_1 inhomogeneities adia-

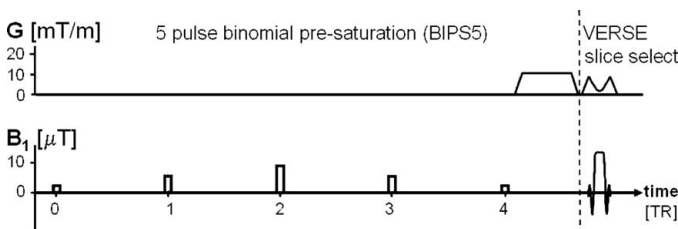


FIG. 1. Gradient and radio frequency (B_1) waveforms for 5 pulse binomial pre-saturation and VERSE slice selection sequence parts. The pre-saturation consists of 5 none slice selective block pulses with a time delay of one TR to saturate the dark band regions. Flip angles: (5.625°), (-22.5°), (33.75°), (-22.5°), (5.625°).

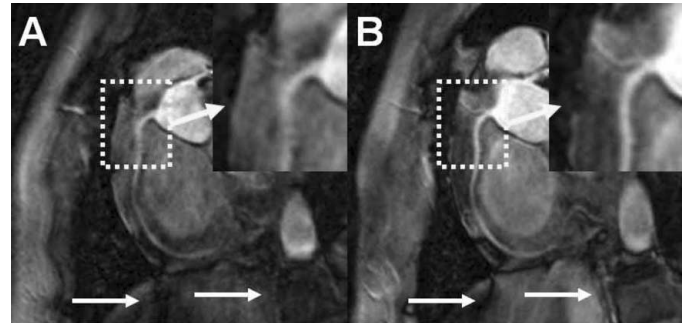


FIG. 2. Coronary angiograms acquired with transient balanced gradient echo sequences applying (A) an alpha-half-TR-half startup and (B) a Kaiser-Bessel flip angle sweep in combination with binomial pre-saturation. The white arrows point at artifacts due to transient signal oscillations in (A), which are suppressed when using the BIPS sequence (B).

batic echo pulses were used in the T2-preparation scheme (8). The BIPS5 and VERSE slice excitation pulse sequence parts are shown in Fig. 1.

After localized shimming and resonance frequency determination based on a measured B_0 -map (9), coronary MR angiograms were acquired from healthy volunteers on a clinical Philips Achieva 3.0T system (Philips, Best, The Netherlands). Free-breathing, navigator-corrected, 3D angiograms of the right coronary artery (RCA) were measured with two different sequences: first, a tbGE sequence with the conventional alpha-half-TR-half (AH) startup (10) and secondly, a tbGE sequence with the BIPS5 scheme as described above. In the AH sequence the repetition time TR was 5.8 ms and in the BIPS5 sequence 5.6 ms. Both startup schemes were applied with 10 dummy excitations. Other parameters were: FOV = 270 mm, matrix = 272×272 reconstructed to 512×512 , 10 slices (3 mm) reconstructed to 20 slices (1.5 mm), acquisition bandwidth = 460 Hz, vector-ecg triggered to the mid-diastolic rest-period as visually determined from a cine acquisition.

Results: Fig. 2 shows images of example coronary MRA. The application of the BIPS5 startup scheme (Fig. 2B) allowed suppression of artifacts (white arrows) which are more prominent in the images acquired with the conventional AH scheme (Fig. 2A). Simultaneously, both a significantly improved visual delineation and contrast in the area of the proximal coronary artery (dotted area) is obtained with BIPS5.

Conclusion: The example in-vivo coronary angiograms demonstrate the effectiveness of artifact suppression when combining VERSE and binomial pre-saturation with a flip angle sweep as compared to the conventional AH sequence. High blood-muscle contrast was achieved with the adiabatic T2-preparation.

REFERENCES

1. Deshpande. MRM 2001;46.
2. Spuentrup. Radiology 2004;231.
3. Deshpande. MRM 2003;49.
4. Foxall. MRM 2005;53.

5. Schär. Proc. ISMRM 2005.
6. Conolly. JMR 1988;78.
7. Le Roux. JMR 2003;163.
8. Nezafat. Proc. ISMRM, 2005.
9. Schär. MRM 2004;51.
10. Deimling. Proc. SMR, 1994.

183. SINGLE BREATH HOLD 3D CINE IMAGING: A NON-ANGULATED ISOTROPIC ACQUISITION USING SENSE ON A 32 CHANNEL SYSTEM.

Vivek Muthurangu, MBChB MRCPCH,¹ Nicholas Noble, PhD,¹ Redha Boubertakh, PhD,¹ Richard Winkelmann, MSc,² Robert Johnson, BA BM MRCP,¹ Peter Börner, PhD,² Derek Hill, PhD,¹ Reza Razavi, MD MRCP MRCPCH.¹ ¹Kings College London, London, United Kingdom, ²Philips Research, Hamburg, Germany.

Introduction: Cardiovascular magnetic resonance (CMR) is an important tool in the assessment of cardiac disease. Two dimensional (2D) cine imaging has been shown to be an accurate method of assessing cardiac anatomy and function. However, it requires complex scan planning and multiple breath-holds. Although isotropic three dimensional (3D) CMR requires minimal planning, and can be reformatted in any plane without loss of resolution it lacks the temporal information needed to assess cardiac function. The optimum solution is isotropic single breath-hold 3D cine imaging. Such imaging requires minimal planning and 3D cine data can be reformatted to allow qualitative and quantitative analysis of function. 3D cine imaging in a single breath-hold requires significant acceleration of imaging. In this study we utilized 2D sensitivity encoding (SENSE) on a 32 channel scanner.

Purpose: The aim of this study was to demonstrate the feasibility of using 3D cine imaging as a method cardiovascular assessment.

Methods: Images were acquired in 8 volunteers on a 1.5T MR scanner using a prototype 32 channel receive coil (Philips Medical Systems, Best, The Netherlands). Single slice 2D cine images were acquired in the long axis (LA) and 4 chamber (4CH) orientations. Multi-slice 2D cine images were acquired in the short axis (SA) orientation for quantification of ventricular function. 3D cine data were acquired in the transverse orientation using a prospectively cardiac gated bSSFP sequence (SENSE factor 2 in the FH and AP direction). Each data set was acquired in a

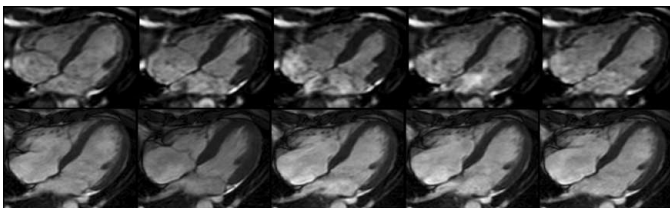


FIG. 1. Reformatted (top row) and conventionally acquired (bottom row) 2D cine images in the 4CH orientation.

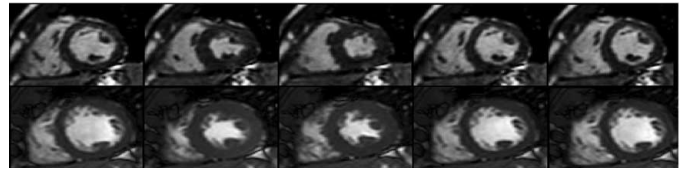


FIG. 2. Reformatted (top row) and conventionally acquired (bottom row) 2D cine images in the SA orientation.

30–35 second breath hold. The acquired voxel size was $3 \times 3 \times 3$ mm, and 10 cardiac phases were acquired. 3D cine data was planar reformatted into the 4CH, LA and SA orientations to produce reformatted 2D cine data. MR volumetry was performed on the multi-slice SA and reformatted SA data and Wilcoxon rank sum tests were used to compare the 2 methods.

Results: Reformatted 2D cine images and conventionally acquired 2D cine images are shown in Fig. 1 and 2. Note the comparable image quality of the reformatted and conventionally acquired 2D cine images. Mean LVEDV was slightly smaller when measured using the reformatted SA data (145.8 ± 22.7 mL vs. 152.9 ± 25.3 mL, $p = 0.64$), while mean LVESV was slightly larger when measured using the reformatted SA data (46.7 ± 10.8 mL vs. 44.7 ± 12.4 mL, $p = 0.87$). Consequently, mean LVSV (99.2 ± 15.3 mL vs. 108.2 ± 14.5 mL, $p = 0.28$) and LVEF ($68.1 \pm 3.9\%$ vs. $71.2 \pm 4.0\%$, $p = 0.38$) were slightly lower when measured using the reformatted data. However, differences did not reach statistical significance.

Conclusions: We have demonstrated the feasibility of acquiring isotropic 3D cine data in a single breath hold. 3D cine data was acquired in the axial orientation and required minimal planning during acquisition. This is a major benefit of this technique, as scanning can be performed by less skilled operators. During post processing arbitrary planar reformatting can be performed allowing qualitative and quantitative assessment of cardiac function. We have demonstrated that 3D cine imaging provides good image quality. In addition, there was reasonable agreement between volume data measured using the 2 methods, with prospective gating and inadequate temporal resolution accounting for the small differences seen. The use of higher SENSE factors will allow improved temporal resolution, shorter breath-holds and the use retrospective gating. This will improve the accuracy of 3D cine imaging. We believe that once optimized this technique will allow the more widespread use of CMR as it will improve ease of use, user independence and patient throughput.

184. FREE BREATHING CINE MRI

Richard Thompson, Angela Leung. *University of Alberta, Edmonton, AB, Canada.*

Introduction: The requirement for a patient breath-hold in studies of cardiac function and cardiovascular hemodynamics (i.e.

blood velocity imaging) is a considerable limitation of cine MRI. The breath-held exam reduces patient comfort and limits the patient populations that can be studied based on to their ability to hold their breath. Infants and young children, in particular, cannot hold their breath on demand. Also, the spatial and temporal resolution of images and their three-dimensional spatial coverage is limited by the practical duration of breath-hold, typically 10 to 20 seconds. Conventional navigator methods are not appropriate for respiratory motion correction of cine imaging experiments due to the time required to excite the navigator tissue, to acquire the information and then establish steady-state conditions for the primary imaging experiment.

Purpose: We will demonstrate a free-breathing cine imaging approach, *cine-navigator imaging*, to correct displacements due to breathing and provide breath-hold-like images.

Methods: The cine-navigator technique incorporates a k-space ordering which allows real-time images to be acquired throughout a conventional gated-segmented experiment, using the same k-space data for both purposes. A radial k-space trajectory is used in this study to allow direct reconstruction of full

field of view, full spatial resolution images from under-sampled k-space data. Each segment of k-space in the cine-navigator experiment is a real-time image. The real-time images are registered using an image-based affine-transformation algorithm. The affine transformation parameters (translation, rotation, scale and shear) are subsequently used to correct every line of k-space prior to the final gated-segmented image reconstruction. Note that because we are using the actual image data as our *navigator*, we do not interrupt the imaging steady-state with a separate navigator acquisition, and we do not lose the time required to collect this extra information. All MR measurements were performed on a Siemens Sonata 1.5 T scanner (Siemens Medical Systems, Erlangen, Germany) using a retrospectively gated radial FISP pulse sequence. Typical imaging parameters: FOV = 360 mm, 256 readout points, 128 to 256 projections, 32 views per segment, 5 mm slice thickness, BW = ± 100 kHz, flip angle = 60 degrees, and TE/TR = 1.5 ms/3.0 ms. Each segment is repeated for ~ 3 heartbeats in order to increase the effective temporal resolution above that provided by 32 segments. Typical acquisition times are 12 to 18 seconds of free-breathing.

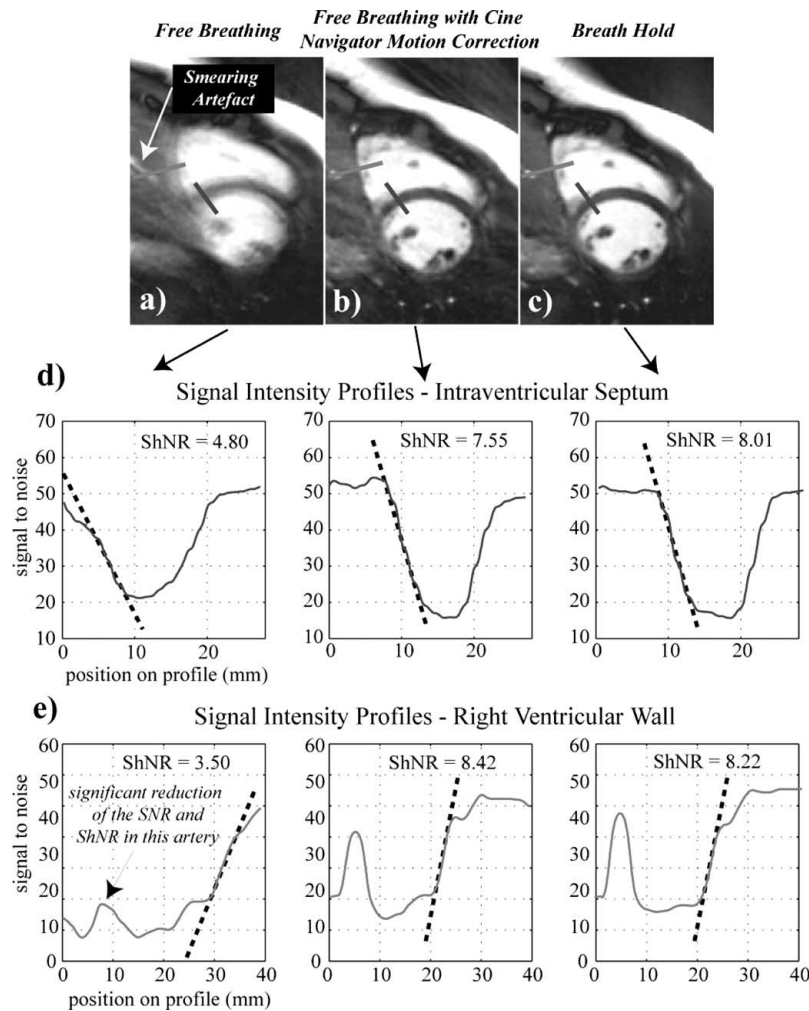


FIG. 1.

Results: Fig. 1a) shows a sample short axis image from cine-series acquired with no breath-hold. The same data, following cine-navigator motion correction is shown in b). As a gold standard, a breath-hold image for same slice prescription is shown in c). Both the free-breathing and breath-hold images were acquired over 15 heartbeats. We use a measure called the sharpness to noise ratio, *ShNR* (the spatial derivative of the signal to noise in the image) to grade the image quality, for quantitative comparison of anatomic images. This measure takes into account the SNR and edge sharpness. The SNR profile and peak *ShNR* along two lines, plotted in a)–c), are shown in d) and e). We have tested this approach with 8 patients to date, with successful results in all studies, regardless of breathing patterns.

Conclusions: It is feasible to image cine mechanical function during free-breathing with negligible loss in image quality, no loss in temporal resolution and without interruption in the imaging steady state, using retrospective affine motion correction and a hybrid real-time/gated segmented imaging sequence.

185. QUANTIFYING MITRAL REGURGITATION WITH CMR MAY AID CLINICAL DECISION MAKING AND HELP OPTIMISE THE TIMING OF MITRAL VALVE SURGERY

Saul G. Myerson, MRCP, Jane Francis, Stefan Neubauer, FRCP. Oxford University, Oxford, United Kingdom.

Introduction: CMR can quantify mitral regurgitation and also left ventricular (LV) dimensions and function accurately but how this information should be used in clinical practice has not been assessed. We sought to examine whether quantification of mitral regurgitation with CMR adds clinically relevant information which may aid the management of these patients, and in particular to optimise the timing of mitral valve replacement/repair.

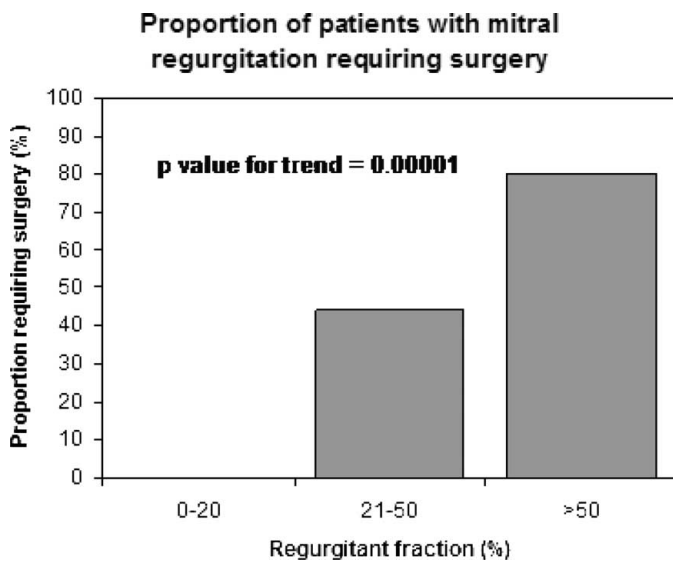


FIG. 1.

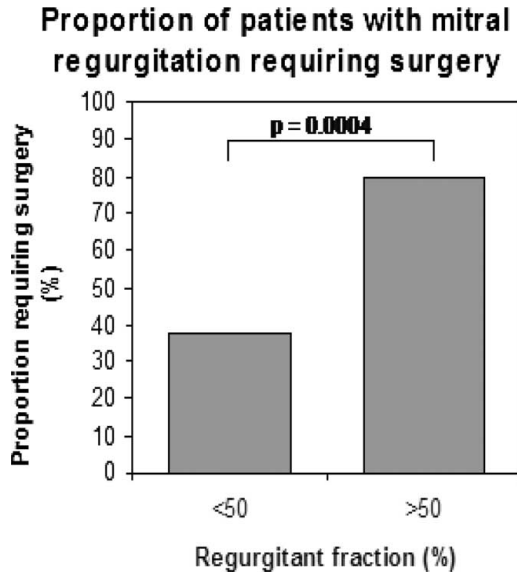


FIG. 2.

Methods: Subjects were identified from clinics and surgical operating lists (for mitral valve repair/replacement) and those with mitral regurgitation (MR) and without other significant valve disease were included. The presence of significant coronary artery disease (either clinically or angiographically) resulted in exclusion. Forty-seven patients were included and had CMR scans with MR quantification prior to any surgery. Those initially treated medically were followed up, and any progression to mitral valve surgery noted. The surgical and conservatively treated groups were compared.

Results: Twenty-four patients underwent surgery and this group, when compared to those treated medically, had a higher mean mitral regurgitant volume (72 vs 44 mLs; $p = 0.003$), regurgitant fraction—MR volume/LV stroke volume $\times 100\%$ (46 vs 33%; $p = 0.006$), LV end-diastolic volume (226 vs 189 mLs; $p = 0.08$), LV stroke volume (151 vs 127 mLs; $p = 0.02$) and LV mass (217 vs 190 g; $p = 0.05$). The likelihood of surgery increased with increasing mitral regurgitant fraction (Fig. 1). Above a 50% regurgitant fraction, the vast majority of patients required surgery, and 2 of the 5 patients initially treated conservatively with regurgitant fractions $>50\%$ required surgery within a year. LV parameters did not prove to be good discriminators between the two groups.

Conclusions: CMR provides valuable information which may help clinical decision making in patients with mitral regurgitation. A mitral regurgitant fraction $>50\%$ seems to be a threshold beyond which the majority of patients require surgery.

186. QUANTIFICATION OF AORTIC REGURGITATION—THE IMPORTANCE OF ACCURATE MEASUREMENT USING RETROSPECTIVE ECG-GATED SEQUENCES

Saul G. Myerson, MRCP, Stefan Neubauer, FRCP. Oxford University, Oxford, United Kingdom.

Introduction: Quantifying aortic regurgitation (AR) is important for monitoring clinical patients. However, prospectively-ECG gated flow sequences may miss the last portion of diastole, and thus underestimate the degree of aortic regurgitation. This is particularly so in the minority of patients whose regurgitation increases with time in diastole.

Purpose: This study examines the importance of ECG gating on the accurate quantification of aortic regurgitation.

Methods: Patients had aortic regurgitation quantified using phase velocity flow mapping, with both prospective and retrospective ECG gating sequences. The prospectively-gated acquisitions were breath-hold while the retrospectively-gated sequences were free-breathing and acquired over 2–3 minutes. Quantification of regurgitation by the two techniques was compared.

Results: Thirteen patients had AR quantified by both methods. Mean \pm standard deviation regurgitant volumes were 38 ± 36 mLs and 44 ± 41 mLs for prospective and retrospectively-gated sequences respectively. Regurgitant fractions (AR volume/aortic systolic flow volume $\times 100\%$) were $21 \pm 15\%$ and $24 \pm 17\%$ respectively. The prospective-gated sequences underestimated total regurgitation by a mean of 6.2 mLs (16% of total). However, in 9 of the 13 patients ($\sim 2/3$ rds), the difference between the two techniques was less than 5 mLs ($p = 0.9$). In the remaining 4 patients, the difference was much greater: 19.8 ± 4.9 mLs; 29% of total, $p = 0.002$ (Fig. 1). In all these patients, the AR persisted throughout diastole, or worsened towards the end of diastole.

Conclusions: Quantification of aortic regurgitation by prospectively-gated flow sequences compares well with retro-

spectively gated sequences in 2/3 rds of patients. In one-third however, it underestimates the amount of aortic regurgitation by a mean of 29%, and retrospectively-gated sequences should be considered for accurate quantification in many cases.

187. TRACKING 3D MYOCARDIAL MOTION USING SLICE-FOLLOWED CINE-DENSE

Bruce S. Spottiswoode,¹ Xiaodong Zhong,² Christine H. Lorenz,³ Ernesta M. Meintjes,¹ Bongani M. Mayosi,⁴ Frederick H. Epstein.² ¹University of Cape Town, Cape Town, South Africa, ²University of Virginia, Charlottesville, VA, USA, ³Siemens Medical Solutions, Baltimore, MD, USA, ⁴Groote Schuur Hospital Cape Town, South Africa.

Introduction: Displacement Encoding with Stimulated Echoes (DENSE) (1) is used to quantify myocardial displacement and strain at high spatial resolution and without the need for tag detection. Two-dimensional (2D) cine-DENSE (2) provides a time series of displacement measurements which can be used to track discrete points in the myocardium as they move through the cardiac cycle (3). By incorporating slice following (SF) (4) and through-plane displacement encoding (5) in the cine-DENSE sequence, we demonstrate the ability to extend cine-DENSE motion tracking to 3D.

Methods: A 2D frame-to-frame tracking algorithm using distance-weighted linear interpolation and temporal fitting of 2D cine-DENSE displacement vectors has previously been developed (3). This algorithm assumes that through-plane motion is uniform, and its direct extension to 3D would require multiple adjacent slices of conventional cine-DENSE data. Instead of imaging a fixed slice position through which the heart moves during the cardiac cycle, the SF technique (4) was used to define and follow an initial plane of myocardium that is to be tracked (Fig. 1a). If this myocardium is displacement encoded in three orthogonal directions, then directly extending the tracking process to 3D becomes possible without the need to image additional slices. The SF method was incorporated into

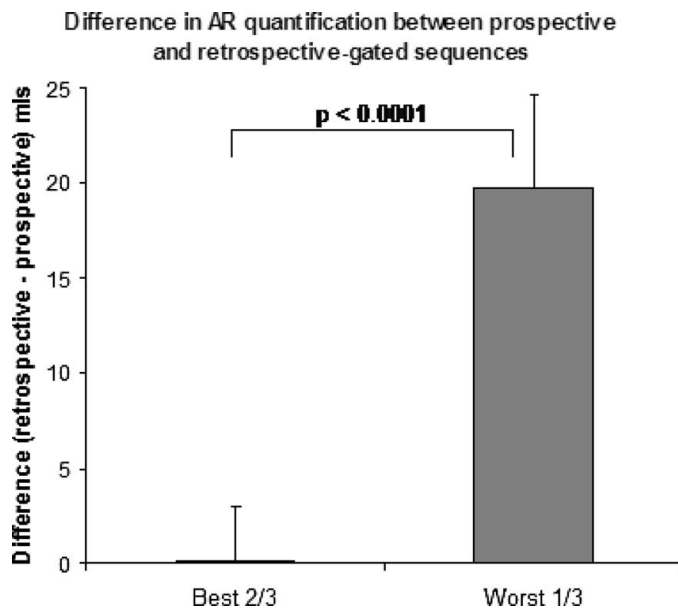


FIG. 1.

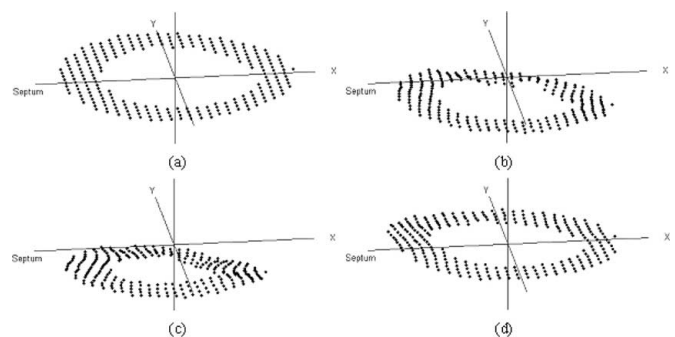


FIG. 1. Three dimensional trajectory positions of a mid short-axis view through the left ventricle of a healthy volunteer. (a) End-diastole, (b) mid-systole, (c) end-systole, and (d) late-diastole.

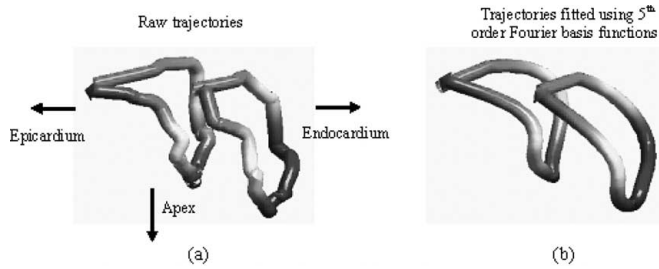


FIG. 2. Two 3D trajectories traversing 75% of the cardiac cycle. (a) Raw, and (b) fitted using 5th order Fourier basis functions. The trajectories are color-coded according to through-plane displacement.

an ECG-gated 2D EPI cine-DENSE sequence (2), and the SF parameters were set as previously described for SF CSPAMM (6). The sequence was run on a 1.5 T Siemens Sonata scanner, with an in-plane resolution of 2.81×2.81 mm and an encoded slice thickness of 8 mm. The accuracy of the SF cine-DENSE 3D tracking algorithm was investigated using a rigid rotating phantom. Also, in accordance with approved protocols and with informed consent, healthy volunteers were imaged. A five pixel median spatial filter was used in each of the ordinate directions to remove noise spikes. The noise in the 3D trajectories was further reduced by fitting 5th order Fourier basis functions to each ordinate direction as a function of time.

Results: For typical ranges of cardiac velocity and displacement, the phantom data demonstrated a 2D in-plane motion tracking accuracy of 0.24 ± 0.15 mm. The tracking accuracy for the through-plane direction was 0.48 ± 0.25 mm, which is lower than the in-plane accuracy because the voxel dimensions are not uniform. Four cardiac phases from a mid-ventricular short-axis slice of a volunteer are shown in Fig. 1. Each point in Fig. 1a represents the centre of a voxel at end-diastole, and Fig. 1b, c and d portray the positions of these points along their trajectories at different cardiac phases. Variations in through-plane motion are evident, as is the radial thickening and circumferential shortening typically seen in tagged images. Figure 2 shows the improvement offered by temporal fitting for two isolated 3D trajectories. Because motion into the imaging plane of previously unexcited protons does not occur in SF imaging, SNR is lower in SF cine DENSE compared to conventional cine-DENSE.

Conclusions: Slice followed cine-DENSE allows 3D myocardial motion to be tracked at a resolution equal to the voxel size. Spatial median filtering and temporal fitting remove noise from the trajectories without any noticeable adverse effects on the deformation. Initial experience in volunteers using SF cine-DENSE, 3D motion tracking, and semi-automatic segmentation suggests that it is now possible to routinely quantify 3D intramyocardial motion with minimal user interaction and high accuracy.

REFERENCES

1. Aletras, et al. *JMR* 1999;137:247–52.
2. Kim, et al. *Radiology* 2004;230:862–71.

3. Spottiswoode, et al. 2005;Proc. ISMRM 778.
4. Fischer, et al. *MRM* 1994;31(4):401–13.
5. Epstein, et al. *MRM* 2004;52(4):774–81.
6. Stuber, et al. *MAGMA* 1999;9:85–91.

188. DYSSYNCHRONY IN LEFT VENTRICULAR MYOCARDIAL CONTRACTION ASSESSED WITH TISSUE DOPPLER IMAGING AND VELOCITY-ENCODED MRI IN PATIENTS WITH CONDUCTION DELAY AND IDIOPATHIC DILATED CARDIOMYOPATHY

Jos J. M. Westenberg, PhD, Hildo J. Lamb, PhD, MD, Rob J. van der Geest, MSc, Gabe B. Bleeker, MD, Eduard R. Holman, PhD, MD, Martin J. Schalij, PhD, MD, Albert de Roos, PhD, MD, Ernst E. van der Wall, PhD, MD, Johan H. C. Reiber, PhD, Jeroen J. Bax, PhD, MD *Leiden University Medical Center, Leiden, The Netherlands.*

Introduction: Cardiac resynchronization therapy (CRT) is the proposed treatment in patients with severe heart failure, depressed left ventricular (LV) function and left bundle branch block (LBBB). Candidates who may benefit are mainly selected on ECG criteria. Still 20–30% of these patients does not respond to CRT, emphasizing the need for additional selection criteria. Several studies demonstrated that the main predictor of CRT response may be the presence of LV dyssynchrony (i.e., mechanical delay between septum and lateral wall contraction), adequately assessed by echocardiography using tissue Doppler imaging (TDI). LV dyssynchrony assessment on TDI has not been compared directly with other imaging modalities. Velocity-encoded (VE) MRI potentially allows direct myocardial wall motion measurement similar to TDI.

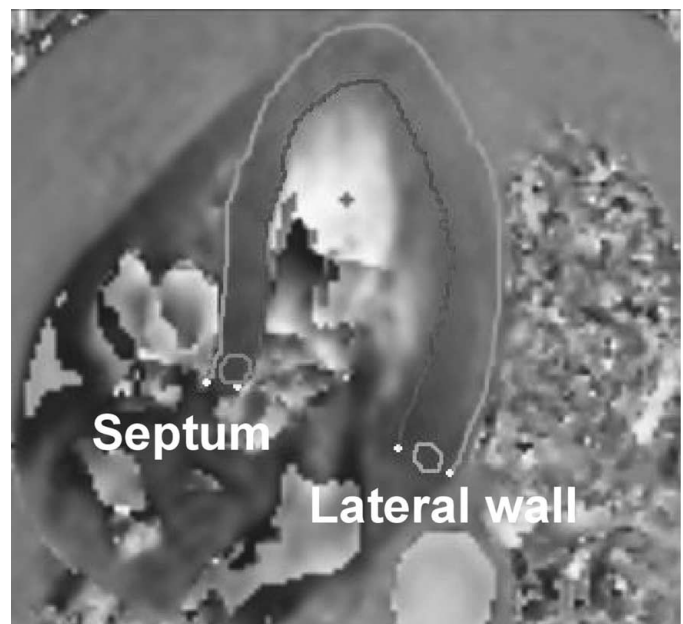


FIG. 1.

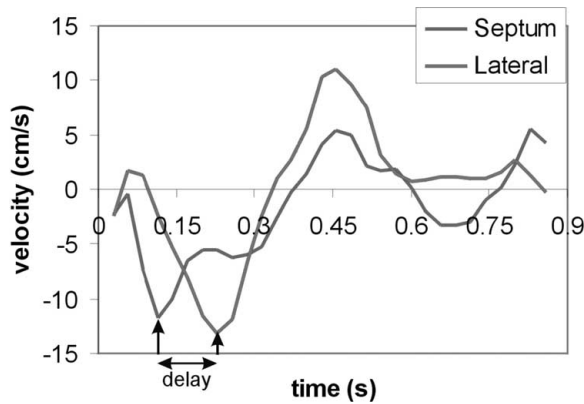


FIG. 2.

Purpose: Comparing TDI with VE MRI for LV dyssynchrony assessment.

Methods: Twenty consecutive patients (15 men, mean age 57 ± 15 years) with heart failure, systolic LV dysfunction, QRS-duration >120 ms, interventricular conduction delay and idiopathic dilated cardiomyopathy were included. Ten normal individuals (8 men, mean age 57 ± 9 years) with QRS-duration <85 ms and normal LV function were evaluated for comparison. TDI Color Doppler data was acquired to study intraventricular LV dyssynchrony. The times of peak systolic velocities were assessed in septum and lateral wall at the basal level, and the difference was defined as intraventricular LV dyssynchrony (ie, septal-to-lateral delay). VE MRI MRI was performed on a 1.5 T MRI scanner (ACS-NT15 Gyroscan; Philips Medical Systems, Best, The Netherlands). A five-element phased-array synergy cardiac-coil was placed on the chest for signal reception. Three-directional VE MRI was performed in the four-chamber orientation. Imaging parameters were: TE/TR = 5.0/6.9, flip angle = 50° , Field-of-View = 370 mm, scan matrix = 128×76 , slice thickness = 8 mm, 4 signal averages, gated cardiac triggering with retrospective reconstruction of 30 phases. Velocity was encoded in 3 directions with a sensitivity of 20 cm/s. From the velocity measured in the basal-to-apical direction, the times of peak systolic velocities assessed in the septum and lateral wall at the basal level (Fig. 1) were determined and the difference defined LV dyssynchrony (Fig. 2). Correlation of LV dyssynchrony assessment with TDI and MRI was determined.

Table 1. Agreement between LV dyssynchrony assessment with TDI and MRI

	MRI		
	<50 ms	50–80 ms	>80 ms
TDI			
Minimal dyssynchrony (<50 ms)	8	0	0
Intermediate dyssynchrony (50–80 ms)	1	5	0
Extensive dyssynchrony (>80 ms)	0	0	6

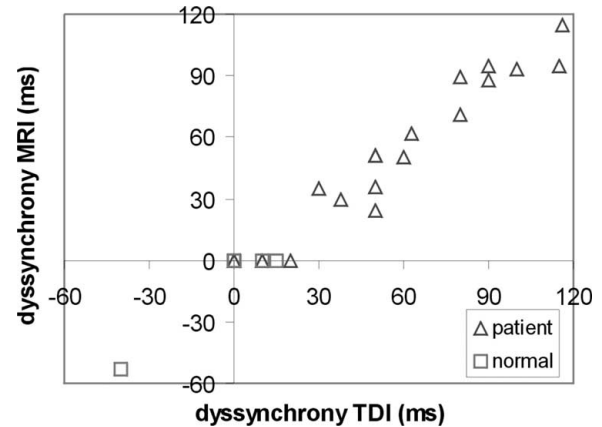


FIG. 3.

Results: None of the normals showed LV dyssynchrony (mean -2 ± 15 ms on TDI; mean -5 ± 17 ms on MRI, $p =$ non-significant (NS)). In patients, the mean LV dyssynchrony was 55 ± 37 ms on TDI, as compared to 49 ± 38 ms on MRI ($p =$ NS). In Fig. 3, LV dyssynchrony measured by MRI is plotted versus LV dyssynchrony measured by TDI. Good correlation between both modalities is observed (linear regression $Y = aX + b$, with a (\pm standard error SE) = 0.99 ± 0.04 and $b \pm SE = -5 \pm 2$, $n = 30$, $r = 0.98$, $p < 0.01$).

MRI exhibited a small, non-significant underestimation of 5 ± 8 ms for LV dyssynchrony as compared to TDI. The confidence intervals ranged from -22 ms to 11 ms. Patients were categorized into three groups, according to the extent of LV dyssynchrony on TDI: minimal (<50 ms), intermediate (50–80 ms) and extensive LV dyssynchrony (>80 ms). The results are presented in a 3×3 table (Table 1). Excellent agreement between MRI and TDI classification was found ($\kappa \pm SE = 0.92 \pm 0.07$, $p < 0.01$), 95% of the patient classification was identical.

Conclusions: Very strong correlation between MRI and TDI for LV dyssynchrony assessment, with both modalities producing similar results. The advantages of MRI over echocardiography (LV volumes, function, scar tissue and LV dyssynchrony can be acquired all in one examination, all potential markers for CRT response) makes this modality very suitable for CRT selection.

189. MAGNITUDE AND CAUSES OF INTEROBSERVER DISCREPANCIES IN CMR VOLUME MEASUREMENTS: CRITICAL IMPORTANCE OF CHOICE OF THE BASAL SLICE

Aaron N. Weaver, MD,¹ Heath U. Jones, MBA,¹ Gerri K. Jelaco, RT,¹ Julie A. Cha, RT,¹ Judy Hall,¹ Kathy Walker, NP,¹ Duane D. Blatter, MD,¹ Jeffrey L. Anderson, MD.²
¹LDS Hospital, Salt Lake City, UT, USA, ²LDS Hospital, University of Utah, Salt Lake City, UT, USA.

Background: MRI provides superior, high-resolution non-invasive cardiac imaging (CMR), capable of highly precise and reproducible measurements of ventricular volumes and masses. However, such potential has not been always realized in clinical practice. Differences in measurement methodology could be a cause of substantial intra- and interstudy variability unrelated to changes in cardiac geometry, but these have not been well studied.

Methods: We tested variability in measuring left and right ventricular (LV, RV) end-diastolic (EDV) and end-systolic (ESV) volumes between 2 experienced physicians reading a set of 21 studies of volunteers without clinical heart disease. Our aim was to assess interobserver sources of variability. Standard cardiac 2, 3, and 4 chamber long-axis, and short axis 1 cm slices (8 skip 2 mm), were obtained on a GE 1.5 Tesla magnet (EXCITE platform, version 11.0) using FIESTA (SSFP), ECG- (n = 20) or peripheral-gated (n = 1) cine sequences. Image analysis was performed independently on a GE Medical Systems ReportCard 1.0 workstation by each observer. Quantitative results were entered prospectively into a database, and computer-assisted manual tracings were saved for later visual comparison. Reading instructions consisted of those given in the workstation manual: unattached papillary muscles were to be included within the LV/RV chambers, and the basal slice was to be at least an “almost complete” muscular circle.

Results: Volunteer age averaged 47 y (range, 40 to 60); BSA averaged 2.1 sq m for men (n = 9) and 1.8 for women (n = 12). All studies were of good quality. Correlations between the 2 readers for LVEDV, RVEDV, LVESV, and RVESV were: 0.95, 0.91, 0.96, and 0.92 respectively (all $p < 0.001$). Simultaneous visual review of individual tracing revealed 3 major sources of interobserver measurement differences: 1) choice of ED/ES frames; 2) choice of the most basal LV, RV short-axis slices; and, 3) approach to endocardial (EC) edge selection. Choice of ED and ES frames differed in 8/42-paired readings (19%), 6 by a single frame. More importantly, a discrepancy in choice of basal slice was present between readers in 8/21 LVEDV (38%), 7/21 LVESV (33%), 7/21 RVEDV (33%), and 8/21 RVESV (38%) series. Average measurement differences between paired readings were substantially increased when a discrepancy in choice of basal slice occurred: LVEDV 19.8 vs. 6.0 ml, $p < 0.00001$; LVESV 27.3 vs. 17.2 mL, $p = 0.09$; RVEDV 33.2 vs. 18.3 ml, $p < 0.01$; and RVESV 49.3 vs. 35.3 mL, $p < 0.01$. These differences translated into corresponding differences in derived measures (ejection fraction, stroke volume, mass, and volume and mass indexes). Finally, visual comparisons revealed moderate differences in EC edge selection as the cause of most of residual measurement variability.

Conclusions: Despite its potential for precise, highly reproducible ventricular volume and mass determinations, CMR is susceptible to major interobserver variability, primarily due to differences in basal slice and EC edge selection, which limit the reproducibility of quantitative measurements. More formal rules

for manual measurements and improved computerized edge detection algorithms are needed to realize the potential of CMR to achieve reliably reproducible quantitative measurements.

190. AUTOMATIC QUANTITATIVE LEFT VENTRICULAR ANALYSIS OF CINE MAGNETIC RESONANCE IMAGES USING THREE-DIMENSIONAL INFORMATION FOR CONTOUR DETECTION

Robert J. M. van Geuns,¹ Timo Baks, MD,¹ Ed Gronenschild,² Jean-Paul Aben,³ Piotr Wielopolski,¹ Filippo Cademartiri,¹ Pim de Feyter.¹ ¹Erasmus MC, Rotterdam, The Netherlands, ²Maastricht University, Maastricht, The Netherlands, ³Pie Medical Imaging, Maastricht, The Netherlands.

Introduction: Accurate and reproducible assessment of left ventricular volumes and ejection fraction is essential for the prognosis of patients with heart diseases and for evaluating therapeutic responses. Because of the limited or partial successful performance of previous reported methods we have developed an automatic boundary detection algorithm that does not make any anatomical assumptions and requires only a set of manual epicardial contours in the two- and four-chamber images at end-systole and end-diastole as single user input. It takes advantage of the three-dimensional information obtained from the MRI system in order to start the segmentation process for both the endocardial and epicardial contours in all short-axis slices.

Purpose: The purpose of our study was to evaluate the automatic boundary detection algorithm of the left ventricle in MR short-axis images with the essential restriction of no manual corrections.

Methods: The study population consisted of 13 patients and 12 healthy volunteers. Fifteen of the subjects were studied twice resulting in a total of 40 data sets available for analysis. A horizontal and vertical long-axis slice and a series of consecutive slices in the short-axis view covering the entire left ventricle were acquired using a steady-state free precession technique. The outline of the left ventricle, including the mitral valve and apex, was indicated manually in the two-chamber and four-chamber images. The intersections of these outlines with the short-axis images served as the starting point for the automatic contour detection. The automatic detected contours were used to calculate endocardial end-diastolic volume (EDV), end-systolic volume (ESV), epicardial volumes, ejection fraction (EF) and mass. For validation, two independent investigators draw the contours in the short-axis slices in all data sets.

Results: Based on the contours manually traced by the two observers, the inter-observer variability for the endocardial volume was 16.1 mL (6.5%) for EDV and 17.7 mL (10.6%) for ESV and for the epicardial volume this was 15.2 mL (3.7%) and 15.4 mL (4.8%), respectively. Automatically derived

volumes were highly correlated with manually derived volumes ($r^2 = 0.98$) with a mean difference in endocardial volume of -8.2 mL (5.1%) for EDV and -6.0 mL (6.7%) for ESV and in epicardial volume -1.3 mL (0.4%) and 12.1 mL (5.3%), respectively. The derived parameters also correlated good with the manual, $r^2 = 0.95$ for EF (mean difference of 1.6 percentage points (5.1%)) and $r^2 = 0.93$ for mass (mean difference of 7.3

g (5.9%)). The automatic contour detection reduced the inter-observer variability to 0.1 ml for endocardial EDV and ESV and to 1.1 ml for epicardial EDV and ESV.

Conclusions: An automated left ventricle contour detection algorithm based on three-dimensional information shows results with an excellent correlation with manually traced contours and substantially reduces inter-observer variability.

Saturday, January 21, 2006

3:30 PM–5:30 PM

Basic Abstracts: Pushing the Limits: New Applications of CMR in Basic Science

191. DETECTION OF ANGIOGENESIS WITH MAGNETIC RESONANCE MOLECULAR IMAGING IN PERIPHERAL VASCULAR DISEASE

Patrick M. Winter, PhD,¹ Shelton D. Caruthers, PhD,² John S. Allen,¹ Todd A. Williams,¹ Elizabeth K. Lacy,¹ Thomas D. Harris, PhD,³ Samuel A. Wickline, MD,¹ Gregory M. Lanza, MD, PhD,¹ ¹Washington University, St. Louis, MO, USA, ²Philips Medical Systems, Cleveland, OH, USA, ³Bristol-Myers Squibb Medical Imaging, Billerica, MA, USA.

Introduction: In peripheral vascular disease, angiogenesis is required for revascularization following vascular occlusion. L-arginine promotes angiogenesis by augmenting the endogenous production of nitric oxide. The $\alpha_v\beta_3$ -integrin is a cellular adhesion molecule that is selectively expressed on angiogenic endothelium but not mature vasculature. X-ray angiography can reliably detect the proliferation of mature vessels in response to L-arginine therapy about 40 days after the ischemic insult, but is not sensitive to the early stages of angiogenesis. $\alpha_v\beta_3$ -integrin-targeted paramagnetic nanoparticles may offer a means for detecting angiogenesis both in native revascularization and in response to pro-angiogenic therapies.

Purpose: The objective of this study was to determine whether molecular imaging with $\alpha_v\beta_3$ -integrin-targeted paramagnetic nanoparticles could detect the neovascular response to L-arginine earlier than traditional X-ray angiography.

Methods: New Zealand white rabbits were fed a 0.5% cholesterol diet for 60 days, followed by surgical ligation of one femoral artery. After surgery, rabbits were switched to normal chow and treated with either 2.25% (wt/vol) L-arginine in drinking water (n = 10) or normal tap water (n = 8). Ten days after ligation, 3D, T1-weighted, black blood, fat suppressed images

(210 μm by 210 μm resolution, 800 μm slices, TR/TE = 37/3.6 ms, 65° flip angle) were collected of both hindlimbs using a clinical 1.5 T scanner and a quadrature birdcage coil. Images were collected before and two hours post intravenous injection of $\alpha_v\beta_3$ -integrin-targeted paramagnetic nanoparticles (1 ml/kg) to assess angiogenesis in both hindlimbs. MRI signal enhancement was determined by pixel-by-pixel image subtraction. The area of enhancement and the average signal increase (both in percent) were multiplied together and the ratio between the ischemic and control hindlimbs was calculated. A third group of rabbits (n = 8) was treated with L-arginine after ligation, but received non-targeted paramagnetic nanoparticles during the MRI exam. X-ray angiography was performed 40 days post-ligation in a separate cohort of L-arginine treated (n = 3) and untreated animals (n = 2).

Results: Molecular imaging 10 days post-ligation showed L-arginine treated rabbits had significantly greater MRI signal enhancement in the ischemic hindlimb compared to the control limb, while untreated rabbits did not show a significant difference. The ratio of MRI enhancement between the ischemic and control hindlimbs was significantly higher in L-arginine treated rabbits compared to both untreated rabbits and rabbits receiving non-targeted nanoparticles (Fig. *p < 0.05). As expected, X-ray angiography 40 days post-ligation confirmed a greater number of mature vessels in the ischemic vs. control limbs of L-arginine treated rabbits and compared to the ischemic limb of untreated animals (Fig. #p < 0.05).

Conclusions: Targeted paramagnetic nanoparticles can be utilized to specifically detect the molecular signatures of angiogenesis in skeletal muscle. These targeted agents may allow evaluation of the response to pro-angiogenic therapies far earlier than traditional X-ray angiography techniques. These novel molecular imaging techniques could provide earlier and closer management of therapeutic interventions in peripheral vascular disease patients.

192. TOMOGRAPHIC FLUORESCENCE AND MR IMAGING OF MYOCARDIAL INFLAMMATION IN THE BEATING MOUSE HEART IN-VIVO

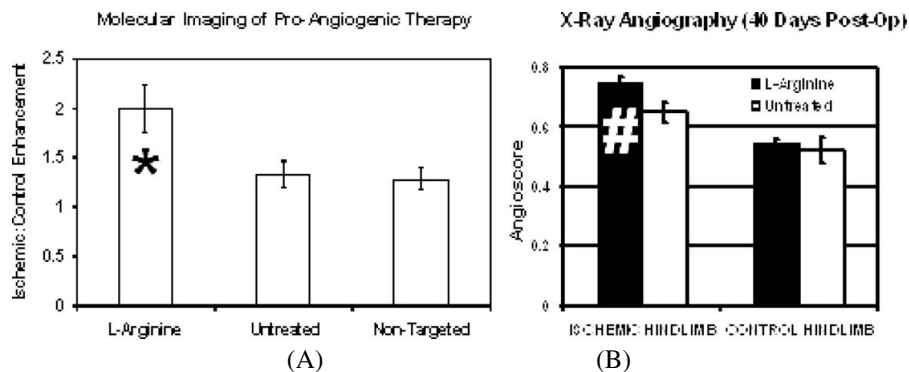


FIG. 1.

David E. Sosnovik, MD FACC, Stephen Windsor, BS, Matthias Nahrendorf, MD, Mikhail Novikov, MD, Anthony Rosenzweig, MD, Lee Josephson, PhD, Ralph Weissleder, MD, PhD, Vasilis Ntzichristos, PhD. Massachusetts General Hospital, Boston, MA, USA.

Introduction: The use of magneto-fluorescent nanoparticles (MNFPs) allows highly complementary MRI and fluorescence data to be acquired with the use of a single probe. We have previously used MNFPs to perform in-vivo MRI and ex-vivo fluorescence reflectance imaging (FRI) in several murine models of cardiovascular disease. Fluorescence tomography (FMT) has numerous advantages over FRI, and does not require sacrifice of the animal to image deep tissues. However, FMT of the heart has not yet been performed in-vivo due to the technical challenges involved. The aim of the present study was thus to investigate the feasibility of cardiac FMT in-vivo, and demonstrate the value of combined tomographic fluorescence (FMT) and MR imaging of the mouse heart in-vivo.

Methods: The MNFP CLIO-Cy5.5, which is taken up avidly by macrophages, was used in a murine model of myocardial inflammation. Thoracotomy and permanent LAD ligation was performed in 7 C57Bl/6 mice, and thoracotomy alone in 5 mice. CLIO-Cy5.5, 20 mg Fe/kg, was injected into the tail vein of all mice 48 hours after surgery. In-vivo MRI (9.4T horizontal bore, Bruker Biospec) and fluorescence tomography were performed 48 hours after probe injection. T2* weighted gradient echo images (TE 3.5–11 ms, slice 1 mm, resolution 150 × 150 μ m), and FLASH cines were acquired in the short axis of the left

ventricle between the papillary muscles and the left ventricular apex. All MR images were gated to both the ECG and respiration. Following MRI, FMT was performed on a custom-built 2nd generation FMT system with 48 illumination spots and a non-contact CCD camera. Intrinsic and fluorescence images at both the transmission (670 nm) and emission wavelengths (700–750 nm) of Cy5.5 were acquired, and the normalized Born ratio was used for tomographic reconstruction. Following the in-vivo MRI and FMT the animals were sacrificed and fluorescence reflectance imaging (FRI) and histology were performed on the excised mouse hearts.

Results: Significant wall motion abnormalities were seen in the anterior and lateral walls of all mice subjected to LAD ligation. A marked reduction in MR signal intensity was seen in the injured myocardium of the infarcted mice, but not in areas of normally contracting myocardium (Fig. 1). Histological sections confirmed the presence of a dense macrophage infiltrate in the infarcted myocardium, suggesting that the reduction in MR signal intensity was secondary to CLIO-Cy5.5 uptake by these infiltrating macrophages. MR signal intensity in the sham operated mice (thoracotomy only) did not show any evidence of regional signal loss consistent with an absence of myocardial inflammation in this model (Fig. 1). FMT imaging revealed a strong fluorescence signal in the livers of all 12 mice, consistent with the known hepatic uptake of CLIO-Cy5.5. However, evidence of a fluorescence signal in the thorax was seen only in the mice subjected to LAD ligation, and not in those subjected to thoracotomy alone (Fig. 1). FRI of the excised hearts showed the presence of CLIO-Cy5.5 only in the infarcted hearts, confirming the accuracy of the in-vivo MRI and FMT images.

Discussion: We demonstrate in this study, for the first time, the feasibility of performing FMT imaging on a rapidly beating mouse heart in-vivo. We furthermore show that the uptake of CLIO-Cy5.5 by macrophages in infarcted myocardium can be imaged in-vivo by either MRI, FMT or both modalities in combination. Future use of the combined MR-FMT approach, using either a single MNFP or tailored combinations of MRI and fluorescence probes, has the potential to provide powerful insights into a variety of cardiac diseases and facilitate the development of novel therapies.

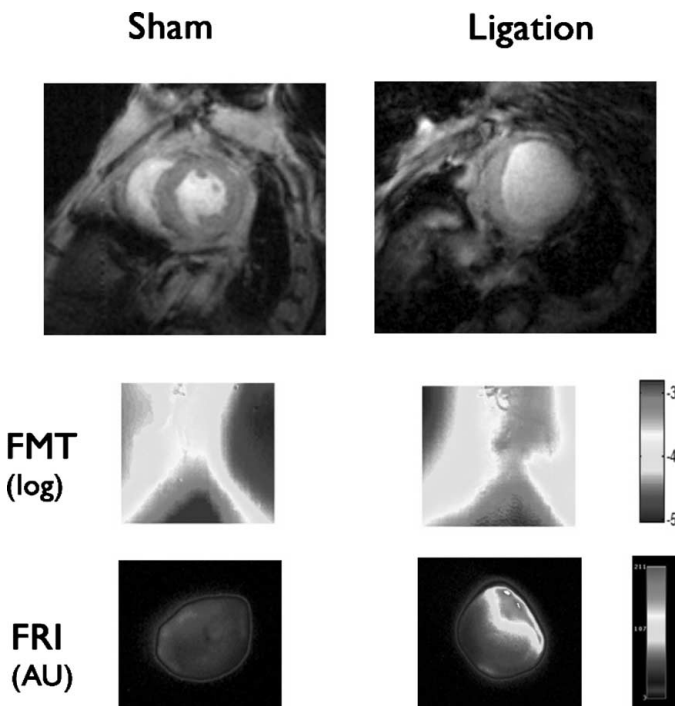


FIG. 1.

193. IMPORTANCE OF INTRAMYOCARDIAL HEMORRHAGE IN ACUTE MYOCARDIAL INFARCTION ASSESSMENT WITH MRI

Jan Bogaert, Maria Kalantzi, Steven Dymarkowski, Stefaan Janssens. Gasthuisberg University Hospital, Leuven, Belgium.

Introduction and Purpose: Intramyocardial hemorrhage (IMH) is frequent complication after mechanical and pharmacological revascularization for acute myocardial infarction. At present it is still an open question, whether these infarcts behave different than infarcts without IMH. The paramagnetic properties of blood

breakdown-products can be exploited to non-invasively detect IMH by using T2-weighted MRI sequences.

Methods: Fifty-two patients with acute myocardial infarction, receiving PCI within 2–12 hours after onset of symptoms, were studied within 1 week (1 W) and 4 months (4 M) after the acute event. T2w- STIR-TSE MRI was used not only to detect myocardial edema (i.e., hyperintense) but also IMH (i.e., centrally hypointense core with peripheral hyperintense rim). Early (i.e., 2–5 min) contrast-enhanced MRI was used to visualize microvascular obstruction (MVO) while late imaging (i.e., 10–25 min) was used for infarct imaging.

Results: While the majority (43/52) of patients showed homogeneous hyperintense signal on T2w MRI, nine patients showed a distinct IMH pattern. All 9 IMH patients showed MVO on early CE-MRI, while MVO was found in 23/43 of the edema group. When comparing both MVO groups, IMH patients showed a trend towards longer time of onset to PCI (380 ± 272 vs. 266 ± 122 min, $p = 0.07$) and higher troponin I levels ($p = 0.086$). While no differences in infarct volume (27.2 ± 19.5 vs. 24.2 ± 12.1 g, $p = 0.5$) between groups, IMH patients showed a trend towards larger MVO volume ($48.7 \pm 29.3\%$ vs. $31.5 \pm 21.8\%$, $p = 0.079$) (i.e., MVO volume normalized to the infarct volume). LV mass index and mean LV wall thickness were larger in IMH infarcts (72.4 ± 16.0 vs. 57.5 ± 9.1 g, $p = 0.006$, and 8.0 ± 1.9 vs. 6.7 ± 1.4 mm, $p = 0.02$, respectively). At 4 M, there was a clear trend towards a larger loss in myocardial tissue (-10.6 ± 8.2 vs. -5.3 ± 9.4 g, $p = 0.1$) and reduction in LV wall thickness in IMH patients (infarcted area: $p = 0.07$, remote area: $p = 0.026$). Global (ejection fraction) and regional function (systolic wall thickening) were found very similar between IMH and non-IMH MVO infarcts early and 4 M after the acute event.

Conclusions: IMH is not an infrequent finding after coronary reperfusion for myocardial infarction, detectable by a central hypointense core and surrounding hyperintense rim on T2w MRI. Current study results suggest a pattern and behavior that is not only very similar but likely even more severe than the one found in MVO infarctions. IMH infarcts seem to occur preferentially in patients with pre-existing LV hypertrophy. Although IMH MVO and non-IMH MVO infarctions behave functionally similar, IMH infarcts seem to be prone to more LV remodeling.

194. FAT SUPPRESSION STRATEGIES FOR OFF-RESONANCE (IRON) IMAGING OF MAGNETICALLY-LABELED STEM CELLS

Saurabh S. Shah, BS,¹ Wesley D. Gilson, PhD,² Robert G. Weiss, MD,³ Bradley P. Barnett, BS,⁴ Jeff W. M. Bulte, PhD,⁴ Dara L. Kraitchman, VMD, PhD,² Matthias Stuber, PhD,^{2,3,5} ¹Department of Biomedical Engineering, Johns Hopkins University, Baltimore, MD, USA, ²Russell H. Morgan Department of Radiology and Radiological Science, Johns Hopkins University School of Medicine, Baltimore, MD, USA, ³Department of Medicine, Johns Hopkins Uni-

versity School of Medicine, Baltimore, MD, USA, ⁴Institute for Cell Engineering, Johns Hopkins University School of Medicine, Baltimore, MD, USA, ⁵Department of Electrical Engineering, Johns Hopkins University School of Medicine, Baltimore, MD, USA.

Introduction: Inversion Recovery with ON-resonant water suppression (I) (IRON) is a positive contrast imaging method that enhances signal originating from susceptibility induced local field variations, by using an on-resonant water suppression prepulse (IRON pulse). It has been used to improve visualization of magnetic nanoparticle-labeled stem cells. However, since the IRON method intrinsically highlights off-resonant protons, unwanted fat signal also appears signal-enhanced. Therefore, effective fat suppression approaches for IRON imaging must be developed.

Purpose: To theoretically and experimentally investigate three different approaches for fat suppression in combination with IRON imaging.

Methods: A theoretical model of the local field variations for an injection of iron-labeled cells was simulated in MATLAB by studying the dipolar field equation for the Lorentz' Sphere (Fig. 1A). Based on theoretical considerations, three strategies were developed to suppress fat signal for the IRON method. The first design, *double IR*, employed a double inversion recovery prepulse ($TI_1 = 400$ ms, $TI_2 = 60$ ms) for T1-nulling of the fat signal (Fig. 1B). The second method, *broadband IRON*, used an IRON pulse with a broad excitation bandwidth (BW) and center frequency set between the resonance peaks of fat and water ($FA = 95^\circ$, frequency offset = -240 Hz, BW = 1020 Hz), therein simultaneously suppressing both water and fat signal (Fig. 1C). The third strategy, *SPIR*, combined the IRON pulse with a spectral presaturation prepulse ($FA = 95^\circ$, frequency offset = -480 Hz, BW = 339 Hz) to selectively suppress fat signal (Fig. 1D). These three approaches were implemented on a

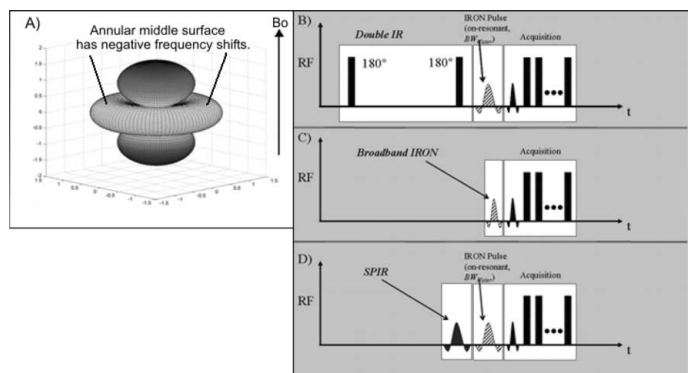


FIG. 1. A) Enhancement pattern for an iron particle in presence of the static magnetic field. Three approaches for fat suppression with IRON imaging are shown here: B) *Double Inversion Recovery (Double IR)* for T1-based nulling of the fat signal; C) *Broadband IRON* where the broad excitation bandwidth of the IRON pulse is used to suppress both water and fat signals simultaneously; and D) *SPIR* prepulse, to selectively suppress the fat signal.

Table 1. SNR and CNR comparison for all the approaches

Imaging Method	SNR _{cells}	SNR _{fat}	SNR _{agarose}	CNR _(cells/agarose)	CNR _(cells/fat)	CNR _(agarose/fat)
1. IRON pulse without fat suppression	95.01	180.47	21.02	73.99	85.46	159.45
2. Fat Suppression using <i>Double IR</i>	40.73	6.61	10.21	30.52	34.12	3.60
3. Fat Suppression using <i>Broadband IRON</i>	38.38	19.89	30.16	8.22	18.49	10.27
4. Fat Suppression using <i>SPIR</i>	78.37	13.52	23.05	55.32	64.85	9.53

Philips 3T Achieva scanner and tested on a gelatin phantom. Three 15mL samples were embedded in the gelatin containing agarose only (doped with CuSO₄), agarose with iron-labeled C17.2 murine neural stem cells (~2 million), or mineral oil. Stem cells were magnetically labeled by magnetoelectroporation(2). Coronal images were obtained using the IRON method with a fast spin-echo acquisition (TE/TR = 10 ms/3000 ms, FA = 90°, FOV/matrix = 220 mm/512, thickness = 3 mm, echo spacing = 10 ms, echo train length = 24). For image analysis, regions-of-interest were manually selected within the agarose, oil and stem cells. Subsequently, signal-to-noise ratio (SNR) for the enhanced cell signal and contrast-to-noise ratio (CNR) between the cells/fat, cells/agarose and agarose/fat were determined for all three approaches.

Results: The MATLAB simulation shows the anticipated shifts in the Larmor frequencies and the characteristic pattern of signal enhancement when a paramagnetic particle is exposed to a static magnetic field (Fig. 1A). Positive frequency shifts are associated with the upper and lower lobes, and negative shifts are associated with the annular middle surface (Fig. 1A-arrows).

Using the IRON method without fat suppression, significant enhancement of the iron-labeled cells was observed but the fat

signal also appeared hyper-enhanced (Fig. 2A). In contrast, the fat signal was effectively suppressed using the *Double IR* strategy optimized for T1-based fat nulling (Fig. 2B). However, SNR and subsequently CNR were significantly reduced relative to the other approaches (Table 1). Using the *Broadband IRON* pulse that suppresses on-resonant protons and fat simultaneously, moderate suppression of water and fat signal was observed, and the enhancement from the negative frequencies was concurrently suppressed, as expected (Fig. 2C, arrows). Excellent fat and water suppression was obtained using the *SPIR* in combination with IRON (Fig. 2D).

Conclusions: Effective fat suppression with IRON imaging was demonstrated *in vitro* for enhanced visualization of iron-labeled stem cells using all three approaches. Excellent signal enhancement and fat suppression were observed using the IRON method with *SPIR* or *Double IR* prepulses. However, *Double IR* may not be appropriate for real-time imaging applications. *SPIR* has superior SNR/CNR among all three strategies. Although suppression was reduced in the *Broadband IRON* approach; the short preparation time lends itself to be useful in rapid imaging strategies.

REFERENCES

1. Stuber, *et al.* Proc. ISMRM 13 2005.
2. Walczak, *et al.*, MRM (2005).

195. FERUMOXTRAN-10 UPTAKE IN THE VESSEL WALL INCREASES WITH ATHEROSCLEROSIS SEVERITY: EX VIVO RABBIT STUDY

Masahiro Terashima, MD, PhD, Michael V. McConnell, MD, MSEE. *Stanford University School of Medicine, Stanford, CA, USA.*

Introduction: Inflammation, including macrophage infiltration, is an important feature of vulnerable atherosclerotic plaques. The ultra-small superparamagnetic iron oxide (USPIO) agent ferumoxtran-10 has been shown to be taken up by macrophages in animal and human atherosclerosis, but quantitative assessment has been limited.

Purpose: To study the relationship between ferumoxtran-10 uptake and the degree of atherosclerosis in a balloon-injured rabbit atherosclerosis model.

Methods: Twelve New Zealand white rabbits underwent aortic balloon injury and high-fat diet for 14 (n = 4) or 26 weeks

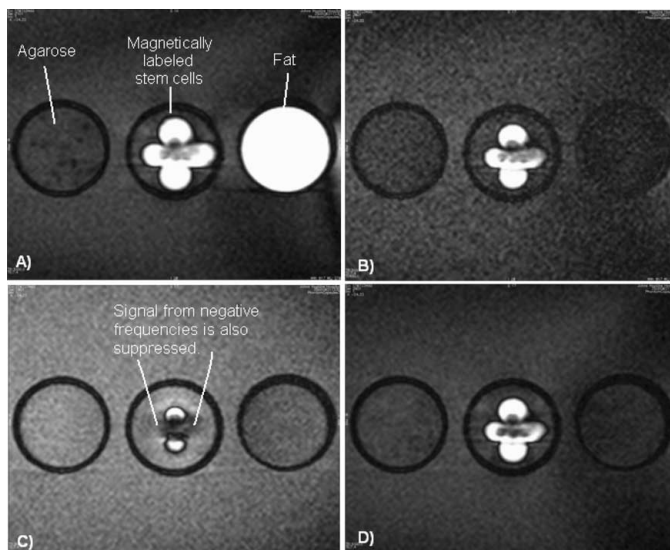


FIG. 2. Phantom images on 3T. From left, tube 1 contains Agarose; tube 2 has magnetically labeled stem cells as point source and tube 3 contains fat. A) IRON method without any fat suppression. B) *Double IR* for fat suppression prior to IRON pulse. C) *Broadband IRON* for both water and fat suppression. D) *SPIR* prepulse for fat suppression prior to IRON pulse.

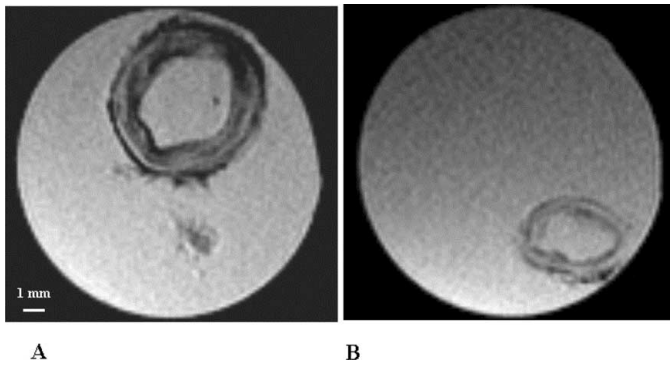


FIG. 1. Representative MR image in rabbits. A. VA = 34.6, WA = 22.2, SI_{wall} = 638, B. VA = 13.75, WA = 8.61, SI_{wall} = 1213.

(n = 8) to induce atherosclerosis. Five days prior to sacrifice, 10 (n = 5) or 25 (n = 7) mgFe/kg ferumoxtran-10 (Combidex[®], Advanced Magnetics, Inc.) was given intravenously. The aorta was removed and underwent perfusion fixation, followed by *ex vivo* MRI and then histology. MRI was performed on a 1.5T whole-body scanner (GE Signa CV/i) equipped with high-performance gradients (40 mT/m, 150 T/m/ms) using a standard 3-inch surface coil. A standard 2D gradient-echo sequence was performed to visualize the negative contrast T2* effect (TR/TE = 450–550/6 ms, NEX = 2, FOV = 8 cm, slice thickness = 2.0 mm, gap = 1.0 mm, Flip angle = 30, Matrix = 512 × 512, in-plane spatial resolution = 156 μm). Vessel area (VA) and lumen area (LA) were traced manually in the thoracic and abdominal aorta on a total of 410 images (34 images per rabbit). Wall area (WA) was calculated as VA-LA. Signal intensity (SI_{wall}) and SNR/CNR of the vessel wall were calculated. On histology, the degree of ferumoxtran-10 uptake in the thoracic aorta was graded by Perl's iron staining: None (positive stain <1% vessel area), Mild (<10% area), Moderate (<50% area), and Severe (>50% area). RAM-11 was used for macrophage staining.

Results: Qualitatively, there were areas of signal loss seen on MRI in all rabbits, indicative of Ferumoxtran-10 uptake (Fig. 1). Quantitatively, the degree of Ferumoxtran-10 uptake, as measured by the decrease in SI_{wall} and SNR/CNR of the vessel wall, was correlated with atherosclerosis severity as measured by WA (SI_{wall} vs. WA: r = -0.35; SNR vs. WA: r = -0.38, CNR vs. WA: r = -0.24, all for p < 0.001). The dose of 25 mgFe/kg of ferumoxtran-10 caused greater signal loss compared to 10 mgFe/kg (SI_{wall}: 919 ± 261 vs. 1028 ± 247, p < 0.001, SNR: 428 ± 135 vs. 465 ± 122, p = 0.004, CNR: -160 ± 104 vs. -83 ± 54, all for p < 0.005). However, the 10 mgFe/kg dose showed better correlation with atherosclerosis severity (SI_{wall} vs. WA: r = -0.38; SNR vs. WA: r = -0.49, CNR vs. WA: r = -0.45, all for p < 0.0001). Histology showed moderate-grade ferumoxtran-10 uptake in the majority of rabbits (7 of 11), with uptake more prominent in the smaller macrophages near the lumen rather than the deeper foamy macrophages (Fig. 2).

Conclusions: Quantitative assessment of ferumoxtran-10 uptake, particularly at 10 mgFe/kg dose, correlated with

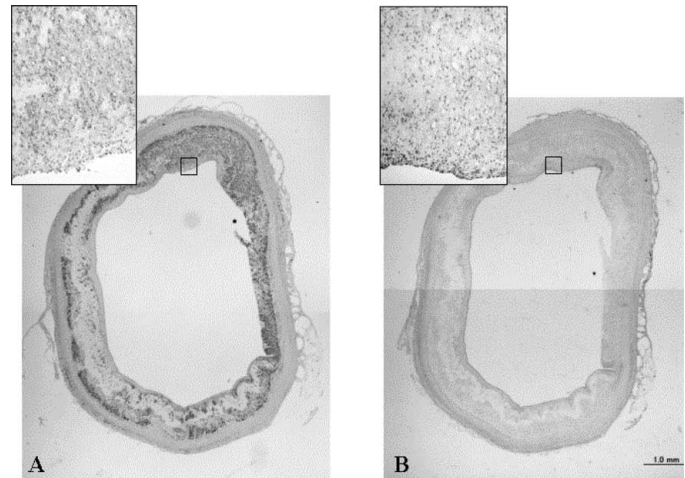


FIG. 2. Histology of the same rabbit aorta as Fig. 1A. A. Macrophage immunostaining with RAM-11 (brown pigmentation). B. Perl's iron staining (blue dots). Insets are the magnified pictures of the boxes in the vessel wall. The uptake of ferumoxtran-10 was more prominent in the smaller macrophages near the lumen rather than the deeper foamy macrophages.

atherosclerosis severity in a rabbit model. Ferumoxtran-10 has the potential to grade plaque inflammation and severity.

196. MRI TRACKING OF THE REGIONAL PERSISTENCE OF FERIDEX-LABELED MESENCHYMAL STEM CELLS IN A CANINE MYOCARDIAL INFARCTION MODEL

Ana Victoria Soto,¹ Wesley D. Gilson,¹ Dorota Kedziorek,² Danielle Fritzges,¹ Izlem Izbudak,¹ Randell G. Young,³ Mark F. Pittenger,⁴ Jeff W. Bulte,² Dara L. Kraitchman¹
¹Russell H. Morgan Department of Radiology and Radiological Science, Johns Hopkins University, Baltimore, MD, USA, ²Department of Radiology and Institute for Cell Engineering, Johns Hopkins University, Baltimore, MD, USA, ³Osiris Therapeutics, Inc, Baltimore, MD, USA, ⁴Division of Cardiology Johns Hopkins University School of Medicine, Baltimore, MD, USA.

Introduction: New methods of cellular therapy for cardiac regeneration after acute myocardial infarction (AMI) are being performed, including those which utilize mesenchymal stem cells (MSCs). To determine the efficacy of these cellular therapies, methods to monitor engraftment, such as magnetic labeling with MRI assessment, are desirable.

Purpose: The purpose of this study was to determine the regional persistence of targeted magnetically-labeled MSCs (MR-MSCs) with respect to the infarction site over an 8 week time-course using MRI.

Methods: Animal Model and Imaging. Seven dogs (25–30 kgs) were subjected to a 90-minute closed-chest coronary artery occlusion followed by reperfusion to create an AMI. Autologous MSCs were isolated from bone marrow and magnetically

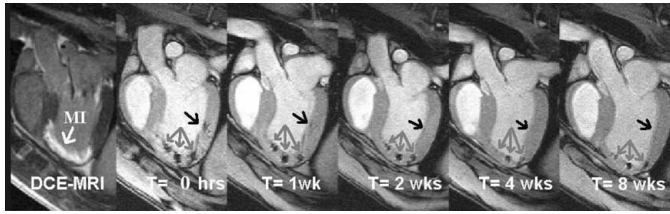


FIG. 1. Delayed contrast-enhanced (DCE) long-axis image (left) demonstrating infarct myocardium (MI). Four MR-MSC injections appear as hypointense areas on fast, gradient echo images immediately after injection (T = 0 hrs, arrows). Serial imaging at 1 week, 2 weeks, 4 weeks, and 8 weeks demonstrates the persistent of the MR-MSC injections. The volume of injections decreases over time. In addition, an injection placed in the normal myocardium (black arrow) can no longer be detected at 4 weeks post-injection.

labeled with $25 \mu\text{g Fe/mL}$ Feridex and 375 ng/mL poly-L-lysine for 24 hours prior to delivery (1). At 72 hours post-AMI (T = 0), delayed contrast-enhanced (DCE) MRI was performed to determine the infarct location. Subsequently, each dog received $30\text{--}190 \times 10^6$ MR-MSCs (7×10^6 MSCs per injection) under MR fluoroscopy (1.5T GE C/Vi) targeted to normal, adjacent, and infarcted myocardium (2). Contiguous fast, gradient echo (FGRE) short-axis images (TR/TE = 6/1.6 ms; $0.5 \times 0.5 \times 5$ mm voxel; 2 NSA; 20° FA; 32 kHz BW) were obtained spanning the left ventricle to localize MSC injection sites. FGRE and DCE imaging was repeated at 1, 2, 4, and 8 weeks post-injection to assess persistence of MR-MSCs. *Image analysis.* A 6-sector per slice model was used to track regional persistence of MR-MSCs. Each sector was classified according to infarct status based on DCE images. Hypoenhanced regions of FGRE images were corresponded to DCE infarct classifications using Amide (3).

Results: At T = 0, hypointense signal voids were present in all three regions, with 59.3% in the infarct, 22.2% in the adjacent, and 18.5% in the normal region. A general trend of disappearance of injections in myocardium was present such that, at 8 weeks, 87.5% of original infarcted region injections were still

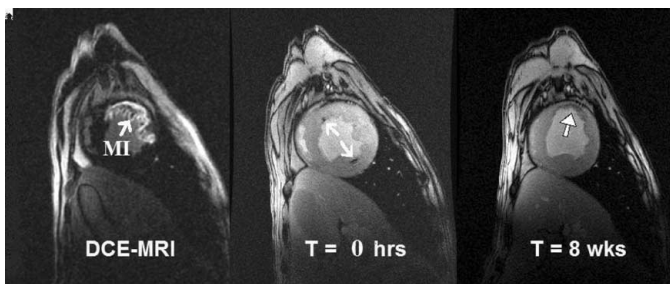


FIG. 2. A short-axis delayed contrast-enhanced (DCE) MRI demonstrates the region of myocardial infarction (MI). Two injections were placed in the peri-infarction area at 0 hours post-infarction (arrows) as seen on fast, gradient echo images immediately after injection (middle). At 8 weeks post-injection, distinct injection sites are no longer visible (right). A large hypointense sub-endocardial rim is demonstrated on the fast, gradient echo images (right). Histological analysis showed that the cells were positive for Feridex, but did not contain cardiomyocyte markers and were not macrophages (data not shown).

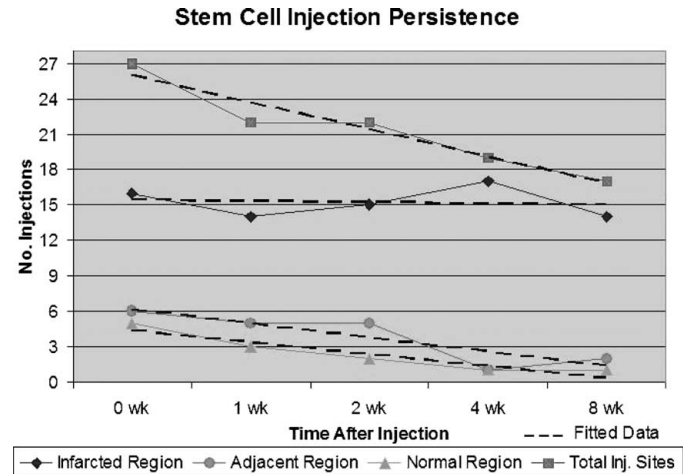


FIG. 3. Number of stem cell injection are shown at 0, 1, 2, 4, and 8 weeks at each region: infarcted, adjacent, and normal. Total injection sites were also plotted for all times. The number of injections decreased over time in all regions, but the normal region showed the greatest diminution of injections as compared to the infarcted and adjacent regions.

present, whereas only 33.3% of the adjacent and 20.0% of the normal regions remained (Fig. 1). A more detailed progression of stem cell injection persistence can be viewed in the graph. In addition, at week 8, the total number of distinct injection sites had decreased by 37.0% from those visualized at week 0. This was in some cases due to marked stem cell migration into the infarcted tissue (Fig. 2). Histological analysis of injection sites in adjacent and infarcted myocardium showed no indication of cardiomyocyte regeneration.

Conclusions: Traditional imaging techniques, such as DCE and high resolution imaging, can be used to accurately target and track stem cells. The higher tendency of the MSCs to remain in the infarcted and peri-infarction site throughout the eight week span indicates that these areas may be the preferred for targeting. The more than 1/3 reduction in injection sites over two months represents a combination of stem cell death and to a lesser extent, stem cell migration within the heart. Serial MR imaging of MR-labeled stem cells could provide a method for tailoring therapy to individual patients as well as for targeting therapy to the areas with the highest likelihood of efficacy.

REFERENCES

1. Kraitchman DL, et al. *Circulation*, 2003;107:2290-3.
2. Karmarkar, et al. *Magn Reson Med* 2004;51:1163-72.
3. Loening, A.M., Gambhir, S.S. *Molecular Imaging*, 2003;2:131-7.

197. THERAPEUTIC ANGIOGENESIS WITH CONTROLLED RELEASE OF VEGF FROM BIODEGRADABLE POLYMER MICROSPHERES IN A RABBIT MODEL OF HIND LIMB ISCHEMIA

Anthony Z. Faranesh, PhD,¹ Dara L. Kraitchman, VMD, PhD,² Elliot R. McVeigh, PhD¹ ¹Laboratory of Cardiac

Energetics, National Heart, Lung, and Blood Institute, National Institutes of Health, Bethesda, MD, USA, ²Russel H. Morgan Department of Radiology and Radiological Science, The Johns Hopkins University, Baltimore, MD, USA.

Introduction: Therapeutic angiogenesis has the potential to be an effective treatment strategy for patients who suffer from ischemic vascular disease. Evidence suggests that the delivery route is important for angiogenic therapy, and it has been proposed that local, sustained release of low amounts of angiogenic protein may be most effective in creating functional vasculature. Biodegradable polymer microspheres are an effective means for providing sustained, localized drug delivery. In this study, non-invasive MR imaging was used to test the efficacy of biodegradable polymer microspheres loaded with vascular endothelial growth factor (VEGF) to treat ischemia.

Purpose: To evaluate the efficacy of VEGF-loaded biodegradable polymer microspheres for achieving therapeutic angiogenesis in a rabbit model of hind limb ischemia.

Methods: Biodegradable polymer microspheres based on poly(DL-lactic-co-glycolic acid) were made to encapsulate VEGF and Gd-DTPA according to methods previously described (1). Two weeks after unilateral femoral artery ligation, animals received one of three treatments: 1) Empty microspheres (Control) (n = 7); 2) Bolus injection (100 μg) of VEGF protein (VEGF protein) (n = 8); or 3) Microspheres encapsulating VEGF (VEGF spheres) (n = 8). Calf blood pressure ratios (BPR) were measured to evaluate global limb perfusion. In addition, dynamic contrast-enhanced MRI using the intravascular contrast agent Gadomer-17 was used to evaluate functional tissue parameters. Quantitative T₁ maps were acquired before and after i.v. administration of 0.05 mmol/kg of Gadomer-17, and data was fit to the Tofts two compartment model (2) to calculate tissue permeability (K^{trans}), interstitial volume (v_e) and plasma volume (v_p), as markers of angiogenesis in the soleus muscle. Measurements were made at the time of treatment (day 14) and two weeks after treatment (day 28). For each measurement, the nonsurgical limb served as control, and a ratio was formed by dividing the value for the ischemic limb by the value for the normal limb. The percent change in the ischemic to normal ratio from day 14 to day 28 was computed.

Results: The percent changes in parameters from day 14 to day 28 are summarized in Table 1. At two weeks post treatment, a significant increase in BPR was observed in the VEGF protein and VEGF spheres groups (P < 0.05), while improvement in the control group did not reach statistical significance. Increases

Table 1. Percent change from day 14 to day 28

	ΔBPR	ΔK^{trans}	Δv_e	Δv_p
Control	27 ± 17	-10 ± 6*	-17 ± 4*	-13 ± 9
VEGF protein	35 ± 10*	-2 ± 14	-6 ± 5	-8 ± 9
VEGF spheres	20 ± 9*	31 ± 20	21 ± 11	2 ± 8

*P < 0.05 day 14 vs. day 28.

in vascular permeability and interstitial volume were observed for the VEGF spheres group, while these parameters decreased for the control and VEGF protein groups. Plasma volume was maintained for the VEGF spheres group, while it decreased for the control and VEGF protein groups.

Conclusions: Controlled delivery of VEGF-165 from biodegradable polymer microspheres results in improved limb perfusion and maintains elevated levels of functional angiogenic markers (tissue permeability, interstitial volume, and plasma volume). This study indicates that controlled delivery of angiogenic therapy can be monitored by MRI and is feasible using biodegradable polymer microspheres with enhanced efficacy over a single bolus administration of protein.

REFERENCES

1. Faranesh AZ, et al. In vitro release of vascular endothelial growth factor from gadolinium-doped biodegradable microspheres. *Magn Reson Med* 2004;51:1265–71.
2. Tofts PS, et al. Estimating kinetic parameters from dynamic contrast-enhanced T(1)-weighted MRI of a diffusable tracer: standardized quantities and symbols. *J Magn Reson Imaging* 1999;10:223–32.

198. GADOLINIUM MIXED-MICELLES: EFFECT OF SIZE ON *IN VITRO* AND *IN VIVO* EFFICACY

Karen C. Briley-Saebo, PhD, Venkatesh Mani, PhD, Vardan Amirbekian, MD, Juan Carlos Frias, PhD, Zahi A. Fayad, PhD. Mount Sinai School of Medicine, New York, NY, USA.

Introduction: Mixed micelles are nanoparticles (15–150 nm) that incorporate phospholipids, biocompatible non-ionic surfactants, and a lipophilic gadolinium complex. The unique properties associated with gadolinium-mixed micelles allow for the development of a variety of potential MR contrast agents including: molecular targeted agents for atherosclerotic plaque, long circulating intravascular agents, and multifunctional or multimodal

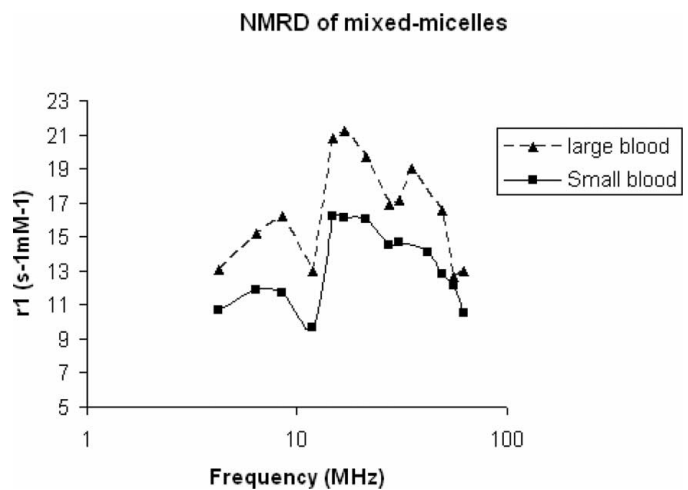


FIG. 1. NMRD of micelles in blood at 25°C.

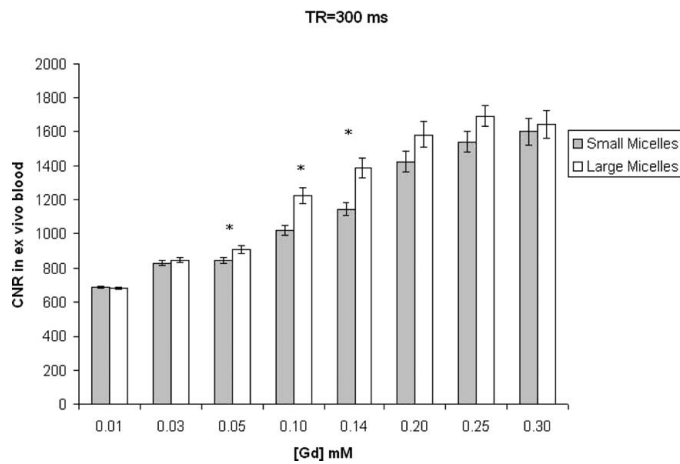


FIG. 2. CNR in whole human blood T1-w TSE at 1.5T.

agents. The hydrated particle size of mixed-micelles is primarily controlled by the phospholipids used to generate the material. Particle size has proven to be a key factor in determining the efficacy, biodistribution and pharmacokinetics of iron based particles. However, unlike iron oxide particles that are rigid spheres, micelles are flexible entities that are able to permeate relative small pores.

Purpose: To determine the effect of gadolinium mixed-micelle size on the *in vitro* relaxation properties of blood and the *in vivo* signal enhancement of atherosclerotic plaque in ApoE knockout mice.

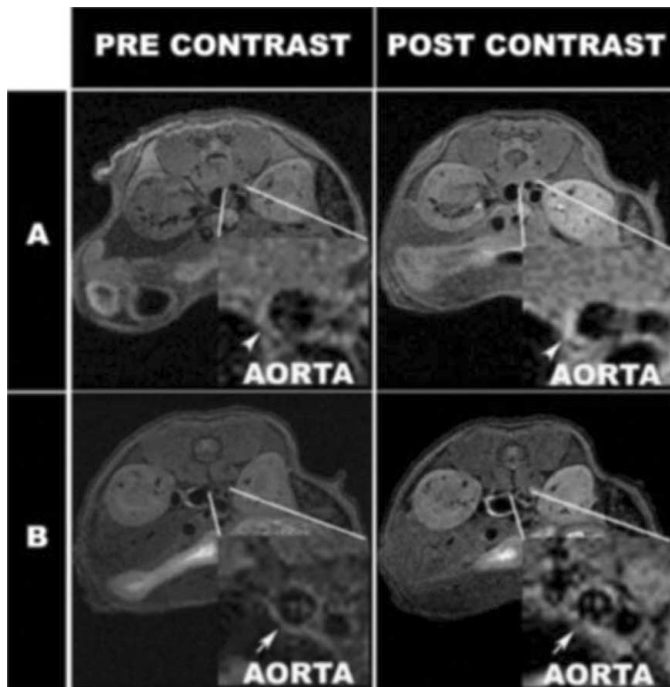


FIG. 3. Images pre and 24 hours post injection of (A) small micelles and (B) large micelles in the aorta of ApoE KO mice at 9.4T.

Table 1.

	Large Micelle	Small Micelle
Normalized Enhancement Ratio of the Aorta	1.19 ± 0.17	1.24 ± 0.15
Percent Enhancement in Aortic Wall	19.2 ± 2.7%	23.7 ± 2.9%
Contrast-To-Noise Ratio (Aorta to Lumen) 24-Hrs Pre-Contrast Injection	8.40 ± 1.9	10.7 ± 2.5
Contrast-To-Noise Ratio (Aorta to Lumen) 24-Hrs Post-Contrast Injection	11.3 ± 2.7	13.5 ± 2.3
Contrast-To-Noise Ratio (Aorta to Lumen) 24-Hrs Post-Contrast Injection	2.82	2.80

Methods: Two micelle formulations were prepared by sonicating 7 w/w% Gd-DTPA-(C₁₈)₂, 14 w/w% Tween 80, and 79 w/w% of either POPC or DPPC. Small micelles (SM, dia. 36 nm) had 270 Gd complex/micelle and large micelles (LM, dia. 106 nm) had 4,100 Gd complex/micelle. Whole human blood was doped with varying concentrations of micelles (0–0.3 mM) and NMRD analysis was performed at 25 Å°C using a field cycling relaxometer (NIH, Bethesda MD). A gel phantom was prepared and the following parameters determined at 1.5T: T2* using multiple double echo sequences, T1 using SPGR sequences, and contrast-to-noise ratios (CNR) relative to blood using fast SE sequences. Thirteen-month-old atherosclerotic ApoE knockout (KO) mice on a high cholesterol diet underwent *in vivo* MR microscopy of the abdominal aorta using a 9.4T MR system. Animals were administered a micelle dose of 0.01 $\hat{I}^{1/4}$ mol Gd/kg and imaging was performed at multiple time-points up to 24-hours post-injection. All imaging was performed using a T1-w black blood (SE) sequence with TR/TE/flip = 600 ms/8.6 ms/30 Å°. Signal intensity measurements were taken using regions of interest on the aortic wall with four points in four quadrants of the aorta and CNR values of aortic wall to lumen were determined.

Results: NMRD data showed that LM gave increased r1 values relative to SM at all fields tested (Fig. 1). Additionally, significant increases in CNR were observed for LMs relative to SMs at concentrations >0.03 mM Gd (Fig. 2). No significant r2* effects in blood were observed for either formulation over the concentration range tested. Fig. 3 shows representative images obtained for the small (A) and large (B) micelles pre and 24 hours post injection. Table 1 summarizes the *in vivo* results obtained for each micelle formulation. No significant differences in the enhancement ratios were observed between the two formulations tested. Additionally, no significant differences in the CNR values (obtained 24 hours post injection) were observed.

Conclusions: Micelle size influences the relaxation properties and signal enhancement of *in vitro* blood. However, the data strongly suggests that the uptake of mixed-micelles into plaque may be driven by mechanisms that are not directly related to micelle size.

199. THE ACUTE ALLOGRAFT REJECTION IS HETEROGENEOUS: NON-INVASIVE IMAGING OF PERICARDIUM-TO-ENDOCARDIUM PROGRESSION OF MACROPHAGE INFILTRATION WITH MRI

Yijen L. Wu, PhD, Qing Ye, MD, Lesley M. Foley, BS, Kevin Hitchens, PhD, Chien Ho, PhD *Pittsburgh NMR Center, Carnegie Mellon University, Pittsburgh, PA, USA.*

Introduction: The current gold standard for diagnosing and staging rejection after organ transplantation is biopsy, which is not only invasive but also prone to sampling errors. We have been establishing non-invasive means for staging allograft rejection after heart transplantation with MRI by in vivo labeling of macrophages with iron oxide particles. Two types of iron oxide particles are used here: (1) dextran-coated ultra-small superparamagnetic iron oxide (USPIO) particles; and (2) micrometer-sized superparamagnetic iron oxide (MSPIO) particles. Our data showed that the infiltration of macrophages in the rejecting allograft hearts is highly heterogeneous and exhibited a reproductive epicardium-to-endocardium progression pattern over time as acute allograft rejection progresses. This spatial distribution of macrophage infiltration can potentially be used for non-invasive staging of acute allograft rejection.

Methods: Animal model: An abdominal heterotopic working heart and lung transplantation model is used using DA to BN transplantation rat pairs. The transplanted hearts exhibit similar cardiac outputs and ventricular pressure close to those in native hearts. Mild (Grade 1A or B) rejection develops by post-operation day (POD) 2.5–3.5; grade 2 rejection develops on POD 4.5–5.5; whereas the moderate to the severe (Grade 3A)

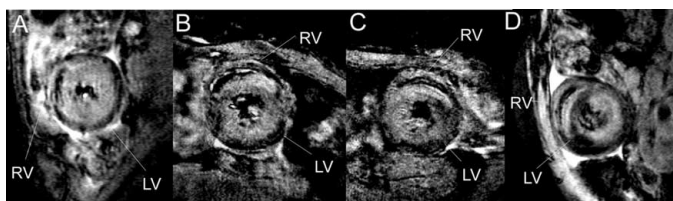


FIG. 1. T2*-weighted image of transplanted allograft hearts 1 day after USPIO (27 nm) administration at (A) POD 3, (B) POD 4, (C) POD 5, and (D) POD 6.

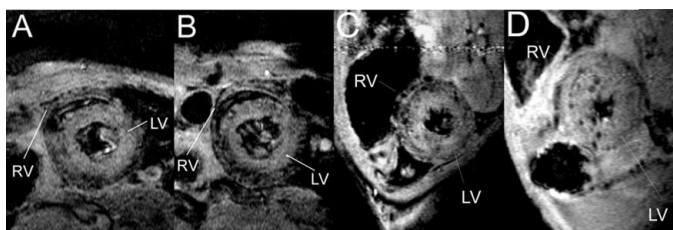


FIG. 2. T2*-weighted image of transplanted allograft hearts 1 day after MSPIO (1 mm) administration at (A) POD 3, (B) POD 4, (C) POD 5, and (D) POD 6.

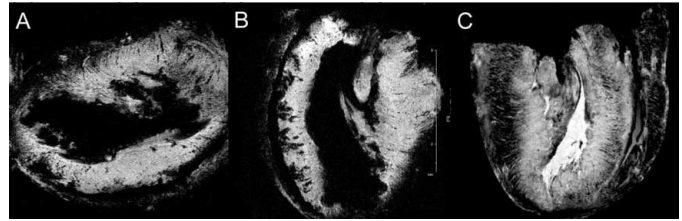


FIG. 3. MRM at 11.7T of allograft hearts after USPIO (27 nm) labeling at (A) POD 4, (B) POD 5, and (C) POD 6.

rejection develops after POD 6–7. MRI methods: EKG and respiration gated T2*-weighted cine imaging on Bruker AVANCE 4.7-T system was used for in vivo imaging with the in-plane resolution of 156 μm . High-resolution 3D imaging is performed at 11.7T with voxel size 46.8 micrometer. Iron oxide particle labeling: Immune cells, mostly macrophages, are labeled in vivo by direct intravenous injection of USPIO or MSPIO (Bangs) particles 1 day prior to MRI scans.

Results: We have previously shown that immune cells, particularly macrophages, accumulated in the rejection sites can be detected non-invasively with MRI by in vivo with direct intravenous injection of iron-oxide particles. Two types of the iron-oxide particles are used here: USPIO particles, which are 27 nm in size; and MSPIO particles, which are about 1 micrometer in size. Macrophage infiltrated foci can be imaged at different rejection stages from post-operation day (POD) 3 to 6. Our data revealed a pericardium-to-endocardium progression of macrophage infiltration as the rejection progresses with both USPIO (Fig. 1) and MSPIO (Fig. 2) labeling. On POD3, with only mild rejection, the macrophage-concentrated areas are limited to the pericardium regions (Fig. 1A and Fig. 2A). On POD 4, macrophage-concentrated areas are slightly larger compared to those at POD 3, but still more concentrated near the pericardium (Fig. 1B & Fig. 2B). On POD 5, more areas are infiltrated with macrophages and more towards the inner parts of LV (Fig. 1C & Fig. 2C). On POD 6, macrophages showed aggressive infiltration throughout inner LV (Fig. 1D & Fig. 2D). MR Microscopy (MRM) of excised hearts showed that the macrophage-infiltration areas resemble peri-vascular structure on POD 5 (Fig. 3B) and the Torrent-Guasp's sheet-like secondary structure on POD 6 (Fig. 3C). The pericardium-to-endocardium progression patterns are confirmed with histology by ED1 macrophages staining.

Conclusions: Our data show that acute allograft rejection after heart transplantation is spatially heterogeneous. MRI is not only non-invasive, but also provides 3-dimensional whole-heart perspectives for the rejection processes. This spatial pericardium-to-endocardium progression can be used for simple and more accurate staging acute allograft rejection.

200. MYOCARDIAL T1 MAPPING: IMPLEMENTATION AND VALIDATION OF AN OPTIMIZED PULSE SEQUENCE VARIANT FOR MODIFIED LOOK-LOCKER

INVERSION-RECOVERY (MOLLI) IN PHANTOMS AND IN HEALTHY SUBJECTS

Daniel R. Messroghli, MD,¹ Andreas Greiser, PhD,² Mirko Froehlich, MD,¹ Rainer Dietz, MD, PhD,¹ Jeanette Schulz-Menger, MD¹ ¹*Franz-Volhard-Klinik, Berlin, Germany,* ²*Siemens AG Medical Solutions, Erlangen, Germany.*

Background: Modified Look-Locker inversion recovery (MOLLI) has been proposed as a reliable pulse sequence for high-resolution single breath-hold cardiac T1 mapping. T1 relaxation times might be used to differentiate between normal and abnormal myocardium. We aimed to optimize pulse sequence parameters for maximum T1 accuracy and to establish normative values for myocardial T1 times.

Methods: An integrated version of the MOLLI pulse sequence was implemented on a 1.5T MR system (Magnetom Sonata, Siemens AG Medical Solutions, Erlangen, Germany). To enhance its utility in a clinical setting, access to all pulse sequence parameters was provided via the standard graphics user interface of the MR system. The original MOLLI scheme consists of 3 ECG-triggered inversion recovery-prepared Look-Locker experiments acquiring 3, 3, and 5 images with initial inversion times of 100, 200, and 350 ms, respectively, resulting in 11 single-shot images within one breath-hold. In order to optimize T1 accuracy in-vitro, MOLLI was performed in 8 Gadolinium-doped agarose gel phantoms (nominal T1: 150–1200 ms) at simulated heart rates from 50–100 beats per minute, varying the following sequence parameters: flip angle 5° to 60° (original: 50°), minimum inversion time 80 ms to 160 ms, increment of inversion time between the 3 Look-Locker experiments 80 ms to 140 ms, and acquisition scheme 3-3-5 vs. 5-3-3 acquisitions. Pulse sequence parameters common to all experiments were TE 1.1 ms, TR 2.2 ms, spatial resolution 2.1 × 1.8 mm, slice thickness 8 mm, steady-state free precession read-out with 20 start-up echoes, and 5/8 partial Fourier reconstruction. T1 values of all phantoms were derived for each variant and compared to nominal T1 values as determined by a standard inversion-recovery spin-echo technique. Using the combination of sequence parameters yielding the highest T1 accuracy in-vitro, MOLLI was performed in mid-cavity short-axis views of 12 healthy volunteers (6 men, mean age 25 ± 5 years) pre and post administration of Gd-DTPA (0.15 mmol/kg). T1 was assessed from the resulting T1 maps using a 6-segment model. Intra- and inter-subject variability of myocardial T1 was calculated.

Results: In-vitro studies revealed that a flip angle of 35°, a minimum TI of 80 ms, a TI increment of 80 ms, and an image acquisition scheme of 5-3-3 images allowed for most accurate and least heart rate-dependent T1 measurements in phantoms (mean T1 error < 3%). Using this pulse sequence scheme, T1 maps of good image quality could be achieved in all subjects. T1 relaxation times in normal myocardium were comparable to data from previous studies, and showed narrow ranges

Table 1. Pre- and post-contrast T1 relaxation times in normal myocardium (n = 12)

Time point	T1 mean ± standard deviation (ms)	Range (ms)
Pre-contrast	939 ± 32	887–1016
1 min	291 ± 24	254–338
2 min	339 ± 27	302–386
3 min	374 ± 28	332–413
4 min	400 ± 26	354–428
6 min	433 ± 28	382–461
8 min	454 ± 28	395–482
10 min	471 ± 29	411–501
20 min	529 ± 31	473–574

both pre and post contrast (Table 1). Linear regression analysis showed no significant heart rate dependency (pre-contrast R2 = 0.01).

Conclusion: We present an optimized implementation of MOLLI for fast T1 mapping with high spatial resolution, which can be integrated into routine imaging protocols. Compared to the original set of pulse sequence parameters, T1 accuracy is superior and heart rate dependency is avoided.

201. HIGH TEMPORAL RESOLUTION PHASE CONTRAST MRI USING SSFP

Vinay M. Pai, PhD, Elizabeth Hecht, MD, Vivian S. Lee, MD, PhD, Leon Axel, PhD, MD. New York University School of Medicine, New York, NY, USA.

Introduction: Phase contrast MRI (PCMRI) provides flow information similar to 2D echocardiography without acoustic window restrictions. High temporal resolution PCMRI may provide valuable information about the flow patterns in the chambers. A new approach, Phase Contrast using Phase Train Imaging (PCPTI), is presented for obtaining high temporal resolution flow information in a breathhold examination. The results obtained compare well with flow results obtained using conventional FLASH-based PCMRI.

Purpose: Very high temporal resolution flow imaging may prove useful for evaluating valvular dynamics and for studying flow patterns in the cardiac chambers.

Methods: 3-echo PCPTI: Recently, a novel multiecho SSFP sequence called phase train imaging (PTI) has been proposed (Fig. 1) which permits acquisition of very high temporal resolutions in a single breathhold. In this approach, while zeroth moments are nulled for all echoes, the first moment nulling at the center of k-space is usually observed only on the odd echoes (echoes 1 and 3 in Fig. 1). Since each echo is acquiring the same line of k-space, this non-nulling of first moment for the even echoes represents an additional phase, which is equivalent to

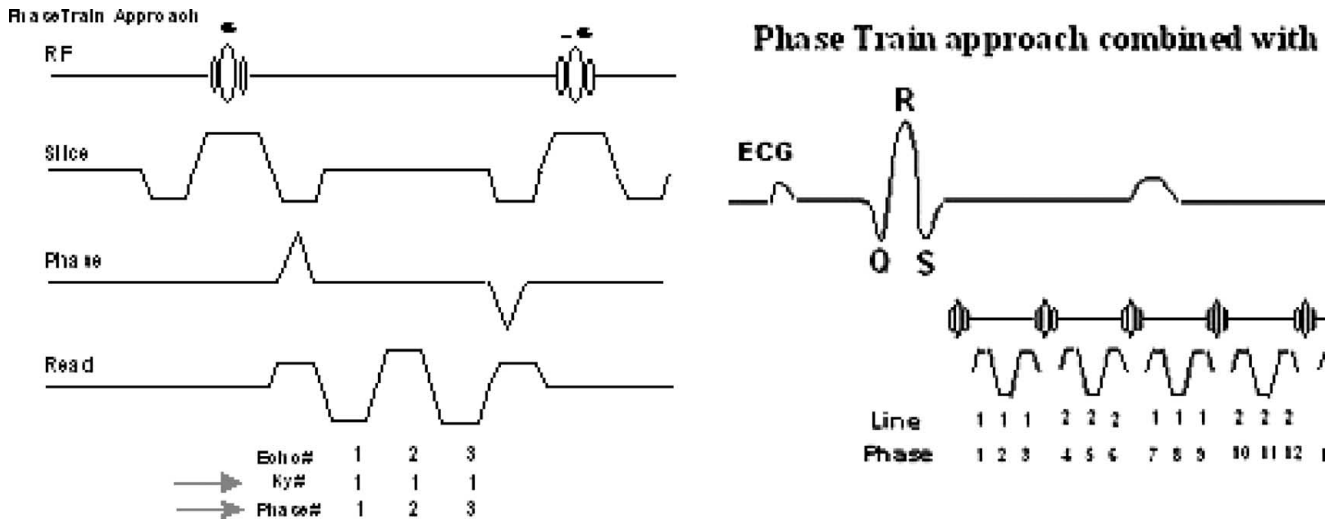


FIG. 1. Phase Train Imaging. (a) Schematic over a single TR. (b) Implementation over a R-R intervals.

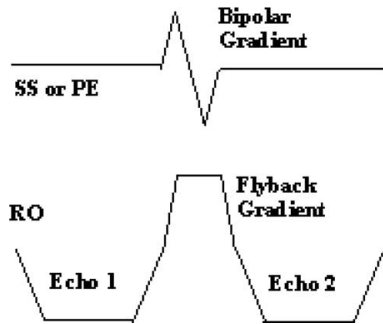


FIG. 2.

the application of a bipolar gradient. By swapping the readout and phase-encode gradient axes, one can use two successive scans to acquire in-plane flow data with this approach. 2-echo PCPTI: An alternative approach (Fig. 2) using 2-echo PCPTI can be used to encode through-plane and in-plane motion. Here, a fly-back gradient is employed between the two readout echoes, and a bipolar flow encoding gradient is played out in either the slice-select or the phase-encoding direction during the duration of the flyback. Thus, the first echo provides the reference data, and the second echo provides the flow-encoded data. For PCPTI, phase difference (PD) is calculated as $PD = \theta_{\text{echo2}} - \theta_{\text{echo1}}$, where $\theta = \tan^{-1}(S_i/S_r)$, and i and r represent the imaginary and real

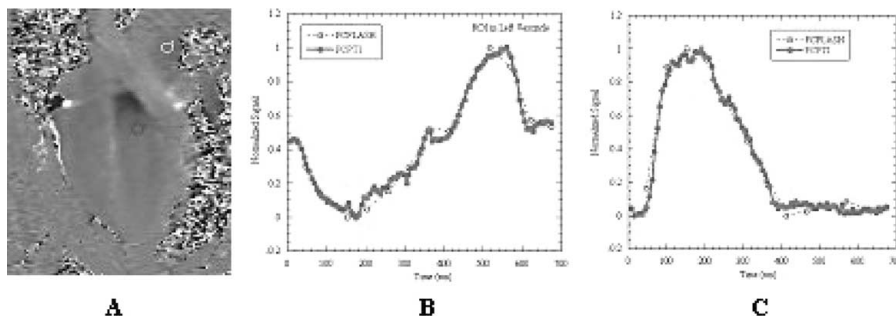


FIG. 3.

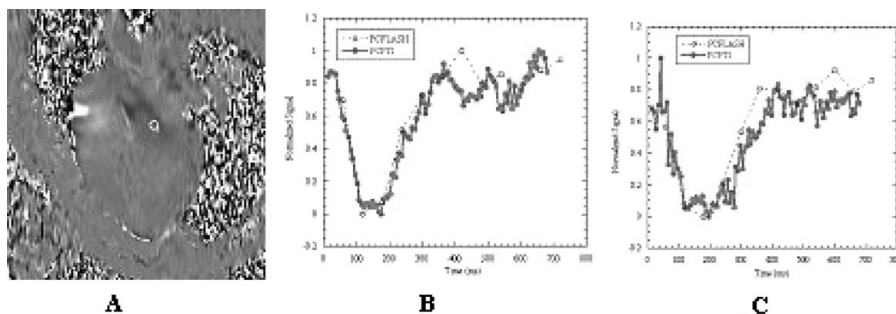


FIG. 4.

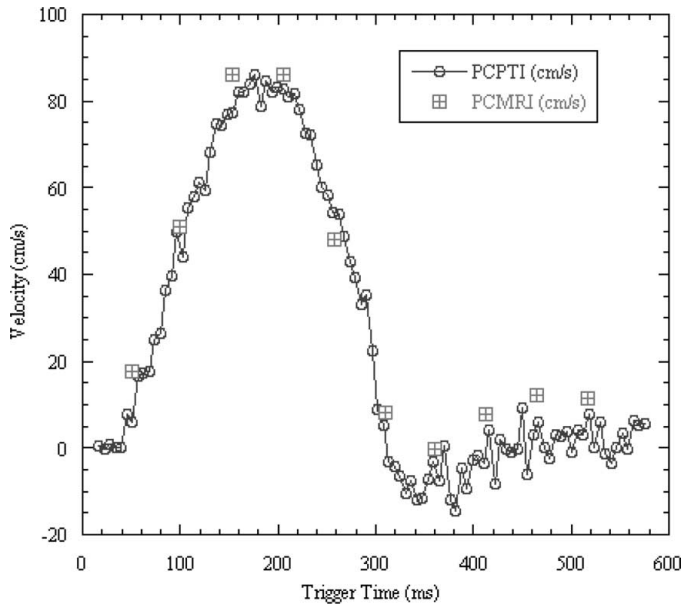


FIG. 5.

parts of the complex signal S. The PCPTI sequence was implemented, in conjunction with TSENSE, on a Siemens Avanto scanner (Siemens Medical Solutions, Malvern, PA) and tested on healthy human volunteers by comparing to a conventional PC-FLASH cine sequence (PCMRI). The coil sensitivity maps were derived from the non-flow-encoded echo (echo 1), and used for both echoes (non-flow-encoded and flow-encoded). In the PCPTI approach, each echotrain (i.e. train of echoes between RF pulses) provides one data point for the PD map.

Results: 3-echo PCPTI: Figs. 3(a, b and c) and 4(a, b and c) show the results for flow encoding in the HF and LR directions respectively. Figs. 3a and 4a shows representative PD images for the two encodings. Normalized signal intensity plots were generated for regions-of-interest (ROIs) placed in the left ventricle (LV) and pulmonary artery (PA). These plots are shown in figures b and c, for the PCPTI and PCMRI approaches. Excellent correlation exists between the two sequences for HF encoding. Due to the conventionally observed lower velocity in the LR direction, both sequences provide noisy data for the LR encoding. 2-echo PCPTI: Fig. 5 shows the through-plane velocity as measured by PCPTI and PCMRI in the ascending aorta for a Dor procedure patient. There is remarkably good overall correlation between the two approaches; however, due to the lower temporal resolution, the PCMRI data misses the dip in the flow at the end of systole (300–350 ms).

Conclusions: The PCPTI approach correlates very well with the conventional PCMRI sequence in tracking the velocity component in-plane and through-plane. The PCPTI sequence provides the highest temporal resolution to-date for looking at in-plane and through-plane flow patterns, with each velocity component being acquired in a single breathhold.

202. CARDIAC CONTRACTILE DYSSYNCHRONY MAPPING USING DENSE DISPLACEMENT IMAGING: PRELIMINARY TESTS IN NORMAL SUBJECTS

Han Wen, PhD, Eric Bennett, PhD, Neal Epstein, MD, Jonathan Plehn, MD. *National Institutes of Health, Bethesda, MD, USA.*

Introduction: Clinical trials of cardiac resynchronization therapy (CRT) in heart-failure patients with contractile dyssynchrony have been shown to improve function, reduce symptoms and improve quality of life (1), and recently echo tissue Doppler imaging (TDI) of inter and intra-ventricular dyssynchrony have been shown to correlate with long term response to CRT (2). When compared with echo TDI, MR displacement imaging (DENSE) (3) of the myocardial wall has several advantages: DENSE measures 3D displacement instead of 1D velocity projection; MRI is not limited by acoustic windows; DENSE strain maps are of higher quality than echo strain maps, and strain based dyssynchrony measures are free of tissue tethering effects; the detailed displacement information allows automatic tissue tracking and image masking which is a saving in image processing time and labor. To attain sufficient temporal resolution for dyssynchrony mapping and spatial resolution for the right ventricular wall, we implemented a respiration-gated DENSE sequence and demonstrated its use in normal volunteers.

Materials and Methods: DENSE with cine acquisition (4) has been shown to achieve 60 ms temporal resolution in breathhold scans. However to reach higher spatial and temporal resolutions, we implemented a respiration-gated cine-DENSE scan with the following parameters: true temporal resolution 21 ms, spatial resolution $1.4 \times 2.8 \times 7.0 \text{ mm}^3$, matrix size 256×48 , 25 cardiac phases, scan time 3.5–4.8 min/slice. To reduce phase encoding steps, one of the two RF pulses in the STEAM preparation was selective in the PE direction. In 5 normal subjects (2F, 3M, age 23–41), 2 short-axis slices (mid-basal and mid-apical) and a 4-chamber slice were acquired. Right ventricular measurements were obtained from the 4-chamber view.

Table 1.

	Inferoseptal	Anteroseptal	Anterior	Anterolateral	Infarolateral	Inferior	RV
Mid LV	356 ± 34	353 ± 42	369 ± 40	382 ± 59	375 ± 48	367 ± 26	343 ± 11
Mid-apical LV	359 ± 48	340 ± 82	362 ± 47	380 ± 54	385 ± 46	356 ± 26	

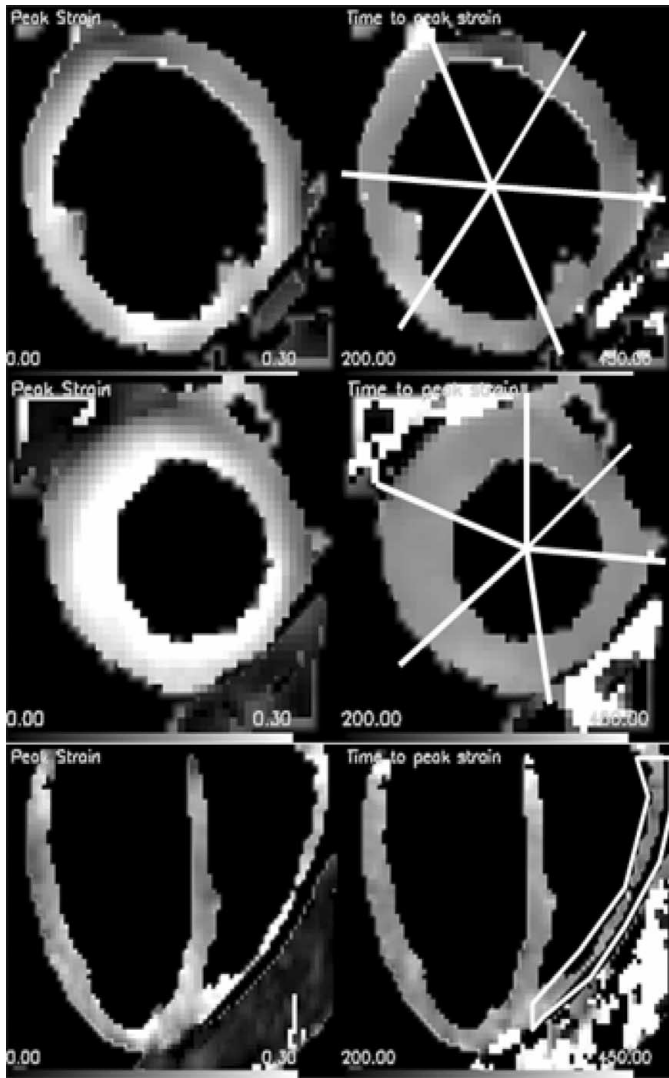


FIG. 1.

Image processing was performed with a custom software (DEN-SEView) which incorporates automatic masking and tissue-

tracking with strain and timing analysis (a separate abstract is submitted). To track the same tissue over time, the displacement field from the starting time to any cardiac phase is regridded by interpolation to a fixed grid at the starting time. Strain as a function of cardiac phase was then calculated for the fixed grid, and a peak strain map (circumferential for short-axis and longitudinal for long-axis) and a R-wave-to-peak-strain map were generated. These were then further segmented manually into different anatomical zones according to the AHA standard. Processing time on a 1.5 GHz laptop was 2 min/slice.

Results: Table 1 shows the magnitude and phase images of a 4-chamber slice for one cardiac phase. The phase maps were the results of automatic masking and unwrapping of the raw phase data.

Fig. 1 shows the peak strain and R-wave-to-peak-strain color maps of a data set from a subject and illustrates the segmentation of anatomical zones in the short axis slices, and separation of left and right ventricles in the 4-chamber view. The left column are peak strain maps, the right are R-wave-to-peak-strain maps. The top two rows are mid-basal and mid-apical slices, the bottom row is the 4-chamber slice. Anatomical segments are marked with white lines and done manually.

Table 1 summarizes the mean and standard deviation of R-wave-to-peak-strain times in the various segments among the 5 subjects, in units of milliseconds.

Conclusion: Cardiac dyssynchrony mapping with MR displacement imaging has several distinct advantages over echocardiography. Respiration-gated cine-DENSE is able to attain sufficient spatial resolution to map right ventricular timing in addition to the left ventricle.

REFERENCES

1. Cazeau S, et al. *N Engl J Med* 2001;344:873–80.
2. Yu CM, et al. *Circ* 2004;110:66–73.
3. Aletras AH, et al. *J Magn Reson* 1999;137:247–52.
4. Kim D, et al. *Radiology* 2004;230:862–71.